Spring 5-15-2017

# Supercooled: An Equilibrium, Melting-Based, Energy Distribution Approach for Describing the Phenomenology of Metastable Liquids

Nicholas Bryan Weingartner
*Washington University in St. Louis*

WASHINGTON UNIVERSITY IN ST. LOUIS

Department of Physics

Dissertation Examination Committee:
Zohar Nussinov, Chair
Jonathan I. Katz
Kenneth F. Kelton
Kater Murch
David Wisbey

# Supercooled: An Equilibrium, Melting-Based, Energy Distribution Approach for Describing the Phenomenology of Metastable Liquids

by

Nicholas Bryan Weingartner

A dissertation presented to
The Graduate School
of Washington University in
partial fulfillment of the
requirements for the degree of

Doctor of Philosophy

May 2017
Saint Louis, Missouri

# Contents

# List of Figures

# List of Tables

# Acknowledgments

I am not a Time Lord, nor am I a superhero. Unlike the Doctor, the Justice League, or the Avengers, I do not have super powers and I have never faced the challenges that these heroes deal with every week. I would posit, however, that many of the challenges and much of the strife that come with pursuing a doctoral degree can sometimes feel just as harrowing as trying to combat the combined might of the Master, the Joker, and Thanos all at once. And just like defeating such a sinister triumvirate would prove impossible for any one of these heroes on their own, navigating the ups and downs of graduate school would have been undoable I were alone. Thankfully, just as the Doctor has his companions, and the Justice League and Avengers have their respective teams, I had the perpetual support of a revolving cast of characters far greater than any you would ever read about in a comic book or see on TV. For this reason, it would be a heinous omission, a proverbial crime even, akin to opening the gates of Arkham itself, to not acknowledge all those who have been with me on this journey.

I would like to first say thank you to my wonderful parents. The support you have given me over the last 27 years, both financial and emotional, has not gone unnoticed or unappreciated. Dad, your many sacrifices so that I never wanted for anything, and so that I could get go to the University of my choice is something I can never repay you for. Nor could I ever express

the depth of my admiration for the example that you set. We may have charted different paths in life, but never doubt that I modeled everything I did after what you taught me. Mom, you have been my closest friend and ally since birth. If you had not listened to my diatribes, and put up with my many idiosyncrasies throughout my college career, I surely would have never survived. Thank you for keeping me grounded, and for all the fun Friday adventures. Those were memories I'll always keep, and are the ones that kept me going these last five years.

Hayden, little buddy, Big H, Grandpa Hayden, Pickleshitz, and whatever other ridiculous thing I've called you over the last seven years, you are my bestest friend. You are too young to know it yet, but you rejuvenated my entire outlook on life when you came into it. All the visits to the park, walks, dinners, movies, and other fun stuff we did over the years when I needed a break from the grind was all that kept me going some weeks. I also cannot thank you enough for all the times that I was feeling low, and doubting myself that you gave me a giant hug and told me I 'was the best'. You, little man, are the best, and I am just lucky to be along for the ride.

Sam and Josh, the 2 tons of tortilla chips and 50,000 gallons of salsa we ate on all those Chevy's Sundays also helped get me through (and get me fat). Thanks for all the good times, and for somehow making such a good looking nephew despite the odds being stacked against you.

Garrett, thanks for being at my defense, and for always paying the bill for the loan I cosigned on, on time. You are a good kid.

Next, I would like to thank the many Bothans who died to bring me the data that was employed throughout this thesis. You have not died in vain.

To my many friends that I made while in graduate school, especially Dr. Ryan Patrick 'Alison' Murphy, Dr. Thomas Crockett, Kelsey Meinerz, Rachel Crouch, and Ivy Love (who I absolutely believe will be President someday), thank you for your friendship. Grad school is rough. We all know that, and the commiseration really does help. That and Risk Legacy and Trump the Game, back when that was still fun. I'd be remiss not to mention separately, my closest friend, Matt Reisman, one of the best, brightest, and most supportive guys anyone could hope to be friends with. I had a blast doing everything from Quantum final projects to playing lots and lots of Love Letter and Naughty Bananagrams with you these last five years.

To Dr. Zohar Nussinov, thank you for your guidance and your mentoring these last years. Thank you for allowing me to provide real input to projects, always contribute my thoughts, even when we disagreed, and pursue my interests. I wholeheartedly believe that we did work of real consequence together, and I look forward to seeing what we can continue to do together. Dr. Ken Kelton, thank you, also, for your guidance. The many chats we had in your office were as illuminating as they were entertaining. Thank you for adopting me into your group as an honorary member, and for including me in social gatherings, and for just being a friend. It was pleasure to work with you.

Finally, thank you to my beloved Jessica. Jessi, the last year and a half with you has been some of the best time of my entire life. I never knew how truly incomplete I was until I

met you. You have strengthened me, encouraged me, inspired me, and comforted me this last year and half. You put up with a lot during the writing and pre-defense part the last 5 months, and I cannot thank you enough for your patience. I love you more than you will ever know, and cannot wait to be with you for the rest of my life. Your love means more to me than this silly degree ever could. Love you baby. But just one question... Is there mail? But was there anything for me?

To President Donald Trump, thank you for setting the bar so low in terms of qualifications for jobs of significance, right as I entered the work force.

To anyone I may have left out, know that it was not intentional, and thank you for everything you did, and for being a part of my life. Salut!

Nicholas Bryan Weingartner

*Washington University in Saint Louis*

*May 2017*

Dedicated to my incredible parents. Everything I am, and ever will be, is because of you.

ABSTRACT OF THE DISSERTATION

Supercooled: An Equilibrium, Melting-Based, Energy Distribution Approach for Describing the Phenomenology of Metastable Liquids

by

Nicholas Bryan Weingartner

Doctor of Philosophy in Physics

Washington University in St. Louis

Professor Zohar Nussinov, Chair

The glass transition remains one of the great open problems of modern physics. This dissertation aims to increase understanding of this topic by studying the rich phenomenology of supercooled liquids, the metastable precursors to the glassy state. Principally, we aim to discover what underlying physics leads to the dramatic, non-Arrhenius increase of the viscosity and relaxation time of supercooled liquids, and what thermodynamic properties govern this physics. We propose a novel framework and associated viscosity function applicable to all supercooled liquids/glassy systems, and rigorously assess both the performance and implications of this model. We demonstrate that the theoretical framework uncovers an underlying universality in the dynamics of supercooled liquids over as much as 16 decades. We extend the model to describe the thermodynamics of supercooled liquids, as well as dynamical features outside of the viscosity/relaxation time. We conclude by discussing a micro structural link, and investigate a growing length scale associated with local rigidity, and percolating clusters of mid range order.

# Chapter 1

# Introduction

## 1.1 Prologue

Solids, liquids, gases. Every elementary school student invariably learns of the three fundamental aggregate states of matter, and the apparent distinctions between them. Solids, they are taught, rigidly maintain their shape, whereas liquids jostle about, and take the shape of their container. Gases, on the other hand have little cohesion and expand to fill any open space. Focusing in on liquids and solids, students are told that at high temperatures, a system will be in its liquid state, and at low temperatures the system will be in its solid state. What separates these two distinct states of matter, as the story goes, is a sharp phase transition at a well defined temperature, known as melting. When a solid is heated to this point, or a liquid cooled to it, one state suddenly changes into the other. Here there is a sharp, and distinct, change of physical properties of the system, and the difference between the two states can be clearly elucidated, with solids being highly ordered at the atomic level, and liquids being more or less random in their arrangement. This dichotomy, while physically true, is not the whole story, however. Much as there are more than simply three states of matter, the distinctions between these states are not always sharp and clear. Some liquids, like honey or tar, are 'thicker' than others, and take a lot longer to 'take the shape of

their container', and if you make them 'cold' they can become so slow that you have to wait a very long time to see them move. What happens if you don't have the patience to wait? In this case the liquid seems solid, but there has not been a transition! So what, then, is the real distinction between the liquid and solid? It turns out this is the very question which underlies one of the most significant open questions in modern physics: the glass transition.

## 1.2 The Phenomenology of Supercooled Liquids and the Glass Transition

### 1.2.1 Broad Introduction

Glasses are ubiquitous. Countless publications over the last five decades have begun with this simple statement, and perhaps the ubiquity of *this statement itself*, has lessened the appreciation of its fundamental truth. Our modern world is, in many ways, built on the usage of glasses, or glassy systems. Device screens, drinkware and cookware, windows, spectacles, jewelry, tools, and more are all commonly made of glass of various types, and new applications are being discovered everyday. The extraordinary elasticity and strain behaviors that result from a lack of crystalline defects in glasses has led to increasing use in machining, biomaterials, and even defensive armor (7; 8; 9; 10; 11; 12). Additionally, the unique energy band structure associated with a lack of periodicity has led to increasing application in the fields of semiconductors and optical recording. It is amazing, then, that something so pervasive in our daily experience, and representing so much potential for innovation, can remain so poorly understood by the scientific community as a whole, but a fundamental understanding of the physics of glasses remains elusive. Why is this the case? What is so mysterious? Naively, a principle difficulty is that glasses are solid, without the structural

regularity of crystals, appearing to form without a phase transition, and are in fact, not even in equilibrium. The unique dynamics and thermo-mechanical properties of glasses, in conjunction with the mysteries surrounding their formation, present a source of tremendous confusion and debate for scientists, but also a source of tremendous opportunity. Indeed, the problem of the glass transition has been called the greatest unsolved mystery of modern condensed matter physics, as true because of the academic curiosity it presents but also the new utilities that can result from understanding it.

In order to understand the properties of glasses, one must first understand the physics of how and why they form at all. Despite decades of intense research, a broadly accepted theory of the glass transition remains elusive. In fact it has been said that there are more theories of the glass transition than there are physicists working in the field to propose them. Regardless of the specific nature or cause of glassiness, it is universally understood that glasses proceed from supercooled liquids, the metastable precursor to the glassy state. In light of this understanding, it is imperative to have a complete understanding and description of the thermodynamics and kinetics of supercooled liquids. It is this understanding that this thesis aims to provide. We must first, however, broadly outline the major facets of supercooled liquid behavior that any theory must account for.

### 1.2.2 Viscosity, Flow, and Phase Transitions

When forces are applied to elastic solids in equilibrium, the solid responds by deforming to a new size or shape, reaching a new equilibrium state, storing energy in deformed (stretched or compressed) bonds. The applied force is traditionally divided by the area over which it is applied to give a quantity called stress. Stresses can be applied perpendicular to the area (elastic stress, tensile stress, pressure) or parallel (shear stress). The reason for defining the stress is because it quantifies the average force experienced by a given

atom/molecule experiencing the force. The resulting deformation of the solid is quantified by a metric known as strain, which is equal to the change in size or shape of the solid, normalized by the original value. Again, this normalization takes into account the individual bonds involved, and allows for a universal description of deformation. In elastic solids, the stress and strain are linearly related via a quantity known as the modulus, ie

$$\sigma = M\epsilon \tag{1.1}$$

where $\sigma$ is the stress, $\epsilon$ is the strain, and $M$, the modulus. There are various moduli corresponding to the specific stress imposed. The one that is most significant to differentiating solids and liquids is the shear modulus, typically denoted as $G_{shear}$. The modulus, regardless of the specific stress, quantifies a solid's resistance to deformation. Thus, for a given perturbation, the solid will deform by a proportional amount according to the strength of its modulus, with the individual atoms/molecules moving to a new equilibrium position, but will not be capable of returning to its original shape via relaxation of the stress. Simply put, solids are rigid. Liquids, on the other hand, are not rigid. When a stress is applied to a liquid, it responds by relaxing away the stress via large scale rearrangements of the constituent atoms/molecules in a process known as flow. This is related to the fact that the shear modulus of liquids is time dependent. As a result, stresses are not proportional to strains, but instead are proportional to strain rates. Additionally, instead of a modulus relating the stress and strain rate, a dynamic quantity called the viscosity relates the two. Mathematically,

$$\sigma = \eta\dot{\epsilon}. \tag{1.2}$$

where $\eta$ is the liquid viscosity. The viscosity is a measure of a liquid's resistance to flow in the same way that a modulus is a measure of a solid's resistance to deformation. A liquid

with a high viscosity does not flow easily, whereas low viscosity liquids flow quite readily. Colloquially, highly viscous liquids are referred to as being 'thick' like honey or molasses, whereas low viscosity liquids, such as room temperature water, are 'thin'. (Throughout this thesis we will use the viscosity and relaxation time interchangeably as they are related via the well known Maxwell relation, $\eta = G_\infty \tau$, where $G_\infty$ is the infinite frequency (instantaneous) shear modulus, which is weakly temperature dependent.) It is possible for the viscous behavior of liquids to change with different conditions. Indeed anyone who has tapped a bottle of ketchup to get it to pour has observed this; some liquids can be made less viscous with applied stress, and vice versa. Stress, however, is not the only control parameter which determines the value of the viscosity of liquids. Quite generally, the liquid viscosity is strongly dependent on temperature, growing with cooling, and typically being quite well described by an Arrhenius form at all temperatures between the melting and vaporization points. The Arrhenius form is given by

$$\eta(T) = \eta_0 \, e^{\frac{G(T)}{k_B T}} \tag{1.3}$$

where $\eta_0$ is the infinite temperature extrapolation of the viscosity, $k_B$ is Boltzmann's constant, and $G(T)$ is a temperature dependent free energy barrier. Typically this free energy barrier is only very weakly dependent on temperature, so the viscosity approximately takes the form,

$$\eta(T) = \eta_0 \, e^{\frac{E_\infty}{k_B T}} \tag{1.4}$$

with $E_\infty$ a temperature independent activation energy. The physical interpretation of this expression is that there is a well defined energy which must be overcome via thermal fluctuations (associated with an energy $k_B T$) or applied forces in order for the liquid to flow. For liquids in equilibrium above the melting point, this activation energy is typically

of the order of the bond energy of the atoms/molecules comprising the liquid. Therefore, for a liquid to flow in response to perturbations, there must be an appreciable amount of energy provided to break the bonds in order for the constituents to rearrange. This picture also quite naturally explains why the viscosity grows with decreasing temperature, as lower temperature implies that thermal fluctuations of an appropriate size to overcome the energy barrier become increasingly scarce at lower and lower temperatures. The value of the activation energy is generally material dependent, being very high for systems with high strength directional bonds, such as silicate systems, and liquids with hydrogen bonds, and low for Van der Waals, metallic, and chalcogenide liquids.

In ordinary liquids, starting at high temperature and quasistatically cooling (lowering the temperature of) the liquid causes the viscosity to increase continuously according to the aforementioned Arrhenius form, until the liquid reaches the melting point. Before moving forward in this description, we must make an important distinction. In most liquids the system does not uniformly melt at a single melting temperature, but instead has a range of temperatures between the liquidus and solidus over which it melts incongruently. Therefore, when we use the term melting temperature, or melting point, we are actually referring to the liquidus. With this point cleared up, we now discuss what happens when the liquid reaches the liquidus. At the melting point, the liquid and crystalline phases are in equilibrium with each other, both possessing the same value of the free energy. For temperatures infinitesimally beneath melting, the crystalline solid phase has a lower free energy, and becomes the equilibrium state. Therefore, the quasistatically cooled liquid will undergo a first order phase transition at melting, giving off a latent heat and rearranging into the extended long range order of the appropriate crystal structure. The crystalline solid ceases being able to flow, having an infinite viscosity/relaxation time. The different dynamical behavior response can now be clearly understood; the rigidity of crystalline solids is due to their long range order (14). In order for the atoms in a crystal to rearrange in response to perturbations,

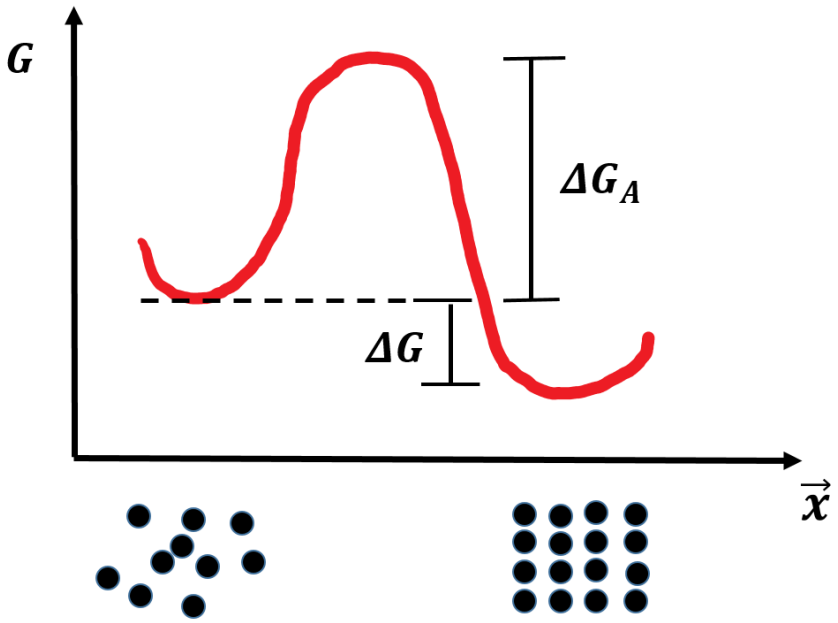


Figure 1.1: (Color Online.) 'Cartoon' representation of the energy barrier associated with interface formation, that creates the kinetic barrier to nucleation.

a massive number of atoms must move together, breaking many strong intermolecular bonds, and necessitating a huge amount of energy. In the liquids, which do not possess any long range order, rearrangement is relatively easy. This is a common underpinning of condensed matter physics: dynamics are determined by structure (15), and the structural change at the thermodynamic phase transition leads to the sharp and drastic change in relaxation/kinetic behavior at the melting point. The process of crystallization that takes place at melting is not instantaneous, it proceeds through nucleation and growth of the crystalline phase. Nucleation is a stochastic process that involves microscopic clusters of the crystalline phase forming within the liquid matrix. While the the clusters are thermodynamically favorable at temperatures beneath melting, the creation of an interface between the cluster and liquid matrix has an associated free energy cost, so that the overall free energy associated with nucleating the crystal is

$$\Delta G = 4\pi r^2 \sigma + \frac{4}{3}\pi r^3 \Delta g_v \tag{1.5}$$

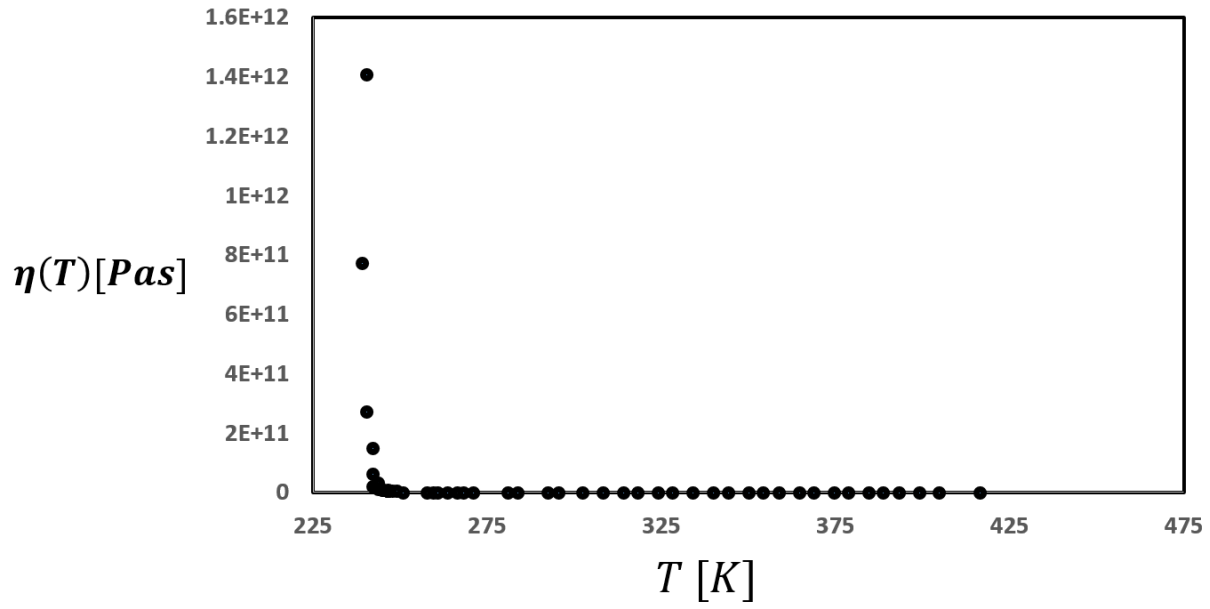


Figure 1.2: (Color Online.) Experimentally observed viscosity data of supercooled OTP.

where $r$ is the radius of the (assumed spherical) cluster, $\sigma$ is the surface tension associated with interface creation, and $\Delta g_v$ is the free energy decrease per unit volume associated with the change of state. It is clear that there will be a critical radius for which clusters of smaller size are thermodynamically unfavorable and will spontaneously breakup, whereas clusters of larger size are stable and will undergo crystal growth. Therefore, the free energy of formation of a cluster with the critical radius forms an activation barrier similar to that depicted in Fig. (1.1). Further use of classical nucleation theory (13) leads to an overall relaxation rate of

$$I_{nuc} = I_0(T)e^{-\frac{\Delta G*(T)}{k_B T}}, \tag{1.6}$$

where $I_0(T)$ is a prefactor which contains several thermodynamic and kinetic factors (13), and is typically inversely proportional to the viscosity, such that more viscous liquids nucleate the crystalline phase more slowly. This makes sense, as nucleation requires

atoms/molecules in the liquid to diffuse through the liquid and rearrange into the crystal structure, and high viscosity implies difficulty in these types of rearrangments, and indeed a lower diffusion coefficient, as the two are usually inversely related via the Stokes-Einstein relation (18). The existence of a nucleation rate means that there exists a nucleation timescale which is roughly the reciprocal of this rate, and is a temperature dependent time for nucleation of the crystalline phase to occur. A byproduct of this kinetic nature of crystallization is that it is possible to cool a liquid sufficiently quickly as to bypass crystallization at the melting point. What does sufficiently quickly mean? It means a rate which is faster than $\frac{1}{\tau_{nuc}}$, such that the temperature of the liquid is lowered before nucleation can occur. As the temperature is further lowered, the viscosity of the liquid will increase, making nucleation more and more difficult. When a liquid is brought beneath its melting point without crystallizing it is said to be supercooled, and exists in a metastable (with regard to the true thermodynamic crystalline ground state) equilibrium.

Once the liquid enters the supercooled state, a number of peculiar thermodynamic and kinetic behaviors and anomalies appear. The most significant of these is that of the temperature dependence of the viscosity/relaxation time, and this will be the principle inquiry of this thesis.

As the temperature of the supercooled liquid is further reduced beneath melting, the viscosity begins to rise incredibly rapidly, by as much as 14 decades over a temperature range as little as 100 Kelvin. This extraordinary increase of viscosity with small change in temperature is fantastically demonstrated by ortho-terphenyl (15), a prototypical glass former, and this is depicted in Fig. (2.7). Eventually, with further cooling, at a material specific temperature, $T_g$, the viscosity of the supercooled liquid reaches a value of $10^{12}$ Pa*s ($\tau = 100s$), and the liquid ceases to flow on physically meaningful timescales, becoming mechanically rigid and behaving as a solid. At first glance this may remind the reader of the phase transition from the liquid to the crystal at the melting temperature, but the glass

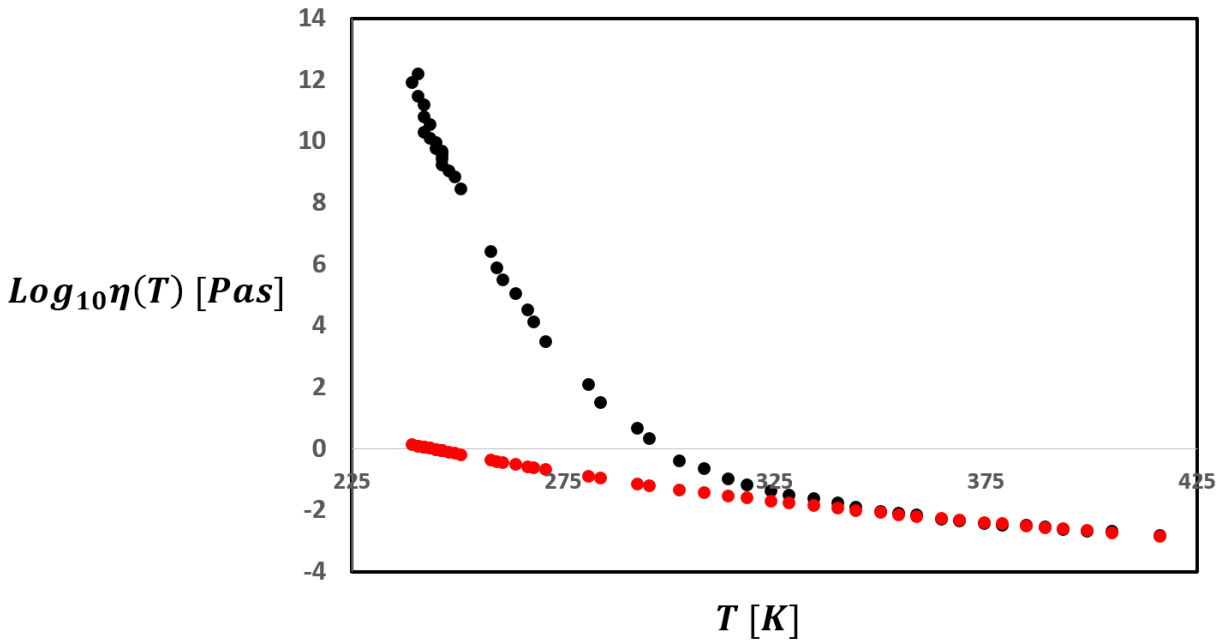


Figure 1.3: (Color Online.) Logarithm of viscosity of OTP plotted as a function of temperature ('upper' black curve) and the extrapolated high temperature logarithm of viscosity ('lower' red curve). A clear departure from Arrhenius behavior occurs at a temperature near T=350 K.

transition is entirely different. First, the glass does not possess an order atomic/molecular arrangement, instead having its constituents arranged in amorphous structure resembling that of the liquid. In fact, radial distribution functions show little change with supercooling the liquid to the glass. Therefore, the rigidity is not associated with a long range order as it is in the crystal. Second, in addition to no apparent structural change, there are none of the usual thermodynamic markers of a first order phase transition at the glass transition temperature, such as latent heats, entropy or enthalpy discontinuities, heat capacity jumps, etc. Indeed, as pointed out, the glass is not an equilibrium state and the glass transition temperature itself is merely operationally defined, and varies with the rate at which the liquid is quenched (cooled). Therefore, the apparent emergence of solid-like features corresponds to dynamical arrest and is not associated with a first order phase transition.

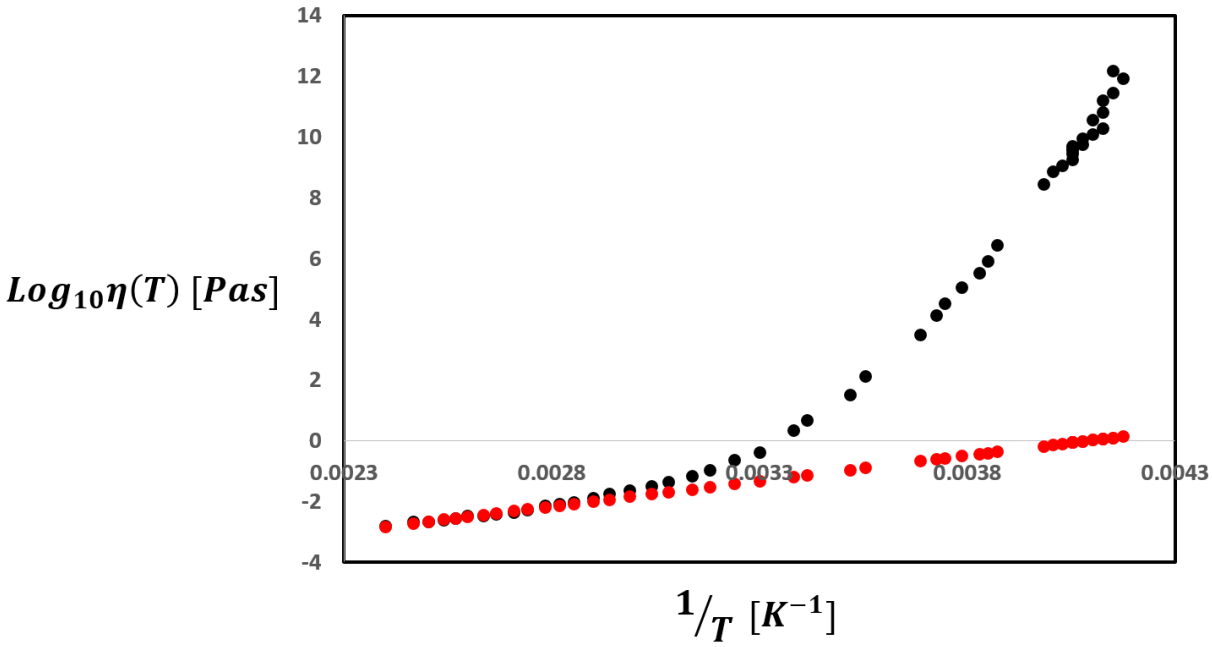


Figure 1.4: (Color Online.) Logarithm of viscosity of OTP plotted as a function of reciprocal temperature ('upper' black curve) and the extrapolated high temperature logarithm of viscosity ('lower' red curve). A clear departure from Arrhenius behavior occurs at a temperature near T=350 K.

With the possibility of a first order transition ruled out, we next turn to other possible explanations for the dramatic slowdown of liquid associated with a rapid viscosity increase. Exponential functions are naturally capable of describing huge increases over small changes of their argument, so we should investigate whether continuing to describe the temperature dependence of the viscosity via an Arrhenius form is appropriate. If this is the case, then the physical picture is quite simple, as the liquid has simply become too viscous to flow on observable timescales. The act of supercooling by removing kinetic energy from the liquid makes it such that rearrangements, which require overcoming the intrinsic energy barrier, will have become incredibly scarce. It is observed, however, that all liquid viscosities depart from the Arrhenius form to some degree, possessing a so-called super-Arrhenius temperature dependence. This is demonstrated in both Figures (1.3) and (1.4), where the logarithm of the viscosity is depicted verus temperature and inverse temperature respectively. In these figures, the Arrhenius viscosity, consistent with high temperature OTP, is shown in red, having been extrapolated beneath melting, and the observed viscosity is shown in black. It is clear that there is a temperature at which the two curves depart from one another, the viscosity becoming 'super-Arrhenius' at this point. This temperature has traditionally been labeled $T_A$, and a number of interesting phenomena appear at this temperature, that will be further discussed later. Complicating matters further, the degree of departure from the Arrhenius function forms a spectrum of behaviors ranging from very little departure for liquids like $SiO_2$ which possess strong directional bonds, and extreme departure for liquids like OTP which do not possess directional bonds. Angell (16) realized that because liquid viscosities tend to have the same limiting value at infinite temperature, and have the same value at $T_g$ by definition, that the logarithm of the viscosity could be plotted versus the inverse temperature scaled by $T_g$ in order to examine this spectrum. An Angell plot of a handful of representative supercooled liquids is shown in Fig. (1.5). Angell additionally defined a useful metric for quantifying the degree of departure which he called the fragility,

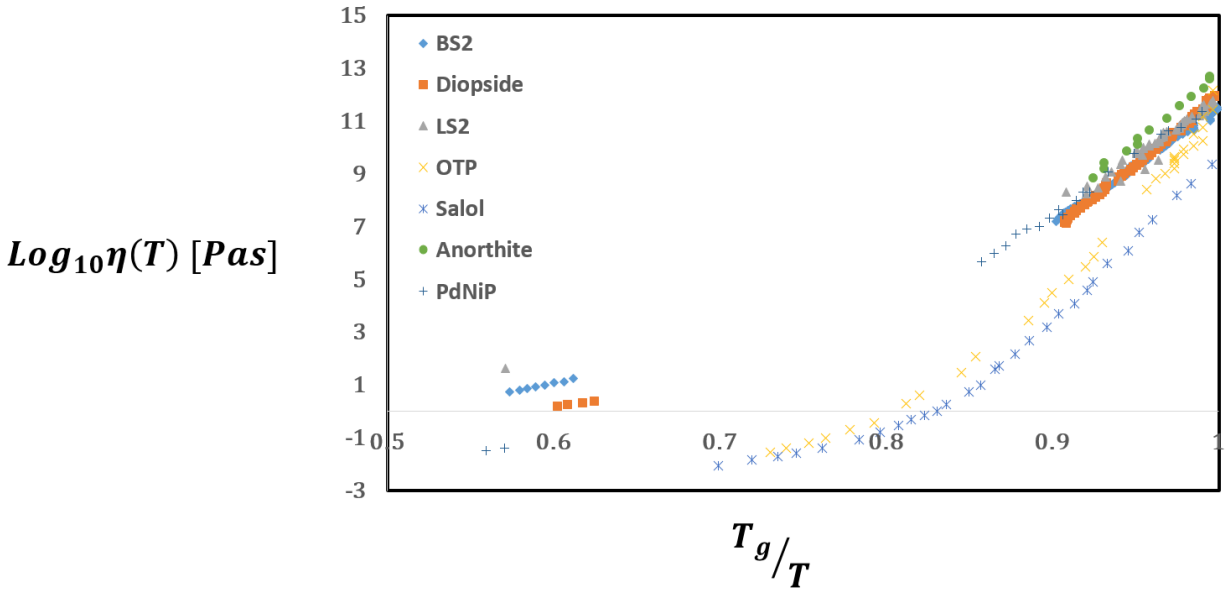


Figure 1.5: (Color Online.) 'Angell' plot of the logarithm of viscosity versus $T_g$-scaled reciprocal temperature for a selection of different liquids. Note the spectrum of different behaviors.

$m$, which is defined mathematically as

$$m = \frac{d\ log\ \eta(T)}{d(\frac{T_g}{T})}|_{T_g}. \tag{1.7}$$

The fragility is an important parameter for describing the dynamics of supercooled liquids, and will be discussed in great detail throughout this thesis.

We have now ruled out both a first order transition, and simple Arrhenius picture for describing the slowdown of supercooled liquids. However, if we recall that the viscosity is related to the relaxation time via the Maxwell relationship, then another possible explanation presents itself. Dramatic increase of the relaxation time of systems is typically observed in the vicinity of *second order* phase transitions, the so-called critical slowing down. In these transitions, the relaxation time diverges at a critical temperature at which the system transitions from one state to another. We have seen that the glass transition at $T_g$ is not

a thermodynamic transition, as it is not between two equilibrium states, and second order thermodynamic discontinuities are also absent. However, the critical slowing down associated with second order transitions sets in at temperatures above the critical point, therefore it is possible that the observed behavior near $T_g$ could be the 'ghost' of an underlying transition at a temperature lower than the glass transition point. The arrest that sets in at $T_g$ due to both the underlying transition and reduced kinetic energy in the liquid, obscures the transition, making it impossible to reach in equilibrium. The divergence of the relaxation time near a critical point is described functionally by a power law dependence, $\tau \propto (T - T_c)^{-zv}$, where $\nu$ is a critical exponent associated with the topology of the system. The exponent $z$ corresponds to the concomitant divergence of an associated correlation length, such that the relaxation time diverges in accordance with a diverging length ($\tau = \xi^{\nu}$). Therefore, if the glass transition is the result of a second order transition, the relaxation time should increase via power law dependence near $T_g$ and there should be an equally diverging lengthscale of some kind. We have discussed that there appears to be little structural change near the glass transition, so a lengthscale associated with structural growth is ruled out. It is quite possible that a lengthscale associated with a more subtle symmetry breaking exists, and indeed we will report on one in Chapter 4, but attempts to find a universally applicable and accepted lengthscale have so-far proved unsuccessful (18; 2; 3; 4; 5; 6) In addition to there being no apparent associated diverging lengthscale, the viscosity (and therefore relaxation time) does not appear to increase in a power law fashion. In Fig. (1.7a)-(1.7c) we demonstrate that plotting the logarithm of the viscosity for the systems listed in the Angell plot versus $T - T_g$ does not lead to a linear variation as would be expected for power law behavior over a wide range. Even if one zooms in to temperatures asymptotically close to $T_g$ to be consistent with ordinary critical behavior, variation from linear dependence is observed, and the results are certainly not universal. Indeed, the depicted data, suggest that there would have to be a large number of universality classes, with exponents significantly greater than any observed experimentally before. While some degree of error could be expected due to using $T_g$ in place

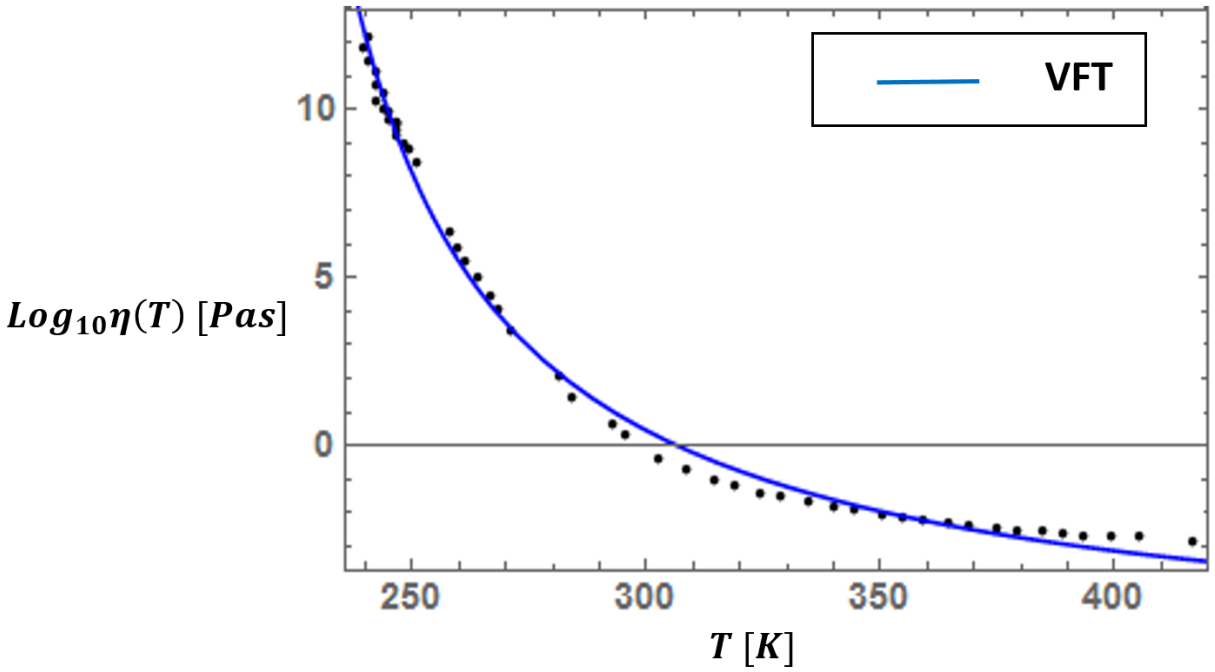


Figure 1.6: (Color Online.) Fits to the viscosity of four sillicate glassformers with the DEH form of Eq. (3.9).

of a lower temperature for the transition, overall there is no evidence suggesting an actual divergence at any temperature beneath $T_g$ (16). Despite this evidence against a transition and associated divergence, many researchers remain unmoved and continue to investigate the existence of a true transition. They are bolstered by the apparent success of the VFT functional form discovered by Vogel, Fulcher, Tammann, and Hesse (28; 30; 29). This form is given by

$$\eta(T) = \eta_0 \, e^{\frac{D \; T_0}{T - T_0}} \tag{1.8}$$

where $D$ is a parameter related to the fragility and $T_0$ is a temperature at which a dynamic divergence occurs. An example of application of the VFT form to the viscosity data of OTP is shown in Fig. (1.6). It is clear from the figure that while, the VFT form does a significantly more accurate job of fitting the experimental viscosity data then either an Arrhenius or power law form, it does display systematic errors in certain temperature regions.

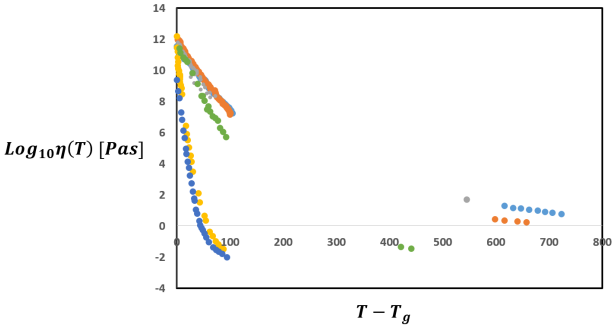


(a)

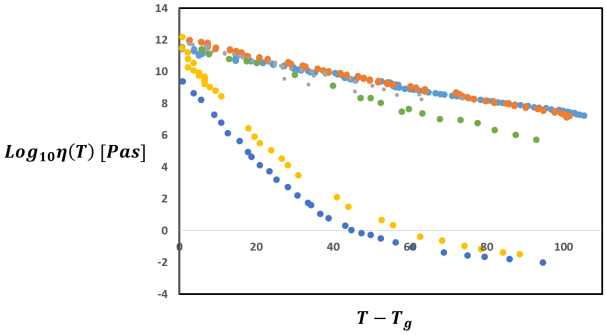


(b)

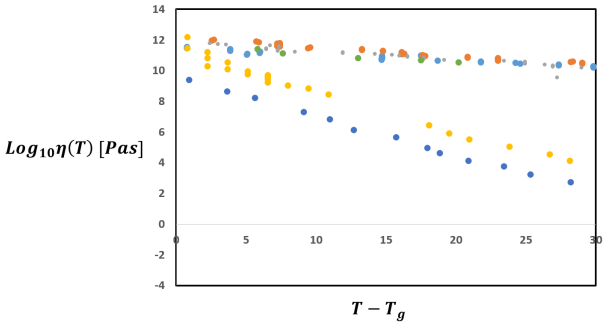


(c)

Figure 1.7: (Color Online.) Zoomed in version of the viscosity collapse data presented in Fig.(3.16). The data is presented in this way to demonstrate that the logarithmic form for the collapse is not masking or suppressing poor fits. Panel (3.17a) focuses on the data in the immediate vicinity of the liquidus temperature. Panel (3.17b) focuses on the mid temperature range. This region is the most sparse, as experimental data in this range is uncommon. Panel (3.17c) shows the lowest temperature region, where the DEH fit is the tightest, and alternative models typically have poorest performance.

More significantly to the theorist, however, is that the VFT form is entirely empirical, not being based in any comprehensive theory. To combat this, numerous theoretical frameworks have been developed over the previous century that aim to 'derive' the VFT form, and some of these will be discussed in Chapters 2 and 3 of this thesis. All of these theories are successful at describing the viscosity over various ranges of temperatures for certain liquids as well as explaining a number of other features of the phenomenology of supercooled liquids, but they all suffer from the same drawbacks. None of the previously proposed theories universally describe all types of liquids at all temperatures successfully, and most have multiple unexplained parameters for the viscosity/relaxation time function, which are not couched in first principles physics. Additionally, many of them lack a complete description of all of the dynamic (such as exponential stretching-which will be discussed in chapter 4) and thermodynamic features of supercooled liquids. Therefore, the field is still quite open. It is our belief, and that of other prominent physicists in the field (38) that any complete theoretical framework for explaining supercooled liquids must possess three major facets, namely it must

1. Explain the super-Arrhenius temperature dependence of viscosity/relaxation time.
2. Explain the non-exponential stretching and anomalous thermodynamics.
3. Be universal, applying to all supercooled liquids regardless of microphysics.

Proposing, investigating, and validating a theory which possesses the above three ingredients is the purpose of this thesis. In the following chapters we will outline a theory which takes as its basis, no special temperatures, relying on the thermodynamic melting temperature (liquidus) as its fundamental temperature, and using properites of equilibrium systems to explain supercoled liquids. This theory can be cast in both a classical and quantum framework, and provides a novel viscosity function which describes the super-Arrhenius growth over the entire range and with only a single parameter. Additionally, the

model is easily extended to all other dynamical and thermodynamical quantities, and also suggests that the dynamics of glass forming liquids are indeed universal.

## 1.3 Overview of thesis

Chapter 2 of the thesis derives the equilibrium, melting-based distribution theory in the classical framework, and applies the resulting viscosity function to 45 different liquids of all types and fragilities. In chapter 3 we recast the theory from a quantum starting point, and extend it to cover other dynamical quantities, as well as various thermodynamic ones. Additionally, we investigate the physics of the single parameter, while also testing more liquids, and extending the theory to temperatures above the liquidus. Finally, in chapter 4, we investigate the structural aspects of the theory, by uncovering a growing lenthscale related to percolating structures, which grows along with the viscosity in a model system.

# References


[1] L. Berthier and M. D. Ediger, Physics Today **69**(1), 40 (2016)

[2] R. Zallen, "The Physics of Amorphous Solids", John Wiley & Sons, Inc., pages 23-32 (1983)

[3] A. L. Greer and E. Ma, MRS Bulletin **32**, 611 (2007)

[4] B. C. Hancock and M. Parks, Pharmaceutical Research **17**, 397 (2000).

[5] M. Telford, Materials Today **7**, 36 (2004).

[6] M. Wuttig, and N. Yamada, Nature Materials **6**, 824 (2007)

[7] A. Cavagna, Physics Reports, **476**, 551-124 (2009) [review]

[8] I. M. Kalogeras and HE. Hagg Lobland, Journal of Materials Education, **34**(3-4): 69-94 (2012) [review]

[9] L. Berthier and F. Biroli, Reviews of Modern Physics, **83**, April-June (2011) [review]

[10] G. L. Hunter and E. R. Weeks, Rep. Prog. Phys. **75**, 066501, (2011) [review]

[11] I. Procaccia, Eur. Phys. J. Special Topics, **178**, 81-122 (2009) [review]

[12] J. S. Langer, Rep. Prog. Phys., **77**,042501 (2014) [review]

[13] K. F. Kelton and A. L. Greer. *Nucleation in Condensed Matter: Applications in Materials and Biology.* Elsevier, 2010.

[14] J. P. Sethna, J. D. Shore, and M. Huang, Phys. Rev. B, **44**, 10 (1991)

[15] G. Brioli, and J. P. Garrahan, The Journal of Chemical Physics **138**, 12A301 (2013)

[16] T. Hecksher, A. I. Nielsen, N. B. Olsen, and J. C. Dyre

# Chapter 2

# The Classical Distribution Theory

## 2.1 Chapter Overview

In this chapter we begin to layout our framework for understanding the phenomenology of supercooled liquids by introducing the main ideas behind the equilibrium, melting-based distribution theory. We fully develop the basic ideas in a classical framework which we call the Energy Shell Distribution Theorem, or ESDT. We take as our starting point, classical statistical mechanical phase space, and recognize that quenching a liquid leads to violation of Liouville's theorem for conservation of trajectories in phase space. Based on this, we develop an extension of sorts, of equilibrium statistical mechanics to metastable supercooled liquids in terms of distributions over classical phase space associated with various effective temperatures. As we described in the first chapter, one of the three principle curiosities of supercooled liquids is the thermal behavior of the viscosity/relaxation time. Therefore, as a first test of the ESDT model, we use this metastable framework to develop an equation for the viscosity of supercooled liquids, and test it by applying the functional form to fit the experimental data of 45 different liquids. The ESDT form links the dynamical evolution of supercooled liquids to the equilibrium melting temperature, and contains only a single fitting parameter, making it experimentally robust, and minimally empirical. Once we have

demonstrated the statistically significant quality of the fits in reproducing experimental data, we observe that this form quite naturally suggests a universality in the dynamics of undercooled liquids. We demonstrate this fact concretely by scaling the data of all 45 liquids using the relevant ESDT variables, and observe a collapse of the data over some 16 decades. We conclude by commenting on the consequences of this apparent universality, and roughly sketching out extensions of the model which will appear in the next chapter.

This chapter is a minimally altered version of a published paper which appeared in *Frontiers of Materials*: N. B. Weingartner, C. Pueblo, F. S. Nogueira, K. F. Kelton, and Z. Nussinov, Front. Mater. 3:50. doi: 10.3389/fmats.2016.00050 (2016)

## 2.2 Introduction

Human kind has been forming and using glasses for millennia. The unique optical, thermal, and mechanical properties, as well as ease of working, that arise from the lack of long-range crystalline order in glasses (1) has lead to their application in a diverse range of fields (7; 8; 9; 10; 11; 12). Despite their ubiquity, a fundamental understanding of the phenomenology associated with glasses and their formation via the vitreous transition remains elusive. In order to understand the structural and mechanical behavior of glasses, we must first understand how and why they form at all. As glasses form from supercooled liquids, this means we must first understand the dynamics of supercooled liquids. Ordinarily, when an equilibrium liquid is cooled to a temperature beneath its melting point it undergoes a first order thermodynamic transition to the ordered crystalline solid. However, if the liquid is cooled sufficiently quickly (at material dependent rate), crystallization can be bypassed, and the liquid enters a metastable (with respect to the crystal) state, and is termed "supercooled". The thermodynamic and kinetic properties of supercooled liquids exhibit a

number of remarkable characteristics, but the most striking is arguably the behavior of the viscosity (and all associated relaxation times) (1; 2; 3; 4; 5; 6). The viscosity of supercooled liquids grows by as much as 14 decades over temperature ranges as small as a few hundred Kelvin, eventually reaching a value of $10^{12} Pa * s$ at the kinetic glass "transition" that occurs at a temperature $T_g$. Calorimetric signatures of the transition into the glassy state have also been observed at the dynamic glass transition temperature $T_g$(63). At temperatures below the glass transition temperature, $T_g$, the increasingly sluggish dynamics lead to the onset of rigidity and solid-like behavior in the liquid on observable timescales. This immense dynamical slowing occurs without any obvious structural change/ordering, and attempts to find an appropriate order parameter or growing length scale have remained inconclusive. As such, explaining the spectacular increase of the viscosity (and associated relaxation time) of supercooled liquids remains an open challenge in material science.

Liquids which are in equilibrium at high temperatures above melting, have a viscosity which is well described by an Arrhenius function, namely

$$\eta(T) = \eta_0 e^{\frac{\Delta G(T)}{k_B T}}, \tag{2.1}$$

with $\Delta G(T)$ a (weakly) temperature dependent Gibb's free energy of activation and $k_B$ Boltzmann's constant. The simple interpretation of this form is that there exists a well-defined energy barrier (associated with bond-breaking) that can be overcome by thermal excitations. As the temperature is lowered, appropriately sized thermal fluctuations become considerably less likely and flow decreases appreciably. If this form were maintained in the supercooled liquid, there would be little mystery. However, all liquids show a degree of departure from the Arrhenius form. This degree of departure forms a continuous spectrum, and is quantified by Angell's fragility parameter (15; 16). According to this scheme, the

most "fragile" liquids (those with the high values of the fragility parameter) display a far more dramatic rise in the viscosity than that predicted by an Arrhenius law whereas the deviation from an Arrhenus law is far smaller in "strong" liquids (having a small fragility). The underlying physics of the departure from Eq. (2.1) is what we aim to explain.

Some of the first attempts to describe the non-Arrhenius character of supercooled liquid viscosity were undertaken in the 1920's by Vogel, Fulcher, Tammann, and Hesse (17). Collectively, they discovered that the functional form,

$$\eta(T) = \eta_0 e^{\frac{DT_0}{T-T_0}} \tag{2.2}$$

was able to adequately describe the viscosity of many supercooled liquids over a fair range of temperatures. In the so-called VFTH form, the parameter $D$ is related to the fragility, and $T_0$ is a material-dependent temperature at which a dynamic divergence is predicted to occur. This form initially appeared as a purely empirical form, with no rigorous theoretical support. However, over the years a number of theoretical frameworks have been proposed (19; 18; 20; 21; 22; 23; 24; 25) to reproduce the VFTH form. While the VFTH form has survived for nearly a century and is widely used, it has consistently been shown to provide an overall poor fit to the viscosity of supercooled liquids of all types (classes, fragilities, bonding types, etc.) over the whole range of data. Additionally, there is no conclusive evidence for a dynamic divergence at any temperature above absolute zero (38). These include tantalizing experiments that employed 20 million year old amber (38; 27). For these and other reasons, a plethora of other functional forms have been proposed in the last 30 years which do not contain a dynamic divergence, and which have rigorous theoretical foundations. A few of these which have been found to accurately describe the viscosity of many glass forming liquids are the KKZNT, Cohen-Grest free volume, parabolic, and MYEGA forms (28; 29; 30; 34; 32; 33; 31).

The aforementioned functional forms have all been shown to do an excellent job of reproducing the temperature dependence of the viscosity of a wide range of supercooled liquids. For example, the KKZNT form (28; 29; 30) has become a favorite of some researchers in the metallic glass community and very accurately describes the behavior of metallic liquids (35), while the MYEGA form (31) has become ubiquitous in the sillicate and oxide glass community, as it works very well for covalently-bonded non-organic liquids. The trouble with these forms, as we will show, is that despite their applicability to some liquids they do not accurately describe all types of supercooled liquids. This is made particularly striking in a review by Angell *et al.* (16), in which the authors list *ten* different functional forms all of which they discuss are accurate only for certain types/classes of liquids. Additionally bothersome is that most of these theories contain at least three adjustable parameters which cannot be uniquely determined by correlations with thermodynamic observables. This is true of the parabolic form (32; 33), which has wide applicability to fragile glasses. It seems reasonable to expect that if any liquid can in principle be supercooled, then there should be some universal mechanism/theory that is applicable across all liquids. Further, the material dependent parameters of a given model should be related to thermodynamic observables, and not arbitrary fitting variables, while reflecting first principles.

In order to remedy the issues discussed above, we will now propose and assess a classical statistical mechanical framework to describe the viscosity of supercooled liquids. An earlier quantum rendition of our theory that mirrors and contains many of the considerations invoked in the classical approach that we discuss here first appeared in (36) and motivated the fit and collapse that we experimentally tested and derive here classically. Within our framework, the temperature dependence of the viscosity contains only a single parameter. Such a functional dependence implies a collapse of the viscosity data. In the current work, we collapse the published viscosity data of 45 supercooled liquids onto a single scaling curve. This collapse is a central result of our work. Additional aspects of our approach

(in particular, the calculation of Angell's fragility parameter and the viscosity above the melting temperature) along with further details concerning our data analysis and fits appear in (37). Regardless of our theoretical bias, the existence of the universal collapse of the viscosity data that we first report on here suggests (as it has in many other arenas for very different problems (38; 39; 40)) an underlying simplicity. Historically, the existence of a collapse in which the data from numerous systems were seen to fall on a universal curve pointed to a commonality in standard equilibrium critical phenomena (40). Historically, the discovery that experimental data for various systems in the vicinity of their liquid to gas phase transition can be made to collapse onto a single curve after a simple rescaling (41) predated current understanding of critical phenomena by many decades and hinted at the universality that permeates equilibrium phase transitions (40; 42). We hope that the viscosity collapse that we find for all studied supercooled liquids will spur further investigation. In the next section, we turn to the rudiments of our classical statistical mechanics approach.

## 2.3 Fundamentals of the Energy Shell Distribution Approach

The macroscopic thermodynamic and dynamical observables (such as viscosity) of a many-body system ultimately result from the average of the microscopic dynamics of the constituent atoms of the system. These microscopic dynamics are governed by the interactions between the system's constituent members, and these are encoded in the system's Hamiltonian, $H$, which is a function of the kinetic and interaction energies of the constituent atoms in the system. We can write down the ***exact*** classical, many-body Hamiltonian for a supercooled liquid of any type as

$$H = \sum_i \frac{\vec{P}_i^2}{2M_i} + \sum_i \frac{\vec{p}_i^2}{2m_e} + \sum_{i>i'} \frac{e^2}{4\pi\epsilon_0 |\vec{r}_i - \vec{r}_{i'}|} + \sum_{ij} \frac{Z_i e^2}{4\pi\epsilon_0 |\vec{R}_j - \vec{r}_i|} + \sum_{j>j'} \frac{Z_i Z_j e^2}{4\pi\epsilon_0 |\vec{R}_j - \vec{R}_{j'}|}. \tag{2.3}$$

where $Z_i$ is the atomic number, $m_e$ is the electron mass, $M_i$ is the atomic mass, $\vec{r}_i$ is the position of the i-th electron, and $\vec{R}_j$ is the position of the j-th nucleus. We consider realistic three-dimensional liquids of $N$ particles (the total number of electrons and nuclei). This Hamiltonian is intentionally general; changing the values of $Z_i$, $M_i$, and the specific form of any additional interaction potentials allows one to describe any and all *specific* liquids. Although the exact Hamiltonian is given by Eq. (2.3), this precise form of the Hamiltonian will be immaterial in the very general analysis that follows. Rather, as we will explain, what matters most in our classical approach (and in its quantum analog (36)) is that the equilibrium properties of this disorder free many body Hamiltonian are empirically well known. Specifically, the realization of Hamlltonian of Eq. (2.3) as it pertains to standard disorder free materials, typically exhibits equilibrium solid or liquid phase at, respectively, low or high energy densities or temperatures.

In what briefly follows, we denote the collection of the momentum coordinates of all particles (electrons and nuclei) by $\vec{\pi}$ and the collection of all spatial coordinates by $\vec{x}$. To compute the dynamics of constituents of the liquid, one needs to solve Hamilton's equations,

$$\begin{aligned} \dot{\vec{\pi}} &= -\nabla_{\vec{x}} H \\ \dot{\vec{x}} &= \nabla_{\vec{\pi}} H \end{aligned} \tag{2.4}$$

corresponding to the Hamiltonian in Eq.(2.3). In general, for many-body systems such as a liquid, this leads to a set of strongly coupled, highly nonlinear, partial differential equations

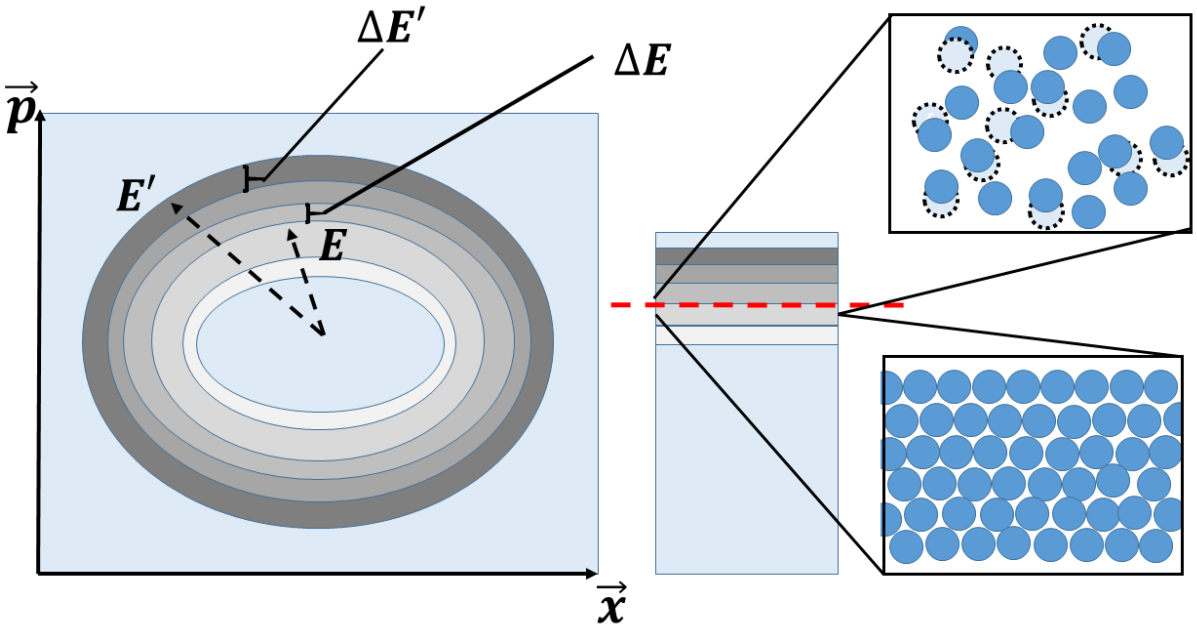


Figure 2.1: (Color Online.) At left is a phase space schematic with fixed energy shells. As described in the text, the microstates change from being "liquid like" at high energy densities (or associated high temperatures) to being "solid like" at low energies (or low temperatures). On the right, we depict a cartoon of the atomic microstates both above and below the energy density associated with melting (dashed line at center).

which are impossible to solve exactly. While methods of approximation do exist to solve the resulting equations, we need only rely on simple statistical mechanics ideas in conjunction with extensively verified experimental observations.

The state of a classical N-body system may be represented by a point labelled by the positions and momenta of each of the particles in 6N-dimensional phase space (a microstate $(\vec{x}, \vec{\pi})$). The time evolution of the system corresponds to a trajectory in this phase space which is governed by the system Hamiltonian and any external constraints. The system is assumed to be in any of the microstates which are allowed by the external constraints of the system (macrostate), with appropriate statistical weights set by the specific ensemble being employed. The calculation of the average values of physical observables $O$ (which correspond to the measured macroscopic values), proceeds by averaging the value of $O$ in each microstate

of the allowed region of phase space. For an isolated system, the allowed phase space is given by a shell centered on the hypersurface of constant energy, $H(\vec{x},\vec{\pi}) = E$, with thickness $\delta E$ set by the uncertainty in specification of the external energy. The statistical weights are constant in the allowed region and zero elsewhere, such that microcanonical averages are given by

$$\bar{O}(E) = \frac{1}{D(E)} \int d^{3N}x \int \frac{d^{3N}\pi}{(2\pi\hbar)^{3N}}\ O(\vec{x},\vec{\pi})\ \delta(H(\vec{x},\vec{\pi}) - E), \tag{2.5}$$

with the density of states

$$D(E) = \int d^{3N}x \int \frac{d^{3N}\pi}{(2\pi\hbar)^{3N}}\ \delta(H(\vec{x},\vec{\pi}) - E). \tag{2.6}$$

When the system is coupled to an external heat bath, all energies are in principle attainable by the system, and the infinitesimally thick shell ($\delta$-peaked) of allowed phase space (Fig. (2.1)) may become smeared and overlap. This leads to averages of the form

$$\bar{O} = \int dE'\ \bar{O}_m(E')\ \rho(E'). \tag{2.7}$$

Here, $\bar{O}_m(E')$ is the microcanonical average at energy $E'$, and $\rho(E')$ is a (normalized) probability distribution in phase space which is not a $\delta$-function. In standard equilibrated systems (such as those corresponding to the disorder free Hamiltonian of Eq. (2.3) that describes equilibrated solids and liquids), the ensemble average of Eq. (2.7) is equal to the long time average of $O$ (which we denote by $O_\infty$) as it evolves according to Eqs. (2.4). Empirically, as we remarked earlier, at high enough temperatures or energy densities, the system of Eq. (2.3) is a fluid while at temperatures or energy densities below that of freezing

the system is an equilibrium solids. Thus, for *any observable* $O$, the microstate average of Eq. (2.5) will change character from featuring equilibrium fluid like features at high energies to solid like behaviors at low energies. When latent heat appears at the equilibrium melting transition (as it nearly always does), there will be intermediate states displaying mixed fluid and solid features. It follows that, when averaged over energy shells in phase space, the microstates themselves change their character across the equilibrium phase transitions. Fig. 2.1 portrays the above simple conclusion.

Since systems in equilibrium, with a well defined temperature, have a canonical partition function,

$$Z = \int_{-\infty}^{\infty} dE\ D(E)\ e^{-\frac{E}{k_B T}}. \tag{2.8}$$

In this case, $\rho(E')$ corresponds o the Gibbs distribution, namely,

$$\rho(E') = \frac{D(E')e^{-\frac{E'}{k_B T}}}{Z}. \tag{2.9}$$

If the system is now cooled quasistatically, equilibrium will be maintained, and the distribution will remain canonical at progressively lower temperatures. This is, in part, guaranteed by Liouville's theorem, which states that the phase space volume along trajectories in phase space is preserved for Hamiltonian systems. This means that as the system is cooled slowly enough, trajectories will neither bunch nor diverge and will map in a "1-to-1" fashion to the newly allowed region of phase space, and the distribution function will adjust accordingly. If instead of slow quasistatic cooling, we rapidly quench the system, it will cease to be in equilibrium and its dynamics will no longer be Hamiltonian. The now dissipative system will violate Liouville's theorem: the trajectories from nearby points in phase space can diverge, and the phase space volume may swell. The initial shape of the initial energy shells will be deformed due to supercooling deform. This deformation is central to our description of the supercooling process. Due to this non-adiabatic evolution, the Gibbs

distribution will no longer be the exactly correct distribution describing the distribution in phase space. If we allow the system to maintain metastable equilibrium then the canonical ensemble is still roughly obeyed. However, in this case, different regions of the initial phase space will map to areas with different effective canonical distribution functions, i.e., with different effective temperatures. This idea, which is seemingly reinforced by the appearance of dynamical heterogeneities (36; 43; 44; 45; 46; 47; 48) and other phenomena implies that the overall system will sample a range of effective global temperatures (necessitated by the apparent spatial distribution of local effective temperatures) consistent with the externally imposed temperature, $T$. This distribution of effective temperatures forms the nub of our "Energy Shell Distribution Theory" (ESDT).

With the system now sampling a smeared out distribution of effective temperatures, the phase space probability distribution for the averages of Eq. (2.7), will now involve a conditional probability density $\rho(E|T')$ for the energy given a specific temperature, namely

$$\rho(E) = \int dT' \ \rho(E|T')\rho(T'). \tag{2.10}$$

Here, $\rho(T')$ is the probability distribution of effective temperatures $T'$. As the system is in a metastable equilibrium, the probability density for a given $E$ at a temperature $T'$ will still reasonably be described by the Gibbs distribution of Eq. (2.9). Similar to Eq. (2.7), the long time average of $O$ for a general distribution $\rho$ including that associated with the supercooled liquid ($sc$) reads (36)

$$\bar{O}_{\infty,sc} = \int dT' \rho(T') \ \tilde{O}_{can}(T'). \tag{2.11}$$

Here, $\tilde{O}_{can}(T')$ is the canonical, equilibrium value of the observable $\mathcal{O}$ at a temperature $T'$. We see, then, that supercooling acts to drive the system into a metastable equilibrium which leads to the system sampling a range of equilibrium value averages over a narrow,

but finite distribution of effective temperatures. The initial "shock" to the system of supercooling causes microscopic effects which broaden the distribution. By virtue of being out of equilibrium, the distribution $\rho$ must have a finite standard deviation. This is so as otherwise the system would be described by a unique uniform effective temperature and be describable by the equilibrium canonical ensemble. However, since the supercooled liquid is out of equilibrium, the standard deviation $\sigma$ associated with the distribution $\rho$ cannot vanish (36). When thermodynamic equilibrium is restored at a uniform global temperature $T$, the distribution $\rho(T')$ becomes a delta function ($\delta(T - T')$) implying an equilibrium Boltzmann distribution (and ensuing equilibrium expectation values for all observables).

With the statistical mechanics ideas in place, we now invoke these to calculate the values of observables of interest. One method of measuring the viscosity of a liquid is by measuring the terminal velocity of a sphere dropped into the liquid. In this case, the viscosity is inversely proportional ($\eta \propto 1/v_\infty$) to the terminal velocity of the sphere. The terminal velocity is a macroscopic property of the system, and therefore can be calculated in our statistical mechanical framework. Setting the observable $O$ to be the vertical velocity of the dropped sphere, $O = v_z$ (36), the observed terminal velocity becomes

$$\bar{v}_{\infty,sc} = \int dT' \rho(T') \; \tilde{v}_{\infty,can}(T'). \tag{2.12}$$

Thus, the viscosity will be given by

$$\eta = \frac{A}{\int dT' \rho(T') \; \tilde{v}_{\infty,can}(T')}, \tag{2.13}$$

with $A$ a constant. As is well known, for an equilibrium system, there exists a cutoff temperature, $T_c$, below which the the terminal velocity must vanish (since the system is completely solid and no long time flow occurs). Thus, in the equilibrium canonical ensemble, only averages of the terminal velocity at temperatures above this cutoff may contribute to

the integral in Eq. (2.13) leading to

$$\eta = \frac{A}{\int_{T_c}^{\infty} dT' \rho(T') \ \tilde{v}_{\infty,can}(T')}. \tag{2.14}$$

If we further assume that the distribution $\rho$ is sufficiently narrowly peaked (as will be verified in the next section and seen from the numerical values of our dimensionless fit parameter) such that the distribution has minimal "leakage" into effective temperatures $T'$ above $T_c$, when the measured global temperature $T < T_c$, then the value of $v_{\infty,can}$ will change very little over the region of appreciable weight. Therefore, we can reasonably replace $v_{\infty,can}(T')$ with $v_{\infty,can}(T_c)$. Thus the viscosity of the supercooled liquid is

$$\eta = \frac{\eta(T_c)}{\int_{T_c}^{\infty} dT' \rho(T')}. \tag{2.15}$$

In order to use this expression to make concrete predictions of the viscosity, we must know what functional form to use for $\rho(T')$. All that is known about the distribution is that it is peaked about the external temperature, $T$, must be normalized, and that it has a small yet finite width. In the absence of additional constraints, the appropriate distribution $\rho$ for the supercooled liquid may be ascertained (36) by maximizing the Shannon entropy $H_I = -\int \rho(T') \log_2[\rho(T')] \, dT'$. As is well known, maximizing the Shannon entropy with the constraints of normalization and finite variance leads to a Gaussian distribution. Therefore, the most probable distribution of effective temperatures is

$$\rho(T') = \frac{1}{\sqrt{2\pi}\sigma(T')} e^{-\frac{(T'-T)^2}{2\sigma(T')^2}} \tag{2.16}$$

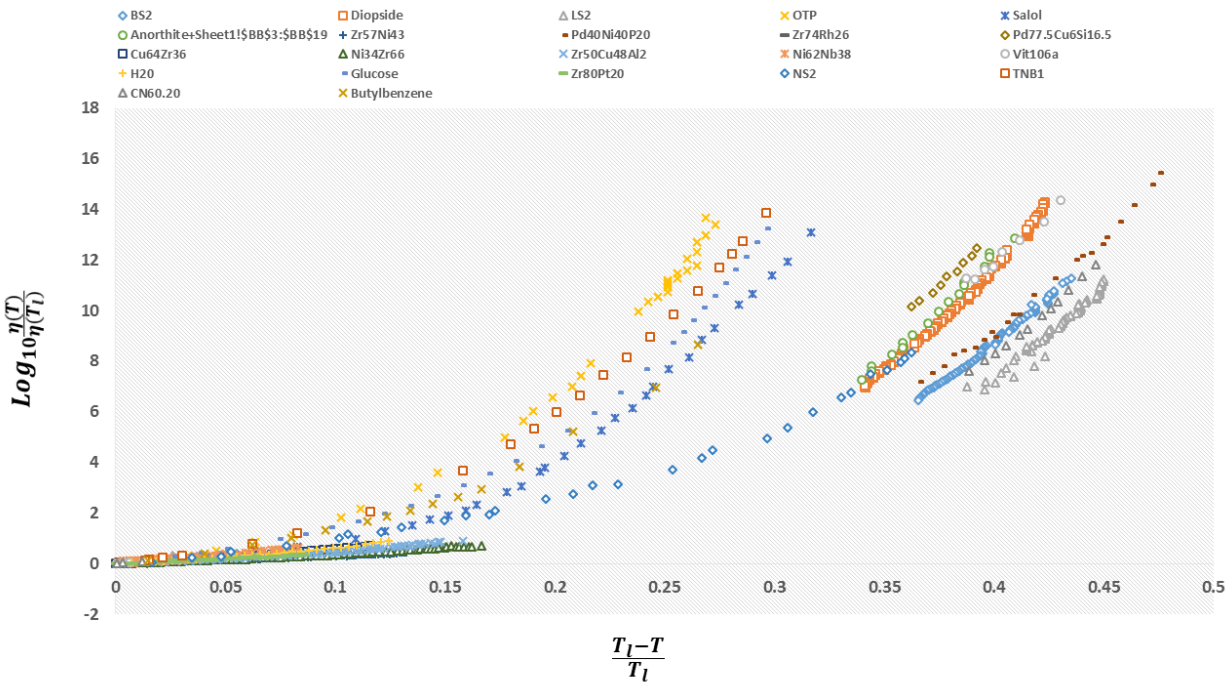


Figure 2.2: (Color Online.) The viscosity, $\eta(T)$, scaled by its value at the melting (or liquidus) temperature $\eta(T_l)$ plotted as a function of the "reduced temperature" $\frac{T_l-T}{T_l}$. When represented this way, a spectrum of behaviors appears, with most glassformers seeming to fall within different 'families' corresponding to fragility classes as defined by experimental values.

where $\sigma(T')$ represents the spread of the distribution and $T$ is the external temperature. Inserting the Gaussian distribution of Eq.(2.16) into Eq.(2.15), we find that the viscosity

$$\eta(T) = \frac{\eta(T_c)}{erfc\left[\frac{T_c-T}{\sqrt{2}\ \sigma(T)}\right]}. \tag{2.17}$$

In what follows, we make two conjectures to complete the form of the viscosity, one involving the cut-off temperature, and one involving the spread of the Gaussian.

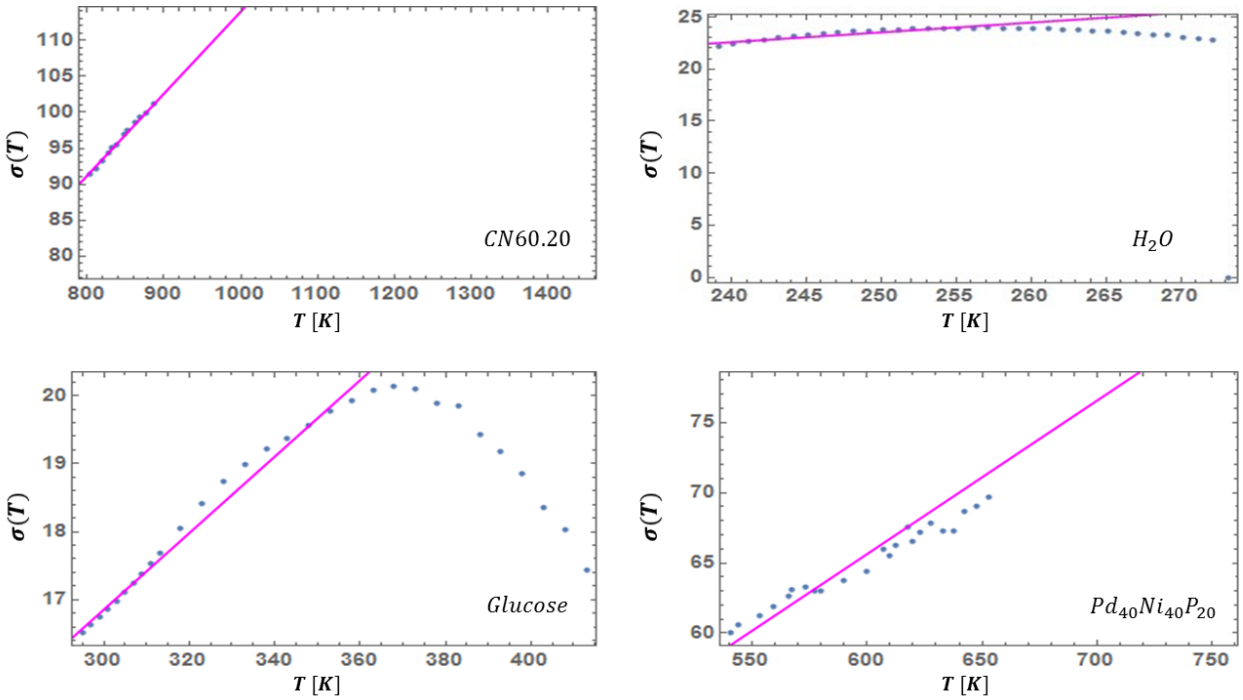


Figure 2.3: (Color Online). The standard deviation $\sigma(T)$ of the probability distribution of Eq. (2.16) as inferred by fitting the experimentally measured viscosity to Eq. (2.19). In most cases that we examined, the approximate linearity relation of Eq. (2.18) holds reasonably well far enough below the liquidus temperature. Here, we also show two well known exceptional liquids: water and glucose. These fluids display anomalies that have been ascribed to putative liquid-liquid transitions, e.g., (60; 61; 62; 63; 64; 65; 66). The crossover of $\sigma$ at high temperature and the one that we similarly found in supercooled salol (37) may be a signature of these putative transitions. Indeed, in salol the crossover temperature at which $\sigma(T)$ deviates from its low temperature linearity (37) coincides with earlier experimentally suggested liquid-liquid transition temperature (68).

### 2.3.1 The cutoff temperature

In choosing a value for the cut-off temperature, $T_c$, we rely on experimental observations. In pure systems, at the melting temperature, the equilibrium system undergoes a first order phase transition from the liquid to the ordered crystalline solid state. At this temperature, in equilibrium, the values of thermodynamic observables transition from their liquid-like values to their solid-like ones. In a perfect crystal (an idealization never realized), the viscosity is infinite (14), and hence the terminal velocity will be zero at temperatures beneath melting.

The idea of linking the glass transition to melting goes back decades and it is easy to understand why (50; 51; 52; 53). By definition, supercooled liquids are formed by avoiding crystallization at the melting transition, therefore the melting temperature implicitly determines at which temperatures a supercooled liquid exists at all. Additionally, the melting transition occurs at a sharp transition temperature, making it a somewhat less arbitrary reference point than the kinetically defined glass transition temperature. Kauzmann, in his seminal paper (37), was one of the first to propose an empirical link between the glass transition and melting. He observed that for all the liquids he studied, on average the glass transition and melting temperatures were related by $T_g \approx \frac{2}{3}T_m$. In the intervening years, a number of researchers have found that this relationship holds, on average, for various types of supercooled liquids/glasses (56; 78). However, deviations from this empirical rule have also been observed for decades. Similar to the argument above, Turnbull reasoned that because nucleation and growth of the crystalline phase became thermodynamically possible at the melting temperature, glass formability may be linked to the gap between the melting temperature and glass transition temperature. He observed that glass formability in metallic liquids could roughly be quantified by what he defined as the reduced glass transition temperature, $T_{rg} = \frac{T_g}{T_m}$ (71; 58; 53), where the best glass formers

had $T_{rg} \approx \frac{2}{3}$. However, as metallic liquids display a range of glass formability, so to does the reduced glass transition temperature. Therefore, in metallic liquids at least, the 2/3 rule does not always hold. Building on the observation of Kauzmann and Turnbull, it appears reasonable to investigate further what links exist between melting and the glass transition. What these empirical relationships fail to do, however, is provide a consistent framework for understanding the dynamics of supercooled liquids and making predictions about the phenomenology based on melting. This is made vivid by examining a simple scaling of the viscosities of several liquids by values associated with melting. In Fig. (2.2) we plot the logarithm of the viscosity scaled by its value at melting (or, more precisely, its liquidus temperature, as will be discussed below) versus the melting-scaled inverse temperature. As the figure demonstrates, a universal description of the viscosity does not immediately emerge by simply using the melting temperature, however "fragility bands" appear, providing more evidence for the link between $T_g$ and $T_m$. This suggests that an "ingredient" is missing. It is our goal to combine the above ideas with our simple statistical mechanical treatment, to ultimately arrive at a complete, predictive theory of supercooled liquids.

In light of the above arguments we will identify the cut-off temperature $T_c$ with the melting temperature, $T_m$. There is an intrinsic difficulty in doing this, however, which must be addressed. Only certain non-monatomic liquids possess a single "melting" temperature. In reality, most liquids have a "melting range" associated with the temperatures between the solidus temperature $T_s$ and the liquidus temperature $T_l$. Additionally, either associated with these temperatures, or the pure-system melting temperature, $T_m$, there will be a range of energies corresponding to the latent heats/enthalpies of formation. Therefore, regardless of which temperature we choose to represent "melting", there will be corrections necessary to account for the melting range. Additionally, many sillicate systems are polymorphic in the crystalline solid state, meaning that at various temperatures below the liquidus, the crystal transitions between different thermodynamically stable crystalline configurations.

These polymorphs and their associated temperatures can have a very large impact on the thermodynamic properties of the system, with minimal apparent impact on the dynamical properties. One may obtain bounds on the viscosity by setting the cutoff or melting temperature in Eq. (2.12) to mean the liquidus temperature (36). If no long time flow appears in this intermediate temperature regime (i.e., if the terminal velocity of Eq. (2.12) vanishes), then this substitution of $T_c = T_l$ in Eqs. (2.15,2.17) will be precise. Thus, because solid-like characteristics will *first appear* at the liquidus temperature, we will take it to define the melting temperature at which point there is a change in the *equilibrium* dynamics of the system. This argument can be further understood in the context of the Lindemann criterion. In Lindemann's model, the break down of solidity and onset of flow at the melting temperature is due to the average amplitude of vibration becoming an appreciable fraction of the lattice length ($\approx 10\%$). At the temperature where this occurs, the lattice destabilizes and constituents become liquid like. The average amplitude of vibration is proportional to the kinetic energy, so this can be seen as the average kinetic energy of the constituents becoming enough to globally overcome the average interatomic bond strength. Observations suggest that a Lindemann-like model also holds for the devitrification of glasses (54). Therefore, viewing this from the perspective of cooling, at the melting (liquidus) temperature, the "stickiness" of the interaction forces/energy first starts to dominate the kinetic energy, and the constituents begin to more strongly interact Inserting the liquidus temperature, $T_l$, into Eq.(2.17), we obtain that $\eta(T) = \frac{\eta(T_l)}{erfc\left[\frac{T_l - T}{\sqrt{2}\ \sigma(T)}\right]}$ We next motivate a specific functional form for the distribution $\sigma(T)$.

### 2.3.2 The width of the distribution

The spread in effective temperatures, $T'$, at a given external temperature, $T$, is quantified by $\sigma(T)$. This spread (related to the variance by a simple square root) is the

fundamental variable in the ESDT, as it is caused by, and leads to, the metastable, non-canonical spread in temperatures/energies Much like the exact distribution of temperatures which it governs, we do not know a priori what its functional form should be. However, there are a number of physical constraints that will ultimately motivate its exact form. As the system is cooled, the peak of the distribution (Eq. (2.16)) shifts downward as it is centered on the external temperature, $T$. The tails, and not the peak, though, control how likely a macroscopic flow event will be. In order that the flow continue to decrease rapidly as the temperature is lowered, the width of the distribution will also have to shrink to "pull" the tail out of sampling the flowing states. Additionally, as the system approaches absolute zero, the third law of thermodynamics will require that the spread in energies (and hence effective temperatures) vanish, such that $\sigma(T)$ must be a decreasing function of temperature. It is also readily obvious, that the only natural energy scale for the metastable supercooled liquid is set by the external temperature. Therefore, it is reasonable to assume that $\sigma(T) \propto T$. We these simple facts in mind, we assert that

$$\sigma(T) = \bar{A}T, \tag{2.18}$$

where $\bar{A}$ is a small, dimensionless, material-dependent parameter. That is, the width $\sigma(T)$ is set by the natural energy (temperature) scale of the system. Additional analysis is provided in (36). To confirm the validity of this approximation, we can invert Eq.(2.17) solving for the spread, $\sigma(T)$, and examine it for experimental viscosity data. Across the different examined liquids, we found this to hold relatively well. In some materials, there are deviations from linearity in the vicinity of their respective solidus and/or liquidus temperatures. This is illustrated in Fig. 2.3. As seen therein, in both glucose and supercooled water (Fig. (2.3)), $\sigma(T)$ exhibits such a crossover. We found an analogous trend in supercooled salol where the crossover temperature associated with $\sigma(T)$ (37) coincided with the earlier reported putative liquid-liquid transition temperature in this system (68). Similarly, supercooled

water and glucose display anomalies that have been ascribed to a liquid-liquid transition (60; 61; 62; 63; 64; 65; 66). Taken together, these data suggest that, if and when present, fragile to strong crossovers or liquid-liquid phase transitions (67) may be associated with deviations in $\sigma(T)$. This will be critically addressed in depth in a follow-up paper where we will further extensively demonstrate that $\bar{A}$ strongly correlates with various thermodynamic parameters and may allow for the prediction of low temperature viscosity from purely high temperature measurements.

For the time being, we stress that $\bar{A}$ constitutes the *only adjustable parameter* in this framework. When combining this with Eq.(2.17), we now arrive, via classical phase space considerations, at our principal result for the viscosity (36),

$$\eta(T) = \frac{\eta(T_l)}{erfc\left[\frac{T_l - T}{\sqrt{2}\ \bar{A}\ T}\right]}. \tag{2.19}$$

It is immediately clear from an examination of Eq. (2.19) that our model does not possess a dynamical singularity. In fact, if one were to calculate the entropy difference between the supercooled liquid and equilibrium crystalline solid, it would be apparent that the excess entropy could only vanish at a point where the temperature distribution becomes a delta function. When this occurs, however, the system will, by definition have returned to equilibrium. Therefore, our approach makes it plain that there cannot be a finite temperature singularity, and that the above excess entropy can only vanish if the system regains equilibrium. The function of Eq.(2.19) relies only on measurable quantities associated with the liquidus and a single parameter. While the specific form of the above equation is only applicable beneath the liquidus temperature, in (37) we derived an extension to all temperatures above the liquidus, completing the theoretical model.

A corollary of Eq.(2.19) is that the viscosity data from all supercooled liquids may be made to collapse onto one master curve. That is, for each fluid, the ratio of the viscosity

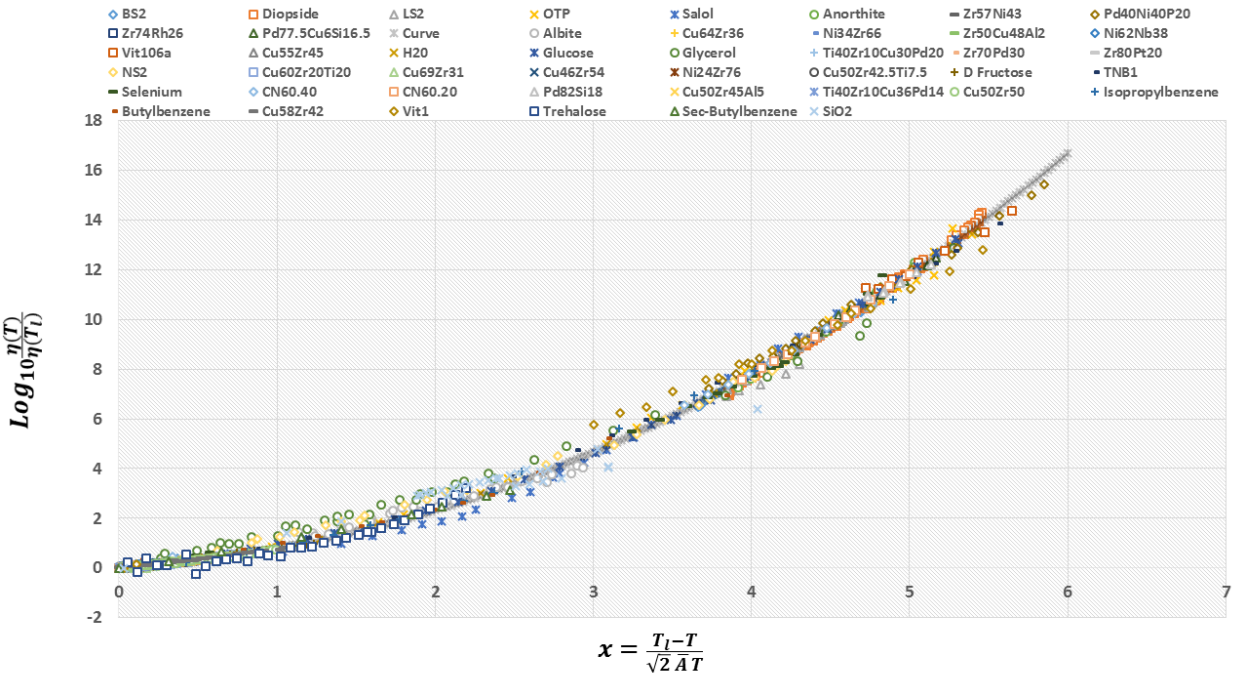


Figure 2.4: (Color Online.) The viscosity data scaled by its value at the liquidus temperature, $\eta(T_l)$, versus $x$, as defined in the figure. The viscosity data of 45 liquids from numerous classes/bonding types (sillicate, metallic, organic) and kinetic fragilities collapse onto a unique curve, suggestive of universality amongst all types of glassforming liquids. Note the exceptional agreement over 16 decades. The deviations of glycerol and $SiO_2$ are discussed in (37). The pertinent liquidus temperature $T_l$ and the viscosity at $T_l$ and our single dimensionless parameter associated with all fluids is provided in Table **??**. The continuous underlying "curve" (seen at the high viscosity end where fewer viscosity data are available) is that predicted by Eq. (2.19).

at temperature $T \leq T_l$ to its viscosity at the liquidus temperature, $(\eta(T)/\eta(T_l))$, is a trivial function of the quotient $(T_l - T)/(\bar{A}\ T)$ with $\bar{A}$ being the single dimensionless parameter that is material dependent. We tested this prediction in Fig. (3.16) and found it is indeed be satisfied. Although the value of $\bar{A}$ does not significantly change across all of the liquids that we examined (see Table **??**), its variations are nevertheless important. In particular, it can be demonstrated that the fragility parameter is a function of both $\bar{A}$ and the reduced glass transition temperature $T_{rg}$ (that are set, in our theory, by the values of the melting temperature and $\bar{A}$ themselves) (37). Thus, albeit being small in size, the changes in the values of $\bar{A}$ in their relatively narrow range (along with the values of $T_{rg}$) differentiate strong fluids from fragile ones. This is clearly seen in Fig. 2.2; if the dependence on $\bar{A}$ between different glass formers were weak the viscosity data in Fig. 2.2 would have collapsed onto a single curve. The contrast between Fig. 2.2 and Fig. 3.16 (in which $\bar{A}$ was, for each liquid, set to the value given by Table **??**) highlights the importance of the deviations in the parameter $\bar{A}$ (the "missing ingredient" the we alluded to above) from one fluid to another.

## 2.4 Methods: A test of the predicted viscosity and a data collapse

Whether or not the dynamics of supercooled liquids are universal has been debated for some time. We demonstrated that the ESDT viscosity form appears to fit the viscosity data of all types of supercooled liquids, thereby providing the "missing ingredient" that prevented a universal description of liquids based on melting. If the ESDT form is to be a complete picture for all liquids, then it should allow for a universal scaling of the viscosity of supercooled liquids. For that reason, we plot the logarithm of the viscosity of all studied liquids scaled by its value at the liquidus, but this time versus the argument of the

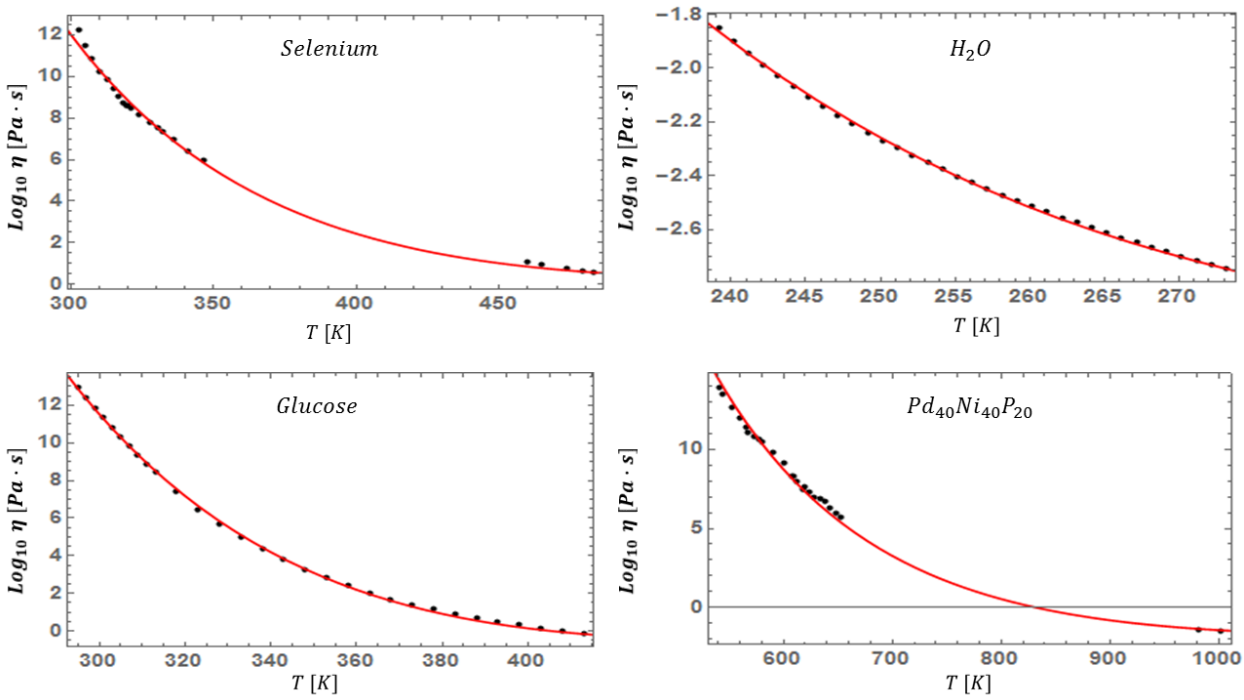


Figure 2.5: (Color Online.) Fits the viscosity of various supercooled fluids (including water) with Eq. (2.19).

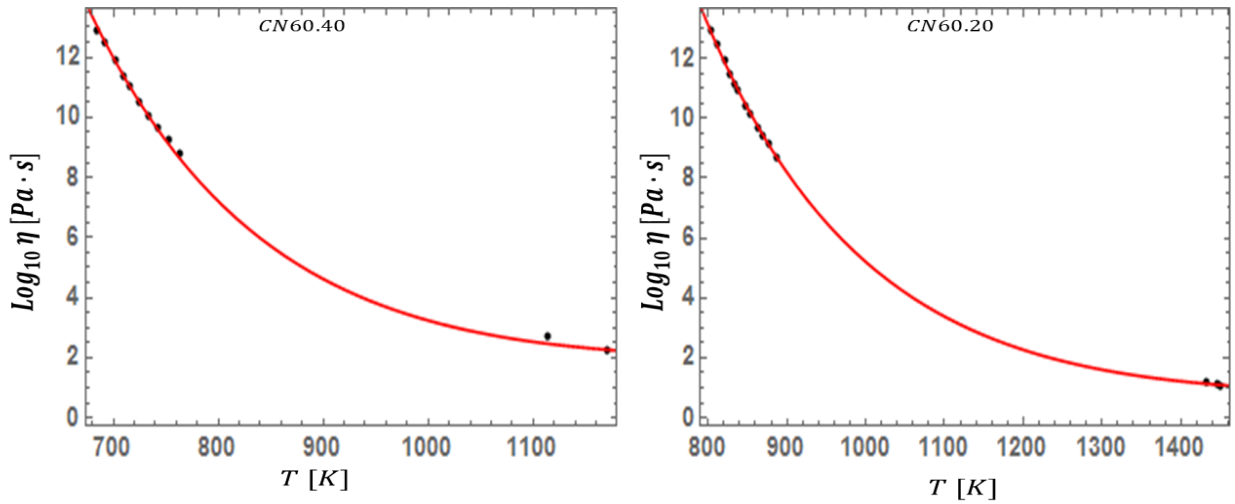


Figure 2.6: (Color Online.) The fit of Eq. (2.19) is tested for CN60.40 and CN60.20, two silicate systems with slightly different molar compositions.

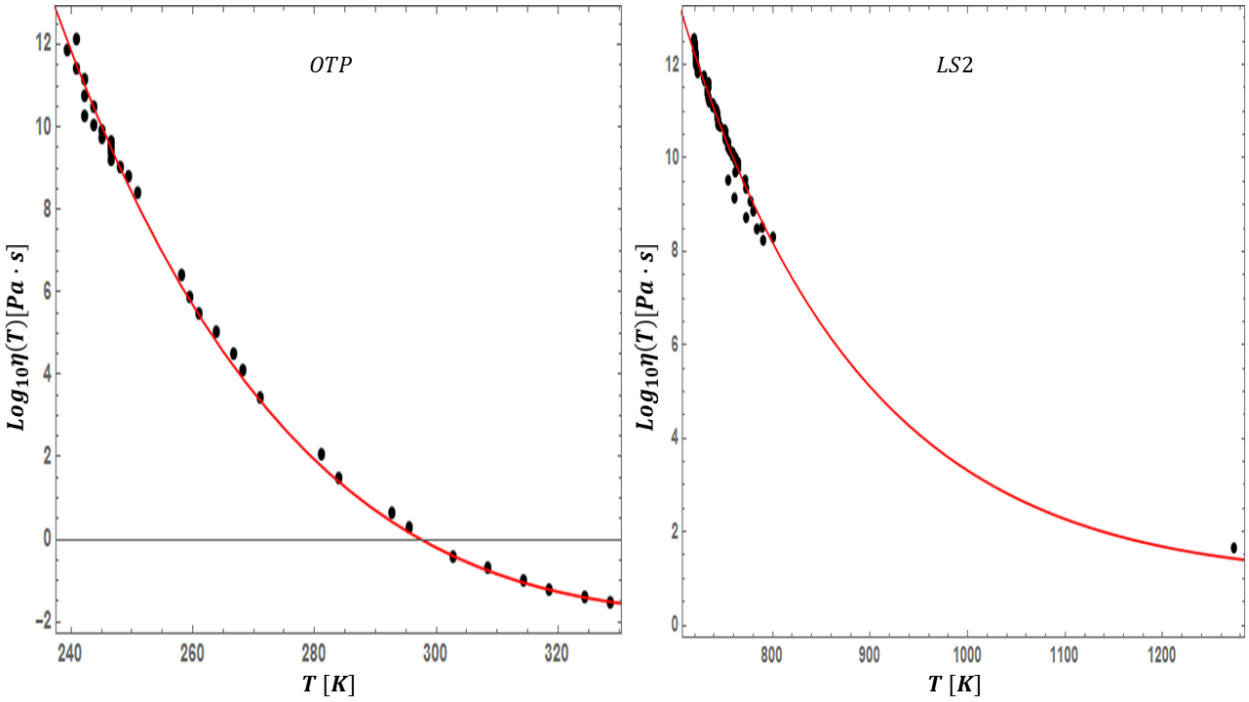


Figure 2.7: (Color Online.) Our viscosity fit of Eq. (2.19) is applied to a very fragile organic glass former (OTP) and very strong silicate glass former (LS2).

complementary error function. The results of this scaling are presented in Figure 3.16. It is immediately clear that this scaling collapses the viscosity data of all liquid types onto a single curve. More significantly, the collapse holds over 16 decades, and for all classes/types of liquids. It should be pointed out that while this scaling arose as a consequence of the ESDT framework, even if the theoretical foundations do not hold, this scaling can always be done. While the analysis of considerably more liquids is ultimately required, this stunning result suggests that there is perhaps an underlying universality to the dynamics of all supercooled liquids.

For completeness, it must be pointed out that all liquids tested in this work undergo congruent melting and can therefore be adequately described by their liquidus temperature. There are numerous liquids, however, that undergo incongruent melting, and a small molar addition of some material can drastically change the liquidus temperature without appreciably effecting the viscosity. This is because the liquidus is where the small crystalline

clusters associated with the addition will first appear, but in small enough concentrations, they cannot impact the dynamical character of the liquid. This presents a difficulty for using the liquidus as the scaling temperature for all liquids. The impact of this will be investigated in a further work, but suggests that for these "pathological" liquids, a description in terms of the solidus or associated temperatures may be more appropriate.

## 2.5 Conclusion

We advanced a classical statistical mechanical framework for understanding the dynamics of supercooled liquids. We demonstrated, both qualitatively and quantitatively, that the resultant expression that is predicted by this classical approach (and by an earlier companion quantum version (36)) for the viscosity of supercooled liquids below the melting temperature can describe/reproduce the behavior of all liquids studied to objectively high accuracy. We demonstrated that the viscosity data of 45 different liquids can be collapsed onto a single scaling curve, suggesting that an underlying universality may be present in the dynamical behavior of supercooled liquids. Further support on our results appears in (37). We hope that our newly found universal 16 decade collapse for the viscosity data of all known liquid types and the theoretical ideas that led us to it will prompt further discussion on the underlying phenomenology of supercooled liquids and the glass transition.

# References


[1] Gupta, P. K. (1996). Non-crystalline solids: glasses and amorphous solids, *Journal of Non-Crystalline Solids 195, 158-164*

[2] Berthier, L. and Ediger, M. D. (2016). Facets of glass physics, *Physics Today 69 (1), 40*

[3] Zallen, R. (1983). "The Physics of Amorphous Solids", John Wiley & Sons, Inc., pages 23-32

[4] Greer, A. L. and Ma, E. (2007). Bulk metallic glasses: at the cutting edge of metals research, *MRS Bulletin 32, 611*

[5] Hancock, B. C. and Parks, M. (2000). What is the true solubility advantage for amorphous pharmaceuticals? *Pharmaceutical Research 17, 397-404*

[6] Telford, M. (2004). The case for bulk metallic glass, *Materials Today 7, 36-43*

[7] Wuttig, M. and Yamada, N. (2007). Phase-change materials for rewriteable data storage, *Nature Materials 6, 824-832*

[8] Cavagna, A. (2009). Supercooled liquids for pedestrians, *Physics Reports, 476, 551-124*

[9] Kalogeras, I. M. and Hagg Lobland, H. E., (2012). The nature of the glassy state: structure and glass transitions, *Journal of Materials Education, 34 (3-4): 69-94*

[10] Berthier, L. and Biroli, G. (2011). Theoretical perspective on the glass transition and amorphous materials, *Reviews of Modern Physics 83, 587-645*

[11] Hunter, G. L. and Weeks, E. R., (2011). The physics of the colloidal glass transition, *Reports on Progress in Physics 75, 066501*

[12] Procaccia, I. (2009). Physics of amorphous solids: Their creation and their mechanical properties, *European Physics Journal Special Topics, 178, 81-122*

[13] Langer, J. S., (2014). Theories of glass formation and the glass transition, *Reports on Progress in Physics 77, 042501*

[14] Yue Y. (2009). The iso-structural viscosity, configurational entropy and fragility of oxide liquids, *Journal of Non-Crystalline Solids 355, 737-744*

[15] Angell, C. A. (1995). Formation of Glasses from Liquids and Biopolymers, *Science 267, 1924-1935*

[16] Angell, C. A., Ngai, K. L., McKenna, G. B., McMillan, P. F., and Martin, S. W., (2010). Relaxation in glassforming liquids and amorphous solids, *Journal of Applied Physics 88, 3113-3157* (2000).

[17] Vogel, H. (1921). The temperature dependence law of the viscosity of fluids, *Physikalische Zeitscrift 22, 645-646*; Fulcher, G. S., (1925). Analysis of recent measurements of the viscosity of glasses, *Journal of the American Ceramic Society 8, 339-355*; Tammann G. and Hesse, W. Z., (1926). The dependancy of viscosity on temperature in hypothermic liquids, *Zeitschrift fur Anorganische und Allgemeine Chemie 156, 245*

[18] Adam, G. and Gibbs, J. H. (1965). On the Temperature Dependence of Cooperative Relaxation Properties in Glass-Forming Liquids, *The Journal of Chemical Physics 43, 139-146*

[19] Cohen, M. H. and Turnbull, D. (1959). Molecular Transport in Liquids and Glasses, *The Journal of Chemical Physics 31, 1164-1169*

[20] Kirkpatrick, T. R., Thirumalai, D. and Wolynes, P. G. (1989). Scaling concepts for the dynamics of viscous liquids near an ideal glassy state, *Physical Review A 40, 1045-1054*

[21] Parisi, G. and Mezard, M. (1999). A first principle computation of the thermodynamics of glasses, *Journal of Chemical Physics 111, 1076-1095*

[22] Lubchenko, V. and Wolynes, P. G. (2007). Theory of structural glasses and supercooled liquids, *Annual Review of Physical Chemistry 58, 235-266*

[23] Leutheusser, E. (1984). Dynamical model of the liquid-glass transition *Physical Review A 29, 2765-2773*

[24] Bengtzelius, U., Gotze, W. and Sjoilander, A. (1984). Dynamics of supercooled liquids and the glass transition *Journal of Physics C 17, 5915-5934*

[25] Gotze, W. *Complex dynamics of glass-forming liquids: A mode-coupling theory* (Oxford University Press, Oxford, 2008).

[26] Mauro, J. C., Through a Glass, Darkly: Dispelling Three Common Misconceptions in Glass Science International Journal of Applied Glass Science 2, **4** 245-261 (2011)

[27] Zhao, J., Simon, S. L., and McKenna, G. B. (2013). Using 20-million-year-old amber to test the super-Arrhenius behaviour of glass-forming systems, *Nature Communications 4, 1783*

[28] Kivelson, D., Kivelson, S. A., Zhao, X., Nussinov, Z. and Tarjus, G. (1995). A thermodynamic theory of supercooled liquids *Physica A, 219, 27-38*

[29] Tarjus, G., Kivelson, S. A., Nussinov, Z. and Viot, P. (2005) The frustration-based approach of supercooled liquids and the glass transition: a review and critical assessment, *Journal of Physics: Condensed Matter 17, R1143-R1182*

[30] Nussinov Z., (2004) Avoided phase transitions and glassy dynamics in geometrically frustrated systems and non-Abelian theories, *Physical Review B 69, 014208*

[31] Mauro, J. C. Yue, Y, Ellison, A. J., Gupta, P. K., and Allan, D. C. (2009). Viscosity of glass-forming liquids, *Proceedings of the National Academy of Sciences of the United States of America 106, 19780-19784*

[32] Elmatad, Y. S., Chandler, D. and Garrahan, J. P. (2009). Corresponding States of Structural Glass Formers, *Journal of Physical Chemistry B 113, 5563-5567*

[33] Elmatad, Y. S., Jack, R. L., Chandler, D. and Garrahan, J. P. (2010). Finite-temperature critical point of a glass transition, *Proceedings of the National Academy of Sciences of the United States of America 107, 12793- 12798*

[34] Cohen, M. H. and Grest, G. S., (1979). *Liquid-glass transition, a free-volume approach, Physical Review B 20, 1077-1098*

[35] Blodgett, M., Egami, T., Nussinov, Z. and Kelton, K. F. (2015). Proposal for universality in the viscosity of metallic liquids, *Scientific Reports 5, 13837*

[36] Nussinov, Z. (2015). A one parameter fit for glassy dynamics as a quantum corollary of the liquid to solid transition, https://arxiv.org/pdf/1510.03875.pdf (unpublished)

[37] Weingartner, N. B., Pueblo, C., Nogueira, F. S., Kelton, K. F., and Nussinov, Z., (2015). A Quantum Theory of the Glass Transition Suggests Universality Amongst Glass Formers, https://arxiv.org/pdf/1512.04565.pdf (unpublished)

[38] Pyrak-Nolte, L. J. and Nolte, D. D. (2016). Approaching a universal scaling relationship between fracture stiffness and fluid flow, *Nature Communications 7, 10663*

[39] West, G. B. and Brown, J. H. (2005). The origin of allometric scaling laws in biology from genomes to ecosystems: towards a quantitative unifying theory of biological structure and organization, *Journal of Experimental Biology 208, 1575*

[40] Stanley, H. E. (1999) Scaling, universality, and renormalization: Three pillars of modern critical phenomena, *Reviews of Modern Physics 71, S358*

[41] Guggenheim, E. A. (1945). The Principle of Corresponding States, *Journal of Chemical Physics 13, 253*

[42] Nishimori, H. and Ortiz, G., (2015). Elements of Phase Transitions and Critical Phenomena, *Oxford Graduate Texts, Oxford University Press*

[43] Sillescu, H. (1999). Heterogeneity at the glass transition: a review *Journal of Non-Crystalline. Solids 43, 81-108.*

[44] Ediger, M. D. (2000). Spatially heterogeneous dynamics in supercooled liquids, *Annual Review of Physical Chemistry 51, 99-128*

[45] Richert, R. (2002). Heterogeneous dynamics in liquids: fluctuations in space and time, *Journal of Physics: Condensed Matter 14, R 703-R738*

[46] Kob, W. C. Donati, S. J. Plimpton, P. H. Poole, and S. C. Glotzer, (1997). Dynamical heterogeneities in a supercooled Lennard-Jones liquid, *Physical Review Letters 79, 2827-2830*

[47] Donati, C. J., Douglas, J. F., Kob, W. Plimpton, S. J., Poole, P. H. and Glotzer, S. C., (1998). Stringlike cooperative motion in a supercooled liquid, *Physical Review Letters 80, 2338-2341*

[48] Gebremichael, Y. , Schroder, T. B., Starr, F. W., and Glotzer, S. C. (2001). Spatially correlated dynamics in a simulated glass-forming polymer melt: Analysis of clustering phenomena, *Physical Review E 64, 051503*

[49] Sausset, F., Biroli, G. and Kurchan, J. (2010). Do Solids Flow? *Journal of Statistical Physics 140, 718-727*

[50] Okui, N. (1990). Relationships between melting temperature, maximum crystallization temperature and glass transition temperature, *Polymer 31, 92-94*

[51] Sakka, S. and Mackenzie, J. D. (1971). Relation between apparent glass transition temperature and liquids temperature for inorganic glasses, *Journal of Non-Crystalline Solids 6, 145-162*

[52] Uhlmann, D. R., (1972). A kinetic treatment of glass formation, *Journal of Non-Crystalline Solids 7, 337-348*

[53] Angell, C. A. (2008). Glass-formers and viscous liquid slowdown since David Turnbull: Enduring puzzles and new twists, *MRS Bulletin 33, 544-555*

[54] Tournier, R. F. (2016). Lindemann?s Rule Applied to the Melting of Crystals and Ultra-Stable Glasses, *Chemical Physics Letters 651, 198-202*

[55] Kauzmann, W. (1948). The Nature of the Glassy State and the Behavior of Liquids at Low Temperatures, *Chemical Reviews 43, 219-256*

[56] Wang, L. M., Angell, C. A., and Richert, R. (2006). Fragility and thermodynamics in nonpolymeric glass-forming liquids, *Journal of Chemical Physics 125 (7), 74505-74505*

[57] Kanno, H. (1981). A simple derivation of the empirical rule $T_G/T_M = 2/3$, *Journal of Non-Crystalline Solids 44, 409-413*

[58] Na, J. H., Demetriou, M. D., Floyd, M. Hoff, A. Garrett, G. R., and Johnson, W. L. (2014). Compositional landscape for glass formation in metal alloys, *Proceedings of the National Academy of Sciences of the United States of America 111, 9031-9036*

[59] Turnbull, D. (1969). Under What Conditions can a Glass be Formed? *Contemporary Physics 10, 473-488*

[60] Mishima, O. and Stanley, H. E. (1989). Decompression-induced melting of ice IV and the liquid-liquid transition in water, *Nature 392, 164-168*

[61] Johari, G. P., Hallbrucker, A., and Mayer, E. (1987). The glass-liquid transition of hyperquenched water, *Nature 330, 552-553*

[62] Ito, K., Moynihan, C. T., and Angell, C. A. (1999). Thermodynamic determination of fragility in liquids and a fragile-to-strong liquid transition in water, *Nature 398, 492-495*

[63] Li Y. Li J., and Wang F. (2013). Liquid-liquid transition in supercooled water suggested by microsecond simulations, *Proceedings of the National Academy of Sciences of the United States of America 110, 12209-12212*

[64] Palmer, J. C., Martelli F., Liu Y., Car R., Panagiotopoulos A. Z., and Debenedetti, P. G., (2014). Metastable liquid-liquid transition in a molecular model of water, *Nature 510, 385-388*

[65] Tyagi, M. and Murthy, S. S. (2006). Dynamics of water in supercooled aqueous solutions of glucose and poly(ethylene glycol)s as studied by dielectric spectroscopy, *Carbohydrate Research 341, 650-662*

[66] Murata, K-I. and Tanaka, H. (2013). General nature of liquid-liquid transition in aqueous organic solutions, *Nature Communications 4, 2844*

[67] Sastry, S. and Angell, C. A. (2003). Liquid-liquid phase transition in supercooled silicon, *Nature Materials 2, 739 - 743*

[68] Mallamace, F. , Branca, C., Corsaro, C., Leone, N., Spooren, J., Chen, S. and Stanley, H. E. (2010). Transport properties of glass-forming liquids suggest that dynamic crossover temperature is as important as the glass transition temperature, *Proceedings of the National Academy of Sciences of the United States of America 107, 22457-22462*

# Chapter 3

# The Quantum Distribution Theory, Critical Assessment, and Extensions

## 3.1 Chapter Overview

In Chapter 2 we introduced the ideas behind the equilibrium melting-based distribution theory and cast them in a classical, statistical mechanical framework in order to derive an expression for the viscosity of supercooled liquids beneath the liquidus temperature. We subsequently demonstrated that this viscosity function accurately described the viscosity of some 45 liquids, while also seemingly uncovering an inherent universality in the dynamics of supercooled liquids. While the classical framework has been demonstrated to be quite successful, it does suffer from two drawbacks: it is unable to appropriately derive an expression for the relaxation time (as opposed to viscosity) from first principles, and it has no natural method of considering corrections associated with the impact of the first order phase transition which takes place at the melting/liquidus temperature. In light of these considerations, in this chapter we will again consider how equilibrium-based distributions describe supercooled liquids, but this time we will work within a quantum mechanical framework, deeming this version of the model the Distributed Eigenstate Hypothesis (DEH).

We again recognize that supercooling perturbs the system, but instead of violating Liouville's theorem in a way which leads to distribution of effective temperatures in phase space, the quantized perturbation leads to a mixing of the energy eigenstates associated with equilibrium liquids and crystals. This leads to the appearance of an *actual distribution* of energies for the supercooled liquid, which has a complete physical interpretation in quantum mechanics. We will observe that following through on these calculations leads to the **same** function for the viscosity as a function of temperature, a major success and suggestion of validity of the distribution approach. Additionally, time-dependent perturbation considerations can be used to find an expression for the relaxation time of supercooled liquids from first principles, and we again find that the calculations predict the **exact same functional form** for the relaxation time as for the viscosity in the classical and quantum frameworks. We apply the relaxation time function to experimental data for 16 liquids, and also test an additional six liquids with the viscosity form, observing strong performance for most liquids. Emboldened by these results, we conduct a rigorous statistical analysis to asses the performance of the DEH, and then make statistical comparisons to the five most widely employed viscosity models. Once we have objectively assessed the strength of the model, we undergo an intensive analysis of the single parameter, and its links to various physical observables. We then work to extend the framework beyond simply describing the viscosity/relaxation time beneath the liquidus, by deriving a high temperature form, explaining dynamic heterogeneity, applying it to jamming, and investigating the thermodynamics of the model. Ultimately, we aim to show that the distributional approach is robust, and is a complete theory of supercooled liquids.

At the time of the writing of this chapter, it was based, with little change, on a publication under revision for resubmission to the Journal of Non-Crystalline Solids.

## 3.2 Introduction.

The glass transition remains one of the most intensely studied and debated phenomena in physics, chemistry, and materials science (1; 2; 3; 4; 5; 6). Uncovering the underlying mechanism of glassy behavior would represent not only a fundamental advance in modern physics, but also would facilitate the ability to better exploit the glass-formation process. This would inevitably lead to the more efficient processing of existing glasses, as well as the production of new types of glass with novel applications. By comparison to their crystalline counterparts, glasses enjoy substantial advantages, e.g., (7; 8; 9). These have led to numerous applications in fields as diverse as pharmaceuticals, semiconductors, biomaterials, optical recording, and many others (9; 10; 11; 12).

A material in its liquid phase is distinguished from a solid by an irregular, non-ordered molecular arrangement, and an associated ability to make large-scale molecular rearrangements in response to fluctuations and perturbations. These rearrangements, known as flow, allow a liquid to relax imposed stresses and deform inelastically. This fundamental property of liquids is quantified by the viscosity ($\eta$), a dynamical measure of a liquid's resistance to flow. The viscosity of a liquid measures the "stickiness" of the local molecular interactions, and as such, is a temperature ($T$) dependent variable.

Liquids in thermal equilibrium at temperatures above their melting point, $T_{melt}$ (or, more precisely, the "liquidus temperature" $T_l$), have temperature-dependent viscosities which are well described by $\eta_{equilibrium} = \eta_0 e^{\frac{G(T)}{k_B T}}$. Here, $\eta_0$, the extrapolated infinite temperature viscosity, and $G(T)$, a Gibbs free energy barrier, are material dependent parameters. The interpretation of the Arrhenius form is that there exists a barrier to molecular rearrangement, which must be overcome by a thermal fluctuation of the appropriate size in order for the rearrangement to proceed. The Gibbs free energy barrier $G(T)$ is, in general, very weakly dependent on temperature above the liquidus, and is typically taken to be a constant, $E$,

such that the viscosity is quite accurately described by a standard Arrhenius form

$$\eta_{equilibrium} = \eta_0 e^{\frac{E}{k_B T}}. \tag{3.1}$$

As the temperature of the liquid is lowered (cooled) quasistatically, such that equilibrium is approximately maintained, the viscosity maintains the form of Eq.(3.1), exponentially increasing with decreasing temperature. When the temperature reaches $T_{melt}$, the liquid reaches the limit of stability, its free energy crossing that of a solid phase (13). At this temperature, the liquid typically gives off a characteristic latent heat. In pure systems, the liquid transforms into a crystal, acquiring long-range structural order and losing its ability to flow. By contrast, when properly computed in the idealized limit of vanishing shear, the viscosity of a solid is infinite (14). As alluded to above, in what follows we will take 'melting' to correspond to the liquidus, the temperature at which nucleation first becomes thermodynamically favorable, and the character of the system begins to change. In actuality, we refer to the *temperature at which the dominant crystalline phase* begins to nucleate, ignoring certain pathological systems where small molar additions of a minor phase can greatly alter the liquidus with little to no change in the viscosity of the liquid.

Because nucleation and growth of the crystalline phase are kinetically controlled, there is an intrinsic time dependence to crystallization. Therefore, a liquid that is cooled sufficiently quickly through $T_l$, may bypass crystallization and be 'supercooled' to a state of metastable equilibrium at temperatures beneath the melting point. As the temperature of the supercooled liquid drops further, its viscosity begins to increase dramatically, by as much as 16 decades over a temperature interval as small as a few hundred Kelvin (this is very clearly demonstrated by the behavior o-terphenyl (15) and many other "fragile" (16; 17) glass formers). Eventually, a "glass transition" temperature ($T_g$) is reached where the viscosity is so large that molecular rearrangements cease on physically meaningful timescales, and

the supercooled liquid is termed a glass. Despite the appearance of various thermodynamic signatures (18) the glass transition appears to be kinetic in nature; the glass transition marks the point at which the timescale of atomic rearrangement (relaxation time) exceeds the relevant experimental timescale and the liquid falls out of equilibrium. In crystalline solids, the dynamical arrest (infinite viscosity) is due to long range structural order that appears with a first order phase transition at melting. Glasses, however, lack the long-range order customarily associated with the stiffness/rigidity of solids, instead possessing amorphous particle arrangement. Understanding the glass transition, then, requires first understanding the temperature dependence of the viscosity of supercooled liquids. It is important to stress that notwithstanding their amorphous character, the formation of structural glasses does not rely on externally imposed disorder. All conventional liquids (and possibly even superfluid Helium and other quantum fluids (19; 20; 21; 22; 23)) may be quenched into amorphous glassy structures by rapid supercooling.

If the rapid rise of the viscosity below the liquidus temperature $T_l$ were simply described by the same Arrhenius form as in Eq. (3.1), or even an Arrhenius form with different constant energy barrier, $E'$, then the glass transition would not be so mysterious. Decreasing the temperature would simply remove more and more kinetic energy from the molecules leading to an ever increasing scarcity in barrier-crossing events that enable molecular rearrangements. The reduction in molecular motion, then, gives the appearance of rigidity on realizable timescales, but is an entirely kinetic phenomenon. This simple behavior is not the case, however, as all glass formers depart from the well-understood form of Eq. (3.1).

Complicating matters further is the fact that different glass forming liquids display a wide spectrum of 'super-Arrhenius' behaviors. These are reflected by an increase of the viscosity (as $T$ is lowered) that may be far more dramatic than that predicted by Eq. (3.1). Some supercooled liquids are approximately Arrhenius, whereas others show drastic departure from the Arrhenius form. There exists a broad array of liquids having behaviors

in between these extremes. Long ago, Angell defined a parameter, called "fragility" (16; 17), that quantifies the degree of departure from Arrhenius behavior, as well as a classification scheme for the spectrum of behaviors. Arrhenius liquids are called strong (i.e., possess a low fragility value) whereas liquids with large departures are termed fragile (high fragility value). It is widely accepted that fragility is a significant parameter characterizing the glass transition, and it is believed that fragility may correlate with both structural and dynamic phenomenon (16; 17; 24; 25; 26; 27). Therefore, any reasonable theory of glass formation and supercooling, must, at the very least, contain a connection with fragility.

The much celebrated Vogel-Fulcher-Tamman (VFT) form (28; 29; 30),

$$\eta = \eta_0 e^{\frac{DT_0}{T-T_0}}, \tag{3.2}$$

has been shown to provide a more reasonable fit than the Arrhenius form to the viscosity of most supercooled liquids over a moderate range of temperatures, and has been in use since the 1920s (28; 29; 30). As seen in Eq. (3.2), the VFT form contains three material-dependent fitting parameters, the prefactor $\eta_0$, the constant $D$, and the temperature $T_0$. These parameters are generally not predictable from first principles. Additionally, despite its apparent successes, the VFT form suffers from two fundamental drawbacks. First, it is a purely empirical function, it is not derived from first principles, or any specific theories of glass formation (although it can be reproduced by certain theories, see (31; 16; 32; 33; 34; 35; 36)). Secondly, it predicts a dynamic singularity at the temperature $T_0$ which exists beneath the glass transition. This temperature has been shown to be in rough agreement with the Kauzmann temperature associated with hypothesized vanishing of configuration entropy (37), leading some to postulate that there exists a true equilibrium thermodynamic phase transition in the limit of infinitely slow cooling to $T_0$. While the notion that the slow dynamics near $T_g$ is associated with the "ghost" of an underlying phase transition is

compelling, any experimental evidence suggesting an "ideal glass transition" remains hidden (38). There are, in fact, several experimental indications that the VFT and similar forms are incorrect, e.g., (39).

As the above discussion hints, rationalizing the mysterious super-Arrhenius increase of the shear viscosity of supercooled liquids has long been an open fundamental problem (40). Towards that end, numerous theories have been proposed that aim to reproduce the behavior of the viscosity upon cooling, and to provide a physical framework that explains the rich phenomenology associated with the glass transition (31; 16; 32; 33; 34; 35; 37; 18). Many such theories have been proposed and tested, all to varying degrees of success (31; 16; 32; 33; 34; 35; 36; 18; 41; 42; 43; 44; 45; 46; 47; 48). In many cases, the functional forms derived for the viscosity are not universal; models that accurately describe metallic liquids may not work well for silicate liquids, for example (49). A complete theory of the supercooled liquids, then, should answer the two most fundamental questions in the field, namely, (i) what is the cause of the super-Arrhenius viscosity and what functional form is most accurate, and (ii) is this form universal to all supercooled liquids regardless of fragility, bonding type, etc.

Recently, a new framework for understanding the behavior of supercooled liquids was introduced based on the framework of equilibrium statistical mechanics (50; 51). As we will briefly review next in Section 3.3, this approach relies on the characteristics of the quantum eigenstates (50) or, correspondingly, on the features of the classical microstates (51) of fixed energy to describe the phenomenology of supercooled liquids and glass formation. The resulting prediction for the viscosity was briefly demonstrated to be quite accurate for liquids of all types and fragilities at all temperatures below their respective liquidus temperatures (51); we succinctly reported on the experimental collapse (that is implied by this prediction) of all available viscosity data onto a universal curve. In the current work, we will critically examine the statistical performance of the predicted form for the viscosity in this approach and extend it to temperatures above the liquidus. Additionally, we will perform a detailed

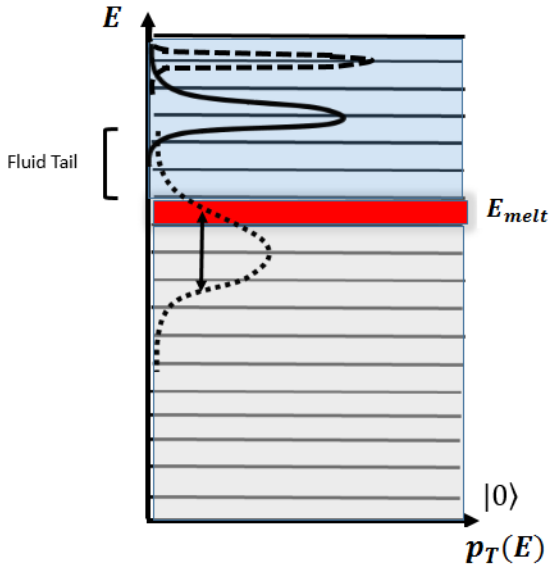


Figure 3.1: (Color Online.) Simple pictorial representation of the basic DEH principle. This simple picture represents the spectral 'hierarchy' of energy eigenvalues, $E$, and their associated eigenstates (horizontal lines), with the various probability densities, $p_T(E)$, overlaid. Distributions shown for (i.) the high temperature equilibrium liquid (narrow dashed curve), (ii.) a high temperature non-equilibrium liquid (solid curve), and (iii.) a supercooled liquid state (dotted curve). For the dotted curve, note that the tail in the fluid-like states is what determines the hydrodynamic relaxation rate (viscosity).

analysis of the physical meaning of the single parameter, and demonstrate that it correlates strongly with various thermodynamic and dynamic quantities. Using these relations, we will demonstrate that it is possible to predict the viscosity at low temperatures, based solely on high temperature data. We will conclude by suggesting extensions of this framework to non-thermal transitions, such as jamming, and show that the framework can quite accurately capture athermal "glassy" dynamics.

## 3.3 The Quantum Non-equilibrium Distribution Hypothesis

The crux of our approach is that *the very same quantum eigenstates (50) or classical microstates (51)* that appear in equilibrium averages suffice to describe supercooled liquids and glasses. That is, to describe glasses, perhaps one need not think about novel states or exotic transitions of one special sort or another but rather employ standard statistical mechanics. The initial impetus to consider such a (seemingly all too simple) possibility was triggered by a general argument. Specifically, in the quantum arena, the eigenstates of the disorder free Hamiltonian (describing the equilibrium solid and liquid) form a complete basis. Thus, any state or probability density (whether that of the equilibrium system or of the non equilibrated supercooled liquid) describing the system may be expanded in terms of this complete set of eigenstates (50). Similar considerations may be enacted, *mutatis muntandis*, for classical phase space states (51). Thus, in our minimal framework, *the only difference* between (i) equilibrium liquids and solids and (ii) the non-equilibrated supercooled liquids and glasses is that of *the probability distributions* that sample this complete set of states are different in both cases; the central idea is that the probability distributions (and long time averages) associated with supercooled liquids and glasses may be rather trivially expressed in terms of those of the equilibrated system. This hypothesis of a trivially extended probability distribution in the energy density (that includes the equilibrated system as a special instance of this distribution that is of vanishing width) underlies our work. In what follows, we summarize several key aspects of the original (quantum) approach of (50) which we dub the "Distributed Eigenstate Hypothesis" (DEH). A direct classical dual of this description (that of the "Energy Shell Distribution Hypothesis" (ESDH)) was introduced in (51). Thus, notwithstanding the viable importance of quantum effects (52; 53) in non cryogenic fluids, we wish to underscore that the results that we will empirically test in great detail in the

current work *do not*, at all, hinge on quantum mechanics. Planck's constant does not appear in our results. The upshot of the below review of (50) is the prediction of Eq. (3.9). This prediction for the viscosity and the universal viscosity collapse that it implies will be assessed and extended in the next Sections.

### 3.3.1 Averages within the DEH theory

The evolution of a general $N$-body system is governed by its Hamiltonian, $\mathcal{H}$. For 'ordinary' glass forming liquids (i.e., systems not requiring ad hoc, 'quenched disorder' (18)) behaving non-relativistically, the correct many body Hamiltonian consists of the kinetic energies of all $N$ particles, as well as the complete set of electrostatic interactions between all nuclei and electrons in a volume $V$. Quite generally, then, one can write down the ***exact*** Hamiltonian of such a general $N$ body system (50). As always, the dynamic evolution of the system, then, is entirely determined by solving the Schrödinger equation corresponding to this Hamiltonian,

$$\mathcal{H}|\phi_n\rangle = E_n|\phi_n\rangle, \tag{3.3}$$

and evolving according to the appropriate time evolution operator. For macroscopic systems, $\mathcal{H}$ contains an astronomical number of interaction and kinetic terms. While methods for obtaining approximate solutions exist, in general, the exact eigenstates and associated energies cannot be determined. In spite of this apparent complication, the mere existence of the eigenstates of Eq. (3.3) (guaranteed by the postulates of quantum theory) allows us to make powerful statements about the dynamical and thermodynamic properties of the system. In order to make these statements, we need only rely on simple, well documented, physical characteristics of the macroscopic thermodynamic properties of equilibrium materials. We

will employ said observations at various temperatures and utilize basic statistical mechanical principles.

In the following calculations, we will assume that our many body system is approximately isolated, and therefore employ the microcanonical (m.c.) ensemble. Computing measurable thermodynamic values for equilibrium systems in the microcanonical ensemble involves taking phase space averages over states within a narrow range of energies (an effective "energy shell") that are consistent with the external constraints. When considering quantum mechanical systems, the energy levels are quantized, and the energy shell encompasses some subset of the allowed eigenstates of the system. Within the microcanonical ensemble, the equilibrium average of any observable $\mathcal{O}$ is given by

$$\langle \mathcal{O} \rangle_{m.c.} = \frac{1}{\mathcal{N}[E - \Delta E, E]} \sum_{E - \Delta E \leq E_n \leq E} \langle \phi_n | \mathcal{O} | \phi_n \rangle, \tag{3.4}$$

where $\mathcal{N}[E - \Delta E, E]$ is the number of eigenstates having energies $E - \Delta E \leq E_n \leq E$ with $\Delta$ an arbitrary (system size independent) width. In the limit in which the width $\Delta E$ of the energy shell is made vanishingly small, only a single eigenstate (or a set of degenerate eigenstates) is effectively encompassed. If only a single, or small range of eigenstates are being averaged over, then the observed thermodynamic values must be properties of the eigenstate(s). Essentially, all observed/measured thermodynamic properties of the macroscopic, equilibrium system will then correspond to such eigenstates. This implies, as we next elaborate on, that we can use experimental observation (that provides the lefthand side of Eq. (3.4)) to classify the properties of allowed eigenstates at various energies (as implied by the average on the righthand side of Eq. (3.4)). It has been empirically known for millennia, that at sufficiently high energies, the equilibrium state of most materials is a liquid (with all the properties therein), whereas the low energy equilibrium state is that of a solid (with associated properties). It can, therefore, be reasonably hypothesized that, on

average (in the sense implied by the righthand side of Eq. (3.4)), the many-body eigenstates will, respectively, exhibit 'liquid-like' or 'solid-like' characteristics, for states with respectively high or low energy densities. Further, as it is observed that liquids and crystalline solids are separated by a first order melting/freezing phase transition, the liquid-like states are separated from the solid-like states by a 'band' of eigenstates corresponding to this melting phase transition range. The width of this melting band corresponds to the latent heat of the associated phase transition. We refer to the states in the melting band as the 'Phase Transition Energy Interval' ($\mathcal{PTEI}$) (50). These states display properties associated with both liquid and solid states. The eigenstates associated with liquids and solids will necessarily possess the observed equilibrium structures of the respective states, in addition to the thermodynamic and kinetic properties. As such, the liquid-like eigenstates will be delocalized in the sense that a system existing in one of these eigenstates can ergodically explore phase space, and will be capable of hydrodynamic flow. Conversely, the solid-like eigenstates will be localized, breaking ergodicity, and possessing the rigidity of the crystalline solid and lacking the ability to flow. Physically, this means that each eigenstate will possess a characteristic structural relaxation time and associated visco-elastic properties, with the solid-like states being assumed ideal (infinite relaxation time). Additionally, the symmetry breaking solid-like states will necessarily have the long-range structural ordering of the equilibrium crystal built in, and the spectrum of 'excited states' lying between the ground state (absolute zero) and the melting band will correspond to various phonon modes.

As discussed above, an isolated equilibrium system explores states within an infinitesimally narrow band of energy densities, and these states possess the system properties. Therefore, we can approximate the equilibrium 'distribution' of energies as a delta function, $\delta(E' - E)$ peaked at the external energy. Starting at high energy, or temperature, (energy and temperature are simply related via the heat capacity) and **quasistatically** lowering the energy/temperature (cooling) will cause the system to transition to eigenstates

of progressively lower energy, with the distribution remaining effectively $\delta$-peaked at the appropriate lower energies. At the $\mathcal{PTEI}$, the system transitions through the mixed states, giving off latent heat, and eventually undergoes the usual first order transition. Consequently, the system then moves into a crystalline, solid-like eigenstate, possessing all of the thermo-mechanical properties of a crystalline solid. As confirmed by experiment, this only happens when equilibrium is maintained. If, instead, the system is rapidly quenched by strongly coupling to a heat bath of some kind, the system will be driven from equilibrium. The quench can be represented by a perturbing Hamiltonian, $\mathcal{H}'(t)$. The augmented Hamiltonian, $\mathcal{H}_{Full} = \mathcal{H} + \mathcal{H}'(t)$, will *not* commute with $\mathcal{H}$ as the system energy (since the expectation value of $\mathcal{H}$ is lowered); the supercooled system will be driven into a new state, $|\Psi_T\rangle$ (where $T$ corresponds to the temperature the system was quenched to). This new state will not be an equilibrium eigenstate of the original Hamiltonian, but because the eigenstates of the original Hamiltonian, are complete, the new state can be expanded in terms of them. Therefore, the post-quench supercooled state, $|\Psi_T\rangle$, can be generically expanded in the basis of equilibrium eigenstates of the original Hamiltonian, $\mathcal{H}$, taking the form

$$|\Psi_T\rangle = \sum_n c_n |\phi_n\rangle. \tag{3.5}$$

We see, then, that the effect of the perturbation (quench) is to *mix* the eigenstates of varying energy densities $E_n/V$, such that the system to no longer exists in a single equilibrium eigenstate. The mixed state encompasses a 'metastable' **distribution** (no longer a delta function) of multiple equilibrium eigenstates; this is a defining property of the Distributed Eigenstate Hypothesis (50). Realistically, there exists a density matrix associated with an open quantum system. To provide the simplest quintessential account of the theory, in what follows, we do not elaborate on the complete treatment involving the full density matrix, essentially focusing on typical states $|\Psi_T\rangle$ that are of high probability (i.e., we will consider those eigenstates of the density matrix for which the corresponding eigenvalues are high).

Consideration of the full density matrix will not impact the final results reviewed herein (50). In the simple single state account, the squared amplitudes $\{|c_n|^2\}$ represent the probability distribution of the eigenstates of Eq. (3.3). Assuming that the many-body eigenstates are vanishingly close together in their energy densities, we will take the continuum limit of this distribution, $|c_n|^2 \to p_T(E')$. A similar distribution $p_T(E')$ will appear when the full density matrix is considered. A cartoon of this continuum limit probability distribution, $p_T(E')$, for various temperatures is depicted in Figure (3.1). As discussed above, the equilibrium state of both the liquid and solid will correspond to a probability density which is "$\delta$-function peaked" (see the dashed curve in Figure (3.1)) and has its support only over a narrow shell of eigenstates that either share the same energy or are nearly degenerate. By comparison to the equilibrated system, the supercooled system exhibits a broadened probability density (see the solid and dotted curves in Figure 3.1) which encompasses many of the equilibrium eigenstates. Long time average (l.t.a.) values will now read (50),

$$\mathcal{O}_{l.t.a.} = \int dE' \; p_T(E')\mathcal{O}(E'). \tag{3.6}$$

In general, the probability density $p_T(E')$ will have a weight originating from both the higher energy delocalized liquid-like states, and the lower energy localized solid-like states. Our central thesis is that the 'mismatch' of characteristics from different types of states is what leads to the phenomenology of supercooled liquids. Generally, the probability density will shift downward as the temperature is lowered, and the width of the distribution will also vary with temperature. Only high energy "liquid-like" equilibrium eigenstates (i.e., states $|\phi_n\rangle$ having an energy density $E_n/V$ exceeding that of the melting energy) contribute *appreciably* to the long time average associated with fluid flow. Setting $\mathcal{O}$ in Eq. (3.6) to be the vertical velocity operator $v$ of a freely falling sphere in the supercooled liquid, recognizing that the terminal speed of free fall in an equilibrium solid is zero, and invoking the Stokes relation

between the terminal speed and the viscosity ($v_{l.t.a.} \propto 1/\eta$), we find that (50)

$$\eta(E) \simeq \frac{\eta^{eq}(E_{melt})}{\int_{E_{melt}}^{\infty} p_T(E')\ dE'} \quad | \quad T \leq T_l. \tag{3.7}$$

Here, $\eta^{eq}(E_{melt})$ is the value of the viscosity of the equilibrium liquid infinitesimally above its melting temperature Since a reduction of flow sets in at the energy density associated with the equilibrium melting/liquidus temperature, in Eq. (3.7), we took this point to define a lower energy cut-off. In reality, the liquidus does not mark a hard cut-off, as states in the $\mathcal{PTEI}$ may enable some level of long time mobility.

### 3.3.2 The scale-free Gaussian distribution and the viscosity function that it implies

In order to obtain an approximate form for the viscosity (and other observables) in the DEH model, we need to have an explicit form for the distribution function, $p_T(E)$. We do not know, *a priori* what this function is, but we do know characteristics it must possess: **(i)** The distribution must be normalized. **(ii)** The probability density must be such that the average of $\mathcal{H}$ is equal to the measured system energy $\langle E \rangle$. **(iii)** Since supercooled liquids are not in full thermodynamic equilibrium, the distribution cannot be a delta function in the energy density. Thus the distribution of the energy density must display a non-vanishing standard deviation in the thermodynamic limit. **(iv)** In the absence of any additional information, the unknown distribution must maximize the Shannon entropy, $H_I = \int dE'\ p_T(E') \log_2[p_T(E')]$, subject to constraints **(i)**- **(iii)**; the distribution maximizing the Shannon entropy subject to the constraint of a fixed standard deviation is, trivially, a Gaussian distribution. Thus,

putting all of the pieces together, in the absence of additional information, the distribution

$$p_T(E') = \frac{1}{\sqrt{2\pi\sigma_T^2}} e^{-\frac{(E'-\langle E\rangle)^2}{2\bar{\sigma}_T^2}} \tag{3.8}$$

uniquely satisfies all of the above requisite characteristics. As is well known, the distribution of the energy density in the equilibrated system is a Gaussian in which the standard deviation scales as $N^{-1/2}$ (and thus vanishing in the thermodynamic limit). Thus, Eq. (3.8) is a trivial extension of the distribution present in equilibrated systems. For completeness, we remark that other Gaussian distributions have, of course, been observed before in disparate contexts. For instance, in (64) and many other works the distributions associated with local low energy "inherent states" in supercooled liquids were analyzed through the prism of Gaussian distributions. To avoid confusion, we wish to stress that the probability density of Eq. (3.8) is that associated with the energy densities of all states (not that of inherent states); we underscore that we do not consider local metastable energy minima in an "energy landscape" and fluctuations about them.

Inserting Eq.(3.8) into Eq.(3.7) will yield the viscosity as a function of energy. In order to compare our theoretical notions to experimental data, we need to express the viscosity as a function of measured temperature (and not the energy density). Towards this end, we will define the average heat capacity in the range $[T, T_{melt}]$ given by $C(T) \equiv \frac{E_{melt}-\langle E\rangle}{T_{melt}-T}$ where $\langle E\rangle$ is the energy of the supercooled liquid at a temperature $T$. In reality, the ratio defining $C(T)$ does not change substantially as a function of temperature $T$; the function $C(T)$ does nevertheless vary with temperature yet its weak temperature will identically drop out in our final result of Eq. (3.9). We will assume that the dimensionless ratio $\bar{A} \equiv \left(\frac{\sigma_T(T_{melt}-T)}{T(E_{melt}-\langle E\rangle)}\right) \equiv \left(\frac{\sigma_T}{CT}\right) \equiv \left(\frac{\bar{\sigma}_T}{T}\right)$ does not vary strongly in the interval of experimentally measured temperatures. An assumption of constant values of the dimensionless ratio $\bar{A}$ and $C \sim \langle E\rangle/T$ is tantamount to asserting that the Gaussian of Eq. (3.8) is scale free. By this

assumption of being "scale free", we mean only energy scale (whether that for the average energy $\langle E \rangle$ or the width $\bar{\sigma}_T$) is set by the temperature $T$. As we emphasized above, any temperature dependence of the average heat capacity defined by the ratio defining $C(T)$ will drop out in the final expression that we provide next. With all of the above, the viscosity of the supercooled liquid is (50)

$$\eta(T) = \frac{\eta_{s.c.}(T_{melt})}{\mathrm{erfc}\left(\frac{E_{melt}-\langle E \rangle}{\bar{\sigma}_T \sqrt{2}}\right)} = \frac{\eta(T_l)}{\mathrm{erfc}\left(\frac{T_l - T}{\sqrt{2}\bar{\bar{\sigma}}_T}\right)} = \frac{\eta(T_l)}{\mathrm{erfc}\left(\frac{T_l - T}{\sqrt{2}\overline{A}T}\right)}. \tag{3.9}$$

The first equality in Eq. (3.9) is obtained by substituting Eq. (3.8) into Eq. (3.7). The last two equalities follow from our definitions of $C$ and $\overline{A}$. If the ratio of $\overline{A}$ does not significantly change with $T$ in the measured temperature range then we may set it to be a constant (as we will in this work). Alternatively, one may arrive at Eq. (3.9) by assuming that the effective temperatures $T_n$ of the equilibrated system (i.e., eigenstates having an energy $E_n = U(T_n)$ with $U$ the internal energy of the equilibrated system governed by $\mathcal{H}$) are distributed in a Gaussian fashion about the imposed external constraint that the supercooled liquid has a temperature $T$. In the above, we largely reviewed the quantum DEH model of (50) that first predicted Eq. (3.9). As we noted earlier, a derivation of the same result in the framework classical statistical physics appears in (51).

The prediction of Eq. (3.9) for the viscosity at all temperatures below the liquidus temperature, $T < T_l$, requires knowledge of the liquidus temperature and the viscosity $\eta(T_l)$ of the supercooled liquid at this temperature. Both of these quantities are given by experiment, and are not fitting parameters of the theory (these numerical values of these measurable quantities are presented in Table I). An objective of the current paper is to critically test the performance of this function that goes beyond the initial analysis conducted in (51).

### 3.3.3 The $\mathcal{PTEI}$ Corrections

In converting Eq.(3.9) from a function of energy to a function of temperature, and indeed when making any such conversions, we have introduced an inherent error into resulting functions/calculations. This error arises from a simple truth, there are a range of energy levels/states (which we have deemed the $\mathcal{PTEI}$) associated with the single temperature $T_l$ and/or range $T_s$-$T_l$, where $T_s$ is the solidus. In the conversion from energy to temperature, and resultant integrations over temperature, we fail to properly consider these states. For some calculations, such as many of the liquid viscosities, the impact of the $\mathcal{PTEI}$ is minimal, but in other cases it can have a profound effect. Unfortunately, it is difficult to probe the energy dependence of various physical observables, and therefore, in many cases the best we can do is to derive corrections for the $\mathcal{PTEI}$ region. Throughout the rest of this paper, we will highlight areas where we suspect the $\mathcal{PTEI}$ region is the cause of discrepancies, and will derive the alluded to corrections where needed.

## 3.4 Tests of the DEH Model.

With Eq. (3.9) in hand, we next compare its predictions to measured viscosity data of various fluids (Section 3.4.1), provide a thorough statistical study of the quality of these viscosity fits that are obtained by this predicted form (Section **??**), compare our predicted to other prevalent fitting functions that have been used throughout the years (Section 3.4.4),

### 3.4.1 Fitting of Viscosity Function

To test the validity of the DEH, we examined how well the functional form of Eq. (3.9) fit actual experimental viscosity data. We applied the DEH form to the viscosities

Table 3.1: Values of Relevant Parameters for all liquids studied

| *Composition* | $\bar{A}$ | $T_l$ *[K]* | $\eta(T_l)$ *[Pa*s]* |
|---|---|---|---|
| BS2* | 0.111107 | 1699 | 5.570596 |
| Diopside | 0.094984 | 1664 | 1.5068 |
| LS2* | 0.12048 | 1307 | 22.198 |
| OTP | 0.049275 | 329.35 | 0.02954 |
| Salol | 0.061654 | 315 | 0.008884 |
| Anorthite | 0.092875 | 1823 | 39.81072 |
| $Zr_{57}Ni_{43}$ | 0.165584 | 1450 | 0.01564 |
| $Pd_{40}Ni_{40}P_{20}$ | 0.10939 | 1030 | 0.030197 |
| $Zr_{74}Rh_{26}$ | 0.132831 | 1350 | 0.03643 |
| $Pd_{77.5}Cu_6Si_{16.5}$* | 0.088303 | 1058 | 0.0446 |
| Albite | 0.073075 | 1393 | 24154952.8 |
| $Cu_{64}Zr_{36}$ | 0.101088 | 1230 | 0.021 |
| $Ni_{34}Zr_{66}$ | 0.148039 | 1283 | 0.0269 |
| $Zr_{50}Cu_{48}Al_2$ | 0.118278 | 1220 | 0.0233 |
| $Ni_{62}Nb_{38}$ | 0.07742 | 1483 | 0.042 |
| Vit106a | 0.094557 | 1125 | 0.131 |
| $Cu_{55}Zr_{45}$ | 0.102192 | 1193 | 0.0266 |
| $H_2O$ | 0.094094 | 273.15 | 0.001794 |
| Glucose | 0.056183 | 419 | 0.53 |
| Glycerol | 0.076957 | 290.9 | 1.9953 |
| $Ti_{40}Zr_{10}Cu_{30}Pd_{20}$ | 0.13109 | 1279.226 | 0.01652 |
| $Zr_{70}Pd_{30}$ | 0.149006 | 1350.789 | 0.02288 |
| $Zr_{80}Pt_{20}$ | 0.119757 | 1363.789 | 0.04805 |
| NS2* | 0.095195 | 1147 | 992.274716 |
| $Cu_{60}Zr_{20}Ti_{20}$ | 0.073101 | 1125.409 | 0.04516 |
| $Cu_{69}Zr_{31}$ | 0.111355 | 1313 | 0.01155 |
| $Cu_{46}Zr_{54}$ | 0.110984 | 1198 | 0.02044535 |
| $Ni_{24}Zr_{76}$ | 0.173226 | 1233 | 0.02625234 |
| $Cu_{50}Zr_{42.5}Ti_{7.5}$ | 0.104828 | 1152 | 0.0268 |
| D Fructose | 0.035443 | 418 | 7.31553376 |
| TNB1 | 0.053509 | 472 | 0.03999447 |
| Selenium | 0.092503 | 494 | 2.9512 |
| CN60.40* | 0.105419 | 1170 | 186.2087 |
| CN60.20* | 0.113965 | 1450 | 12.5887052 |
| $Pd_{82}Si_{18}$ | 0.097314 | 1071 | 0.03615283 |
| $Cu_{50}Zr_{45}Al_5$ | 0.083885 | 1173 | 0.03797 |
| $Ti_{40}Zr_{10}Cu_{36}Pd_{14}$ | 0.097406 | 1185 | 0.0256 |
| $Cu_{50}Zr_{50}$ | 0.117874 | 1226 | 0.02162 |
| Isopropylbenzene | 0.052216 | 177 | 0.086 |
| ButylBenzene | 0.060151 | 185 | 0.0992 |
| $Cu_{58}Zr_{42}$ | 0.093316 | 1199 | 0.02526 |
| Vit 1 | 0.07862 | 937 | 36.59823 |
| Trehalose | 0.050244 | 473 | 2.71828 |
| Sec-Butylbenzene | 0.056631 | 190.3 | 0.071 |
| $SiO_2$ | 0.06431 | 1873 | $1.196 \times 10^8$ |

Table 3.2: Values of Relevant Parameters for all liquids studied

| *Composition* | $\bar{A}$ | $T_l$ *[K]* | $\eta(T_l)$ *[Pa*s]* |
|---|---|---|---|
| Xylitol | 0.072217 | 367 | -22.3 |
| Sorbitol | 0.057043 | 368 | -21.7 |
| D20* | 0.071461 | 1761 | 1.5427 |
| CKN* | 0.05432 | 438 | -23 |
| Dioctyl Phlatate | 0.036182 | 223 | -9.9 |
| Benzophenone | 0.079421 | 321 | -23.1 |
| Bisphenol A | 0.02092 | 285 | -11.9 |
| 2D LJ | 0.316259 | 0.7468 | 3.35 |
| Propanol | 0.065266 | 147 | 2.9 |
| phenylphthaleindimethylether | 0.04169 | 373 | -17.758 |
| Borate | 0.056409 | 723 | 10.325 |
| Sodium Borate | 0.0570181 | 1039 | 2.67 |
| LB2* | 0.0781628 | 1190 | -1.5636 |
| Indomethacin | 0.048729 | 424 | -21.1 |
| Toluene | 0.07999 | 178 | -22.3 |
| Ethylene Glycol | 0.107532 | 260 | -19.7 |
| Ethanol | 0.098953 | 160.71 | -21 |
| Sucrose Benzonate | 0.020335 | 373 | -8.8 |
| Butyronitrile | 0.041008 | 116 | -10.4 |
| Propylene Glycol | 0.048486 | 215 | -12.6 |
| Propylene Carbonate | 0.057808 | 218 | -20.9 |

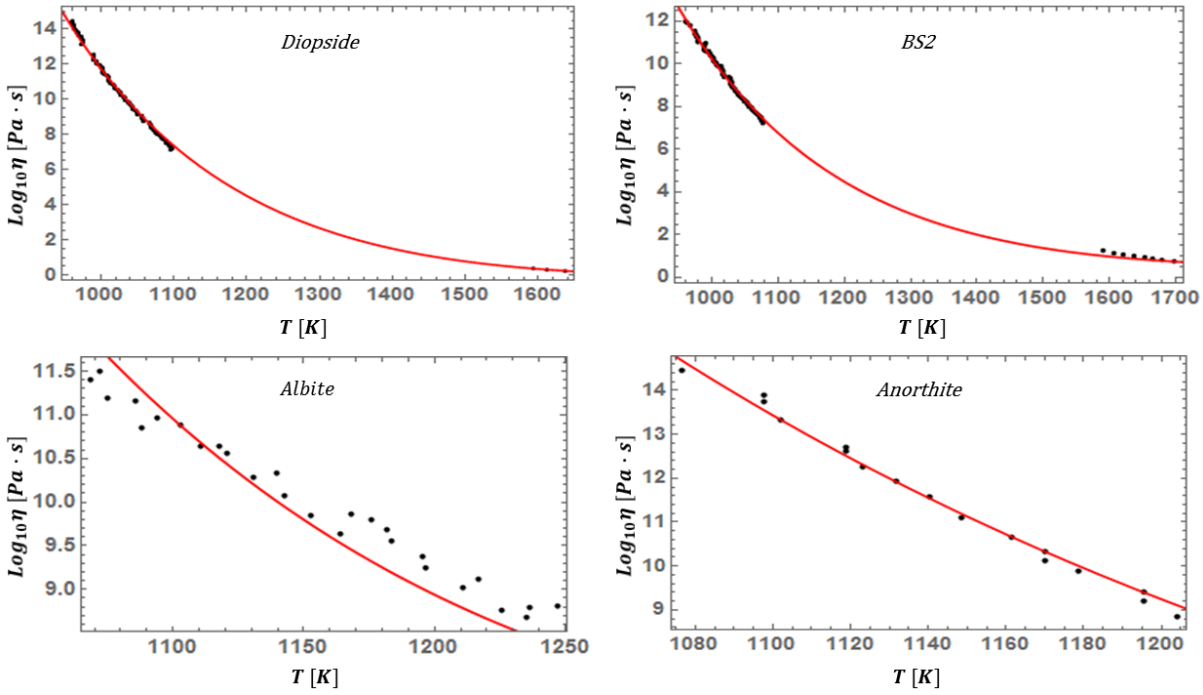


Figure 3.2: (Color Online.) Fits to the viscosity of four sillicate glassformers with the DEH form of Eq. (3.9).

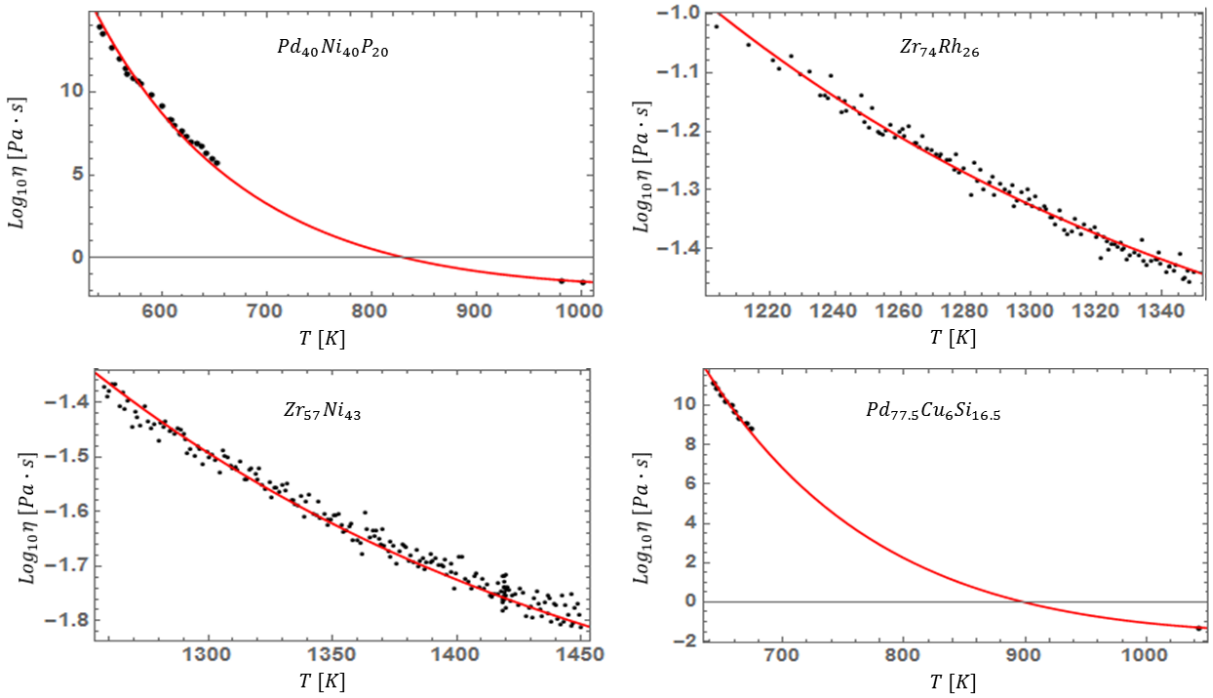


Figure 3.3: (Color Online.) Fits of the DEH form for the viscosity, Eq. (3.9), to four metallic glassforming liquids.

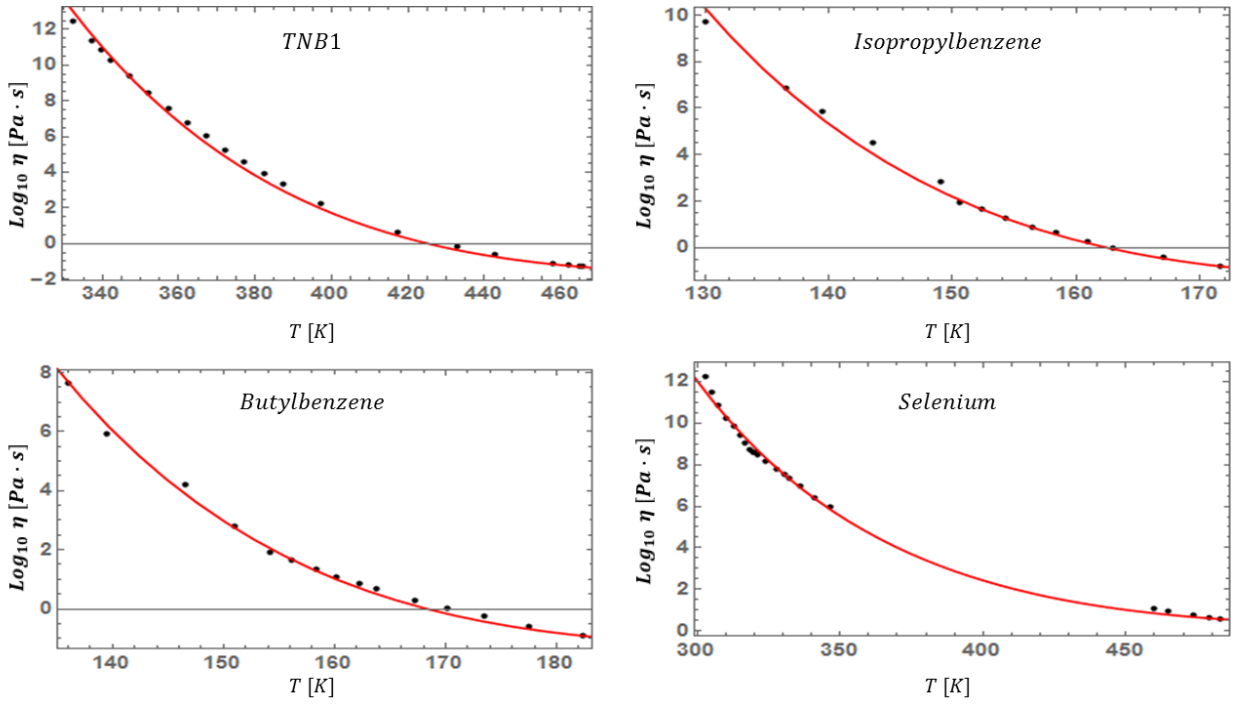


Figure 3.4: (Color Online.) Fits of the DEH form for the viscosity, Eq. (3.9), to various benzene and chalcogenide liquids.

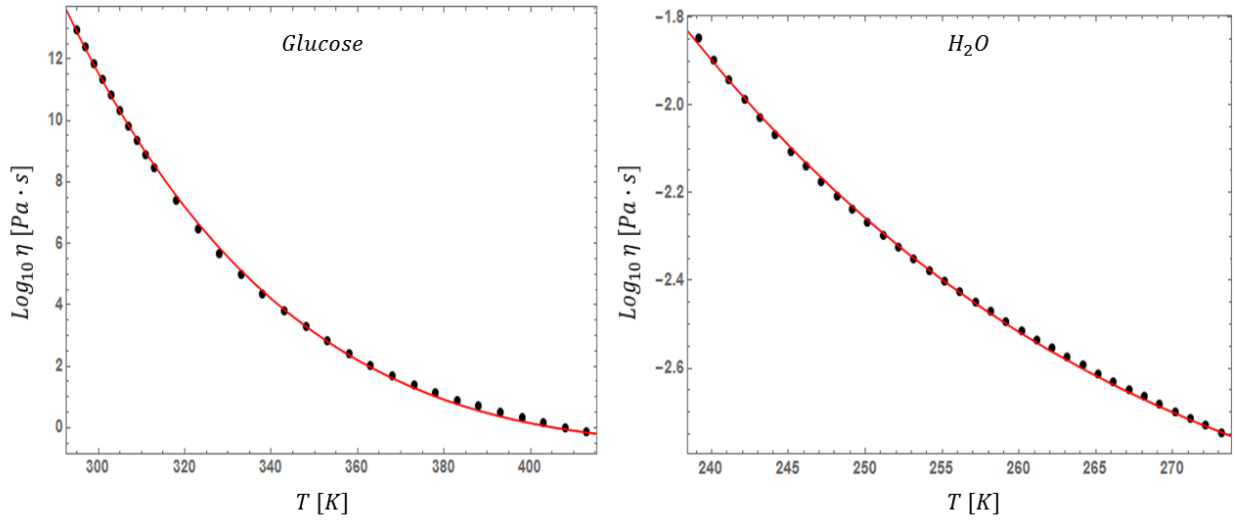


Figure 3.5: (Color Online.) Fits of the DEH form for the viscosity, Eq. (3.9), to supercooled glucose and supercooled water.

of 45 different glass forming supercooled liquids. As the DEH is meant to be universal across all types of supercooled liquids, we selected glassformers of all classes, bonding types, fragilities, and physical and chemical features. We studied silicate liquids, organic liquids, metallic liquids, elemental liquids, sugars, chalcogenides, and even supercooled water. The experimental viscosity data for the various supercooled liquids was either measured "in-house" by one of the authors or extracted from previously published works. The published data that was present only in graphical form was converted to tabular form using data digitization software. Nonlinear curve fitting methods and error minimization were employed to extract the best-fit value of the single parameter, $\bar{A}$. The natural logarithm of the DEH form of the viscosity (Eq. 3.9) was fitted to the experimental viscosity data for all temperatures at and below the liquidus, using the experimental values for the liquidus temperature, $T_l$, and viscosity at the liquidus, $\eta(T_l)$ (data presented in traditional base-10 format for consistency). In some cases, a data point was not present exactly at the liquidus temperature, requiring interpolation of the value of $\eta(T_l)$. In most cases, the standard error

in the calculation of $\bar{A}$ from the nonlinear fitting algorithm was of $\mathcal{O}(10^{-3})$. Associated p-values supported the null hypothesis that the values of $\bar{A}$ were statistically significant from zero (54).

Figures (3.2)-(3.5) show the viscosity data, with DEH fit applied, in logarithmic form as a function of temperature. Qualitatively, the data in the figures suggest that the DEH form is capable of reproducing the data for the silicate, metallic, organic, and sugar-based glass forming liquids as well as supercooled water, with minimal residual error. A notable exception is the case of Albite. The closest data points to the melting point for this liquid were within approximately 100 K on both sides of the $T_l$. This necessitated a large interpolation of the data to extract $\eta(T_l)$. While it was observed that the DEH fits are significantly less sensitive to changes in the value of $\eta(T_l)$, than either $T_l$ itself, or $\bar{A}$, this is still likely the cause of this discrepancy.

### 3.4.2 Statistical Measures of Goodness of Fit

We have demonstrated qualitatively that the DEH form can reasonably reproduce the temperature dependence of the viscosity of a large number of supercooled liquids. However, purely visual fitting results are subjective, and the validity of a physical model must rest on objective measures. Therefore, in order to bolster the claim that the DEH model is the correct model for describing supercooled liquids, we also performed a quantitative analysis, to assess the statistical significance of our results. In what follows, we calculate various statistical measures of the goodness of fit of the DEH model to the experimental viscosity data, as well as perform a statistical comparison with previous theories. While we perform these analyses on 45 of the liquids studied, but we will use OTP, LS2, and $Pd_{40}Ni_{40}P_{20}$ as 'case studies' throughout the next sections. These liquids are seen to be good representatives

for their various classes, and will allow us to do detailed calculations with lower computational cost.

Statistical measures allow one to quantify the error, or goodness of fit (GoF) of the performance of a model. Typically, the first step to assessing the statistical GoF is to analyze the residuals of the fit. In our case, using the raw viscosity data, the residuals are defined as

$$Res(T) \equiv \sum_i (\eta_{exp}(T_i) - f(T_i)). \tag{3.10}$$

Here, $f(T)$ is the temperature dependent model function being tested (in this section, the DEH model of Eq.(3.9). Figures (3.6) and (3.7) display the results of the residual analysis for a random sample of the supercooled liquids studied. When examining the residuals of a fit, one wants to note both the magnitude of the residuals and the distribution of the residuals about zero. In all liquids studied the magnitude of the residuals is very small, and this is true for LS2 and OTP (with the exception of two outlying points for OTP). This low magnitude suggests that the DEH form is capable of reproducing the approximate values of the measured viscosity. The distribution of the residuals about zero is a measure of how well the model captures the actual trend of the data. An accurate model should have residuals which, roughly, approximate the random error associated with measurement error. Examination of the residuals of the DEH shows that in many cases the residuals are more or less random. There are some minor exceptions, which might be due to the fact that most viscosity data is reported in the literature without error bars, and not considering these error bars in the fits is likely the culprit in the minor skewing of residuals. This hypothesis is bolstered by the fact that other models of supercooled liquids tested in the next section tend to show the same skewing, or bias in the residuals suggesting possible error inherent to the data itself. The next step in performing a rigorous statistical analysis of the quality of a model is to calculate various quantitative measures of the GoF. For each of the liquids

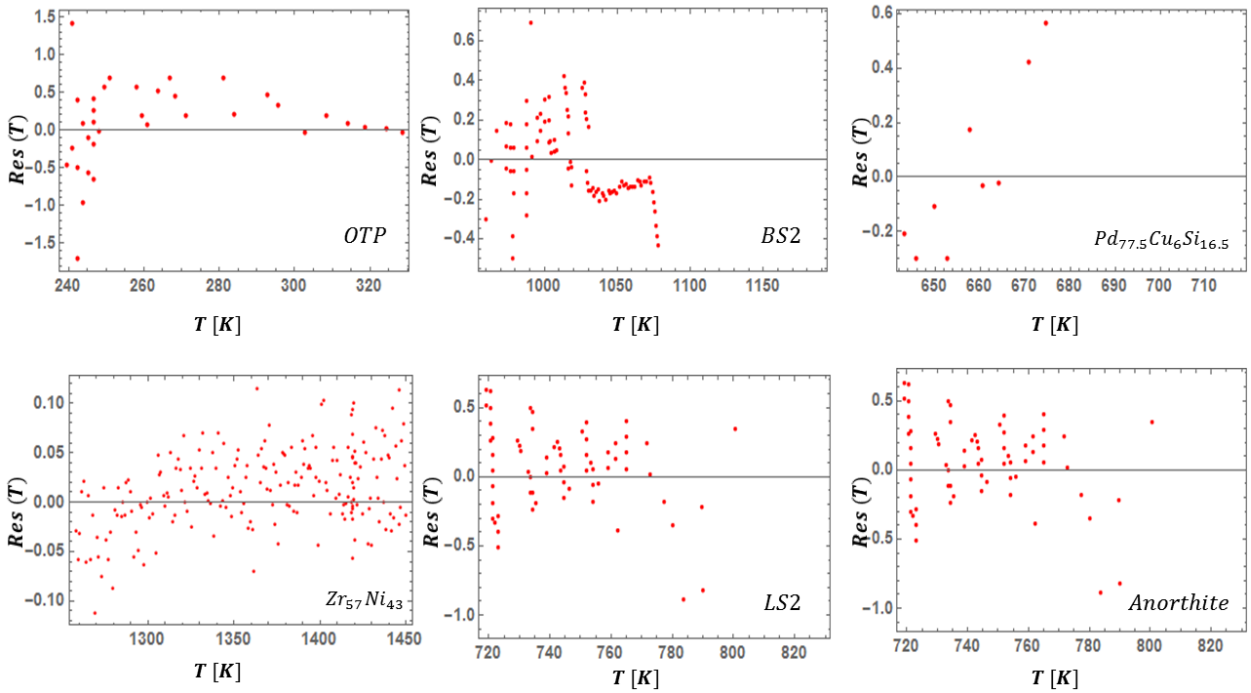


Figure 3.6: (Color Online.) Residuals as computed from Eq. (3.10) associated with fits of Eq. (3.9) for six different supercooled liquids. Residuals corresponding to accurate fits typically possess random scatter about zero. For a discussion of possible bias in the residuals, see the main text.

Table 3.3: Statistical Measures of GoF

| *Composition* | *Function* | $(SSE)$ | $\chi^2_{red}$ | $R^2$ |
|---|---|---|---|---|
| OTP | DEH | 10.617 | 0.312264 | 0.997247 |
| | VFT | 24.5584 | 0.767451 | 0.993632 |
| | KKZNT | 8.67516 | 0.279844 | 0.997751 |
| | CG | 9.66624 | 0.30207 | 0.997494 |
| | BENK | 8.91119 | 0.270036 | 0.997689 |
| | MYEGA | 12.3813 | 0.386916 | 0.99679 |
| LS2 | DEH | 14.8497 | 0.215213 | 0.983678 |
| | VFT | 16.5523 | 0.247049 | 0.981807 |
| | KKZNT | 13.3202 | 0.201821 | 0.985359 |
| | CG | 14.8216 | 0.221218 | 0.983709 |
| | BENK | 13.3526 | 0.196361 | 0.985324 |
| | MYEGA | 24.9113 | 0.371811 | 0.972619 |
| $Pd_{77.5}Cu_6Si_{16.5}$ | DEH | 0.789078 | 0.0876754 | 0.998759 |
| | VFT | 10.2834 | 1.46905 | 0.983823 |
| | KKZNT | 0.235779 | 0.0392965 | 0.999629 |
| | CG | 0.203843 | 0.0291204 | 0.999679 |
| | BENK | 0.334157 | 0.0417696 | 0.999474 |
| | MYEGA | 1.31174 | 0.187391 | 0.997937 |
| Salol | DEH | 17.1643 | 0.553687 | 0.993136 |
| Diopside | DEH | 13.1776 | 0.0941259 | 0.997362 |
| Anorthite | DEH | 2.25807 | 0.141129 | 0.991396 |
| BS2 | DEH | 4.902 | 0.0505361 | 0.998646 |
| Albite | DEH | 13.3105 | 0.511942 | 0.87503 |
| $Zr_{74}Rh_{26}$ | DEH | 0.115181 | 0.000984452 | 0.983959 |
| $Pd_{40}Ni_{40}P_{20}$ | DEH | 12.3782 | 0.515757 | 0.993153 |
| $Zr_{57}Ni_{43}$ | DEH | 0.351164 | 0.00172139 | 0.977947 |
| $Cu_{64}Zr_{36}$ | DEH | 0.190441 | 0.00307162 | 0.984655 |
| $Ni_{34}Zr_{66}$ | DEH | 0.121782 | 0.00162376 | 0.993343 |
| $Zr_{50}Cu_{48}Al_2$ | DEH | 10.617 | 0.312264 | 0.997247 |
| $Ni_{62}Nb_{38}$ | DEH | 0.448888 | 0.00487922 | 0.9841 |
| Vit106a | DEH | 6.23195 | 0.623195 | 0.996508 |
| $Cu_{55}Zr_{45}$ | DEH | 0.223386 | 0.00314628 | 0.987581 |
| $H_2O$ | DEH | 0.00731595 | 0.000215175 | 0.999412 |
| Glucose | DEH | 1.48859 | 0.0513308 | 0.999499 |
| Glycerol | DEH | 76.0137 | 1.85399 | 0.945217 |
| $Ti_{40}Zr_{10}Cu_{30}Pd_{20}$ | DEH | 0.395717 | 0.00316573 | 0.988712 |
| $Zr_{70}Pd_{30}$ | DEH | 0.080497 | 0.00134162 | 0.996159 |
| $Zr_{80}Pt_{20}$ | DEH | 0.077876 | 0.00162242 | 0.971562 |
| NS2 | DEH | 20.9749 | 0.723273 | 0.981462 |
| $Cu_{60}Zr_{20}Ti_{20}$ | DEH | 0.196626 | 0.0012063 | 0.985095 |
| $Cu_{69}Zr_{31}$ | DEH | 0.756104 | 0.00804366 | 0.950419 |
| $Cu_{46}Zr_{54}$ | DEH | 0.650675 | 0.00971157 | 0.910136 |
| $Ni_{24}Zr_{76}$ | DEH | 0.0453595 | 0.0008584 | 0.991683 |
| $Cu_{50}Zr_{42.5}Ti_{7.5}$ | DEH | 0.0535541 | 0.00172755 | 0.982531 |
| D Fructose | DEH | 0.554086 | 0.0240907 | 0.946689 |
| TNB1 | DEH | 8.97792 | 0.448896 | 0.996155 |
| Selenium | DEH | 6.43906 | 0.292684 | 0.995906 |
| CN60.40 | DEH | 0.746426 | 0.0678569 | 0.998937 |
| CN60.20 | DEH | 0.147407 | 0.0105291 | 0.999883 |
| $Pd_{82}Si_{18}$ | DEH | 1.2915 | 0.1435 | 0.998916 |
| $Cu_{50}Zr_{45}Al_5$ | DEH | 0.109111 | 0.000742252 | 0.992842 |
| $Ti_{40}Zr_{10}Cu_{36}Pd_{14}$ | DEH | 0.195736 | 0.00163113 | 0.92674 |
| $Cu_{50}Zr_{50}$ | DEH | 0.235607 | 0.00420727 | 0.976969 |
| Isopropyl benzene | DEH | 4.47953 | 0.344579 | 0.993307 |
| Butylbenzene | DEH | 1.97384 | 0.140989 | 0.995543 |
| $Cu_{58}Zr_{42}$ | DEH | 0.551631 | 0.0108163 | 0.966384 |
| Vit 1 | DEH | 46.5891 | 2.58828 | 0.956556 |
| Trehalose | DEH | 8.93373 | 0.288185 | 0.934837 |
| Sec-Butylbenzene | DEH | 1.27723 | 0.159653 | 0.976809 |
| $SiO_2$ | DEH | 57.7053 | 1.98984 | 0.660326 |

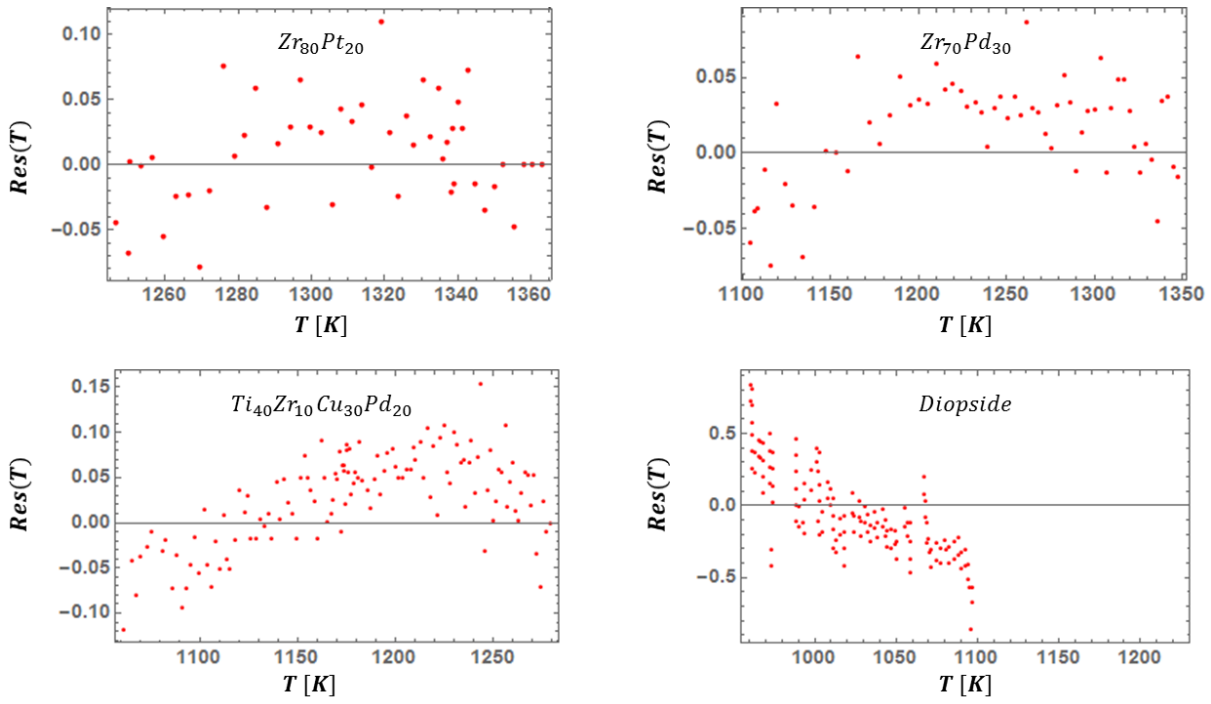


Figure 3.7: (Color Online.) Residuals as computed from Eq. (3.10) associated with fits of Eq. (3.9) for four different supercooled liquids which receive cross validation analysis.

studied we compute the sum of squared errors (SSE),

$$SSE \equiv \sum_i (\eta(T_i) - f(T_i))^2, \tag{3.11}$$

r-squared value ($R^2$),

$$R^2 \equiv 1 - \frac{SSE}{SST} = 1 - \frac{\sum_i (\eta(T_i) - f(T_i))^2}{\sum_i (\eta(T_i) - \bar{\eta})^2} \tag{3.12}$$

and reduced chi-squared value, $\chi^2_{reduced}$ (There are multiple definitions of the $\chi^2$ statistic for goodness of fit. We have chosen one of the more common ones),

$$\chi^2_{reduced} = \sum_i \frac{(\eta(T_i) - f(T_i))^2}{n_{data} - n_{parameters}}. \tag{3.13}$$

The calculated values of the statistical GoF measures are listed in Table (3.3), in the rows labeled "DEH". Statistically significant GoF is typically taken to correspond to $\chi^2_{reduced}$ values less than one, $R^2$ values asymptotically close to one and low values for the SSE. Examining the values in Table (3.3) makes clear that the lowest values of $\chi^2_{reduced}$ do not always correspond to the highest values of $R^2$. In some cases the various statistical measures can report differing levels of GoF. Therefore, it is important to consider all measures simultaneously. We can examine the "worst-case examples" to assess a bound on the DEH GoF measures. We see that the lowest value of $R^2$ corresponds to $SiO_2$ which we will discuss in more detail in the SI. Otherwise, with the exception of Albite which was discussed above, the $R^2$ values all exceed 0.9. This indicates that the DEH model is able to accurately account for the natural variability in the data. As seen in the table, the highest values of $\chi^2_{reduced}$ are approximately 1.9 for $SiO_2$ and 1.8 for glycerol. With these exceptions, the remainder of the liquids studied all have values of $\chi^2_{reduced}$ which are significantly less than one. This is indicative that the DEH model is capable of representing the viscosity data in a statistically significant way, while simultaneously suggesting that specific liquids may possess certain anomalies (see SI). If one were to go further and examine actual p-values associated with the various $\chi^2$ values, they would also confirm that the DEH model provides a statistically significant reproduction of the experimental data.

### 3.4.3 Cross Validation

The statistical measures employed up to this point to assess the performance of the DEH have demonstrated that the model is capable of fitting the experimental viscosity data of a large number of supercooled liquids to a high degree of statistical accuracy. The drawback to the methods employed previously, however, is that they merely reflect the ability of the model to fit the data given, and do not describe how well the model can make

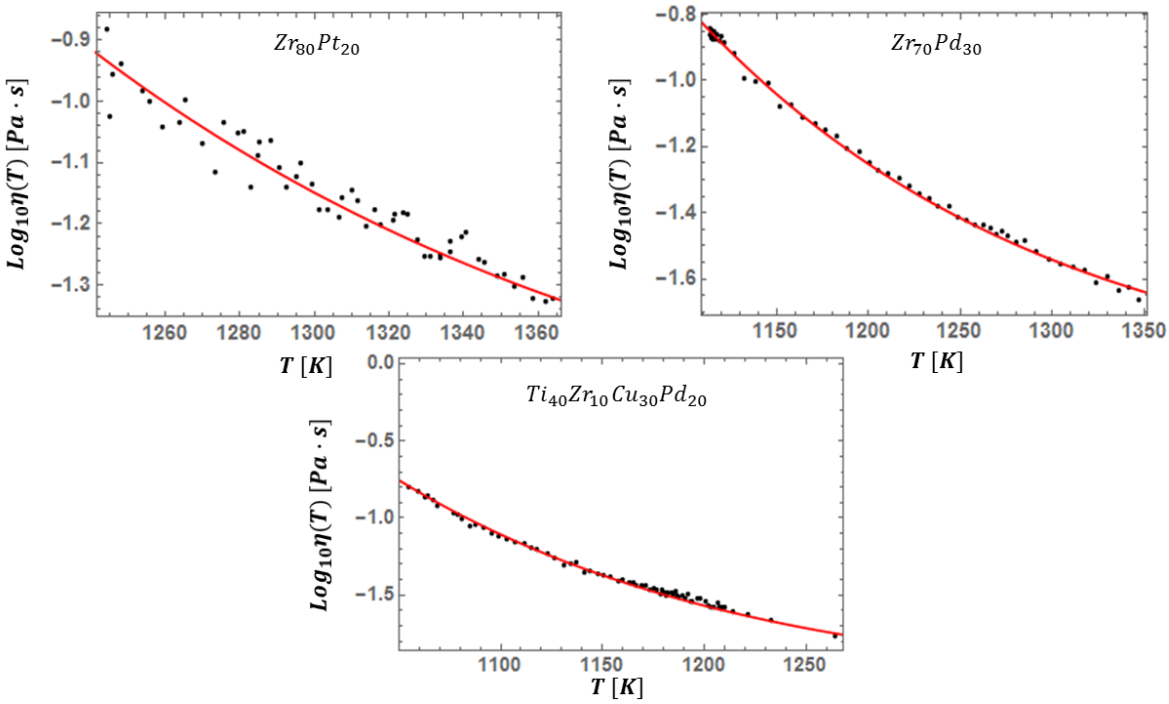


Figure 3.8: (Color Online.) Results of cross validation of the DEH model for three supercooled liquids where multiple data sets were available. Using values of $\bar{A}$ extracted by fitting the data of one set, we applied the form of Eq. (3.9) to a second set to assess the reproducibility of the model. For more information, see Section VC.

Table 3.4: Cross Validation Statistics

| *Composition* | *Cross Validation* $\chi^2_{reduced}$ |
|---|---|
| $Zr_{80}Pt_{20}$ | 0.0043631 |
| $Zr_{70}Pd_{30}$ | 0.000973443 |
| $Ti_{40}Zr_{10}Cu_{30}Pd_{20}$ | 0.00193925 |
| Diopside | 0.097273 |

predictions based on those fits or whether or not the model over fits the data. In order to assess the ability of the fits to predict 'new' data for a given liquid we must employ cross validation schemes. In cross validation, we use the value of the parameter, $\bar{A}$ that comes from fitting one set of experimental viscosity data for a given liquid and apply it (using Eq. 3.7)) to an independently measured set of data for the same system. We employed this analysis for multiple independent data sets that we had available for metallic liquids. Using the values of $\bar{A}$ reported in Table (3.2), we apply the DEH form to alternative data sets for three metallic liquids. The results are shown in Fig. (3.8). For liquids that did not have multiple data sets available for cross validation we applied a 5-fold cross validation scheme to the single data set available. The example case that we examined is for diopside, and the results of this 5-fold cross validation are presented in Fig. (3.9). Qualitatively it is clear from the cross validation studies performed here, that the parameter values extracted from fitting experimental data sets will generalize to new data for the same liquid, providing more support that the DEH provides a statistically accurate model of supercooled liquid viscosity data. We can quantify this by examining the values of $\chi^2_{reduced}$ that result from the cross validated fits. These results are given in Table (3.4). Comparing these values with those in Table (3.3) for the original fits shows that they are roughly comparable in magnitude, further validating the general applicability of the DEH fit accommodate 'new' data.

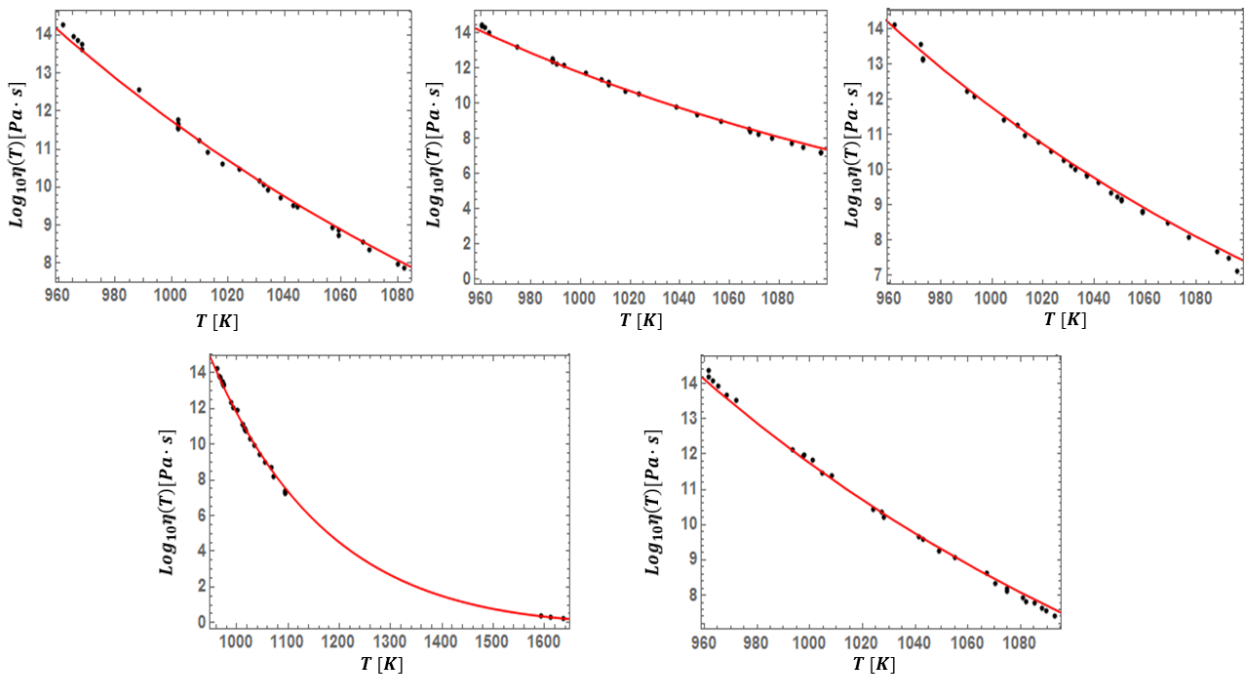


Figure 3.9: (Color Online). Results of 5-fold cross validation of single diopside dataset. We randomly separated the single dataset for diopside into 5 subsets and iteratively used 4 subsets to fit and extract $\bar{A}$ to apply the fit of Eq.(3.9) to the fifth subset to assess the reproducibility of the model. For more information, see Section VC.

Overall, the various statistical measures and analyses employed to assess the validity and goodness of fit of the DEH model appear to objectively suggest that the functional form of Eq. (3.9), is able to accurately describe the phenomenology of the super-Arrhenius growth of the viscosity. This was demonstrated for 45 distinct and diverse supercooled liquids, and makes a strong case for the DEH as a descriptor of the glass transition.

### 3.4.4 Statistical Comparison With Other Theories

We have demonstrated both qualitatively and quantitatively, that the DEH model and functional form for the viscosity is able to accurately describe and reproduce the temperature dependence of the viscosity of supercooled liquids using only a **single** fitting parameter. It is important, however, to examine the DEH in comparison with existing theories and models of the glass transition, some of which even provide for collapse of the viscosity data (55). To that end, we statistically compare and contrast the DEH with five of the most widely used models of supercooled liquids, and their associated functional forms for the viscosity. We selected a glass forming liquid from three of the classes considered, namely organic (OTP), silicate (LS2), and metallic ($Pd_{77.5}Cu_6Si_{16.5}$) and fit the viscosity functions arising from the KKZNT avoided critical point model (56; 57; 58),

$$\ln \eta = \ln \eta_0 + \frac{E_\infty}{T} + \frac{T_A}{T} B [\frac{T_A - T}{T_A}]^z \Theta(T_A - T) \tag{3.14}$$

Cohen-Grest free volume model (59),

$$\ln \eta = \ln \eta_0 + \frac{2B}{T - T_0 + \sqrt{(T - T_0)^2 + CT}} \tag{3.15}$$

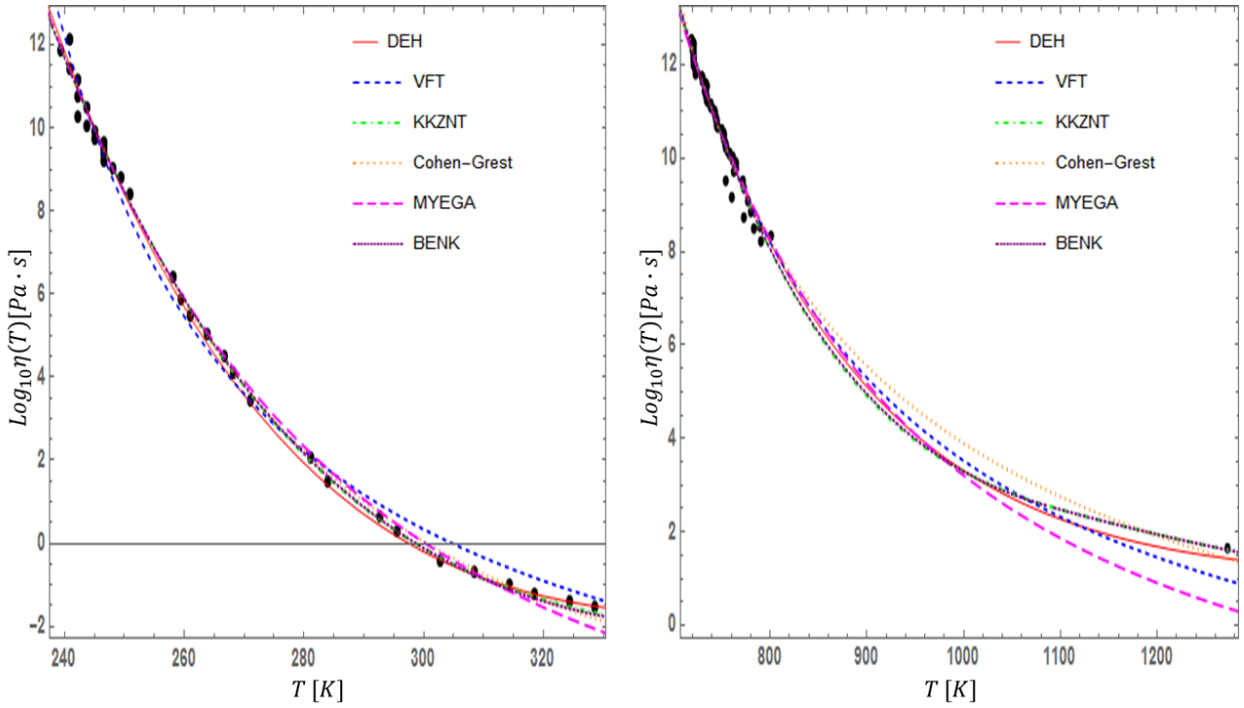


Figure 3.10: (Color Online.) Comparison of DEH [Eq. (3.9)], VFT [Eq. (3.2)], KKZNT [Eq. (3.14)], Cohen-Grest [Eq. (3.15)], MYEGA [Eq. (3.17)], and BENK [Eq. (3.16)] forms for the viscosity as applied to fragile OTP and strong LS2.

BENK modified parabolic model (55; 60; 61),

$$\ln \eta = \ln \eta_0 + \frac{E_\infty}{k_B T} + J^2 (\frac{1}{T} - \frac{1}{\tilde{T}})^2 \Theta(\tilde{T} - T) \tag{3.16}$$

MYEGA entropy model (62),

$$\ln \eta = \ln \eta_0 + \frac{K}{T} e^{\frac{C}{T}} \tag{3.17}$$

and the oft-employed VFT form (Eq. 3.2).

Each one of these functional forms (including VFT) has at least two parameters that (at this point) cannot be determined from first principles. In order to determine the parameters of the various forms for the three test liquids, we fit the natural logarithm of the viscosity data as a function of temperature. As the DEH form of Eq. (3.9) is applicable only below

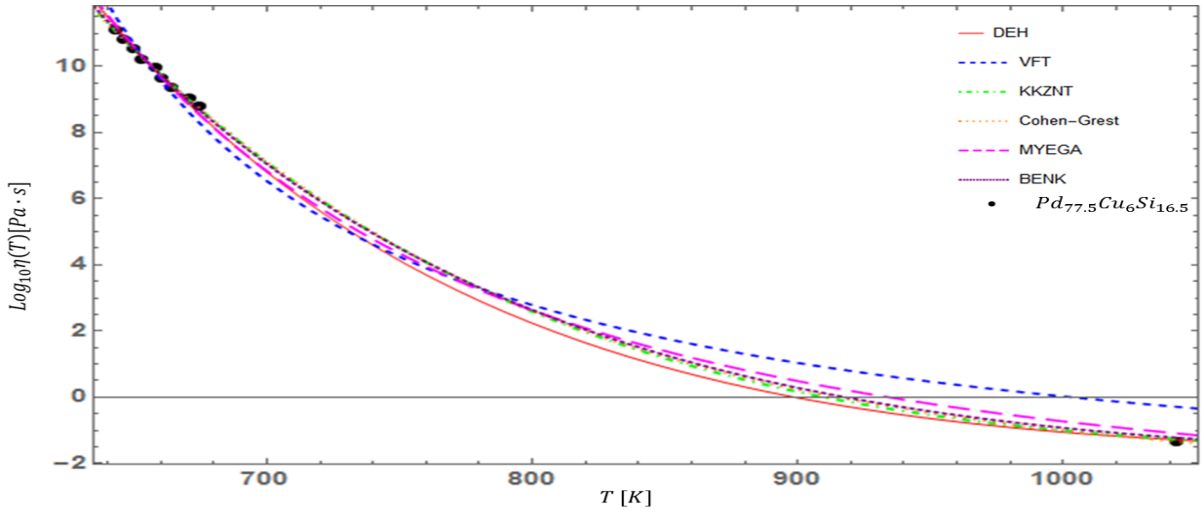


Figure 3.11: (Color Online.) Comparison of DEH [Eq. (3.9)], VFT [Eq. (3.2)], KKZNT [Eq. (3.14)], Cohen-Grest [Eq. (3.15)], MYEGA [Eq. (3.17)], and BENK [Eq. (3.16)] forms for the viscosity as applied to the metallic liquid $Pd_{77.5}Cu_6Si_{16.5}$.

the liquidus temperature, $T_l$, we needed a 'fair' metric for comparison between the above theories whose functional forms apply to the entire temperature range of measured data. To that end, in all cases, we first applied a linear fit to the high temperature Arrhenius (above the crossover temperature) regime as a function of inverse temperature. This allows us to extract values of the prefactor, $\eta_0$, and the extrapolated high temperature activation energy, $E_\infty$, where relevant. For each liquid, we fixed these values and then fit the various models over the remaining temperature range from $T_l$ and below, to extract the values of the remaining parameters. In the case of KKZNT, we also constrained the parameter $z$ to be $\frac{8}{3}$ (see (56) for discussion). The results of the fitting with the extracted parameters are depicted in Figures (3.10) and (3.11). The functional forms of all studied theories are shown along with the DEH fits. In Figure (3.12) we plot the residuals of all the forms together. A visual comparison of the fits against the data makes clear that the VFT form consistently provides the worst fit to the experimental data. Qualitatively, it is difficult to distinguish the goodness of fit of the remaining models. In order to resolve these differences, we examine the residuals of the fits in Fig. (3.12) and compute statistical measures. The residuals are more or less consistent across the forms, with the exception of VFT, which as expected shows

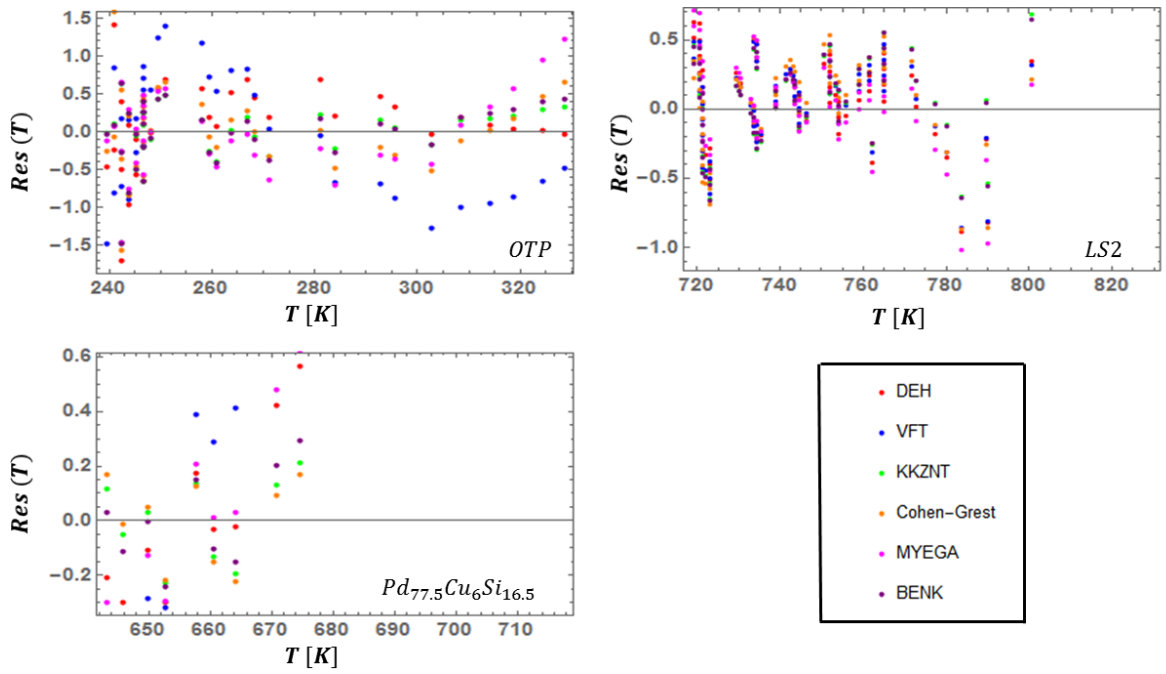


Figure 3.12: (Color Online.) Comparison of the residuals from Eq. (3.10) of the DEH [Eq. (3.9)], VFT [Eq. (3.2)], KKZNT [Eq. (3.14)], Cohen-Grest [Eq. (3.15)], MYEGA [Eq. (3.17)], and BENK [Eq. (3.16)] forms of the viscosity.

significant bias, especially in the case of OTP. This provides support to the argument that the non random nature of the residuals is likely related to measurement error in the data. The calculated statistical values are provided in Table (3.3) in the rows corresponding to the various model designations. Examining the calculated values makes clear that the DEH model consistently outperforms both the VFT and MYEGA forms across all three liquids. The Cohen-Grest form appears to be roughly similar to the DEH form, whereas the KKZNT and BENK forms consistently outperform the DEH. This result is not surprising, as the KKZNT and BENK forms have many more open parameters than the DEH form. In fact, it can be shown that forcing the values of the "special temperatures" that appear in these forms to correspond to experimental values causes the fit performance to worsen significantly. This is consistent with previous results that suggested that the KKZNT form does not perform well for silicate glassformers and that the MYEGA form does not perform well for metallic glass formers. This leads to the conclusion that in numerous cases, the optimal values of the

parameters are often inconsistent with the underlying theoretical motivations. This suggests that the various models contrasted with the DEH are unable to universally describe the phenomenology of supercooled liquids of all types, unlike the DEH model.

### 3.4.5 Fitting of the Relaxation Time

As we have discussed, the viscosity acts, in many ways, as a proxy for the relaxation time of the supercooled liquid in response to some perturbation, and the two are generally linked via Maxwell's relation. However, in many cases the infinite frequency shear modulus is itself mildly temperature dependent (in fact, at least one model is based upon this dependence cite Shoving Model), and the viscosity reports a sort of average relaxation time for the fluid, whereas raw relaxation times are the most probable. These facts make it imperative that we have a method for computing the relaxation time in the supercooled liquid state, without the requirement of using the viscosity equations first. The relaxation time, however, is not an ensemble averaged quantity, and therefore, cannot simply be averaged over using the thermal or energy distribution approach of the classical framework. This is, perhaps, the first case where the quantum approach possesses an inherent advantage to classical one, as we can extend the above derivation to include relaxation times.

Once the state of the fluid has reached its post-quench thermal mixed state, $|\Psi_T\rangle$, the relaxation time can be measured by many methods, such as exposing a liquid to an electric field and measuring the decay of the polarization. The external fields employed to evoke a measurable response can be treated as a time-dependent potential which the system evolves under during measurement. This has the effect of being an evolution operator with the potential, $U'(t)$, and therefore, elements of time dependent perturbation theory can be employed. We assert that the relaxation rate of the system due to the time dependent

perturbing potential will be similar to that of Fermi's golden rule, namely,

$$r_{s.c.} = \frac{d}{dt} \sum_m |\langle \phi_m | U'(t) | \Psi_T \rangle|^2 \tag{3.18}$$

Inserting the expression for the thermally mixed state into the above equation, and recognizing that $r_n \equiv \frac{d}{dt} \sum_m |\langle \phi_m | U'(t) | \phi_n \rangle|^2$, in traditional time dependent perturbation theory, leads to the expression

$$r_{s.c} = \int dT' p_T(T') r(T'). \tag{3.19}$$

for the relaxation rate in the DEH framework. We assume the same distribution as in the viscosity case, and argue that the Eyring relaxation rate for the equilibrium liquid, when multiplied by our relatively peaked distribution, can be well approximated by its value at the liquidus, thus leading to the expression

$$r_{s.c} = r(T_l) \int_{T_l}^{\infty} dT' p_T(T') \tag{3.20}$$

for the relaxation rate. Placing this expression into the relation $\tau = \frac{1}{r}$, and again using the Gaussian distribution leads to the final form for the supercooled liquid's relaxation time,

$$\tau_{s.c.} = \frac{\tau(T_l)}{\text{erfc}\left(\frac{T_l - T}{\sqrt{2}\hat{A}T}\right)}. \tag{3.21}$$

It is immediately recognizable that this result is identical to the functional form of the expression for the viscosity. This is not surprising, as we would expect the two to obey a similar form, but in this way, it is rigorously derived from the first principles of the DEH model, instead of merely conjectured. We can test whether the relaxation time truly does obey this form in the same way the viscosity does, by fitting raw relaxation time data for various liquids. Fig. (3.13) shows the relaxation time data (measured by dielectric

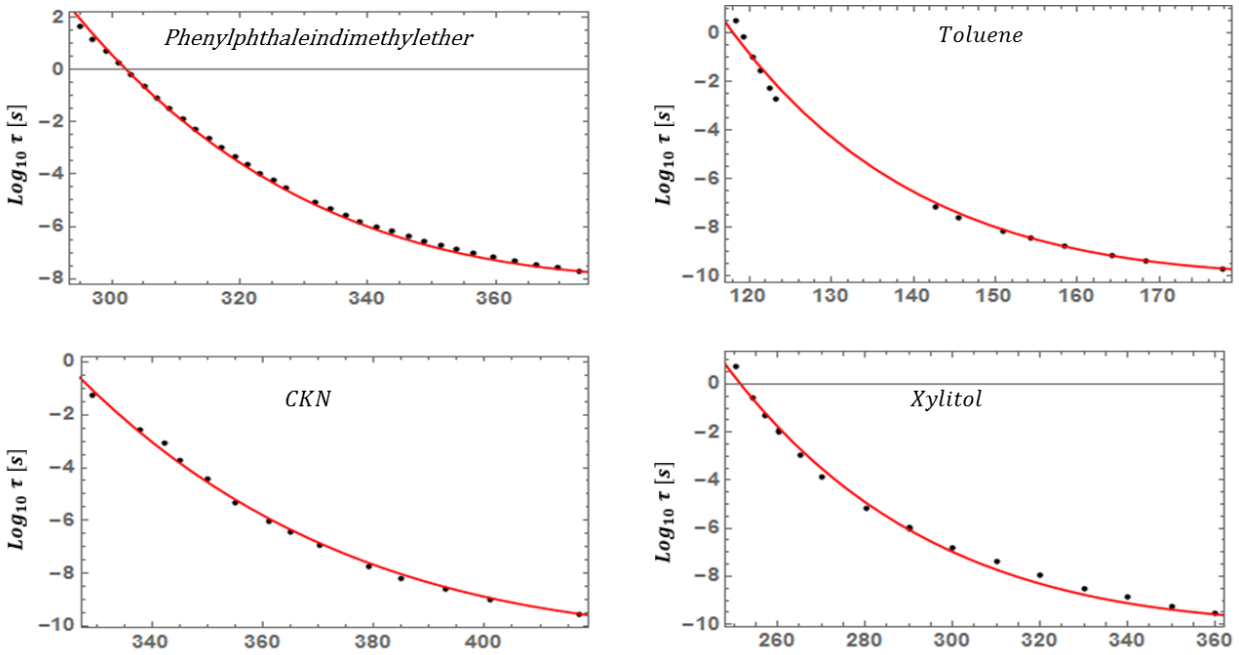


Figure 3.13: (Color Online.) Log base-10 representation of the relaxation time data scaled by its value at the liquidus, $\tau(T_l)$, versus $x$, as defined in the figure for various liquids. The data of 11 distinct liquids is observed to lie upon a single curve.

relaxation and other methods) for four different liquids of various types. Overall, we see that the DEH relaxation formula does well in describing their behavior. Two particular interesting cases are that of CKN (**?** ) and Phenlalalallalalall (**?** ). The former is one of the most studied supercooled liquids, and the latter is a Van der Waals liquid which has been shown to be difficult to describe with previous fitting functions. We must point out that, as in the viscosity case, the DEH relaxation time function does not perfectly reproduce the behavior of all liquids studied, and these cases and possible explanations are discussed in the supplementary information.

## 3.5 Universality Amongst Supercooled Liquids

The DEH viscosity function of Eq. (3.9) has only one dimensionless parameter ($\bar{A}$). The two other quantities appearing in Eq. (3.9) (the liquidus temperature $T_l$ and the viscosity of the supercooled liquid at the liquidus temperature $\eta(T_l)$) are both fixed by experiment. Thus, the DEH theory (50) implies that the viscosity data of supercooled fluids may be collapsed onto one master curve with the judicious value of this single parameter $\bar{A}$. In (51), we succinctly verified this prediction of a universality in the viscosity data. Here, we expand on this newfound universality. In Section 3.4, we demonstrated that the DEH model can accurately reproduce the viscosity of all types of supercooled liquids, over many decades. Thus, since Eq. (3.9) holds over the experimentally relevant temperature range, it follows the glass transition phenomenon possesses some form of universality that may be unearthed with the aid of the single parameter $\bar{A}$. The virtue of the universality implied by Eq. (3.9) is that the only temperature and viscosity scales are the equilibrium liquidus temperature and the viscosity at this temperature. There are no assumptions about exotic temperatures such $T_0$ of Eq. (3.2). Rather, the only pertinent temperature in the DEH framework is that associated with a known equilibrium transition. Previously, many investigations attempted to scale the viscosity data of all liquids studied in some meaningful way, to see if they can be collapsed onto a single curve by appealing to various "special" temperatures such as the just noted "ideal glass transition temperature" $T_0$, the dynamic glass transition temperature $T_g$ (at which the viscosity reaches the rather arbitrary threshold value of $10^{12}$ Pascal $\times$ sec) that often coincides with a weak thermodynamic signature (63), or the Arrhenius cross-over temperature $T_A$ (61; 56; 57; 58) above which the activated Arrhenius form of Eq. (3.1) holds and below which deviations from Eq. (3.1) fails and rigidity and collective phenomena emerge (75; 76; 77). Within the DEH model, the equilibrium liquidus temperature $T_l$ constitutes the only temperature of significance. As we discussed above, Eq. (3.9) implies that a universal

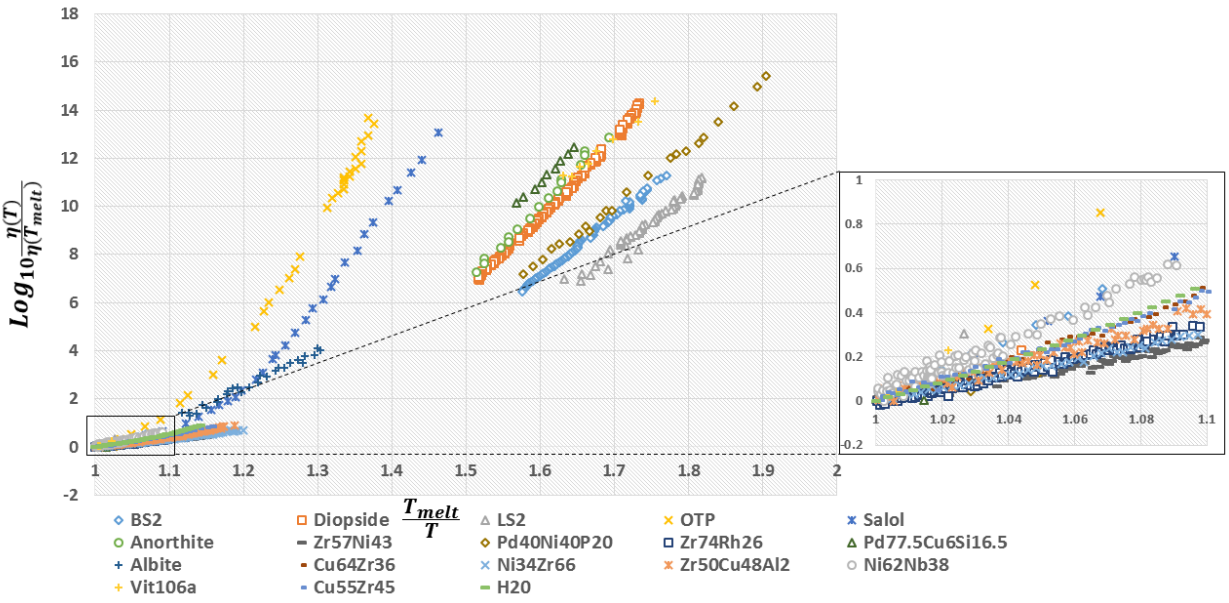


Figure 3.14: (Color Online.) The logarithm of the viscosity, $\eta(T)$, scaled by the viscosity at the liquidus, $\eta(T_l)$, versus the scaled temperature, $\frac{T_l}{T}$ for a subset of the studied liquids. When represented this way universal behavior does not appear, however, a spectrum of behavior approximating the fragility does appear. A careful inspection of the plot indicates that most glassformers seem to fall within different 'families' corresponding to fragility classes as defined by experimental values.

data collapse of the viscosity occurs relative to the ratio $(T_l - T)/T$ when it is scaled by the single dimensionless parameter $\bar{A}$ of the DEH theory.

In Fig 3.14, we plot the logarithm of the viscosity data as a function of the reciprocal temperature with both quantities scaled by their respective values at $T_l$. A moment's inspection reveals that this scaling does not lead to a data collapse. However, an interesting result does appear in the fact that the viscosity data appears to fall into a spectrum of "fragility bands" in much the same way the standard Angell plot does. This suggests that fragilities appear quite naturally in the DEH model using $T_l$ (a well defined temperature) instead of $T_g$ (an occasionally arbitrarily defined temperature) as the fundamental scaling temperature. This is not unreasonable, as the Kauzmann "2/3" rule (78) suggests that on average $T_g = \frac{2}{3}T_l$. Therefore, we would expect that Angell-like fragility scaling should appear in the plot versus the reciprocal melting temperature, as it is, in many cases, proportional to the glass transition temperature. This will be discussed more in the next section (for a summary of earlier attempts to relate the glass transition to melting see, e.g., (51)). Since the DEH model contains only a single fitting parameter, and is able to reproduce the viscosity of a disparate cross section of supercooled liquids using only this single parameter, it seems natural to include $\bar{A}$ in any scaling attempts. In our previous work (96) we demonstrated that by plotting the logarithm of the scaled viscosity, $\eta(T)/\eta(T_l)$, versus the argument of the complementary error function in the DEH form for the viscosity (Eq. 3.9) (namely $x \equiv \frac{T_l - T}{T\bar{A}\sqrt{2}}$) led to a collapse of the viscosity data of some 45 liquids to a universal scaling curve (the reciprocal of a raw complementary error function). Here we attempt this same scaling for the relaxation time data of 17 different liquids in Fig. (3.15) and observe that the scaling relation holds for relaxation time as well. The fact that the logarithm of the scaled relaxation time has the same functional form as that of the scaled viscosity means that the relaxation time and viscosity can be placed on the same scaling curve. Therefore, in Fig. (3.16) we combine the relaxation time data of 17 liquids, as well as the viscosity data of the original 45

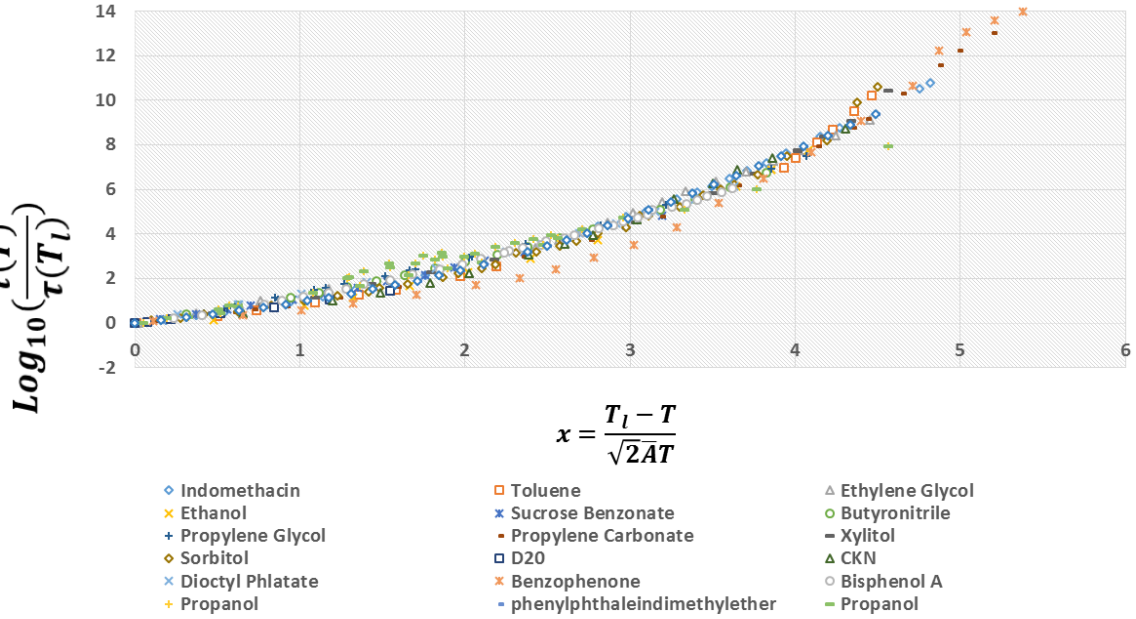


Figure 3.15: (Color Online.) Log base-10 representation of the relaxation time data scaled by its value at the liquidus, $\tau(T_l)$, versus $x$, as defined in the figure for various liquids. The data of 11 distinct liquids is observed to lie upon a single curve.

liquids and 5 additional liquids *for a total of 67 different liquids studied and collapsed to the same universal curve*, over 16 decades and using only a single parameter. The collapse in Fig. 3.16, to our knowledge, represents one of the first times that data for all types of supercooled liquids has been collapsed over this many orders of magnitude for this many diverse liquids. This result is perhaps the most important finding in the entirety of this thesis, as regardless of the whether the theoretical framework we have proposed is correct, this data scaling clearly demonstrates an underlying universality. This result suggests that the physics of supercooling and ultimate mechanism of the glass transition is, in fact, universal across all liquids, and warrants significant further investigation. In the preceding section we undertook a rigorous statistical analysis to objectively assess the performance of the DEH model. The statistical analysis performed on the individual compositions is equivalent to performing a statistical analysis of the goodness of fit for the universal collapse curve, so a separate analysis of the universal curve itself will not be undertaken. However, in Figure 3.17a-3.17c we "zoom in"

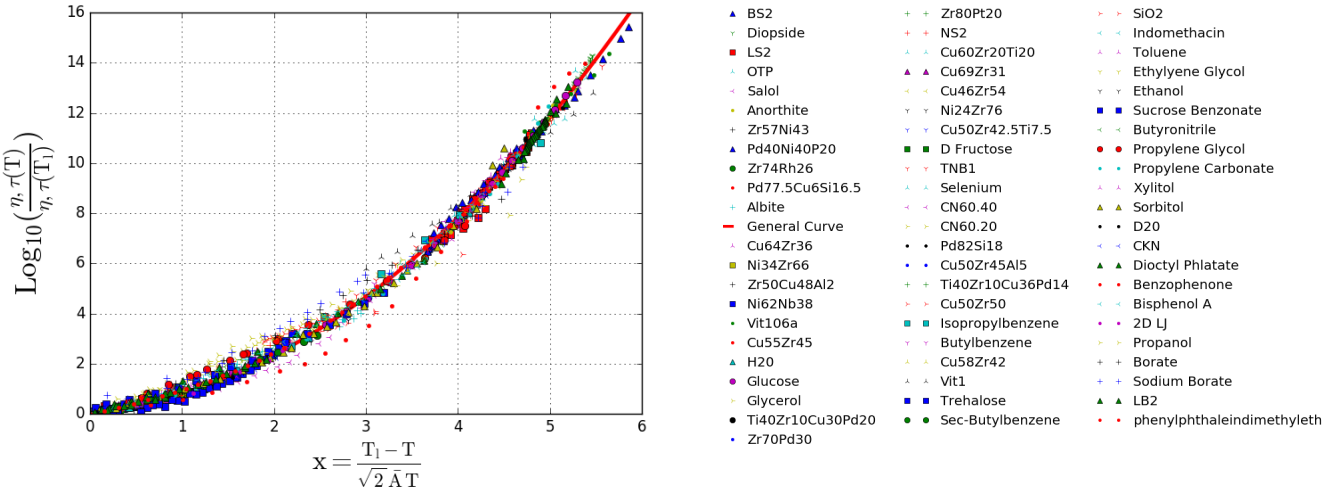


(a) (b)

Figure 3.16: (Color Online.) Log base-10 representation of both the viscosity data, and relaxation time data, scaled by their respective values at the liquidus, $\eta, \tau(T_l)$, versus $x$, as defined in the figure for all studied liquids. The data of all 66 liquids, of all types and kinetic fragilities, is observed to fall upon ('collapse onto') a single, universal scaling curve. This result is suggestive of an underlying universality in the behavior of supercooled liquids. Note the exceptional agreement over 16 decades.

on the three major regimes in the universal curve, namely temperatures very near melting, midrange temperatures, and temperatures corresponding to deeply supercooled liquids where glassy effects are strongest. The objective of this "zooming" is to demonstrate that we are not "sweeping anything under the rug", so-to-speak, by representing the data in this way. It is standard to plot the logarithm of viscosity data when demonstrating collapse-like curves, but in the interest of total transparency, we show that even at higher "resolution" the data fits the curve of the DEH with only minor spread. From the figure it is clear that in the deeply supercooled region, the collapse is very tight, with little visible spread. Indeed, in the two regions immediately beneath melting, the data also falls along the universal curve with minimal spread, but what spread does exist, is likely due to the influence of the $\mathcal{PTEI}$ region discussed at length above. With this visual understanding of the accuracy of the DEH model in focus, we now move on to make objective, quantitative measures of said accuracy.

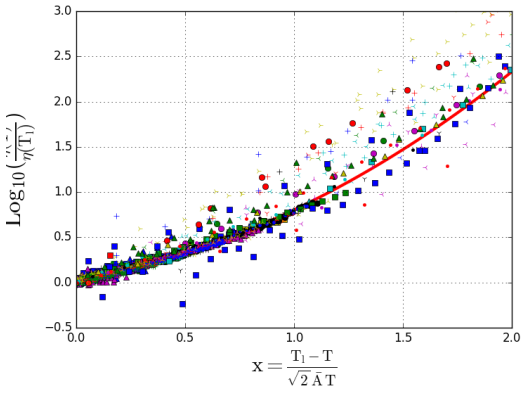


(a)

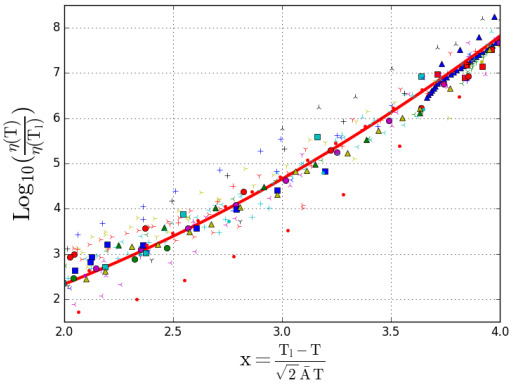


(b)

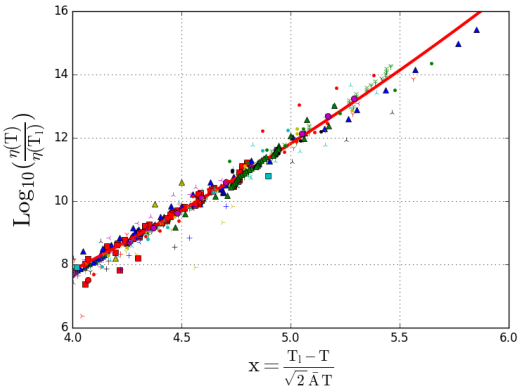


(c)

Figure 3.17: (Color Online.) Zoomed in version of the viscosity collapse data presented in Fig.(3.16). The data is presented in this way to demonstrate that the logarithmic form for the collapse is not masking or suppressing poor fits. Panel (3.17a) focuses on the data in the immediate vicinity of the liquidus temperature. Panel (3.17b) focuses on the mid temperature range. This region is the most sparse, as experimental data in this range is uncommon. Panel (3.17c) shows the lowest temperature region, where the DEH fit is the tightest, and alternative models typically have poorest performance.

## 3.6 What is $\bar{A}$?: The Physics of the Single DEH Parameter

### 3.6.1 Temperature Dependence of $\bar{\sigma}_T$

A major assumption of the DEH model is that the width, $\bar{\sigma}_T$, of the distribution of eigenstates has an approximately linear temperature dependence, i.e. $\frac{d\bar{\sigma}}{dT} = const \equiv \bar{A}$. As this notion is fundamental to the form of the viscosity function applied throughout this paper, it is imperative that the validity of this assumption be checked. Assuming that all other facets of the DEH model up to the assumption of the temperature dependence of $\bar{\sigma}$ are correct, Eq. (3.9) can be inverted to solve for the temperature dependence of $\bar{\sigma}_T$ using the experimental viscosity data. The results of this analysis for 12 various example liquids is presented in Figures (3.18) and (3.19). Examining the results in the figures makes clear that in most cases the assumption of linearity of the width is accurate over a wide range of temperatures. In some of the cases, such as many of the metallics, the seeming bend as $T_l$ is approached is likely due to the precarious limit that arises as the temperature approaches $T_l$ from below in the inverted expression for $\bar{\sigma}_T$. There are also cases where a clear crossover in the behavior of $\bar{\sigma}_T$ takes place at various temperatures. These anomalies may be linked to various kinetic crossovers or hypothesized phase transitions. Although the linear assumption is generally valid, in some cases it appears as though a nonzero intercept may improve the fit quality. This would introduce a second parameter, and only make marginal improvements in the fit quality. For these and other reasons, a zero intercept is assumed for all liquids.

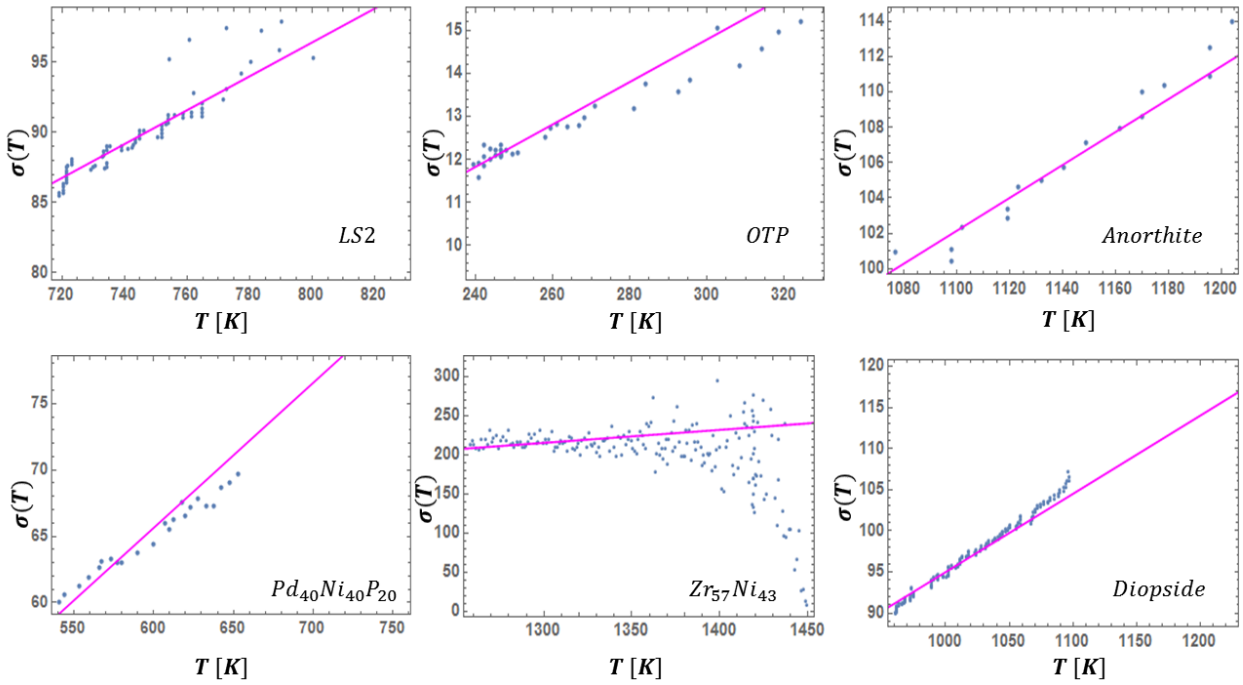


Figure 3.18: (Color Online.) Plot of $\bar{\sigma}_T$ as a function of $T$, found by inverting the expression in Eq.(3.9) and applying it to experimental data. The fit from the linear assumption is shown to work very well for most cases, especially at temperatures far below melting.

Having established in previous sections that the DEH model ably describes the behavior of supercooled liquids of all types with only a **single** fitting parameter, it is prudent to attempt to understand the physical meaning of $\bar{A}$. By definition, $\bar{A}$ governs the temperature dependence of the width of the distribution of eigenstates, which underlies the metastable features of the supercooled liquid. However, it is quite possible that it is linked to various thermodynamic or kinetic properties of the system. Uncovering any correlations between $\bar{A}$ and other physical quantities may help in increasing the understanding of both the DEH model and the glass transition itself. Additionally, finding a link between $\bar{A}$ and other measurable quantities may allow for the prediction of $\bar{A}$ and reduce the DEH model to a zero parameter theory. In what follows, we examine the relationship between $\bar{A}$ and certain physical observables, and find a number of interesting correlations.

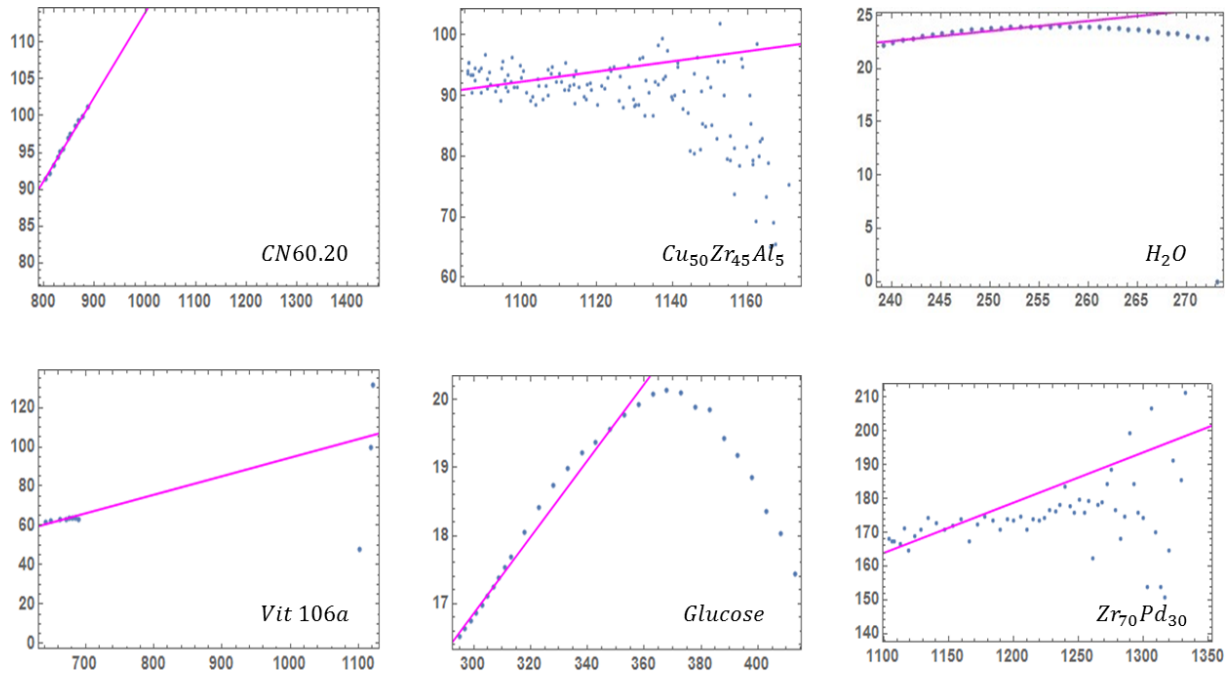


Figure 3.19: (Color Online). Additional examples of $\bar{\sigma}_T$ as a function of $T$. The linear fit well approximates most systems over much of the temperature range. Glucose displays anomalous behavior which is discussed in the Supplementary Information (S.1).

### 3.6.2 Fragility.

It is almost universally accepted that the concept of fragility in glass science is intimately linked to dynamics and structure in supercooled liquids, and not merely an artificial scaling property. Indeed, recent studies have shown that fragility can be related to the temperature dependence of the structure factors, and radial distribution functions upon supercooling, and therefore represents a measurable physical quantity of significance to glass theory (70). Therefore, we must briefly examine the nature of fragility in the DEH. We saw in Section III D that a fragility spectrum similar to Angell's classic plot (16) appeared quite naturally when scaling the viscosity and reciprocal temperatures about melting. We can take this further by using the definition of the fragility parameter, $m$, as outlined in (16). Using this definition and the functional form of the viscosity in the DEH (3.9), an explicit

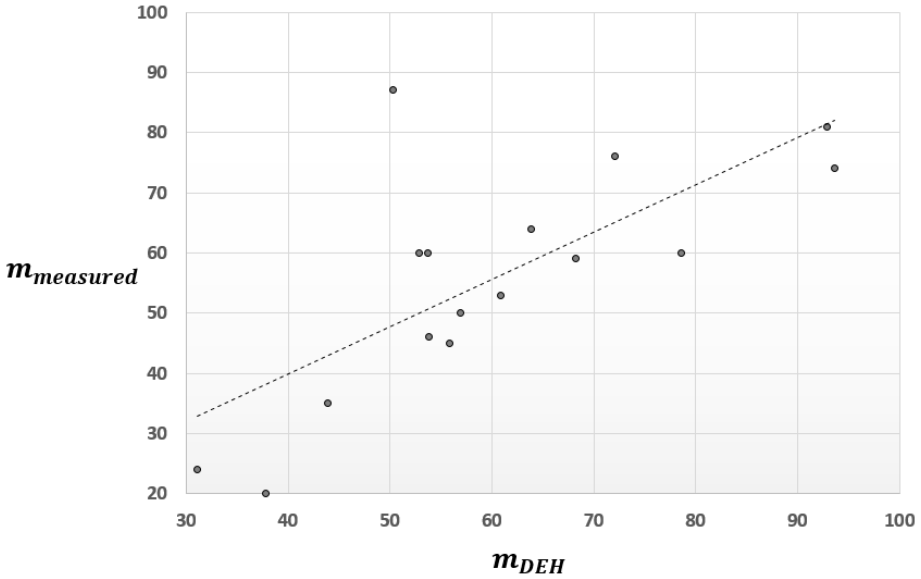


Figure 3.20: (Color Online.) Experimental values of the fragility, $m_{measured}$, versus the values computed ($m_{DEH}$) using Eq. (3.22). Overall, the correlation is strong, suggesting broad agreement between the DEH and experiment. However, the slope of the dashed line is not exactly equal to one, indicating a prefactor may be necessary, despite the strong correlation.

expression for the fragility can be derived within the DEH framework as

$$m \equiv \left.\frac{d\log_{10}\eta(T)}{d(T_g/T)}\right|_{T=T_g} = \frac{\sqrt{\frac{2}{\pi}}}{\ln(10)}\frac{T_l}{T_g}\frac{1}{\bar{A}}\frac{e^{-\left(\frac{\frac{T_l}{T_g}-1}{\sqrt{2}\bar{A}}\right)^2}}{\operatorname{erfc}\left[\frac{\frac{T_l}{T_g}-1}{\sqrt{2}\bar{A}}\right]}. \tag{3.22}$$

Strikingly, and perhaps surprisingly, the reduced temperature from the Turnbull criterion (71; 72) for glass forming ability (GFA), $T_{red} \equiv \frac{T_g}{T_l}$, appears throughout this expression. This provides further support to a link between fragility and GFA. We can calculate the values of the fragility using Eq. (3.22) and compare with the experimental values reported in (73; 61). The results of this comparison for a cross-section of the studied liquids are presented in Table (3.5) and in Figure (3.20). From Fig. (3.20), it is clear that there is a correlation between the predicted and experimental values of the fragility. The slope of the line of fit is not exactly equal to unity, but this may be related to differences in the measurement of $T_g$.

Table 3.5: Relevant Temperatures

| *Composition* | $T_l$ *[K]* | $T_g$ *[K]* | $m_{measured}$ | $m_{DEH}$ |
|---|---|---|---|---|
| BS2 | 1699 | 973 | N/A | 47 |
| Diopside | 1664 | 933 | 59 | 68 |
| LS2 | 1307 | 727 | 35 | 44 |
| OTP | 329 | 240 | 81 | 93 |
| Salol | 315 | 220 | 76 | 72 |
| Anorthite | 1823 | 1113 | 69 | 54 |
| $Zr_{57}Ni_{43}$ | 1450 | 722 | N/A | 33 |
| $Pd_{40}Ni_{40}P_{20}$ | 1030 | 560 | 50 | 57 |
| $Zr_{74}Rh_{26}$ | 1350 | 729 | N/A | 40 |
| $Pd_{77.5}Cu_6Si_{16.5}$ | 1058 | 632 | 64 | 64 |
| Albite | 1393 | 1087 | 24 | 31 |
| $Cu_{64}Zr_{36}$ | 1230 | 800 | N/A | 36 |
| $Ni_{34}Zr_{66}$ | 1283 | 760 | N/A | 24 |
| $Zr_{50}Cu_{48}Al_2$ | 1220 | 675 | N/A | 46 |
| $Ni_{62}Nb_{38}$ | 1483 | N/A | N/A | N/A |
| Vit106a | 1125 | 672 | 45 | 56 |
| $Cu_{55}Zr_{45}$ | 1193 | N/A | N/A | N/A |
| $H_2O$ | 273 | 136 | N/A | 100 |
| Glucose | 419 | N/A | 72 | N/A |
| Glycerol | 291 | 190 | 53 | 61 |
| $Ti_{40}Zr_{10}Cu_{30}Pd_{20}$ | 1280 | 687 | N/A | 41 |
| $Zr_{70}Pd_{30}$ | 1351 | N/A | N/A | N/A |
| $Zr_{80}Pt_{20}$ | 1364 | N/A | 45 | N/A |
| NS2 | 1147 | N/A | N/A | N/A |
| $Cu_{60}Zr_{20}Ti_{20}$ | 1125 | 647 | N/A | 106 |
| $Cu_{69}Zr_{31}$ | 1313 | N/A | N/A | N/A |
| $Cu_{46}Zr_{54}$ | 1198 | N/A | N/A | N/A |
| $Ni_{24}Zr_{76}$ | 1233 | 626 | N/A | N/A |
| $Cu_{50}Zr_{42.5}Ti_{7.5}$ | 1152 | 677 | N/A | 48 |
| D Fructose | 418 | N/A | N/A | N/A |
| NB1 | 472 | N/A | N/A | N/A |
| Selenium | 494 | 308 | 87 | 50 |
| CN60.40 | 1170 | N/A | N/A | N/A |
| CN60.20 | 1450 | N/A | N/A | N/A |
| $Pd_{82}Si_{18}$ | 1071 | N/A | 106 | N/A |
| $Cu_{50}Zr_{45}Al_5$ | 1173 | 701 | N/A | 71 |
| $Ti_{40}Zr_{10}Cu_{36}Pd_{14}$ | 1185 | 669 | N/A | 64 |
| $Cu_{50}Zr_{50}$ | 1226 | 651 | 60 | 53 |
| Isopropylbenzene | 177 | 126 | 74 | 94 |
| Butylbenzene | 185 | 128 | 60 | 79 |
| $Cu_{58}Zr_{42}$ | 1199 | N/A | N/A | N/A |
| Vit 1 | 937 | 625 | 54 | 46 |
| Trehalose | 473 | 380 | N/A | 54 |
| Sec-Butylbenzene | 190.3 | 127 | N/A | 102 |
| $SiO_2$ | 1873 | 1475 | 20 | 38 |

### 3.6.3 The Crossover Temperature $T_A$ and Structural Considerations

In the previous section we discussed the behavior of the fragility in the DEH framework. The fragility represents the degree of departure from Arrhenius behavior of the viscosity, and this deviation sets in at a crossover temperature, commonly known as $T_A$. It is natural to consider what meaning this crossover temperature will have within the DEH model, as the fragility appeared quite naturally in this framework. It is worth briefly outlining the general phenomenology of the crossover temperature, $T_A$, before proceeding. $T_A$ marks the temperature at which the super-Arrhenius growth of the viscosity sets in, the Stokes-Einstein relation breaks down, phonons delocalize, and cooperative motion of atoms/molecules/polymer chains in the liquid first begins (18; 74; 75; 76). The onset of the above phenomenon has been shown, in molecular dynamics simulations, to be correlated with the onset of structural changes associated with the formation, and subsequent percolation, of locally-preferred structures, which may or may not be subunits of the low temperature crystalline order (75; 76; 77). All of these features are associated with the metastable, supercooled liquid. It seems reasonable, then, that upon cooling, the temperature at which these phenomena onset corresponds to the temperature at which the eigenstate distribution first has appreciable weight in the solid-like eigenstates (50). At high enough temperatures, even a distribution of nonzero width will not have a tail that has weight in the solid-like states, so flow should not be uninhibited, and structures in the supercooled liquid should more-or-less be consistent with structures present in the equilibrium liquid. It is clear that as temperature is lowered, the distribution widens, and shifts to lower energy states. At a certain temperature, the distribution over eigenstates will begin to have appreciable weight in the solid-like states. Structural and dynamical properties of these solid-like states should then start to play a role in the behavior of the liquid. We postulate that the temperature at which this occurs should be identified as the crossover temperature, $T_A$. With this idea

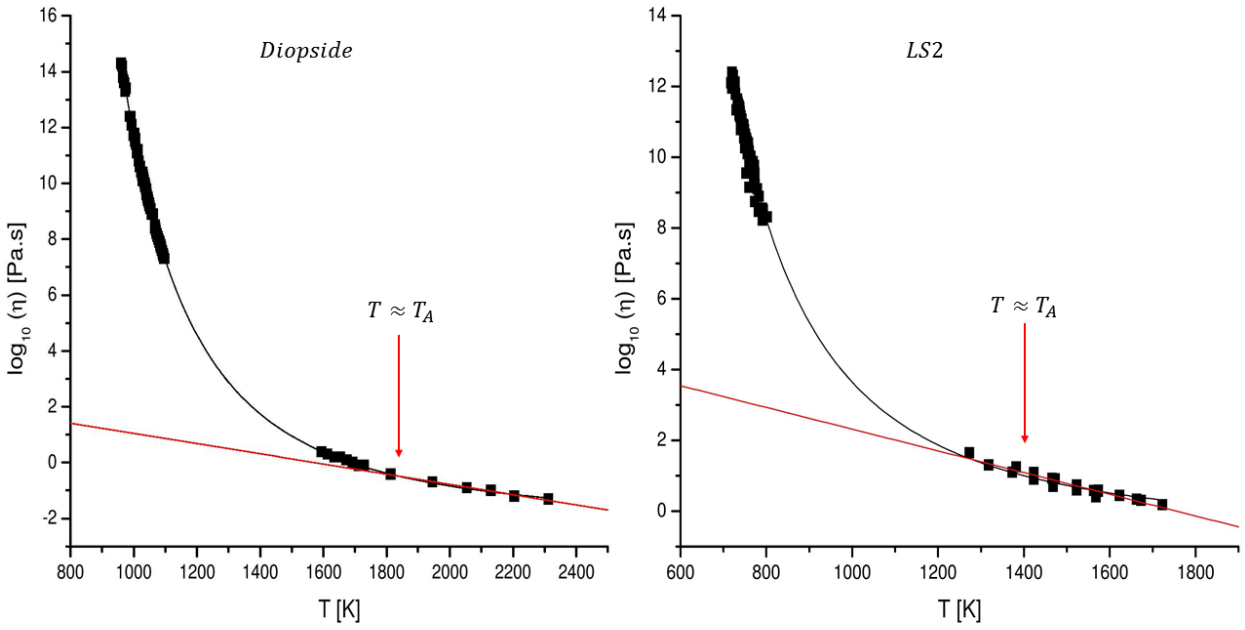


Figure 3.21: (Color Online). Log base-10 viscosity Data as a function of temperature for Diopside and LS2. The changeover from Arrhenius behavior appears to occur in the vicinity of 1900 K for diopside and 1450-1500 K for LS2, roughly agreeing with predicted values for the crossover temperature $T_A$.

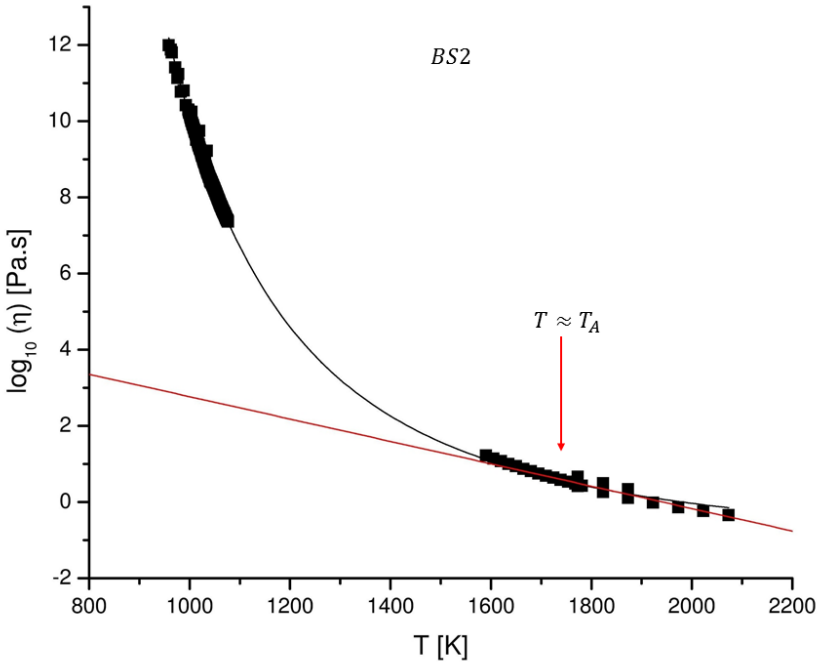


Figure 3.22: (Color Online.) Log base-10 viscosity data as a function of temperature for BS2. The changeover from Arrhenius behavior appears to occur in the vicinity of 1750 K. The predicted crossover temperature $T_A$ was 1911 K. This agrees to within roughly ten percent.

in mind, we can make a rough approximation as to how $T_A$ should relate to the distribution in the DEH model. Assuming that at $T_A$ the width first spans the 'distance' between the crossover temperature and the liquidus temperature, $T_l$ so as to have weight in the solid-like states, we can conjecture that at $T_A$ the $\bar{\sigma}_T$, namely, $\bar{\sigma}_T = \bar{A}T$, is such that it extends up to energy density at the melting temperature $T_l$, i.e.,

$$\bar{\sigma}_{T_A} \simeq \bar{A}(T_A - T_l). \tag{3.23}$$

This then yields (50),

$$T_A \simeq \frac{T_l}{1 - \bar{A}}. \tag{3.24}$$

Eq. (3.24) constitutes a rough approximation. The notion of 'appreciable weight' is rather

arbitrary and there may be a prefactor that is necessary, and perhaps material dependent, in Eq. (3.23) (this will be investigated in an upcoming work). Despite this, we can examine the predicted values for $T_A$. The values of $T_A$ that are predicted by Eq. (3.24) are listed in the Table (3.6). Previous studies of OTP and $Pd_{40}Ni_{40}P_{20}$ found $T_A$ values of approximately 350 K and 1157 K, respectively, which is in exceptional agreement with the values predicted from our approximation. Approximating $T_A$ from measured viscosity data is achieved by finding the temperature at which the viscosity ceases to be Arrhenius. In Fig. (3.21) we display the viscosity data for both Diopside and LS2. Visually, it appears that deviations from Arrhenius behavior onsets at about 1839 K and 1486 K, respectively. These values are in good agreement with those predicted from our approximation. It is worth noting, however, that Eq. (3.24) does not apply for all 45 liquids studied. Eq. (3.24) predicts a value of 1911 K for BS2, which is clearly too high in comparison to the crossover point in Fig. (3.22). A discrepancy in values was also observed in the case of $Pd_{77.5}Cu_6Si_{16.5}$. Overall, for a sample of the studied liquids where $T_A$ values are reported in literature [cite], we present the actual values versus predicted in Fig (3.23). We see a strong positive correlation. A more detailed investigation of the exact relation between $\bar{A}$ and $T_A$ is clearly necessary yet preliminary results are promising. The possible link between $\bar{A}$ and $T_A$ is significant not only because of the implications to the physics of the DEH model, but also because it may predict $\bar{A}$. Subsequently, this will enable the prediction of the viscosity in the entirety of the low temperature range, solely from high temperature data. This idea warrants more investigation, and further considerations for predicting $\bar{A}$ from high temperature data are discussed in Section S.1. It makes physical sense that having substantial weight of solid-like states for $T \leq T_A$ corresponds to the formation of locally preferred solid structures. The low-temperature locally preferred atomic structures would either be inherent to the equilibrium crystalline eigenstates, or result from the spatial mismatch of multiple crystalline ordered states in the distribution. In fact, the macroscopically disordered atomic arrangement of the glass logically results from overlap of multiple crystalline states of differing phonon

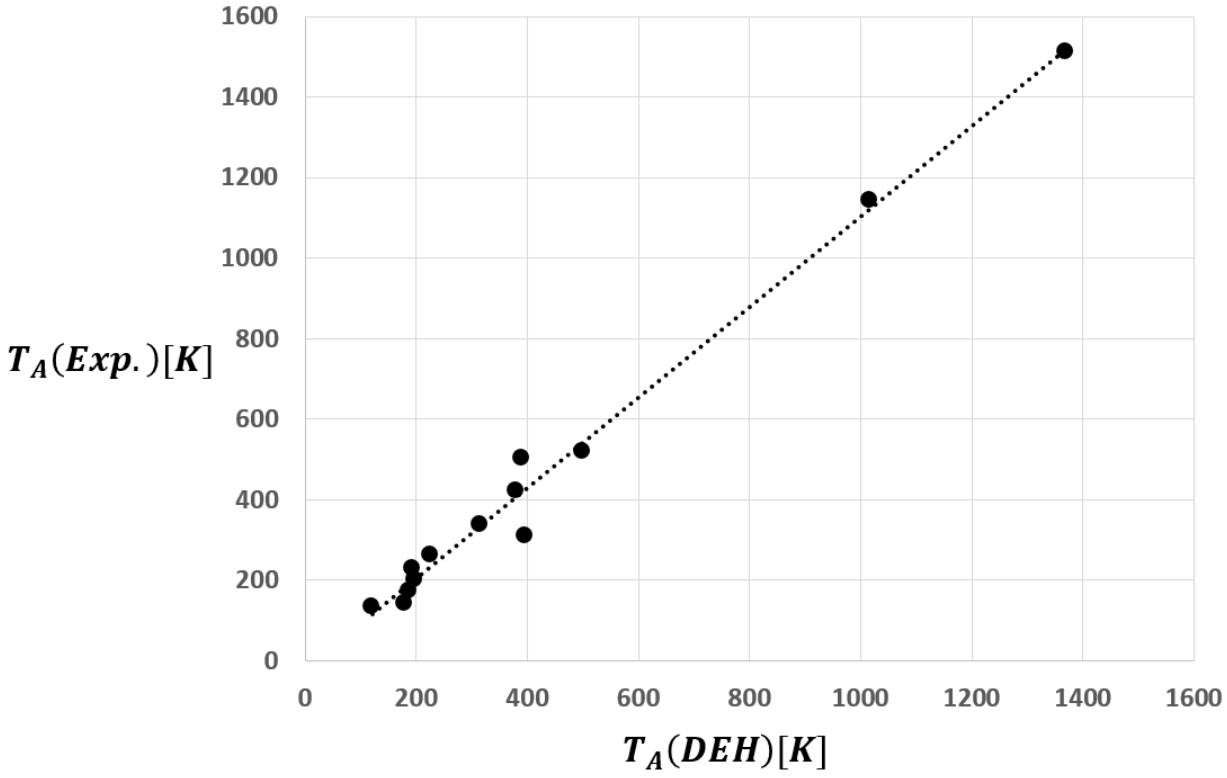


Figure 3.23: (Color Online.) Plot of the experimentally observed values of the Arrhenius crossover temperature $T_A$ versus the values of $T_A$ predicted within the DEH model for a sample of the liquids studied. A strong correlation is apparent.

Table 3.6: Predicted Values of Crossover Temperature, $T_A$

| *Composition* | $T_A$ *[K]* |
|---|---|
| BS2 | 1911 |
| Diopside | 1839 |
| LS2 | 1486 |
| OTP | 346 |
| Salol | 336 |
| Anorthite | 2010 |
| $Zr_{57}Ni_{43}$ | 1738 |
| $Pd_{40}Ni_{40}P_{20}$ | 1157 |
| $Zr_{74}Rh_{26}$ | 1557 |
| $Pd_{77.5}Cu_6Si_{16.5}$ | 1160 |
| Albite | 1503 |
| $Cu_{64}Zr_{36}$ | 1368 |
| $Ni_{34}Zr_{66}$ | 1506 |
| $Zr_{50}Cu_{48}Al_2$ | 1384 |
| $Ni_{62}Nb_{38}$ | 1607 |
| Vit106a | 1242 |
| $Cu_{55}Zr_{45}$ | 1329 |
| $H_2O$ | 302 |
| Glucose | 444 |
| Glycerol | 315 |
| $Ti_{40}Zr_{10}Cu_{30}Pd_{20}$ | 1472 |
| $Zr_{70}Pd_{30}$ | 1587 |
| $Zr_{80}Pt_{20}$ | 1549 |
| NS2 | 1268 |
| $Cu_{60}Zr_{20}Ti_{20}$ | 1214 |
| $Cu_{69}Zr_{31}$ | 1478 |
| $Cu_{46}Zr_{54}$ | 1348 |
| $Ni_{24}Zr_{76}$ | 1491 |
| $Cu_{50}Zr_{42.5}Ti_{7.5}$ | 1287 |
| D Fructose | 433 |
| TNB1 | 499 |
| Selenium | 544 |
| CN60.40 | 1308 |
| CN60.20 | 1637 |
| $Pd_{82}Si_{18}$ | 1186 |
| $Cu_{50}Zr_{45}Al_5$ | 1280 |
| $Ti_{40}Zr_{10}Cu_{36}Pd_{14}$ | 1313 |
| $Cu_{50}Zr_{50}$ | 1390 |
| Isopropylbenzene | 187 |
| Butylbenzene | 197 |
| $Cu_{58}Zr_{42}$ | 1322 |
| Vit 1 | 1017 |
| Trehalose | 498 |
| Sec-Butylbenzene | 202 |
| $SiO_2$ | 2002 |

modes and structural excitations. One can imagine cutting and superposing patches of elastically deformed lattice structures with given phonon modes associated with the relevant distribution of eigenstates. This would lead to the emergence of an overall 'amorphous' structural arrangement. At this stage, this is an unproven conjecture. As we alluded to above, numerous studies have shown that various crystal-like or polyhedral structures begin to form at this temperature, $T_A$ . e.g., (75; 76; 77). Further arguments based on uncertainties bolster these conclusions (50).

### 3.6.4 Correlation of $\bar{A}$ with Various Physical Quantities

It has been demonstrated that the parameter, $\bar{A}$, appears in expressions for the fragility and crossover temperature within the DEH framework. Additionally, it is seemingly apparent from the raw values of $\bar{A}$ presented in Table (3.2) that trends in the values may exist for similar liquid types. In light of these observations, it is reasonable to hypothesize that $\bar{A}$ may be linked to other macroscopic kinetic and thermodynamic properties of the supercooled liquid and glassy state. Toward this end, we investigated possible relationships between $\bar{A}$ and various physical properties that are relevant to the glass transition phenomenology. We begin by examining the possible relationship between $\bar{A}$ and two of the dynamical characteristics of glass forming liquids, namely the kinetic fragility parameter, $m$ (discussed in much more detail in Section VA), and the glass transition temperature, $T_g$. No direct discernible correlation was found with either quantity.

This is not so surprising, as the exact expression for the kinetic fragility which was derived in Section V:A contained multiple other factors. Turning now to thermodynamic variables, we examine the relationship between $\bar{A}$ and the liquidus temperature, $T_l$ and the reduced glass transition temperature, $T_r \equiv \frac{T_g}{T_l}$, defined by Turnbull (71). Panel (a) of Fig. (3.25) shows the behavior of $T_l$ versus $\bar{A}$. While there is no direct correlation between these

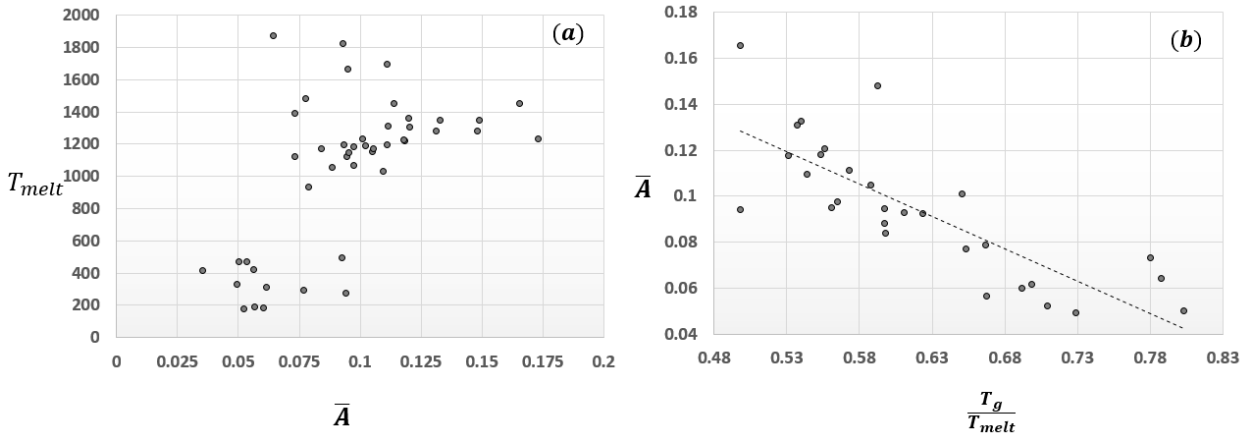


Figure 3.24: (Color Online.) Correlation of $\bar{A}$ with various physical quantities: (a) $T_l$ versus $\bar{A}$ and (b) $\bar{A}$ versus Turnbull's reduced temperature, $T_r \equiv \frac{T_l}{T_g}$. $\bar{A}$ is seen to have a strong correlation with $T_r$, possessing a correlation coefficient of $r \approx 0.88$.

two quantities, an interesting behavior does appear. There seems to be a 'jump' in the data such that liquidus temperatures below 600 K have values of $\bar{A} \leq 0.1$ and systems with liquidus temperatures greater than 800 K have values of $\bar{A}$ approximately $\geq 0.075$. The exact meaning of this behavior is unclear. The first real correlation appears when examining the relationship between $\bar{A}$ and $T_r$. It is evident from panel (b) of Fig. (3.25) that there exists a strong correlation between these quantities. Making this more quantitative, the value of the Pearson's correlation coefficient between $\bar{A}$ and $T_r$ was $r \approx 0.8$. This result is very interesting, and perhaps not surprising. In the years since Turnbull's original paper (71), the reduced glass transition temperature, $T_r$, has been used as a measure of glass forming ability in metallic liquids. The Turnbull temperature essentially quantifies how wide of a temperature range a liquid has to avoid crystallization. It is clear from our data, that higher levels of glass forming ability (GFA) correspond to smaller values of $\bar{A}$. This is consistent with the DEH framework. As the temperature is lowered, and the distribution over eigenstates shifts to lower energy states (the displacement of the distribution peak is governed by the heat capacity and is discussed in the next section).

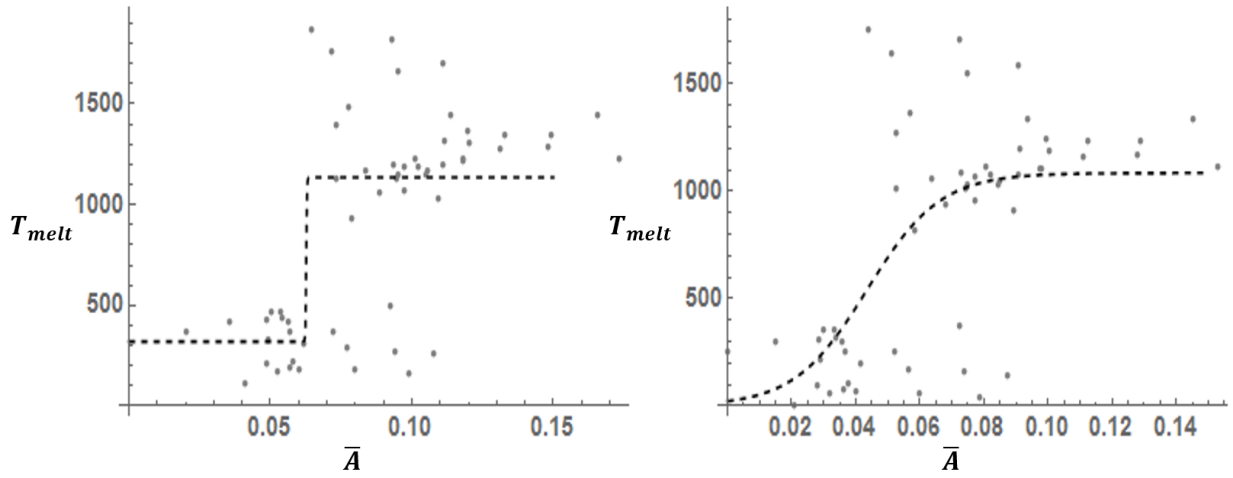


Figure 3.25: (Color Online.) $T_{melt}$ versus $\bar{A}$ with two fitting functions applied. In panel (a) the fit is of a Heaviside function, and panel (b) is a 'Fermi function'. The exact meaning of this result is unclear, but is evidence that perhaps $T_{melt}$ can be predicted from $\bar{A}$.

In addition to making good physical sense, and helping to facilitate an understanding of the physics underlying parameter, $\bar{A}$, this correlation may, in fact, allow for the prediction of the viscosity in the supercooled range. Using the equation of the linear fit in panel (b) of Eq. (3.25), $\bar{A} = 0.268 - 0.2806T_r$. This enables a calculation of $\bar{A}$ from $T_g$ and $T_l$. This, in turn, enables the prediction of the temperature dependence of the viscosity in the undercooled regime. Thus, if $T_g$ can be measured in a thermodynamic sense, through calorimetric measurements of the heat capacity or specific volume, then the kinetic properties of the system can be entirely determined up to some error. Additionally, this would also potentially allow for the prediction of the liquidus temperature (associated with the dominant crystal phase), if one were to replace the parameter $\bar{A}$ in the fitting function with the reduced temperature, and fit with $T_l$ as the parameter. Both of these predictive abilities would represent major advances for the field of supercooled liquids. For many of the metallic liquids studied, thermodynamic data related to the density and its temperature dependence were available at the liquidus temperature. We examined the correlation of $\bar{A}$ with the density at the liquidus, $p_{T=T_l}$, rate of change of density with temperature at the liquidus,

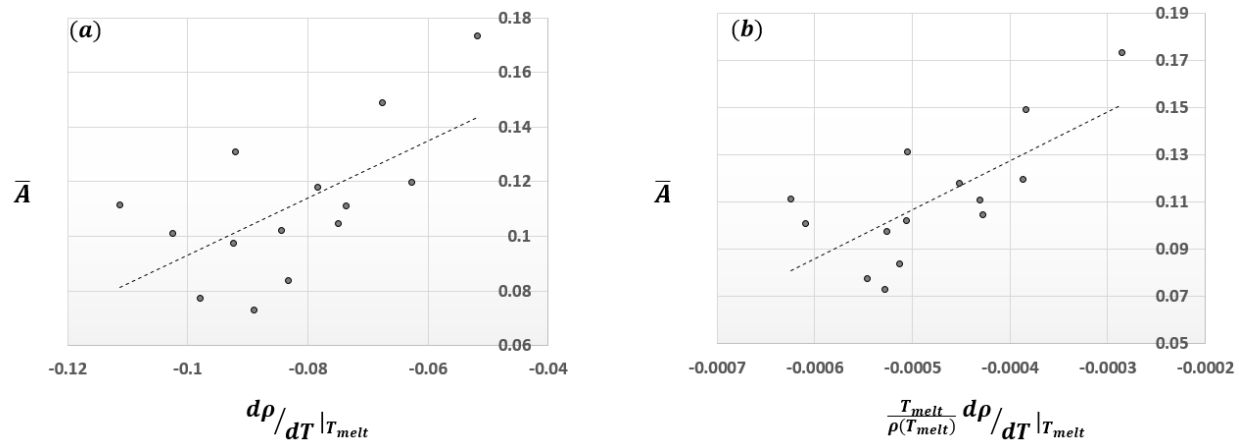


Figure 3.26: (Color Online.) Correlation of $\bar{A}$ with the rate of change of density at melting in both the (a) bare and (b) scaled cases. A positive correlation is apparent, which can be rationalized in the DEH framework.

$\frac{dp_T}{dT}|_{T_l}$, expansion coefficient at the liquidus, $\alpha(T_l)$, and the scaled rate of change of density with temperature at the liquidus, $\frac{T_l}{p_{T=T_l}}\frac{dp_T}{dT}|_{T_l}$ for 14 metallic glass forming liquids. We saw no discernible correlation with either the density or expansion coefficient evaluated at the liquidus. Correlations with the rates of change of density are presented in panels (a) and (b) of Fig. (3.26). From the figure, a quantifiable correlation between $\bar{A}$ and the rate of change of the number density, $p_T$ (both bare and scaled) at the melting temperature seems apparent. This result indicates that $\bar{A}$ may in fact be linked to equilibrium thermodynamic values. More strikingly, the rate of change of density at the melting point, is connected to both the nature of the potential for the given liquid, as well as the way the system 'jams' as it is cooled. This not only suggests that $\bar{A}$ is linked to the microstructural interactions, but also that it may be able to connect the DEH with other concepts such as free volume, unifying many of the theories of the glass transition under the DEH 'umbrella'. The DEH naturally rationalizes these, and many other experimentally observed trends. At a given temperature, $T$, a larger value of $\bar{A}$ means there is a wider distribution of states. If the equilibrium expansivity is temperature dependent (i.e. different for low and high energy eigenstates), then as temperature is varied, contributions from a broader range of these will

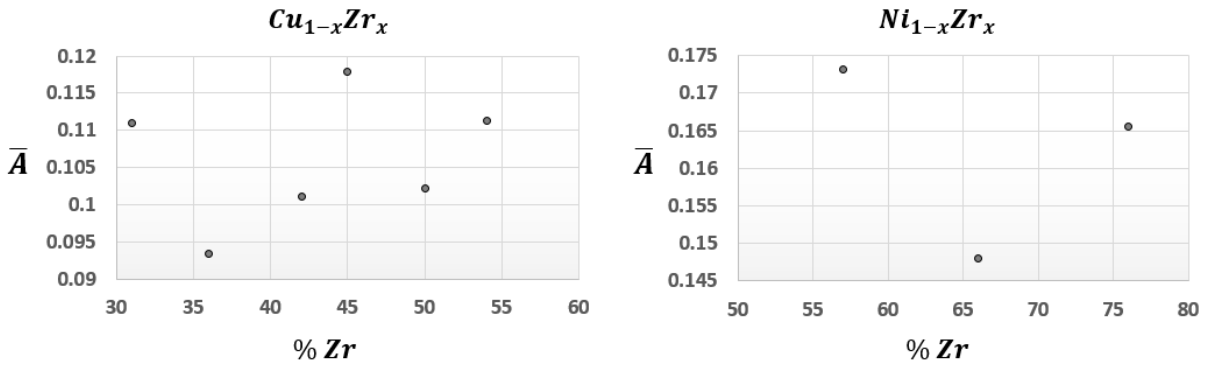


Figure 3.27: (Color Online.) Correlation of $\bar{A}$ with the zirconium content of the binary systems $Cu_{1-x}Zr_x$ and $Ni_{1-x}Zr_x$. The CuZr system has well defined peaks in the value of $\bar{A}$ where it has been shown the expansivity also has peaks.

lead to a greater rate of change of density, consistent with the observed results. Finally, it was demonstrated in (79) that the expansivity for a range of compositions in the $Cu_xZr_{1-x}$ system, possesses well defined local maxima at specific zirconium fractions. This intriguing result inspired us to analyze the behavior of $\bar{A}$ as a function of the zirconium fraction of supercooled metallic liquids in the $Cu_xZr_{1-x}$ and $Ni_xZr_{1-x}$ systems. These results are presented in Fig. (3.27). From the figure, it is apparent, and surprising, that $\bar{A}$ also seems to 'oscillate' with well defined local maxima at various zirconium fractions. Preliminary results suggest these maxima may occur at similar zirconium fractions as the results in (79) for the $Cu_xZr_{1-x}$ systems. The exact meaning of these results will be considered in a future work.

### 3.6.5 Prediction of $\eta(T)$ from High T Data

In Section 3.6.4, it was demonstrated that $\bar{A}$ showed a strong correlation with the reduced glass transition temperature, $T_r$. It was suggested that knowing the value of $T_g$ and $T_l$ would then allow for the prediction of $\bar{A}$ and consequentially, the viscosity of the supercooled liquid. It may seem dubious that it would be necessary to use the glass transition

temperature, which marks the lower limit of the supercooled regime, to predict the kinetics of the supercooled liquid. Additionally, it can be quite difficult to experimentally determine the value of $T_g$. By contrast, high temperature data, and associated features are often easier to measure in the laboratory. It would seem beneficial, then, to relate $\bar{A}$ to high temperature (melting and above) data. Recently,an empirical relationship between the glass transition temperature, $T_g$, and the high temperature activation energy, $E_\infty$, of the viscosity in the Arrhenius regime for metallic liquids was found (80). In that work, it was discovered that for all metallic liquids the relationship, $E_\infty \approx 11 k_B T_g$ holds. Taking advantage of this, as well as the equation of the linear fit, $\bar{A} = 0.268 - 0.2806 T_r$, resulting from the relationship displayed in panel (b) of Fig. (3.25), we can estimate the value of $\bar{A}$ for a metallic liquid within a bound associated with the average error in the fit. We applied this method to two metallic glass forming liquids, the results of which are depicted in Fig. (3.28). In the figure, the red (solid) curve represents the fit to the data associated with the fitting as described in Section II. The blue (dashed) and green (dotted) curves represent the fits associated with the values of $\bar{A}$ on both sides of the predicted boundary. It is clear that the blue curve does a reasonable job of predicting the viscosity of the supercooled liquid using purely high temperature data. The specific values of $\bar{A}$ predicted will depend on how tightly the relationship of (80) holds, as well as the sensitivity of the linear fit in the high temperature Arrhenius regime to the extraction of $E_\infty$. These results will need to be made more rigorous, but the preliminary results suggest that the viscosity of supercooled liquids can be predicted to reasonable accuracy using data which is more readily available than measuring the viscosity in the lab. These results will likely be of particular interest to researchers working in industry. To conclude this section, we point out that the relationship found in (80) also holds for organic/molecular liquids, and a similar relationship for network formers, $E_\infty \approx m k_B T$, with m, the fragility, was suggested. This result was not able to be verified here, but represents an exciting research opportunity and possible extension of the DEH.

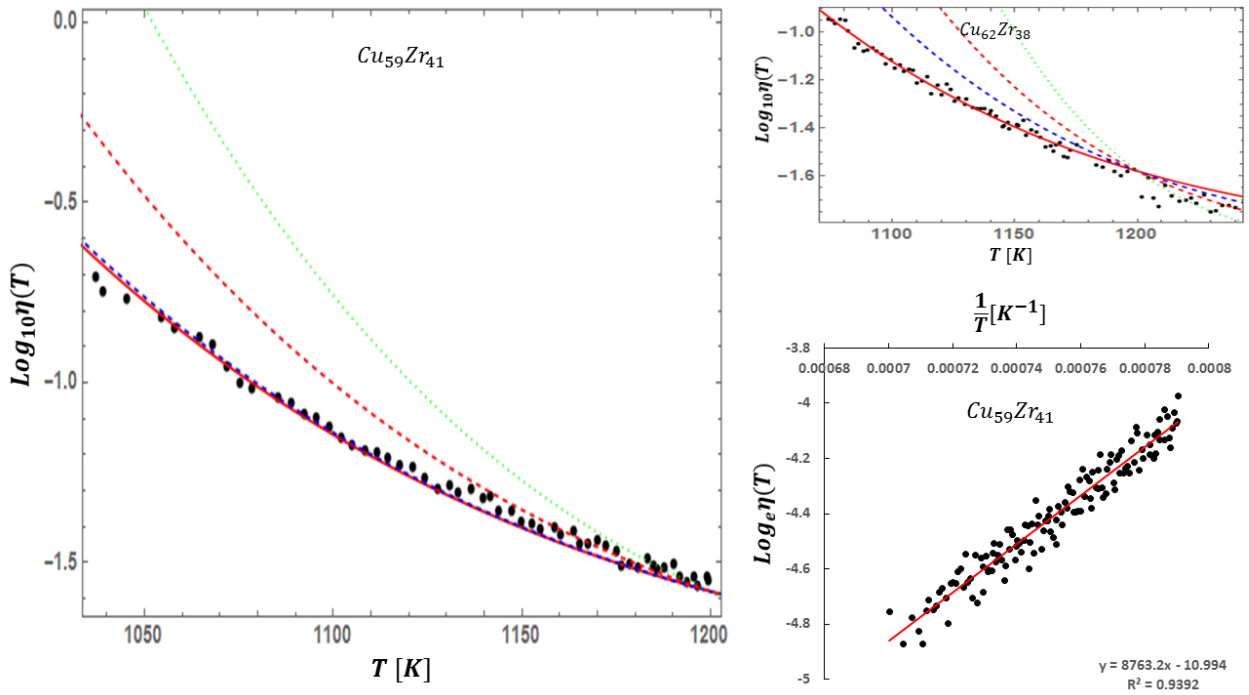


Figure 3.28: (Color Online.) Viscosity data for two metallic liquids with the DEH viscosity function, Eq. (3.9) (solid red curve) applied. Using the correlation found in Figure (3.26b) and the relationship between $E_\infty$ and $T_g$ discussed in Section VII, we predict the value of $\bar{A}$ from purely high temperature data as seen in the bottom right panel. The dashed, blue curve represents the fit using this predicted value. The green, dotted curve represents an 'upper bound' on the prediction by considering the average error in the correlation involving $\bar{A}$ and high temperature measurements, whereas the blue dashed curve is a lower bound using the same error. The central red dashed curve is the 'average' predicted value associated with the average value of $\bar{A}$. Overall, the blue curves are seen to do a fairly reasonable job representing the data at low temperatures using only high temperature measurements, but refinements are required.

## 3.7 The DEH Viscosity Above Melting

Until now, we focused on the viscosity of supercooled liquids below their liquidus temperature, $T_l$. In Section 3.4.4, we contrasted the DEH with a series of alternative models for the viscosity of supercooled liquids, ultimately concluding that the DEH model more accurately described experimental data, with fewer parameters. These alternative models, however, apply to the entire temperature range in which viscosity measurements can be made. Therefore, it is imperative that the DEH model be able to make statements about the viscosity above melting. In deriving the DEH expression for the viscosity (Eq. (3.9)), we began from the expression in Eq. (3.7). Using this expression and arguments laid out more concretely in (50), at temperatures above the liquidus, the viscosity is given by

$$\eta(T) = \frac{\tilde{\eta}}{\int_{T_l}^{\infty} C_v'(T')r'(T')p_T(E(T'))\ dT'}. \tag{3.25}$$

Here, $\tilde{\eta}$ is a constant, $C_v'$ is the constant volume heat capacity of the equilibrium liquid at a temperature $T'$, while $r'(\propto \exp(-\frac{\Delta G(T')}{k_B T'}))$, and $E'$ denote, respectively, the equilibrium relaxation rate and internal energy. As we have done earlier, we will, once again, invoke a Gaussian $p_T[E'(T')] \propto \exp(-\frac{(T'-T)^2}{2\bar{\sigma}_T^2})$. With these, Eq. (3.25) becomes

$$\eta(T) = \frac{\tilde{\eta}}{\int_{T_l}^{\infty} C_v'(T')e^{-\frac{\Delta G(T')}{k_B T'}}\frac{1}{\sqrt{2\pi\bar{\sigma}_T^2}}e^{-\frac{(T'-T)^2}{2\bar{\sigma}_T^2}}\ dT'}. \tag{3.26}$$

For $T$ close to yet above the liquidus temperature, the distribution $p_T(E(T'))$ can still be assumed to be localized to a narrow range of $T'$ about the temperature, $T$. In this narrow range, $C_v'(T')$ is essentially constant. As the system is supercooled, a temperature will eventually be reached where solid-like characteristics begin to set in. We have already met

such a temperature, the crossover temperature, $T_A$. The integrand vanishes approximately over a temperature range of order $\bar{\sigma}_T$ that is centered on $T \approx T_A$. When $\frac{\bar{\sigma}}{T} \ll 1$ (as is empirically the case), we may Taylor expand the heat capacity and free energy barrier about $T' = T$,

$$\begin{aligned} C_v'(T') \approx \quad & C_v'(T) + \frac{\partial C_v'}{\partial T'}(T' - T) + \cdots, \\ \Delta G(T') \approx \quad & \Delta G(T) + \frac{\partial \Delta G}{\partial T'}(T' - T) + \cdots \\ = \quad & \Delta H(T) - T\Delta S(T) \\ & + \frac{\partial \Delta H}{\partial T'}(T' - T) - T'\frac{\partial \Delta S}{\partial T}(T' - T) + \cdots . \end{aligned} \tag{3.27}$$

In Eq. (3.27), we used $\Delta G = \Delta H - T\Delta S$, where $H$ is the enthalpy (at a fixed volume, the enthalpy would be replaced by the internal energy $E$), and $S$ is the entropy of the equilibrated system at a temperature $T'$. Noting that $\frac{\partial \Delta H}{\partial T'} = C_p'(T')$ and $\frac{\partial \Delta S}{\partial T'} = C_v'(T')/T'$, and using the fact that we are working in the regime where $T \approx T_A$, we have

$$\begin{aligned} \Delta G(T') \approx \quad & (\Delta G(T) - \Delta G(T_A)) + \Delta H(T_A) - T\Delta S(T_A) \\ & + C_v'(T_A)(T' - T) - T\frac{C_p'(T_A)}{T}(T' - T) \\ & + \cdots . \end{aligned} \tag{3.28}$$

We recognize that $C_v'(T_A)(T' - T) - T\frac{C_p'(T_A)}{T}(T' - T) \approx (C_p'(T_A) - C_v'(T_A))(T' - T) = V(T_A)T_A\frac{\alpha(T_A)^2}{\beta(T_A)}(T' - T) \approx c_1(T' - T)$ (with $c_1$ a $T'$ independent constant). Here, $\alpha(T_A)$ and $\beta(T_A)$ are, respectively, the thermal expansion coefficient and the isothermal compressibility at $T_A$. Setting $\Delta G(T_A) \equiv E_\infty$, the viscosity becomes

$$\eta(T) \approx \frac{\tilde{\eta}\sqrt{2\pi\bar{\sigma}_T^2}}{C_v'(T)Ae^{-(\frac{\Delta G(T) - E_\infty}{k_B T_A})}\int_{T_l}^{\infty} e^{-c(T'-T) - \frac{E_\infty}{k_B T'} - \frac{(T'-T)^2}{2\bar{\sigma}_T^2}}\, dT'}. \tag{3.29}$$

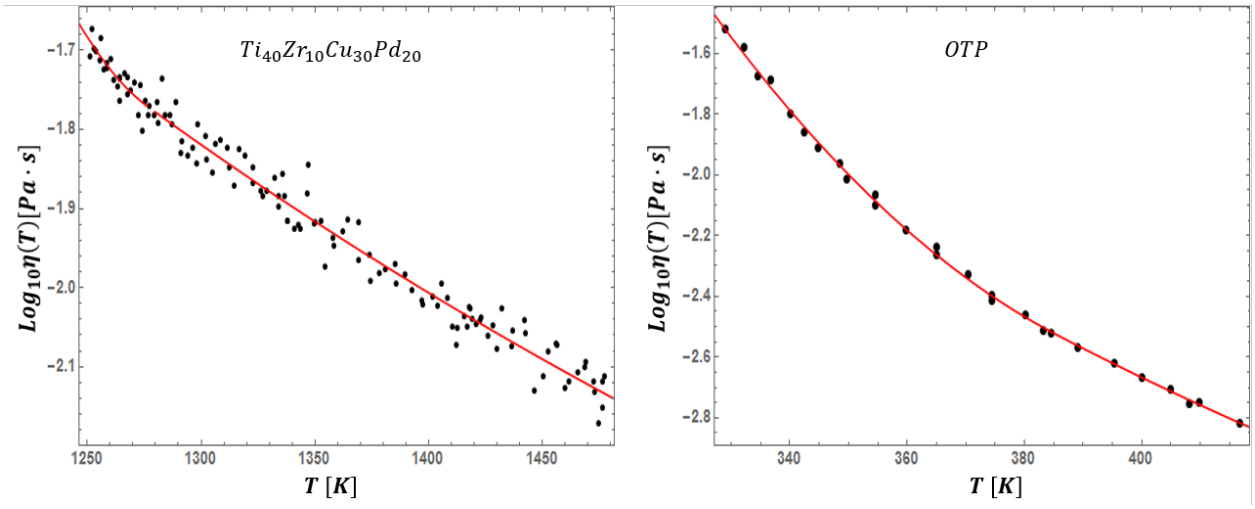


Figure 3.29: (Color Online.) The high temperature form for the DEH viscosity, Eq. (3.31) applied to experimental data of a metallic system ($Ti_{40}Zr_{10}Cu_{30}Pd_{20}$) and the archetypal organic fragile glass former (o-Terphenyl (OTP)).

In Eq. (3.29), $c = c_1 + c_2$ where $c_2 = (\Delta G(T) - E_\infty)/(k_B T_A^2)$. The Gaussian has its support in the narrow range of order $\mathcal{O}(\bar{\sigma}_T)$ about $T$, essentially forcing $T'$ to be close to $T$. If the three functions $\bar{\sigma}_T$, $C_v'(T)$, $\Delta G(T)$ do not vary significantly in the interval $[T_l, T_A]$, then for this range of temperatures, the viscosity

$$\eta(T) \approx \eta_0 e^{\frac{E_\infty}{k_B T}} e^{\frac{(T-T_A)^2}{2a^2}}, \tag{3.30}$$

where $a \equiv \bar{\sigma}_{T_A}$ and $\eta_0$ is a constant. In Eq. (3.30) we pulled out the Arrhenius factor of $e^{\frac{E_\infty}{k_B T}}$ (a factor that does not markedly change in the range $T_A > T > T_l$). This was done so that a trivial extension of Eq. (3.30) that we write below will be valid at temperatures $T > T_A$. Far above $T_l$, the equilibrium Arrhenius form of Eq. (3.1) follows from Eq. (3.25) when $\Delta G(T')$ is weakly temperature dependent (and essentially equal to $E_\infty$). Thus, putting all of the pieces together, the viscosity for temperatures $T > T_l$ is, approximately,

$$\begin{aligned} \eta(T) &\approx \eta_0 e^{\frac{E_\infty}{k_B T}} e^{\frac{(T-T_A)^2}{2a^2}\Theta(T_A - T)} \\ &\equiv \eta_{equilibrium}(T) e^{\frac{(T-T_A)^2}{2a^2}\Theta(T_A - T)}. \end{aligned} \tag{3.31}$$

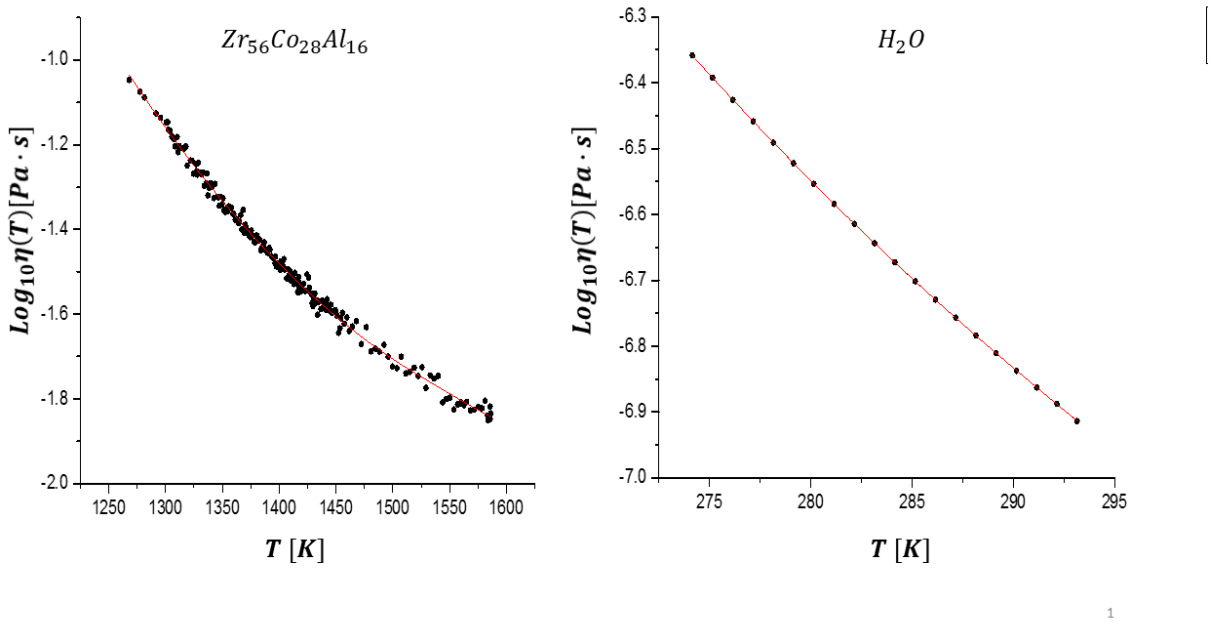


Figure 3.30: (Color Online.) The high temperature form for the DEH viscosity, Eq. (3.31) applied to experimental data of a metallic system ($Zr_{56}Co_{28}Al_{16}$) and supercooled water.

Similar to Eqs. (3.14, 3.16), we explicitly inserted the Heaviside function $\Theta(x)$ that enables a crossover to the high temperature (Arrhenius) equilibrium form of the viscosity. We see, then, that the supercooled viscosity below $T_A$ is equal to the viscosity of the equilibrium liquid that is multiplied (and increased) by the reciprocal of a Gaussian This is reasonable since for temperatures below $T_A$, the weight $P_T(E')$ associated with the solid-like states (those states with energies $E' < E_{melt}$, the internal energy of the system at melting) will increase and the associated probability of a flow event will, correspondingly, decrease (and thus the viscosity will increase).

It is worth pointing out that Eq. (3.31) bears a striking resemblance to the BENK form (61) of Eq. (3.16) and the earlier associated parabolic fits of (55; 60). Our derived viscosity of Eq. (3.31) is exponential in a quadratic form in $T$ instead of $(1/T)$ as appears in (55; 60; 61). In these previous works, the parabolic functional form was presented without a theoretical framework justifying it. Here we directly derived Eq. (3.31) within the DEH theory. Since

the erfc appearing in Eq. (3.9) leads to an asymptotic Gaussian at low temperature (50) and as at temperatures above the melting temperatures, we find the Gaussian form of Eq. (3.31), we conclude that the pure Gaussian form appears in both the high and low temperature regimes of the DEH in a very physical manner. An added benefit of this form is that it holds down to $T_l$, and therefore, will allow for estimation of $\eta(T_l)$ if such a value is not available. This makes using the form of Eq. (3.9) easier, without having to do an interpolation.

Finally, we briefly demonstrate the quality of fit of Eq. (3.31) to experimental data. Fig. (3.29) shows the viscosity data for both $Ti_{40}Zr_{10}Cu_{30}Pd_{20}$ and OTP with Eq. (3.31) fit to the high temperature data. We leave all four parameters open, but note that we can easily constrain $E_\infty$ and $\eta_0$ with very high temperature data. This process can be volatile and prone to error with outliers from bad experimental data, so in this brief study we allow all parameters to be open. We see that the fit to $Ti_{40}Zr_{10}Cu_{30}Pd_{20}$ has $R^2 = 0.9776$ and $\chi^2_{reduced} = 0.00219$ and OTP has $R^2 = 0.99879$ and $\chi^2_{reduced} = 0.00111$, both indicating statistically good fits. The predicted value of $T_A$ (1276-1286K and 386K, respectively) are reasonable, and the values for $a$, are such that $\frac{a}{T_A} << 1$, as assumed.

## 3.8 Dynamical Heterogeneities

The super-Arrhenius temperature dependence of the viscosity, or relaxation time, of supercooled liquids is one of the two defining kinetic characteristics of glassy behavior. The other is the existence of non-exponential relaxation of perturbations/fluctuations. In ordinary, equilibrium liquids, the linearity of the physical equations and processes underlying the approach to equilibrium lead to perturbative responses decaying exponentially with a timescale set by the appropriate relaxation time of the system at a given temperature. In supercooled liquids, it is widely observed that relaxation processes are not exponential, and

are instead reasonably described by a stretched exponential or so-called KWW function,

$$\phi(t) = \phi_0 e^{-(\frac{t}{\tau})^\beta} \tag{3.32}$$

where $\phi$ is the relaxation function and $\beta$ is the stretching exponent. The value of $\beta$ is between zero and one, with $\beta = 1$ corresponding to simple exponential relaxation. The commonly held view of the physics underlying the non-exponential relaxation of the supercooled liquid is that there is a spatial *distribution* of relaxation times throughout the liquid, and this is referred to as dynamical heterogeneity. Essentially, at any given moment, the liquid is comprised of various dynamic regions, or clusters, each relaxing at their own rate, with relaxation times distributed about the observed overall system relaxation time. Within these clusters, MD results have shown that the relaxation process is exponential. Therefore, the overall relaxation of the liquid as a whole, which is a simple spatial average of all of the relaxing dynamic clusters, will be the integral of relaxation functions weighted by some distribution function, ie,

$$\phi_{total}(t) = \int d\vec{x}\ \Phi(\tau(\vec{x}))\ e^{-t/\tau(\vec{x})}. \tag{3.33}$$

The metastability of supercooled liquids requires that they retain their ergodicity, and thus, over long times all particles in the liquid at one point belong to both fast and slow clusters. The major consequence of this is that spatial averages are equal to ensemble averages, and thus the overall relaxation can be found from typical statistical mechanics techniques. Numerous studies have been conducted which aim to work backwards from relaxation data to uncover the distribution of relaxation times, and distributions such as skew-normal, lognormal, truncated normal, and more (106) have been observed. Given these findings, and the above discussion of the theory of a distribution of relaxation times, it seems that the DEH model must quite naturally explain non-exponential relaxation, as it inherently

contains distributions over states. It seems prudent, then, to test this, by examining what the relaxation function would look like in the DEH framework. The relaxation function of a supercooled liquid can be defined in any number of ways and in terms of any number of different correlation functions. One such prevalent example, is that of the normalized intermediate scattering function,

$$F(\vec{k},t) \equiv \langle \rho_{-\vec{k}}(0)\rho_{\vec{k}}(t)\rangle_T. \tag{3.34}$$

This function is the Fourier transform of the Van Hove function, and quantifies the temporal decay of density fluctuations in the liquid in k-space. The intermediate scattering function is a spatial average over the liquid, but as discussed above,it is equal to a corresponding ensemble average, and as an ensemble averaged quantity, it can be computed within the DEH framework in the usual way, by integrating its value at a given temperature over the DEH distribution. In this way, the intermediate scattering function for the supercooled liquid would be,

$$F_{s.c.}(\vec{k},t) = \int_0^\infty C_v(T')\ dT' p_T(T') \langle \rho_{-\vec{k}}(0)\rho_{\vec{k}}(t)\rangle_{T'}. \tag{3.35}$$

As discussed, the individual clusters relax exponentially, and so too, do the equilibrium thermal states of the system, so we can make the approximation that

$$\langle \rho_{-\vec{k}}(0)\rho_{\vec{k}}(t)\rangle_T \approx f(\vec{k}) e^{-\frac{t}{\tau(T)}}, \tag{3.36}$$

where $f(\vec{k})$ is a function of the wavevector alone. We can further assume that the *corresponding equilibrium relaxation time in each equilibrium state maintains an Arrhenius temperature dependence*, and use the experimentally observed fact that the relaxation time

of perfect equilibrium crystals is infinite. Taken together, this leads to the assumptions,

$$\begin{aligned} \tau(T) &\to \infty \qquad T < T_l \\ \tau(T) &= \tau_0 e^{\frac{E_\infty}{k_B T}} \qquad T \geq T_l. \end{aligned} \tag{3.37}$$

and thus the overall form for the relaxation function in the supercooled liquid in this model is

$$\begin{aligned} F_{s.c.}(\vec{k},t) = & \int_0^{T_l} C_v(T')\ dT' p_T(T') \\ + & \ f(\vec{k}) \int_{T_l}^{\infty} C_v(T')\ dT' p_T(T') e^{-\frac{t}{\tau(T')}}. \end{aligned} \tag{3.38}$$

After carrying out the first two integrals, this can be simplified to

$$\begin{aligned} F_{s.c.}(\vec{k},t) = & \ erf\left[\tfrac{T_l - T}{\sqrt{2}\bar{A}T}\right] - erf\left[-\tfrac{1}{\sqrt{2}\bar{A}}\right] \\ + & \ f(\vec{k}) \int_{T_l}^{\infty} C_v(T')\ dT' p_T(T') e^{-\frac{t}{\tau(T')}}. \end{aligned} \tag{3.39}$$

The error function terms contain no time dependence and will only scale the relaxation function up and down the y-axis as a function of temperature, so we focus only on the remaining integral part of the equation. Recalling that the relaxation function is defined as the intermediate scattering function normalized by its value at t=0, we assert

$$\phi(t) \approx \int_{T_l}^{\infty} C_v(T')\ dT' p_T(T') e^{-\frac{t}{\tau(T')}} \tag{3.40}$$

where $\phi(t)$ is the relaxation function. At this point, we must point out that relaxation function in supercooled liquids does not just simply follow a stretched exponential time dependence, but is also, in fact, multi-stepped. It is typically observed that supercooled liquids first undergo a fast relaxation mode, deemed $\beta$-relaxation, which is usually exponential and corresponds to vibrational relaxation. The liquid then enters a 'plateau' in

the relaxation function at which point the particles in the liquid are confined to vibrations in cages of other atoms, before finally undergoing the stretched exponential relaxation with the observed, super-Arrhenius, relaxation time, in a process called the $\alpha$-relaxation mode. Beta relaxation will not appear in this function, as in the DEH model, it is hypothesized that the beta relaxation corresponds to the time to come to steady-state, in which the distribution takes it's Gaussian form. What we mean by this is that when the system is rapidly quenched to a given temperature, the initial shock leads to the system not yet being in a metastable equilibrium, and possessing energy flows throughout the liquid. After a given time, the $\beta$-relaxation time, the flows will have reached a steady state, and a well defined spatial effective temperature distribution will have set in in the liquid. This distribution corresponds to our phase space distribution, and therefore, the initial relaxation is concerned with reaching the Gaussian distribution of the DEH. Therefore, while the beta relaxation has a natural understanding in this framework, it will have to be considered separately, and the alpha relaxation will be what appears in the relaxation function in the equation above. We test this expression for an example system, to see if exponential stretching does indeed appear in the DEH framework. For this example, we take the case of toluene whose high temperature Arrhenius behavior has been observed to be $\tau(T) = 5.67 * 10^{-14} e^{\frac{1367}{T}}$, with a liquidus temperature $T_l$=178K. Inserting these values into Eq.(3.40) for various representative temperatures both above, and below the liquidus, lead to results which showed little to no stretching in the relaxation. This result is easy to understand, as we don't consider any relaxation time values between the value at the liquidus and infinity in the above expression. In almost all cases, where the relaxation time distribution was found experimentally, it was observed that the distribution was nonzero at all values of $\tau$ from some lower cutoff to infinity. The solution to this problem comes from properly considering the $\mathcal{PTEI}$. Within the $\mathcal{PTEI}$ the energy states which contain all possibles mixtures of liquid and crystal structures, will possess a large range of relaxation times that *continuously* evolve from the value at the liquidus to infinity as the energy is lowered to the bottom

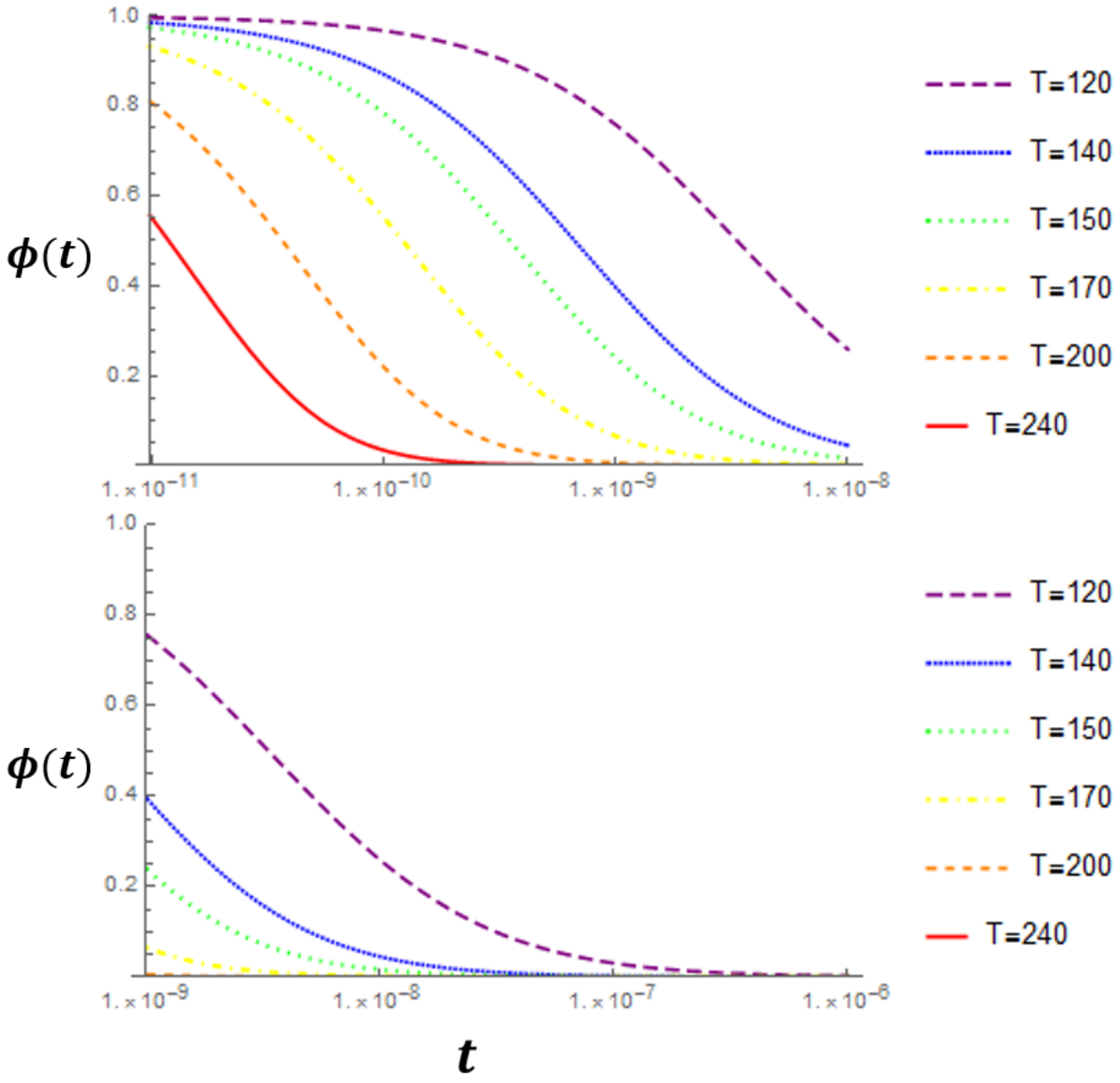


Figure 3.31: (Color Online.) Predicted DEH relaxation function for toluene at various temperatures above and beneath the liquidus. A degree of stretching is apparent.

of the interval. This range of relaxation times will result from the continuous evolution of ever-increasing amounts of solid-like regions until the liquid reaches the bottom of the interval. The corresponding weights should rapidly decrease into the lower relaxation time values which correspond to higher energies, and the Gaussian form assumed in the DEH will deliver this effect. The exact functional dependence of the relaxation time on energy in the $\mathcal{PTEI}$ is a priori unknown, and it is possible that the behavior of $\sigma(E)$ could be different from linear in this region as well.Therefore, to observe the impact of properly considering the $\mathcal{PTEI}$ we can choose some physically meaningful form for the dependence of $\tau(E)$ and add the $\mathcal{PTEI}$ term to the expression in Eq. (3.40). We choose to continue the Arrhenius form, and integrate across all temperatures from zero to infinity to approximate the weighted consideration of the energies in the interval. This is an acceptable means of approximating the behavior, as the entirety of the temperature range with an Arrhenius dependence of the relaxation time will be equivalent to sampling all relaxation times in the $\mathcal{PTEI}$ as they map to each other. The results are shown in Fig (3.31). A considerable amount of exponential stretching is observed, making clear that the DEH naturally explains dynamic heterogeneity and stretching. While convincing, this can be made more concrete by making a simple change of variables. This transformation from energy dependence to $\tau$ dependence via a simple change of variables *guarantees* that the DEH form should align with the $\tau$ distributions observed experimentally. By making the simple change of variables assuming an Arrhenius relationship between the energy and relaxation time, we arrive at

$$\phi(t) = k_B T \int \frac{d\tau}{\tau} e^{-\frac{(k_B T)^2}{2}\left(\frac{ln(\tau)-ln(\tau')}{\sigma_E}\right)^2} e^{-\frac{t}{\tau}} \tag{3.41}$$

as an equivalent expression for the relaxation function. We immediately see that something resembling a log normal distribution naturally appeared within the DEH framework, and therefore, agreement with experimental results is roughly observed.

Before concluding this section, it must be mentioned that in addition to the observation of dynamical heterogeneity, it is also observed that there is a corresponding dynamical heterogeneity lengthscale, $\xi_D$, which gives the typical length of the dynamical clusters. Additionally, this lengthscale is observed to increase with supercooling. It is natural to inquire as to whether the existence and growth of $\xi_D$ can be explained in the DEH, and while a rigorous derivation is beyond the scope of this paper, we will briefly remark on a likely explanation. It is observed that in equilibrium liquids the dymamics of the constituent particles is largely uncorrelated, with maximum correlation lengths only slightly larger than an atomic diameter. In crystals, however, it has been observed that the dynamics are correlated over much larger distances, which have some relationships to the phonon spectra (114). It is not unreasonable to argue, then, that the distribution having weight in crystal and liquid states, will have some average of the properties, and as the system cools and has more weight in the crystal states and less in the liquid, it will pick up more of the correlation associated with those crystal states, thus growing the length over which the dynamics are correlated in the supercooled liquid. This rather simple cartoon description makes clear that it is indeed possible to describe the dynamic heterogeneity lengthscale in this framework, although we don't undertake it here.

## 3.9 Thermodynamic Considerations

### 3.9.1 Free Energies and Response Functions

Heretofore we have focused solely on dynamical quantities within the DEH framework, such as the viscosity, relaxation time, and relaxation function, but the nature of the DEH model is such that it applies to thermodynamic quantities as well as well as dynamical ones. Indeed, a principle facet of the DEH is that the **same distribution** should apply to all values

of physical observables in the supercooled state, both dynamic and thermodynamic. An example of this was already encountered in motivating the Gaussian form for the distribution of energies. The second characteristic listed in Section 3.3.2 that the distribution must obey was that

$$U_{s.c} = \int dE' p_T(E')\ \bar{E}', \tag{3.42}$$

with over bars denoting equilibrium ensemble average values. Therefore, the average energy over all states sampled by the distribution must be equivalent to the observed supercooled energy of the liquid. This was not only a reasonable constraint, but a necessary one if the thermodynamics of the model are to have any meaning. This notion, then, naturally extends to any quantity which corresponds to an ensemble average in ordinary statistical mechanics, as the average value at a given energy can then be integrated with the DEH distribution to give the supercooled average, such that

$$O_{s.c.}(E) = \int dE' p_T(E')\ \bar{O}(E'), \tag{3.43}$$

where $O$ is any thermodynamic observable. Typically, observables are not measured as a function of energy, but as a function of temperature. Therefore, like we did in the case of the viscosity, we convert to functions of temperature by assuming $E \approx CT$, such that observable averages become,

$$O_{s.c.}(T) = \int dT'\ C_v(T')\ p_T(T')\ \bar{O}(T'). \tag{3.44}$$

In general, when converting from integration over the energies to corresponding temperatures, one must use the heat capacity as a conversion factor as the energy and temperature are related via it. We have included that in Eq. (3.42), but will leave it out going forward, as the distribution gets a reciprocal heat capacity in converting from a

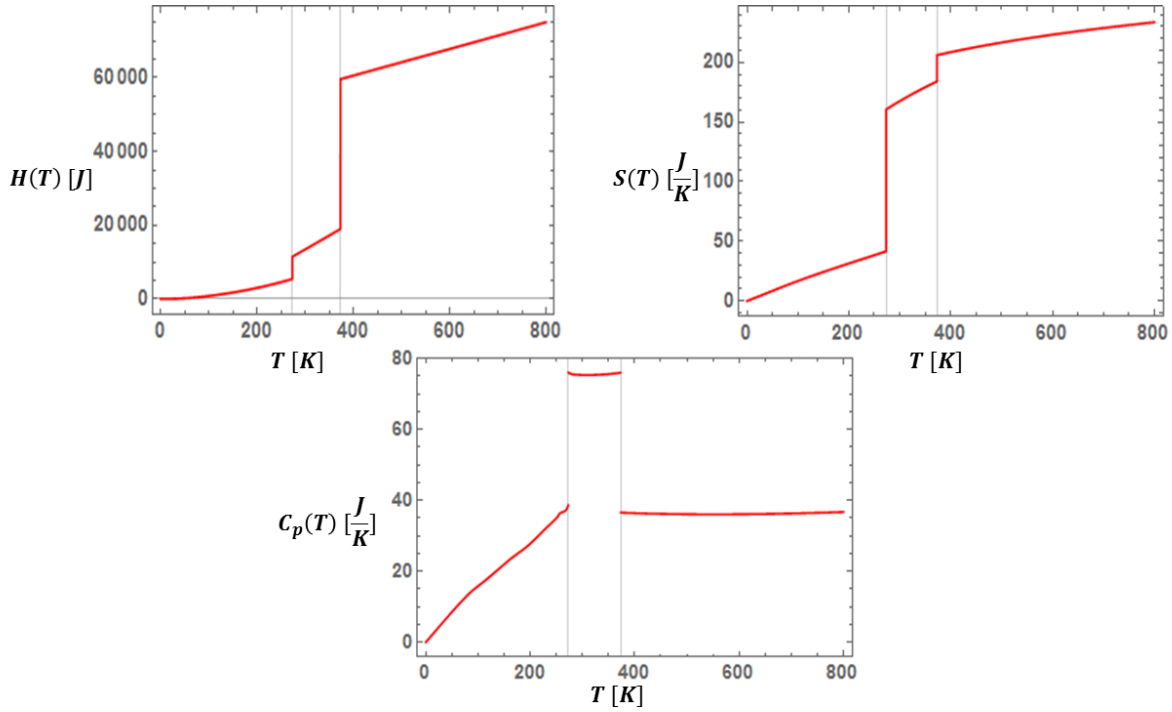


Figure 3.32: (Color Online.) Enthalpy, entropy, and heat capacity functions for equilibrium water at all temperatures based on interpolation/extrapolation of experimentally measured values.

function of energy to temperature, associated with the conversion of $\sigma_E$. Additionally, it is important to point out that only quantities which correspond to ensemble averages can be averaged over again with the DEH distribution; response functions such as heat capacities and susceptibilities cannot, as the equilibrium values do not correspond to ensemble averaged state variables, but derivatives of them. Therefore, to compute the form of response functions in the supercooled state, one must first compute the corresponding state variable in the DEH supercooled regime, and then take the appropriate derivative. For instance, the enthalpy in equilibrated systems is $H = \bar{E} + P\bar{V}$, so the enthalpy in the supercooled liquid will be given by

$$\begin{aligned} H_{s.c.}(T) &= \int dT' \; p_T(T') \; [\bar{E}(T') + P\bar{V}(T')] \\ &= \int dT' \; p_T(T') \; \bar{H}(T'), \end{aligned} \tag{3.45}$$

and the supercooled liquid heat capacity (at constant pressure) would be given by

$$C_{p,s.c.} = (\frac{\partial H_{s.c}}{\partial T})_p$$
$$= \frac{\partial}{\partial T} \int dT' \; p_T(T') \; \bar{H}(T'). \tag{3.46}$$

In calculating the heat capacity using the above expression, only $p_T(T')$ contains the variable $T$, and therefore the derivative will only act on the distribution, leading to the expression for the supercooled heat capacity in the DEH framework (see SI for derivation),

$$\begin{aligned} C_{p,s.c} = & -\frac{1}{T} \int dT' p_T(T') \; \bar{H}(T') \\ & -\frac{1}{\bar{A}^2 T^3} \int dT' \; p_T(T') T' \; \bar{H}(T') \\ & +\frac{1}{\bar{A}^2 T^4} \int dT' \; p_T(T') T'^2 \; \bar{H}(T') \end{aligned} \tag{3.47}$$

To calculate the entropy and other free energies in the supercooled liquid, one need only follow standard thermodynamic procedure, and utilize the computed heat capacity. $C_{p,s.c}$ can be integrated to calculate both the entropy and enthalpy of the supercooled liquid, and to test these expressions, we use the heat capacity data of an example system, namely $H_2O$ in the ice (109), water (110), and vapor (110) phases. We begin by using experimental equilibrium heat capacity data (at constant pressure) to interpolate the equilibrium enthalpy and entropy at all temperatures. These values for the heat capacity, enthalpy, and entropy of this system are shown in Fig. (3.32). The values for the heat capacity, enthalpy, and entropy in the supercooled state as calculated using the above equations and equilibrium data are depicted in Fig. (3.33). Examination of the calculated enthalpy, entropy, and heat capacity in the supercooled liquid reveals that the functions possess the correct form as observed in experiments, but with crossovers at temperatures higher than observed experimentally, and with 'gaps' or small 'jumps' at the liquidus temperature, which are not observed experimentally. In supercooled liquids, it is typically observed that the enthalpy does not

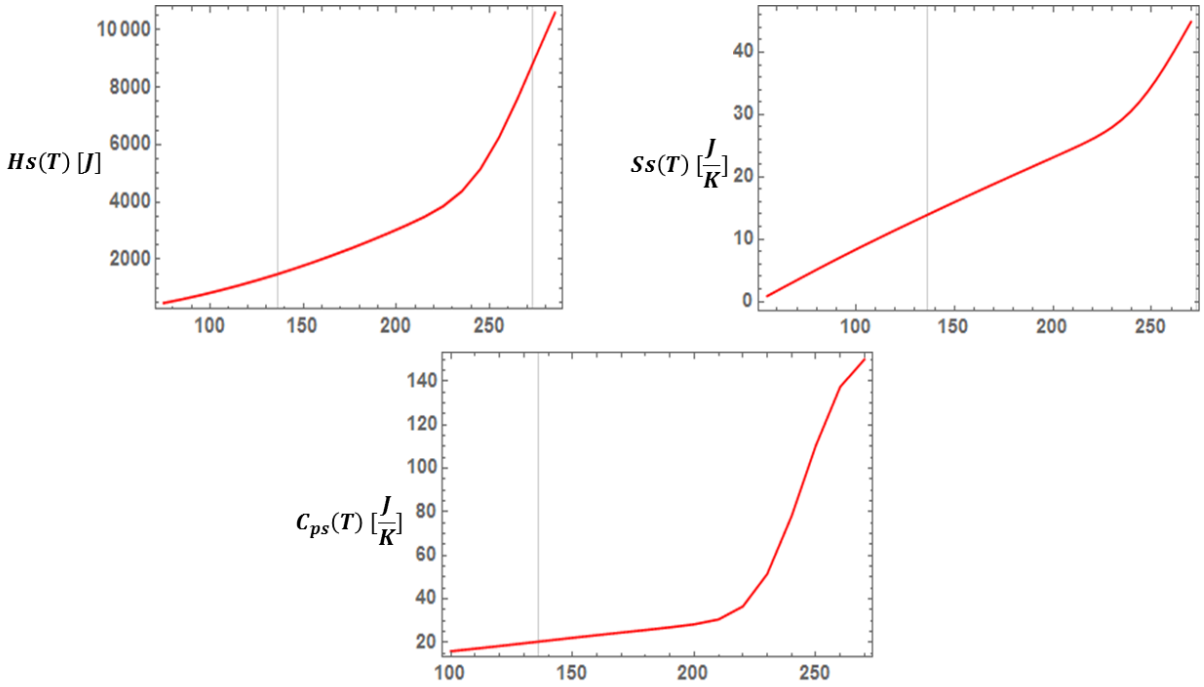


Figure 3.33: (Color Online.) Enthalpy, entropy, and heat capacity functions predicted from the DEH model. The exact functional form appears to have some discrepancies which we hypothesize to be the result of not properly considering the $\mathcal{PTEI}$.

'turn over', and the heat capacity does not have a drop until at or near the glass transition temperature. It makes sense that the DEH model would not predict these features at $T_g$, as they are widely accepted to occur due to the freezing out of degrees of freedom, solely due to observation times not being long enough to allow appropriate equilibration. Therefore, these changes are not thermodynamic changes, but kinetic ones. The DEH represents a metastable extension of the statistical mechanics of liquids, so its predictions should hold regardless of observation time.

However, we know from experimental observations, that there should be no bending or turning over in the free energies, etc. of the supercooled liquid until at least the glass transition temperature, regardless of whether or not these are physical. Therefore, we must rectify the apparent crossover that happens in the DEH predictions of the enthalpy, entropy, and heat capacity, at a temperature well above $T_g$. We again postulate that the influence

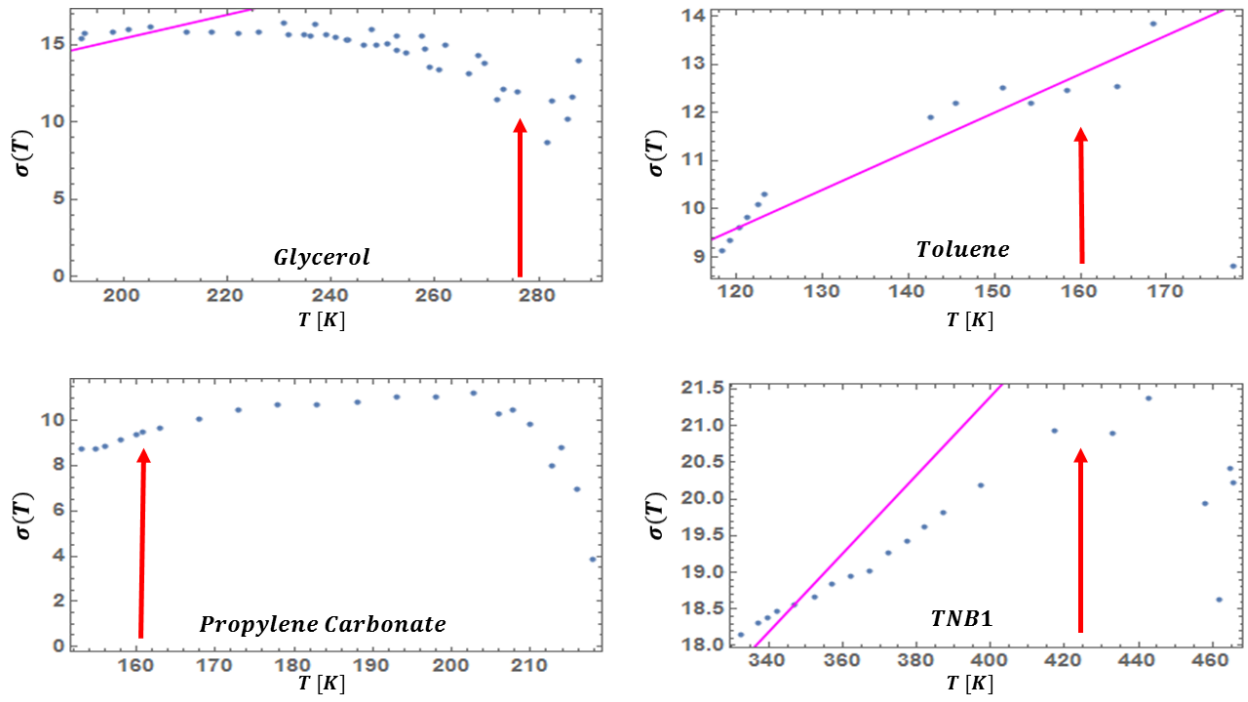


Figure 3.34: (Color Online.) $\sigma(T)$ data with location of experimentally suggested crossover/liquid-liquid phase transition marked via the red arrows.

of the energy states in the $\mathcal{PTEI}$ region will play a significant role in determining the thermodynamic functions of the supercooled liquid, and that omission of these states is what causes the discrepancy. It is beyond the scope of this thesis to test this claim, as experimental values of thermodynamic functions are rarely reported as functions of energy, making the relevant $\mathcal{PTEI}$ integrals difficult to carry out. We hope to take this up in the future.

### 3.9.2 Liquid-Liquid Phase Transitions

Much of the current and previous research into supercooled liquids and the glass transition has focused on whether or not there is an associated equilibrium phase transition at a temperature at or beneath $T_g$ to a so-called 'ideal glass'. In recent years, however, research into another hidden phase transition in the supercooled liquid has become quite popular,

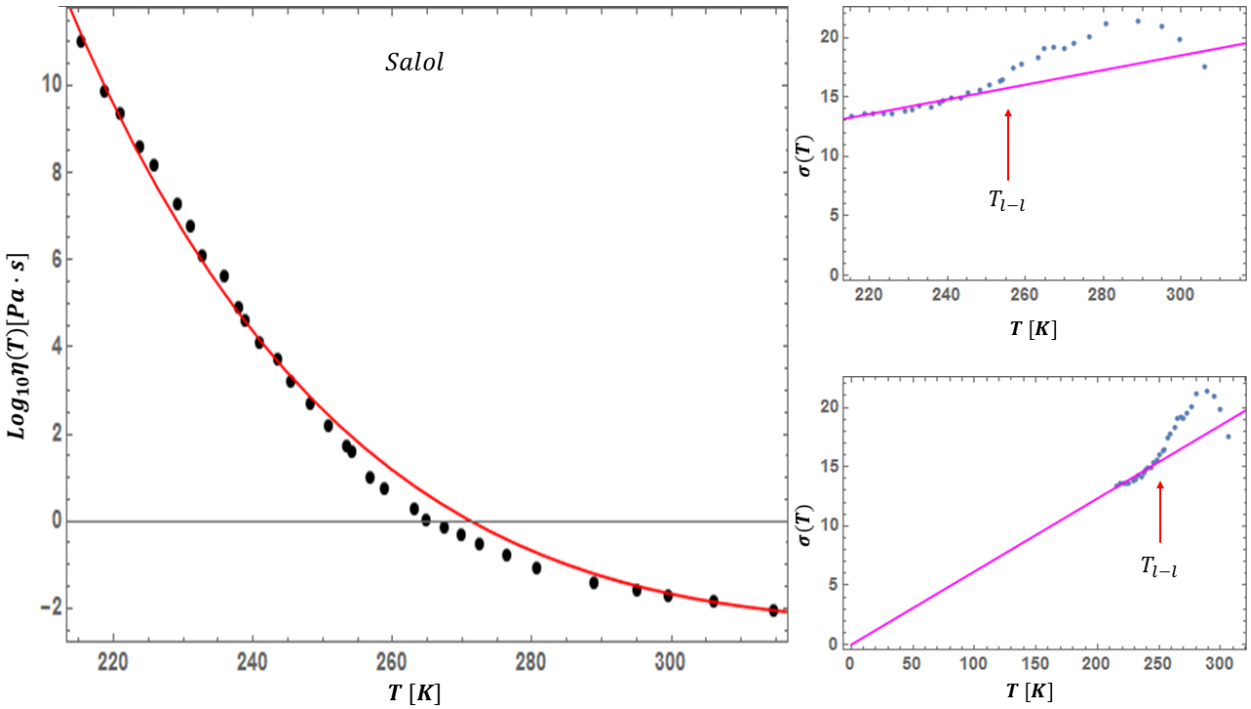


Figure 3.35: (Color Online.) Left: DEH fit to the viscosity of Salol. The intermediate region of data where the DEH fit appears to "fail" corresponds to the region where the linear approximation breaks down and, in fact, to a temperature where a putative liquid-liquid phase transition was earlier suggested to occur (see text). Right: (Top) The temperature dependence of $\bar{\sigma}_T$. The linear approximation fit from Eq. (3.7) (shown in magenta) works well over a large range of temperatures, but appears to break down upon approach to $T \approx 256K$ from below. (Bottom) $\bar{\sigma}_T$, this time with the range extended to the origin.

that of the supposed liquid-liquid phase transition. Briefly, a liquid-liquid phase transition, is a hypothesized true thermodynamic transition between two different liquid structural forms somewhere in the supercooled liquid regime. Typically these liquid-liquid phase transitions are such that the liquid goes from a low density liquid to a high density liquid. Experimental results suggesting that the heat capacity shows a signature of this transition have previously been reported (107). Additionally, a dynamical crossover, which may or may not coincide with the liquid-liquid phase transition, has also been widely reported in the literature (112). This crossover is from the previously described super-Arrhenius thermal dependence of dynamical quantities back to an Arrhenius dynamics at some temperature between the glass transition and the liquidus. If either of these transitions exists for all liquids, then the DEH framework, if it is to be the complete theory of supercooled liquids that we purport it to be, should show some signature of the transition. We observed in section XX, that the temperature dependence of $\sigma$ in many cases appeared to show a crossover at a temperature in the supercooled range. Therefore, we investigate whether or not this crossover point is at all correlated with the previously proposed liquid-liquid or Arrhenius crossover temperatures. It was shown in (66), that salol may undergo a so-called "fragile-strong" crossover in the range $T_g \leq T \leq T_l$ and the exact temperature of its occurrence was suggested to be at $T_{l-l}$=256 K (66). Other investigations have suggested a very similar temperature (111). Examining the behavior of $\sigma(T)$ in Figure (3.35) for salol, it is clear the the linear approximation breaks down at exactly the same temperature at which the putative liquid-liquid transition supposedly occurs, $T \approx 256K$! Therefore, it may be possible for the DEH form to predict the existence and location of liquid-liquid phase transitions or crossovers, based on a change in the behavior of $\bar{\sigma}_T$. In Fig. (3.34), we display the $\sigma$ data for four additional liquids with arrows denoting the location of proposed crossover temperatures (**?** ). For propylene carbonate and TNB1, it appears as though these temperatures do coincide with a change in behavior of $\sigma(T)$. The relationship is not as clear for toluene or glycerol. If a change in behavior is existent in $\sigma(T)$ for all liquids, this could help explain some of the poor fit quality

of the DEH model for certain liquids. These links between the temperature dependence of $\sigma$ and possible liquid-liquid/Arrhenius transitions requires further investigation.

Before concluding this section, we briefly remark on what the physical interpretation of these transition/crossovers would be in the DEH framework. Quite simply, we hypothesize that they correspond to the temperature in the supercooled liquid at which the system has 'used up' the energy of fusion. As we discussed, it is observed that in equilibrium systems, the energy discontinuously decreases by an amount equal to the latent heat at the liquidus temperature, whereas the energy of the supercooled liquid continuously decreases with temperature. At a certain temperature, say $T_{-}$, the energy of the supercooled liquid will have decreased by an amount equal to the latent heat energy, and the influence of the $\mathcal{PTEI}$ states will have effectively been reduced to zero. We believe that the temperature $T_{-}$ where this occurs coincides with one, or both of the above mentioned transitions in the supercooled liquid. To test this, we examine the observed Arrhenius crossover temperatures of Mallamace et al (111) for seven liquids. If these temperatures do in fact correspond to the point at which the latent heat is used up by the supercooled liqud, then there should be a correlation between the heat of fusion and the difference in temperature between the liquidus and crossover, ie $\Delta H_{fus} \propto (T_l - T_{-})$. This implicitly assumes that the supercooled liquid heat capacity doesn't show much of a temperature dependence in this region, which is observed to be a fairly reasonable approximation. For the sample of liquids for which data was available and tested, we observed a strong positive correlation between the enthalpy of fusion and the temperature difference, $r = 0.71$, and using statistical methods, observed that this result is statistically significant despite the small sample size. Therefore, we take this as a positive result that our interpretation of the liquid-liquid/Arrhenius transition/crossovers is the correct one, and that the DEH framework can naturally describe this. More rigorous investigations of these results and conjectures are required, and will be taken up in a future paper.

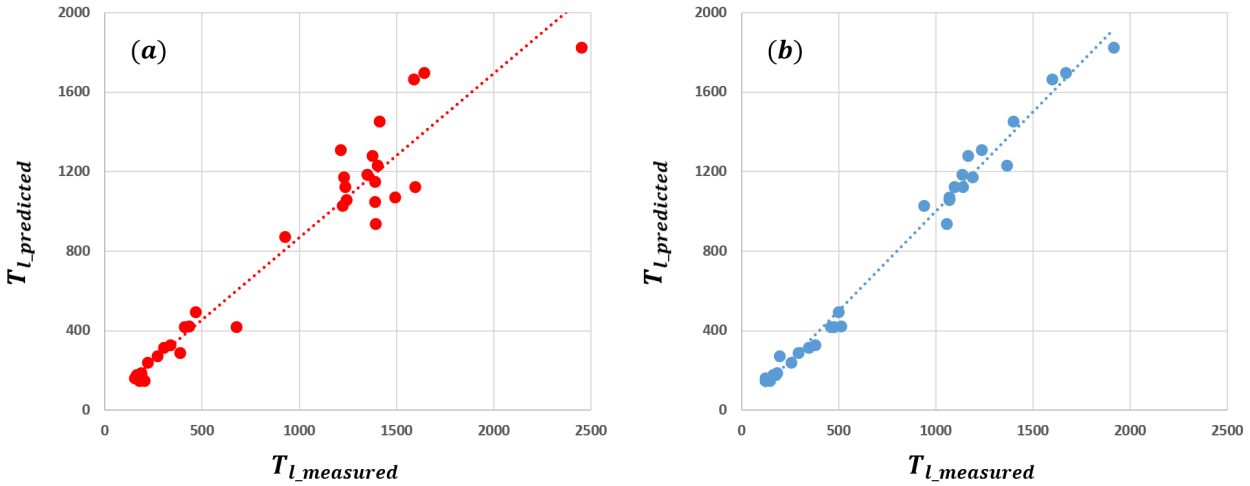


Figure 3.36: (Color Online.) (a) Prediction of the liquidus temperature by fitting the viscosity data with the liquidus and $\eta(T_l)$ left as parameters. (b) Prediction of the Liquidus using the observed correlation between it and $T_g$.

### 3.9.3 Predicting the Liquidus Temperature

Throughout the preceding sections, we have both argued and demonstrated, that the liquidus temperature is fundamental to not only the DEH framework, but the physics of supercooling in general. Indeed, the low temperature viscosity function depends on having an appropriate value for the liquidus of a given material in order to say anything about its supercooled viscosity. However, experimentalists frequently report that accurate measurements of the liquidus temperature are very difficult to achieve, whereas viscosity measurements are much simpler and easier. Therefore, having a theoretical/functional means of estimating the liquidus temperature in general systems, would represent a major advance in the study of the thermodynamics of fluids. As such, it has been suggested that the DEH viscosity equation, Eq. (3.9), could be inverted to use viscosity data to predict the liquidus. We aimed to test this notion, by using the viscosity data of a large fraction of the liquids studied.

In order to predict the liquidus temperature using the DEH model, we fit the viscosity data using the DEH form of Eq. (3.9), but let the liquidus temperature and log of the viscosity at the liquidus be fitting parameters in addition to $\bar{A}$. The inherent constraint that the viscosity be equal to its value at the liquidus for the liquidus temperature should be enforced naturally by the functional form of the viscosity, so as to naturally force consistency. The difficulty in getting reasonable values of the parameters, then, results from the fact that the parameter space is filled with a huge number of local minima that the standard gradient descent algorithm can easily get stuck in, and lead to the prediction of highly nonsensical parameter values. To combat this, we used the observed relationship between $\bar{A}$ and the Turnbull reduced temperature discussed in Section 3.6.4, in conjunction with the observed range of $\bar{A}$ values ( 0.025-0.16) to place broad constraints on $\bar{A}$ and the liquidus temperature. The results of this analysis for a random subset of the studied liquids is depicted in panel (a) of Fig. (3.36). It is observed that while the predicted and experimental values are linearly correlated as they should be, there is much scatter in the predicted $T_l$ with reference to the actual value, with the average percent error being 12.5%. This level of error suggests we need to refine our method of predicting the liquidus in the DEH framework. In studying correlations between the DEH parameters and various thermodynamic variables, we observed that there is a strong correlation between the glass transition temperature, $T_g$, and the liquidus temperature, $T_l$ (see Fig. (3.37)), such that $T_l$ can be predicted from the value of $T_g$ using a simple linear regression. The results of this analysis are depicted in panel (b) of Fig. (3.36). We see that the value of the liquidus using Tl is slightly more accurate than the values predicted from the DEH viscosity equation, with an average percent error of about 7.52%. We next attempted to use the the predicted $T_l$ values from both the DEH equation and the $T_g$ relation to fit a multiple regression to the data. The results of this analysis are depicted in panel (a) of Fig. (3.38), and we observe that they are better than the raw DEH prediction, but marginally worse than the $T_g$ prediction with an average percentage error of about 7.74%. We next decided to use the $T_g$ predicted value of the iquidus and the average

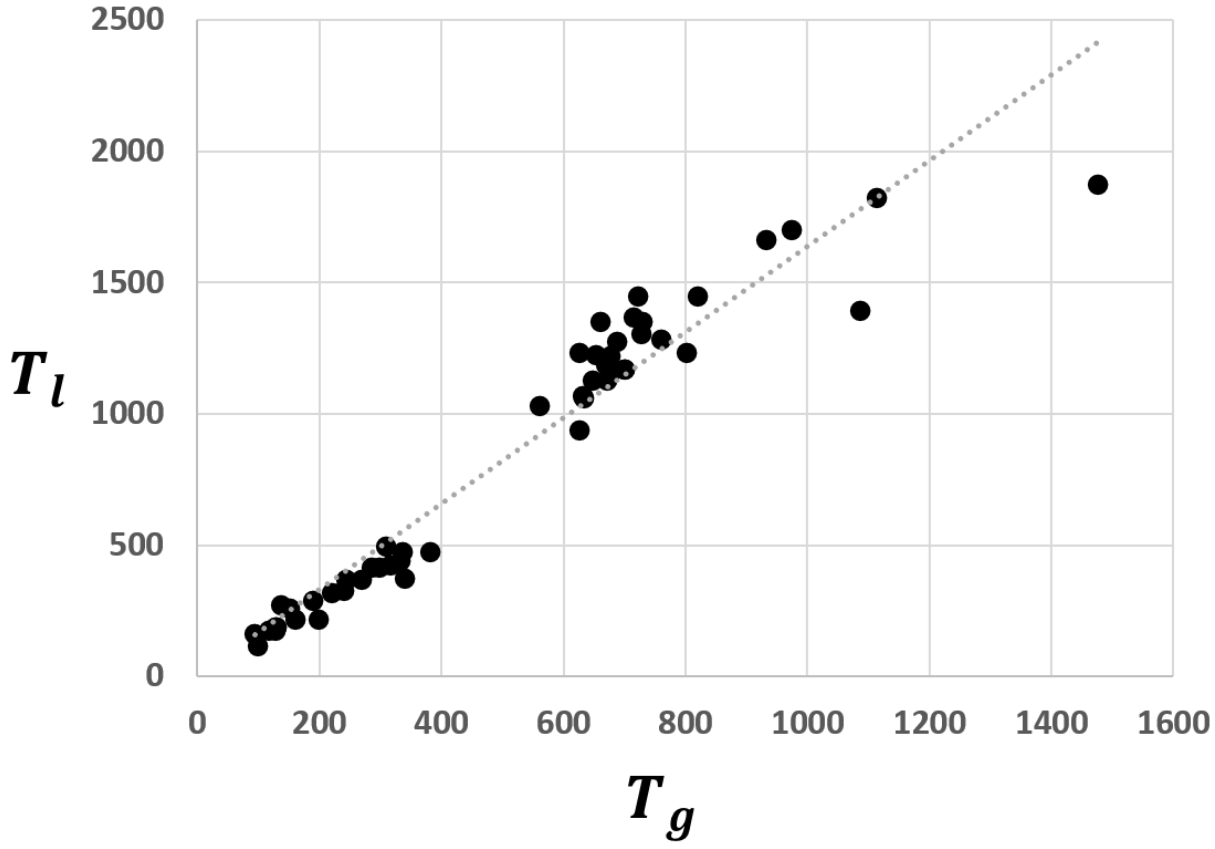


Figure 3.37: (Color Online.) Correlation between the experimental $T_l$ and the glass transition temperature $T_g$.

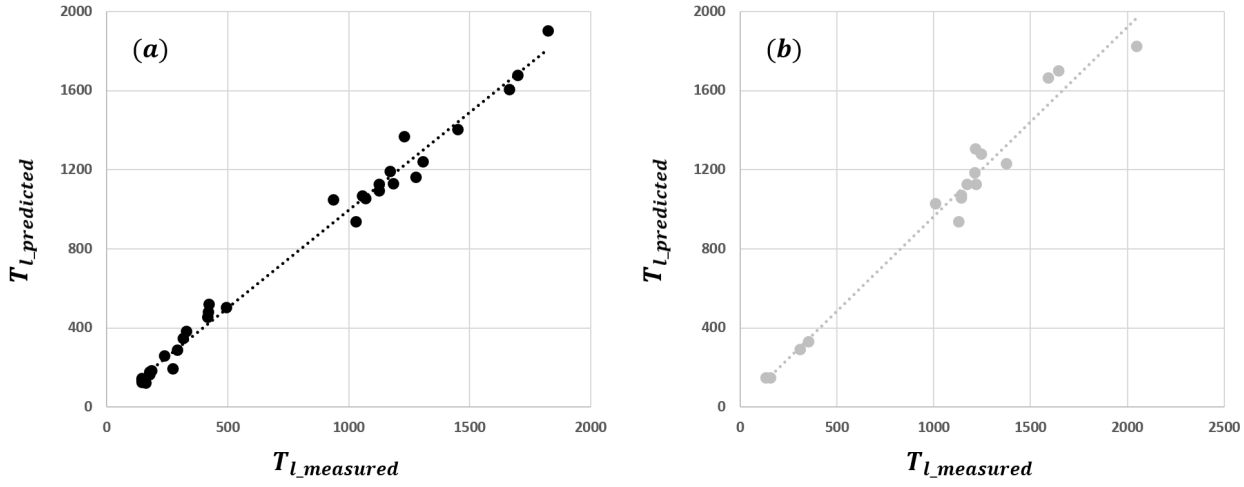


Figure 3.38: (Color Online.) (a) Predicted value of $T_l$ resulting from OLS regression. (b) Prediction of $T_l$ using the $T_g$-predicted value to constrain the fitting of the DEH viscosity with $T_l$ and $\eta(T_l)$ as parameters.

Table 3.7: Actual and Final Predicted Liquidus Values For Sample of Studied Liquids

| Composition | Measured $T_l$ | Predicted $T_l$ |
|---|---|---|
| 3bromopentane | 147 | 156 |
| Anorthite | 1823 | 2048 |
| BS2 | 1699 | 1644 |
| $Cu_{60}Zr_{20}Ti_{20}$ | 1125 | 1172 |
| $Cu_{64}Zr_{36}$ | 1230 | 1374 |
| Diopside | 1664 | 1592 |
| Glycerol | 291 | 311 |
| LS2 | 1307 | 1216 |
| OTP | 329 | 352 |
| Pd40Ni40P20 | 1030 | 1008 |
| $Pd_{77.5}Cu_6Si_{16.5}$ | 1058 | 1143 |
| $Pd_{82}Si_{18}$ | 1071 | 1141 |
| Propanol | 147 | 135 |
| $Ti_{40}Zr_{10}Cu_{30}Pd_{20}$ | 1279 | 1247 |
| $Ti_{40}Zr_{10}Cu_{36}Pd_{14}$ | 1185 | 1211 |
| Vit 1 | 937 | 1130 |
| Vit106a | 1125 | 1219 |

error associated with it, to set new boundaries for prediction using the DEH equation. We left the same range of allowed $\bar{A}$ values based on the observed values of all liquids, but constrained the predicted $T_l$ to lie within the range $T_{l,g} - 0.07 * T_{l,g} \leq T_l \leq T_{l,g} + 0.07 * T_{l,g}$, where $T_{l,g}$ is the liquidus value predicted using the $T_g$ relationship. In this case, the values of $T_l$ were in considerably better agreement with the experimental values, as depicted in panel b of Fig. (3.38), *with only an average percent error of 7.1%* for a subset of the previous liquids tested. In a number of cases, the predicted liquidus value bumped up against the end of the allowed interval, and increasing the interval width led to changes in the predicted value. This is easily understood as likely being the result of overfitting. Given a wide enough range of possible values, any function would aim to choose parameters that fit every point of available data with little regard for physical reasonableness. We expect that the fits will not be perfect due to experimental error and other factors, so do not expand the range of allowed values. Taken together, these results suggest that it is possible to use the DEH model to predict the liquidus using viscosity data, and that if researchers know that the liquidus must fall within a smaller range, they can increase the accuracy of the prediction.

## 3.10 Jamming and other non-thermal transitions

Glassy dynamics are ubiquitous in nature and appear in arenas that extend beyond the confines of the diverse collection of supercooled liquids (wherein a rapid lowering of the temperature drives the system into a glassy state) that we examined in the earlier sections of this paper. It is thus natural to investigate the possible links between the dynamics of non-thermal liquids and traditional supercooled liquids. As we will explain in this section, the formalisms of (50; 51) are generally applicable to more than traditional supercooled liquids. To make this lucid, we remark that the DEH eigenstates discussed hitherto (as well as the classical phase space regions of (51)) may not only be classified by the energy

density or temperature but (in systems in which the volume and particle number are not both fixed) also by the number density and all other quantum numbers that describe them. The density matrix associated with the quenched, metastable system state will, generally, lead to an extension (50) of the long time average of Eq. (3.6) by an average with a probability distribution that depends on parameters other than the energy density (such as the volume fraction) if these parameters are allowed to vary. Similarly, in the classical approach of (51), the long time average of Eq. (3.6) will be performed over microstates that have different particle number and other parameters. Now, here is a new idea that we wish to introduce and explore in this section: if the quantum eigenstates or classical microstates change from being 'liquid-like' to 'solid-like' as the number density (or other parameter) is increased then quenching will lead to a state for which much of our above ideas can be reproduced with the temperature $T$ replaced by the volume fraction (or other parameter) describing the macrostate of the system.

For concreteness, we will now explicitly consider the case of liquids which undergo a jamming transition (19; 81; 82; 83; 84; 85; 86; 87; 88; 89; 90; 91; 92; 93; 94). The control parameter in this case is not the temperature but rather the volume fraction $\phi$. In, e.g., hard sphere (or colloidal) systems, $\phi$ is the fraction of the volume occupied by the hard spheres (or colloids). The system will again have a general Hamiltonian and associated eigenstates, and these eigenstates will intrinsically possess the macroscopic properties of equilibrium systems, including system sizes and atomic arrangement. For simplicity, the eigenstates can be associated with a many body energy, which will in turn depend on the volume fraction, $\phi$, instead of the temperature, $T$. Similar to the supercooled case, if the system starts out at as an equilibrated liquid (at volume fractions $\phi < \phi_{melt}$) and the volume fraction is then quasi-statically elevated then the system will remain in equilibrium and will transition to the crystalline state (when the volume fraction $\phi = \phi_{melt}$). By contrast, if the system is very rapidly compressed, it will be driven out of equilibrium, and by the same arguments

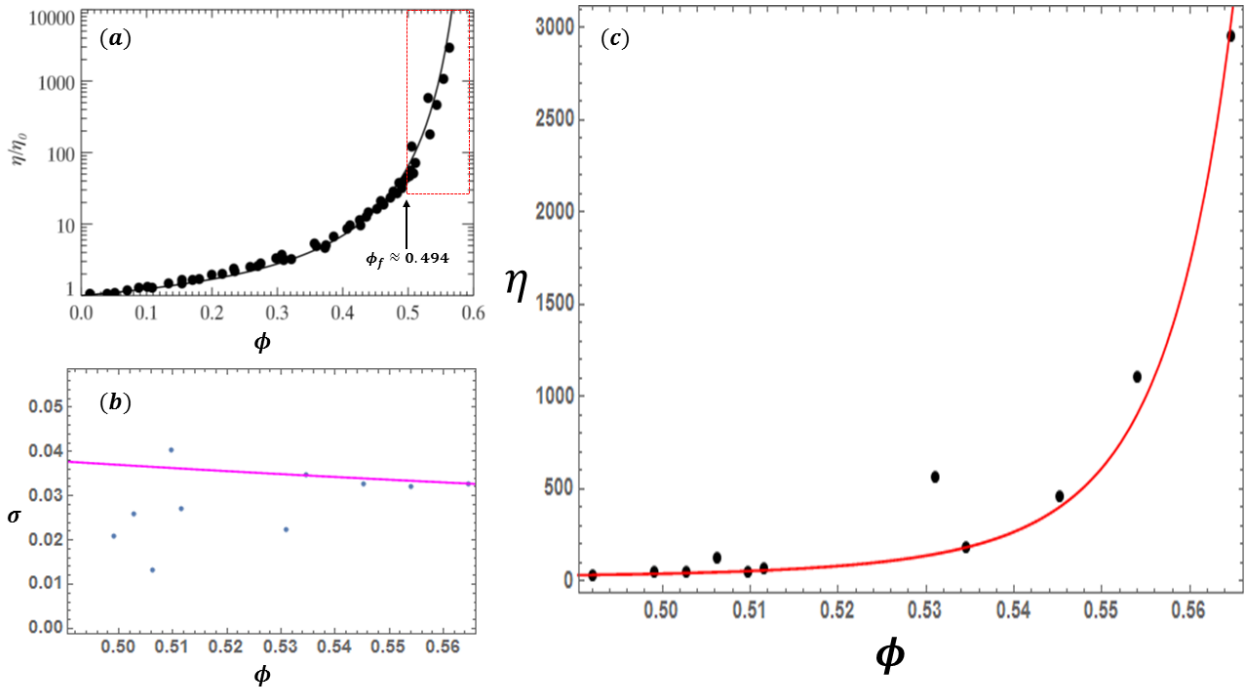


Figure 3.39: (Color Online.) (a) Reproduction of scaled experimental hard sphere viscosity data as a function of volume fraction, from (95). The equilibrium 'freezing' volume fraction is marked and the metastable 'supercooled/pre-jamming' region is highlighted in the dashed, red box. (b) Plot of the spread, $\sigma_\phi$, for the hard sphere data, found by inverting Eq.(3.48). The magenta line is the curve $\sigma_\phi = \frac{\bar{J}}{\phi}$ using the value of $\bar{J}$ obtained from fitting Eq.(3.50) to the data. (c) Hard sphere viscosity data with DEH fit applied. The DEH model is seen to do an exceptional job of reproducing the viscosity of a jammed hard sphere liquid, demonstrating the universality of the underlying physics of disordered solids.

that we provided here and in (50; 51) for supercooled liquids, the distribution ($p_\phi(E')$) will no longer be a $\delta$-function, but rather a (Gaussian) distribution parameterized by $\phi$ over the energy states that is of finite width. Thus, following rapid quenching, the quantum density matrix (or classical probability density) may generally contain both liquid-like and solid-like states. This mixed character will lead to the observed sluggish/glassy dynamics. Assuming that only liquid-like states are capable of flow, such that the melting energy marks a cut-off and replicating, *mutatis mutandis*, the earlier steps that led to Eq. (3.7), we arrive at an functional form for the viscosity of jammed liquids as a function of the energy that is

identical to that of the supercooled liquids that we discussed earlier, namely

$$\eta(T) = \frac{\eta_{jam}(E_{melt})}{\text{erfc}\left(\frac{E_{melt}-\langle E\rangle}{\bar{\sigma}_E\sqrt{2}}\right)}. \tag{3.48}$$

In order to make predictions, we need to convert this equation from being a function of energy levels to that of the relevant control parameter. In the case of jamming, the control parameter is the volume fraction, $\phi$ and not the temperature, $T$. We briefly sketch how, in the simplest approximation, the energy depends upon the volume fraction to make the necessary conversion. In the supercooled liquid case, the energy and temperature were simply related via an effective average heat capacity by $E = CT$. In systems where the volume can change, with fixed particle number, the energy changes correspond solely to volume changes (at constant pressure) and the energy $E = -PV$. The volume $V$ and the volume fraction $\phi$ are reciprocally related to one another ($V = \frac{const.}{\phi}$). Thus, in terms of volume fraction, the energy is $E = -\frac{const.\times P}{\phi} \equiv -\frac{\mathcal{P}}{\phi}$. Insertion of this relation into Eq. (3.48) leads to

$$\begin{aligned}\eta(\phi) &= \frac{\eta_{jam}(\phi_{melt})}{\text{erfc}\left((\frac{1}{\phi_{melt}} - \frac{1}{\phi})\frac{\mathcal{P}}{\bar{\sigma}_E\sqrt{2}}\right)} \\ &= \frac{\eta_{jam}(\phi_{melt})}{\text{erfc}\left(\frac{\mathcal{P}\ (\phi-\phi_{melt})}{\bar{\sigma}_E\sqrt{2}\phi\phi_{melt}}\right)}.\end{aligned} \tag{3.49}$$

Since the energy $E$ and volume fraction $\phi$ are inversely related to one another, for small standard deviations (which we implicitly assume), we asymptotically have that $\sigma_E \approx \frac{\mathcal{P}\sigma_\phi}{\phi^2}$. If we further postulate that $\sigma_\phi = \frac{\bar{J}}{\phi}$ where $\bar{J}$ is a small material-dependent constant (similar to $\bar{A}$), then we finally obtain that for $\phi \geq \phi_{melt}$ the viscosity of the jammed fluid is

$$\eta(\phi) = \frac{\eta(\phi_{melt})}{\text{erfc}\left(\frac{(\phi-\phi_{melt})\phi^2}{\sqrt{2}\bar{J}\phi_{melt}}\right)}. \tag{3.50}$$

Similar to our earlier relation of Eq. (3.9), the viscosity of Eq. (3.50) utilizes only a single parameter ($\bar{J}$), which controls the rate at which the width of the distribution changes with $\phi$, and a thermodynamically measured 'freezing' point. In Fig. (3.39) we fit the viscosity function of Eq.(3.50) to hard sphere data taken from (95). As seen in the figure, the DEH model is capable of very accurately reproducing the viscosity of the hard sphere liquid in the metastable, pre-jammed state. This result is highly significant, as it demonstrates the generality of the energy-distribution framework to different classes of amorphous solids, and provides a link between the jamming and glass transitions. Further, it begs the question as to whether phenomena such as shear thickening/thinning could also be explained using this framework with similar resulting functional dependencies of the viscosity on parameters such as applied stress. More investigation is required to answer this question, and it will be addressed in an upcoming paper.

## 3.11 Conclusion and Outlook.

In this work, we expounded on a new framework for understanding supercooled liquids and the glass transition. Crucially, we tested the predictions of this theory (the distributed eigenstate hypothesis (DEH)) by analyzing the viscosity of *all* currently known supercooled liquid classes. We demonstrated, both qualitatively and quantitatively, that the DEH model can capture the temperature dependence of the viscosity of all of these liquid types to a statistically significant degree using only a **single** fitting parameter. We established that the viscosity of 65 disparate supercooled liquids below their melting temperature can be collapsed onto a universal curve over 16 decades by using the single parameter, $\bar{A}$. Coincident with the theoretical premise underlying the DEH theory, we unveiled correlations between this single parameter and various properties of supercooled liquids and glasses. Our results further strongly hint that it may be possible to predict viscosity of supercooled liquids

below their melting temperature using only viscosity data above this temperature. Notably, we also derived a new form for the viscosity above melting and assessed the validity of this functional form by examining experimental data. Taken together, our results suggest an underlying universality of the glass transition that enables a natural crossover from an activated Arrhenius form at high temperatures to a very marked rise of the viscosity (most pronounced in fragile systems) at low temperatures. While the predictions of the DEH framework led to our analysis and observations, it is possible that other approaches might also rationalize and complement our findings. We hope that our observations of *universal* behaviors in all known supercooled liquid types will spur further investigations.

# References


[1] A. Cavagna, Physics Reports, **476**, 551-124 (2009) [review]

[2] I. M. Kalogeras and HE. Hagg Lobland, Journal of Materials Education, **34**(3-4): 69-94 (2012) [review]

[3] L. Berthier and F. Biroli, Reviews of Modern Physics, **83**, April-June (2011) [review]

[4] G. L. Hunter and E. R. Weeks, Rep. Prog. Phys. **75**, 066501, (2011) [review]

[5] I. Procaccia, Eur. Phys. J. Special Topics, **178**, 81-122 (2009) [review]

[6] J. S. Langer, Rep. Prog. Phys., **77**,042501 (2014) [review]

[7] L. Berthier and M. D. Ediger, Physics Today **69**(1), 40 (2016)

[8] R. Zallen, "The Physics of Amorphous Solids", John Wiley & Sons, Inc., pages 23-32 (1983)

[9] A. L. Greer and E. Ma, MRS Bulletin **32**, 611 (2007)

[10] B. C. Hancock and M. Parks, Pharmaceutical Research **17**, 397 (2000).

[11] M. Telford, Materials Today **7**, 36 (2004).

[12] M. Wuttig, and N. Yamada, Nature Materials **6**, 824 (2007)

[13] A mixed phase appears instead of a solid phase in various alloy and silicate systems.

[14] F. Sausset.,G. Biroli, and J. Kurchan, Journal of Statistical Physics **140**, 718 (2010)

[15] E. Rossler, and H. Sillescu, "Organic Glasses and Polymers", Materials Science and Technology, ISBN: 3527313958 (2006)

[16] C. A. Angell, Journ. Phys. and Chem. of Solids, **49**, 863-871 (1988)

[17] C. A. Angell, Science **267**, 1924 (1995).

[18] A. Cavagna, Physics Reports, **476**, 551-124 (2009) [review]

[19] Z. Nussinov, A. V. Balatsky, M. J. Graf, and S. A. Trugman, Physical Review B **76**, 014530 (2007)

[20] B. Hunt, E. Pratt1, V. Gadagkar, M. Yamashita, A. V. Balatsky, and J. C. Davis, Science **324**, 632 (2009)

[21] Giulio Biroli, Claudio Chamon, and Francesco Zamponi Phys. Rev. B **78**, 224306 (2008); Z. Nussinov, Physics **1**, 40 (2008)

[22] M. Boninsegni, N. Prokof'ev, and B. Svistunov, Phys. Rev. Lett. **96**, 105301 (2006)

[23] Z. Nussinov, P. Johnson, M. J. Graf, and A. V. Balatsky, Physical Review B **87**, 184202 (2013)

[24] L. M. Martinez and C. A. Angell, Nature **410**, 663 (2001)

[25] N. A. Mauro, M. L. Johnson, J. C. Bendert, and K. F. Kelton, J. of Non-Crystalline Solids **362**, 237 (2013)

[26] N. A. Mauro, M. Blodgett, M. L. Johnson, A. J. Vogt, and K. F. Kelton, Nature Communications **5**, 4616 (2014)

[27] G. Tarjus and C. Alba-Simionesco, arXiv:1401.2812 (2014)

[28] H. Vogel, Z. Phys. 22,**645** (1921)

[29] G. S. Fulcher, J. Am. Ceram. Soc. 8, **339** (1925)

[30] G. Tamann and W. Z. Hesse, Anorg. Allgem, Chem. 156, **245** (1926)

[31] L. Berthier and F. Biroli, Reviews of Modern Physics **83**, 587 (2011)

[32] I. Procaccia, Eur. Phys. J. Special Topics, **178**, 81-122 (2009)

[33] I. M. Kalogeras and H. E. Hagg Lobland, Journal of Materials Education, **34(3-4)**: 69-94 (2012)

[34] G. L. Hunter and E. R. Weeks, Rep. Prog. Phys. **75**, 066501 (2011)

[35] J. S. Langer, Rep. Prog. Phys., **77**, 042501 (2014)

[36] G. Adam, and J. H. Gibbs, J. Chem. Phys., **43**, 139-146 (1965)

[37] W. Kauzmann, Chem. Rev. **43 (2)**, 219-256 (1948)

[38] J. C. Mauro, International Journal of Applied Glass Science 2, **4** 245-261 (2011)

[39] J. Zhao, S. L. Simon, and G. B. McKenna, Nature Communications **4**, 1783 (2013)

[40] P. W. Anderson, Science **267**, 1615 (1995)

[41] T. R. Kirkpatrick, D. Thirumalai, and P. G. Wolynes, Phys. Rev. A, **40**, 1045 (1989)

[42] T. R. Kirkpatrick and D. Thirumalai, Phys. Rev. Lett., **58**, 2091 (1987)

[43] T. R. Kirkpatrick and D. Thirumalai, Phys. Rev. B, **36**, 5388 (1987)

[44] T. R. Kirkpatrick and P. G. Wolynes, Phys. Rev. B., **36**, 8552 (1987)

[45] T. R. Kirkpatrick and D. Thirumalai, Phys. Rev. B., **37**, 5342 (1988)

[46] T. R. Kirkpatrick and D. Thirumalai, J. Phys. A, **22**, L149 (1989)

[47] D. R. Reichman, and P. Charbonneau, J. Stat. Mech: Theory and Experiment, Issue 05, 05013 (2005)

[48] F. Ritort and P. Sollich, Adv. Phys., **52**, 219-342 (2003)

[49] Angell, C. A., Ngai, K. L., McKenna, G. B., McMillan, P. F., and Martin, S. W., (2010). Relaxation in glassforming liquids and amorphous solids, *Journal of Applied Physics 88, 3113-3157* (2000).

[50] Z. Nussinov, arXiv: 1510.03875 (2015)

[51] N. B. Weingartner, C. Pueblo, F. S. Nogueira, K. F. Kelton, and Z. Nussinov, Front. Mater. 3:50. doi: 10.3389/fmats.2016.00050 (2016)

[52] For completeness, we note that in recent years, a growing body of research has focused on apparent connections between traditionally quantum ideas/quantities and observables (e.g., the viscosity) of high energy/temperature "classical" systems (98). In the current context, a link has been posited between the prefactor, $\eta_0$ in the high temperature Arrhenius expression of Eq. (3.1) for the viscosity, and Planck's constant (53; 99; 100; 61). Further suggestions have been raised of quantum mechanics playing a role in certain "special liquids" (101). Quantum jamming transitions (102) may might appear in systems in which the interatomic separations is of the order of the relevant thermal wavelength.

[53] Z. Nussinov, F. S. Nogueira, M. Blodgett, and K. F. Kelton, arXiv;1409.1915 (2014)

[54] R. L. Waaerstein and N. A. Lazar, The American Statistician **70**, 129 (2016); F. Dorey, Clinical Orthopaedics and Related Research **468.8**, 2297 (2010)

[55] Y. S. Elmatad, D. Chandler, and J. P. Garrahan, J. Phys. Chem. B, **113**, 5563-5567 (2009)

[56] D. Kivelson, S. A. Kivelson, X. Zhao, Z. Nussinov, and G. Tarjus, Physica A, **219**, 27-38 (1995)

[57] G. Tarjus, S. A. Kivelson, Z. Nussinov, and P. Viot, J. Phys: Condens Matter, **17**, R1143-R1182 (2005)

[58] Z. Nussinov, Phys. Rev. B, **69**, 014208 (2004)

[59] M. H. Cohen and G. S. Grest, Phys. Rev. B, **20**, 1077-1098 (1979)

[60] Y. S. Elmatad, R. L. Jack, D. Chandler, Jamd . P. Garrahan, PNAS, **107**, 12793-12798 (2010)

[61] M. Blodgett, T. Egami, Z. Nussinov, and K. F. Kelton, Nature Scientific Reports, **Volume 5**, id. 13837 (2015)

[62] J. C. Mauro, Y. Yue, A. J. Ellison, P. K. Gupta, and D. C. Allan, PNAS, **106**, 19780-19784 (2009)

[63] Y. Yue, Journal of Non-Crystalline Solids 355, 737 (2009)

[64] M. D. Ediger and P. Harrowell, J. Chem. Phys. 137, 080901 (2012)

[65] D. Cranmer and D. R. Uhlmann, J. Non-Crystalline Solids, **45**, 283-288 (1981)

[66] F. Mallamace, C. Branca, C. Corsaro, N. Leone, J. Spooren, S. Chen, and H. E. Stanley, PNAS, **107(52)**: 2245722462 (2010)

[67] G. S. Parks, L. E. Barton, M. E. Spaght, and J. W. Richardson, Journ. Applied Phys. **5**, 193 (1934)

[68] K. H. Tsang, S. K. Lee, and H. W. Kui, J. App. Phys, **70**, 4837-4841 (1991)

[69] A. Dehaoui, B. Issenmann, and F. Caupin, PNAS **112(39)**, 12020-12025 (2015)

[70] N. A. Mauro, M. Blodgett, M. L. Johnson, A. J. Vogt, and K. F. Kelton, Nature Comm. **5**, 4616 (2014)

[71] D. Turnbull, Contemp Phys, **10**,473488 (1969)

[72] D. Turnbull, J. Chem. Phys. **18**, 198 (1950).

[73] M. Nascimento, and C. Aparicio, J. Phys. and Chem. of Solids, **68**, 104-110 (2007)

[74] T. Iwashita, D. M. Nicholson, and T. Egami, Physical Review Letters, **110**, Issue 20, id. 205504 (2013)

[75] R. Soklaski, Z. Nussinov, Z. Markow, K. F. Kelton, and L. Yang, Phys. Rev. B, **87**, 184203 (2013)

[76] Ryan Soklaski, Vy Tran, Zohar Nussinov, K.F. Kelton, and Li Yang, Phil. Mag. **96**, 1212 (2016)

[77] N. B. Weingartner, R. F. Soklaski, K. F. Kelton, and Z. Nussinov, Phys. Rev. B **93**, 214201 (2016); N. B. Weingartner and Z. Nussinov, J. Stat. Mech. 094001 (2016)

[78] H. Kanno, Journal of Non-Crystalline Solids **44**, 409 (1981)

[79] Volume expansion measurements in metallic liquids and their relation to fragility and glass forming ability  an energy landscape interpretation, J. C. Bendert, A. K. Gangopadhyay, N. A. Mauro, and K. F. Kelton, Physical Review Letters, 109, 185901 (2012)

[80] Abhishek Jaiswal, Takeshi Egami, Kenneth F. Kelton, Kenneth S. Schweizer, and Yang Zhang, PRL **117**, 205701 (2016)

[81] A.J. Liu and S. R. Nagel, Nature (London) **396**, 21 (1998)

[82] A. J. Liu and S. R. Nagel, Annu. Rev. Condens. Matter Phys. 1, 347 (2010)

[83] C. S. O?Hern, S. A. Langer, A. J. Liu, and S. R. Nagel, Phys. Rev. Lett. **88**, 075507 (2002)

[84] C. S. O?Hern, L. E. Silbert, A. J. Liu, and S. R. Nagel, Phys. Rev. E **68**, 011306 (2003)

[85] J. A. Drocco, M. B. Hastings, C. J. Olson Reichhardt, and C. Reichhardt, Phys. Rev. Lett. **95**, 088001 (2005)

[86] L. E. Silbert, A. J. Liu, and S. R. Nagel, Phys. Rev. Lett. **95**, 098301 (2005)

[87] O. Dauchot, G. Marty, and G. Biroli, Phys. Rev. Lett. **95**, 265701 (2005)

[88] A. R. Abate and D. J. Durian, Phys. Rev. E **74**, 031308 (2006)

[89] A. R. Abate and D J. Durian, Phys. Rev. E **76**, 021306 (2007)

[90] A. S. Keys, A. R. Abate, S C. Glotzer, and D. J. Durian, Nature Phys. **3**, 260 (2007)

[91] F. Lechenault, O. Dauchot, G. Biroli, and J.-P. Bouchaud, Europhys. Lett. 83, 46003 (2008)

[92] T. Hatano, Phys. Rev. E **79**, 050301(R) (2009)

[93] P Charbonneau, EI Corwin, G Parisi, F Zamponi Physical Review Letters **109**, 205501 (2012)

[94] P. Charbonneau, J. Kurchan, G. Parisi, P. Urbani, and F. Zamponi, arXiv:1605.03008 (2016)

[95] G. L. Hunter and E. R. Weeks, Rep. Prog. Phys. **75** (2012) 066501

[96] N. B. Weingartner and Z. Nussinov, in preparation

[97] G. E. H. Hentschel, S. Karmakar, I. Procaccia, and J. Zylberg, Phys. Rev. E **85**, 061501 (2012)

[98] F. Kovtun, D. T. Son, and A. O. Starinets, Phys. Rev. Lett, **94**, 111601 (2005)

[99] H. Eyring, J. Chem. Phys, **4**, 283 (1936).

[100] H. Eyring, J. Chem. Phys, **3**, 107 (1935)

[101] T. E. Markland, J. A. Morrone, K. Miyazaki, B. J. Berne, D. R. Reichman, and E. Rabani, J. Chem. Phys, **136**, 074511 (2012)

[102] Z. Nussinov, P. Johnson, M. J. Graf, and A. V. Balatsky, Physical Review B **87**, 184202 (2013)

[103] C. A. Angell, Heat Capacity and Entropy Functions in Strong and Fragile Glass-Formers, Relative to Those of Disordering Crystalline Materials, Chapter Two in book: Glassy, Amorphous and Nano-Crystalline Materials. estk J, Mare JJ, Hubk P, editors. Berlin: Springer; 2011.p. 21-40

[104] D. J. Cronin, J. T. Wenzel, and D. A. Kauffman, American Mineralogist, **68**, 1083-1088 (1983)

[105] P. Lunkenheimer, S. Kastner, M. Kohler, and A. Loidl,

[106] C. Liu, E. Pineda, and D. Crespo, Metals **5**, 1073-1111 (2015)

[107] S. H. Chen, Y. Zhang, M. Lagi, S. H. Chong, P. Baglioni, and F. Mallamace, J. Phys.: Condens. Matter **21** 504102 (2009)

[108] F. Mallamace, C. Corsaro, H. E. Stanley, and S. H. Chen, Eur. Phys. J. E **34**: 94 (2011)

[109] http://www.engineeringtoolbox.com/ice-thermal-properties-d_576.html

[110] https://en.wikipedia.org/wiki/Water_(data_page)

[111] F. Mallamace, C. Branca, C. Corsaro, N. Leone, J. Spooren, S-H. Chen, and H. Eugene Stanley, PNAS **107**, 22459 (2010)

[112] C. Liu, E. Pineda, and D. Crespo, Metals **5**, 1073-1111 (2015)

[113] T. Hecksher, Relaxation In Supercooled Liquids: Linear and Nonlinear, Mechanical and Dielectric Studies of Molecular Liquids, Thesis

[114] I. Jeong , T. Proffen , F. Mohiuddin-Jacobs , and S. J. L. Billinge, J. Phys. Chem. A, **103** (7), pp 921924 (1999)

## 3.12 Supplementary Information

### S.1 Exceptional Cases: Poor Fits and Possible Anomalies

In the text it was demonstrated that the DEH form for the viscosity provided a statistically 'good' fit to the experimental data for a disparate group of supercooled liquids. Furthermore, we were able to collapse the data of all these liquids to a universal curve, representing both an underlying universality in the glass transition phenomenology, and a universality in the DEH formalism. It must be pointed out, however, that a few exceptional cases did appear in our analysis, with the DEH form not providing a reasonable fit to the data, despite all but one of the liquids being collapsed onto the universal curve. In Figs. (3.35 and (S1), data are presented for 5 exceptional case liquids with the DEH form applied, and it is clear that the function of Eq. (3.9) does not accurately describe the data as depicted. A multitude of reasons may exist for this discrepancy. In the cases of Vit 1 and Trehalose it seems likely that there is measurement error in the data. In the case of $SiO_2$, in addition to the pronounced scatter in the data, this liquid is also at the very extreme of strong behavior, and is traditionally difficult to describe with models. We are not sure exactly why this is the case. In the case of glycerol, there is data (103) showing that the heat capacity has drastically different behavior from other supercooled liquids, and that a so-called liquid-liquid phase transition may exist in this liquid. Salol possesses similar anomalies.

The reader will have noticed that the behavior of $\bar{\sigma}_T$ for glucose shows a stark crossover from increasing to decreasing at a sharp temperature in the supercooled range, yet the DEH model accurately fit the experimental data. It is possible that glucose may have a liquid-liquid transition, but this is masked in the DEH model, as the slope in the increasing range has the same magnitude in the decreasing range. The fact that the magnitude of the slope

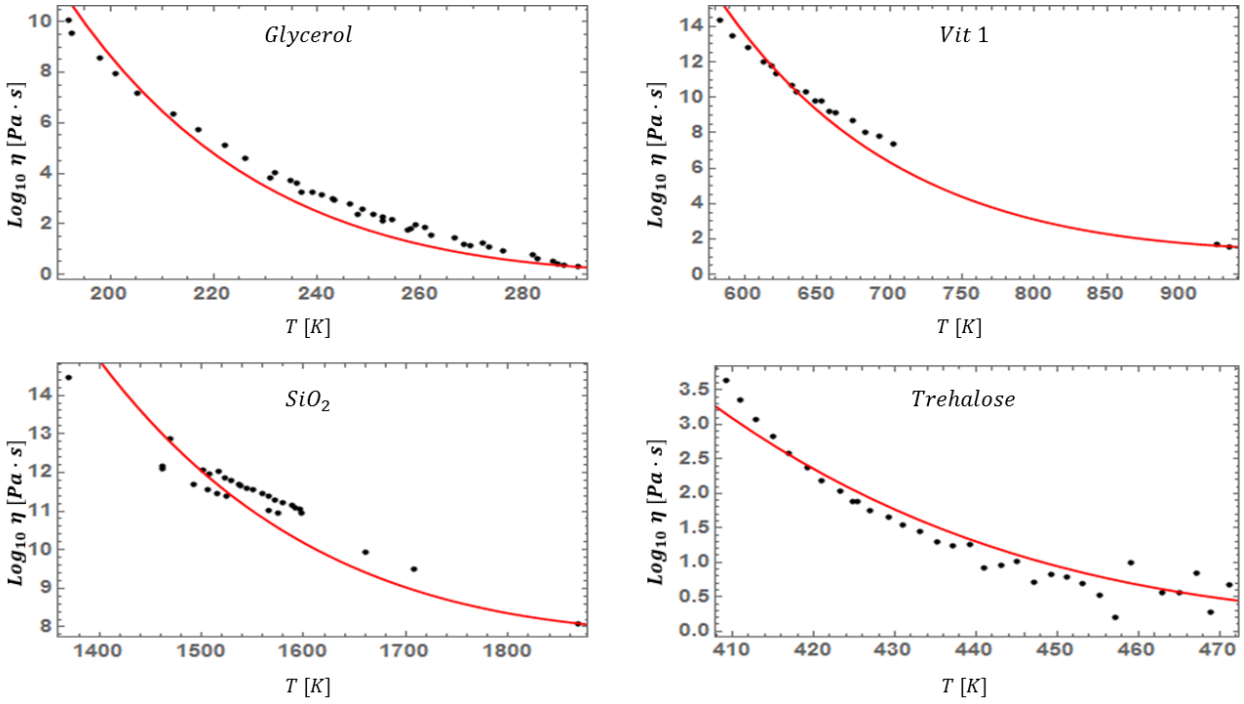


Figure S1: (Color Online.) The four examples of worst performance of the DEH fit of Eq. (3.9). Various possibilities for the relatively poor performance are discussed above.

remained roughly the same will allow the DEH form to accurately predict the experimental viscosity data.

Overall, many reasons may exist for the discrepancies observed in the fits of the above 5 liquids, ranging from experimental error to liquid-liquid phase transitions. The exact reasons will require further investigation, and will need to be understood to strengthen the validity of the DEH model.

# Chapter 4

# A Dramatically Growing Shear Rigidity Length Scale in a Supercooled Glass Former ($NiZr_2$)

## 4.1 Chapter Overview

In the previous chapter we demonstrated that the crossover temperature $T_A$, which has been linked to the development of locally preferred structures in the supercooled liquid, had an interpretation in the DEH framework, as the temperature at which the solid-like states begin to appreciably contribute to the overall state of the system. We suggested that as these states, which possess the perfect crystalline order of the equilibrium solid, gain more influence, the overall solidity of the liquid increases in terms of structure as well as dynamics. We hypothesize that the mismatch of crystalline ordered states with different phonon modes active, corresponding to the spectrum of equilibrium crystal eigenstates, leads to the formation of the locally preferred structures in the supercooled liquid. As such, the existence of 'solid-like' structures with a degree of rigidity, forming a sort of backbone over some length in the liquid is a natural byproduct, and likely requirement of the equilibrium

melting-based distribution approach. Therefore, we must investigate whether or not such a rigidity length appears to exist in supercooled liquids. In this chapter, we examine a typical metallic glassforming liquid, $NiZr_2$, and its response to a shear perturbation applied at the boundary of the system in the equlibrium liquid, supercooled liquid, and glassy states. We aim to find a growing lengthscale over which the shear perturbation will propagate into the liquid, which should be associated with the emergence of locally-ordered clusters. We demonstrate, through the use of MD simulations, that the proposed rigidity length does indeed exist in this system, and that it grows dramatically with supercooling. We also observe that appreciable growth of this lengthscale does not occur until the temperature $T_A$, reinforcing our hypothesis above and in the previous chapter. We conclude by discussing the structural correlations with this lengthscale, and the connections with various facets of the phenomenology of supercooled liquids.

This chapter is a combination of published papers appearing in Physical Review B (Weingartner et al, Physical Review B **93**, 214201 (2016)), and a special edition of the Journal of Statistical Mechanics (Weingartner et al, JSTAT **2016** (2016)).

CITATIONS

## 4.2 Introduction

When a liquid is cooled sufficiently quickly to temperatures well below its melting temperature, nucleation is avoided and the transition to the crystalline state, possessing both extended long-range structural order and absolute minimum free energy, is bypassed. A liquid maintained beneath its melting temperature exists in metastable equilibrium, and is said to be supercooled. A supercooled liquid lacks the long range structural order characterstic of the underlying crystalline ground state, instead maintaining the amorphous

atomic arrangement typical of a liquid. As the temperature of the supercooled liquid is lowered further, the viscosity (and relaxation time) increases dramatically, by up to some 14 decades over a temperature range as small as 100 K. Eventually, a temperature, $T_g$, is reached at which the viscosity (and hence, relaxation time) is so large ($>10^{13}$ Poise/100 s) that structual rearrangments cease to take place on any reasonable timescale, and the liquid behaves rigidly in response to fluctuations and perturbations. By definition, the liquid is then out of equilibrium, and this is deemed the glass transition. The 'transition' occuring at $T_g$, is in fact not a thermodynamic transition, but instead a kinetic crossover. There is no thermodynamic driving force (energy saving) associated with $T_g$, and a structural rearrangment and associated symmetry breaking is apparently absent. In addition to the smooth emergence of rigidity at $T_g$, the glass transition is accompanied by a rich phenomenology and wide range of interesting features that cannot be enumerated here, but are discussed in a variety of exceptional reviews, e.g. (1; 2; 3; 4; 5; 6).

The two most puzzling aspects of the glass transition are the onset of structural rigidity without apparent long range structural order (with associated long-time, non-zero shear modulus), and the dramatic, faster than Arrhenius increase of the viscosity/relaxation time found in the so-called fragile glass formers (7; 8). Both features seem to call for, and likely require, the existence of a growing length scale, intimately connected to the propagation of some form of amorphous order or increasingly cohesive, extended network. In fact, while the notion of a growing activation energy barrier is clearly tied to cooperative motion, even more fundamentally, simple intuitive reasoning suggests that a dramatically growing (or diverging) timescale to relaxation should be coupled to a similarly increasing (and possibly diverging) length scale. Recently, rigorous bounds mandating the existence of a concomitant growth of spatial length scale with relaxation time have been proven to exist (9).

The notion of a growing length scale underlying the dynamic slowdown of the glass transition is a principle feature of most theories of glass formation, such as that of Adam and

Gibbs, Random First Order Transitions, Mode-Coupling Theories, Kinetically Constrained Models, and others (1; 2; 3; 4; 5; 6; 10; 11; 12; 13; 14; 15; 16; 17; 18). Some of these theories predict an underlying phase transition at a temperature below $T_g$, with the glass transition serving as a kinetic "ghost" preceding the actual thermodynamic change. Others posit that there is no true thermodynamic transition besides the melting/freezing transition, and that the length scale corresponds to a geometrically arrested structural ordering which is still capable of bringing about rigidity. As such, the quest to find physical, verifiable, and suitably increasing length scales has been underway for decades. Many proposals for appropriate length scales have been made including those associated with liquid-like defects, the lowest eigenvalues of the relevant Hessian matrix for a system, various point-to-set lengths, elasticity lengths (19; 20; 21; 22; 23**?** ; 24; 25; 26; 27; 28; 29; 30; 31; 32; 33), and dynamical heterogeneity lengths (34; 35; 36; 37; 38; 39; 40; 41; 42) and computer vision methods to ascertain both static and dynamic length scales (43). "Hybrid" correlation length scales, that have mixed static/dyanmical charactersitics, have also been found, as in (44). Each of the previously proposed length scales is exceptionally interesting in their own right (and perhaps many can eventually be found arise from the same underlying mechanism), but many display the same drawbacks. Previous numerical and experimental work has shown that these length scales evade experimental verification, and/or do not display an exceptional growth upon approach to $T_g$. For instance, in the case of the lengthscale investigated in (44), the behavior of the lengthscale and underlying physics bears a passing resemblance to the investigation done in this work, but that lengthscale, which arises in response to internal perturbations associated with thermal fluctuations, requires knowledge of individual particle displacements, making it difficult to experimentally detect. It is natural to expect that propagating amorphous order should be able to be revealed experimentally, and our proposed correlation length has the benefit of being readily measurable with methods beyond scattering experiments.

It is also worth noting that in (45), the authors found evidence of a **decreasing** correlation length upon cooling toward the glass transition temperature, $T_g$, in kinetically strong glassforming liquids. This was found to be indicative of a lambda transition in the vicinity of the glass transition. It was further suggested that for kinetically fragile liquids, the behavior would be the opposite, with the correlation length increasing upon approach to $T_g$. While this general behavior is consistent with our findings, we found no evidence suggestive of a lambda transition in this system, and further, the correlation length investigated in (45), was purely dynamical in nature.

In light of the above discussion, and based upon suggestions made in previous theoretical work (43; 46), we perform molecular dynamics simulations of $NiZr_2$, an excellent representative of a fragile glass (47). *We provide evidence for the rapid increase of the shear penetration depth*, defined as the length over which a supercooled liquid rigidly responds to externally imposed forces. We find that the near divergence of the penetration depth as the system becomes glassy is not far off the mark of Ising-like scaling.

## 4.3 The Shear Penetration Depth

In ordinary critical phenomena, the correlation length scale is defined as the typical spatial extent of a fluctuation of the thermodynamically relevant order parameter. It can also be interpreted as the average length over which a perturbation by the appropriate conjugate "generalized force" will appreciably propagate. For example, in the Ising Model, the correlation length corresponds to fluctuations in the typical size of magnetic domains (the order pameter is the magnetization, $\vec{M}$), and the also corresponds to the distance over which an applied magnetic field, $\vec{\mathcal{B}}$ (the conjugate force) will influence the system. As it is known that in crstalline solids, the rigidity is due to long range order, we can apply this idea to the

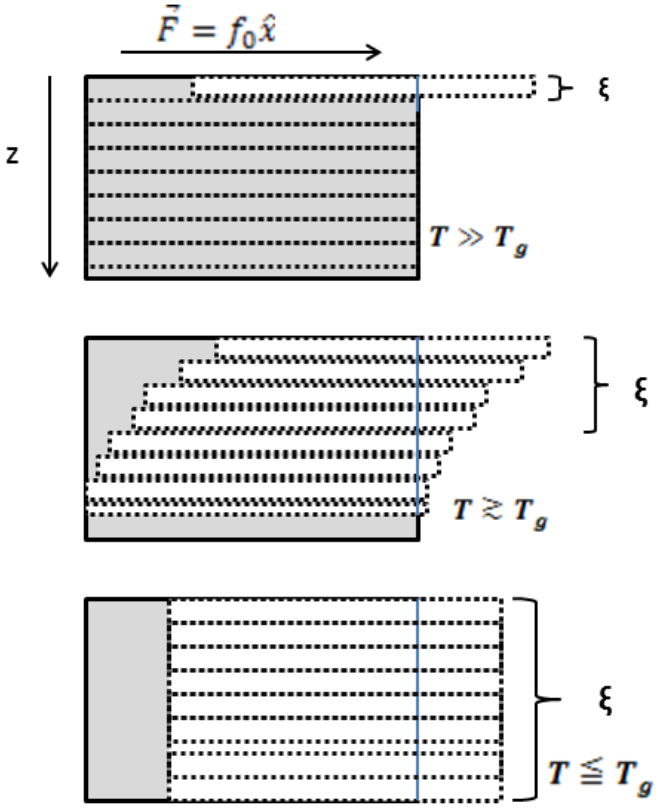


Figure 4.1: (Color Online) Representation of the proposed response of general supercooled fluid systems. The solid lines represent the original box shape before perturbation. The dashed regions represent the successive layers that respond to the perturbation at temperatures above and around Tg. At high temperatures only the layers experiencing the external stress move appreciably, but as temperature, T, is lowered and the cooperativity becomes pronounced, the perturbation is transmitted deeper into the material, reflecting increasing rigidity. Note that the extent to which the layers move as depicted, have been greatly exaggerated for clarity.

glass transition problem. In this case the ordering should be short range at temperatures just below melting, and grow as temperature as lowered. We can quantify this by subjecting the liquid to a shear perturbation on the boundary, and tracking how it penetrates the liquid transverse to the applied stress. Liquids, by definition, are capable of rearrangement to dissipate shear stress; a shear force applied to the top of a liquid will only propagate appreciably through a finite number of layers below the perturbation before fully decaying. Intuitively, one would expect that a high temperature liquid, having relatively low viscosity, would respond to the external force in a manner such that only the forced layer experiences a substantial displacement relative to the opposite boundary. As the temperature is lowered and the viscosity increases, one expects an associated increase in the liquids effective, short-lived rigidity. This, we argue, corresponds with increasing structural ordering and kinetic cohesion of network-like structures in the liquid. At moderate supercooling, then, one expects a deeper penetration of shear perturbations and associated displacements sustained by layers of the liquid that are increasingly distant from the applied perturbation. As depicted in Figure 1, the shear is applied to the top layer of the simulation box, transverse to the vertical (z) direction. The penetration depth is defined as the distance (along the z axis) up to which appreciable effects of shear are observed. At $T_g$ when solid-like rigidity has set in, one expects that the whole block of material will roughly slide together, such that the penetration depth is the length of the material. This is consistent with results that show the continuous emergence of a finite shear modulus for temperatures below $T_g$ (48). This process is pictured, schematically, in Figure (4.1). Ultimately this length scale is agnostic to the specific type of structural ordering, but can be related to cooperativity and the idea of a divergent correlation length in ordinary critical theory.

## 4.4 Models and Methods

Molecular dynamics (MD) simulations were employed using the LAMMPS package (49). The atoms in the simulation evolved under the influence of a semi-empirical Finnis-Sinclair type Embedded Atom Model potential created by Mendelv et al (50) with periodic boundary conditions. The parameters and coefficients associated with the potential were fitted using X-ray diffraction data as well as enthalpy of mixing values, and volume measurements in the liquid state. This potential has been shown to excellently reproduce both the high temperature liquid as well as glassy states of $NiZr_2$ (50).

The simulations were run in the NPT ensemble with N=5000 atoms and a target external pressure of P=0. Thermostatting and barostatting were employed using a Nose-Hoover thermostat, and barostat respectively, and the velocity-verlet algorithm was utilized to integrate the equations of motion. A 5fs timestep was employed. The initial configurations were generated randomly and the atoms were then allowed to melt and evolve naturally for 0.25 ns at a temperature of 2200 K to allow for equilibration. The system was then quenched to various target temperatures ranging from 300 K up to 1900 K using a quench rate of $\mathcal{Q} = 10^{13}$ K/s. After the quench, the system was allowed to evolve unperturbed for an additional 0.1 ns. The process was repeated, starting from independent initial configurations, for $T_g$ as well as all sampled temperatures below $T_g$ and some representative temperatures above.

As the glass transition is a kinetic phenomenon without a thermodynamic driving force, the glass transition temperature $T_g$ is not a constant, and weakly depends on cooling rate, and external timescale. Therefore, one has to be careful in identifying its precise location. Typically, various thermodynamic parameters show a crossover at the glass transition, associated with falling out of equilbrium (the system loses its translational degrees of freedom on the timescale of observation). One such property that shows a change in behavior at the

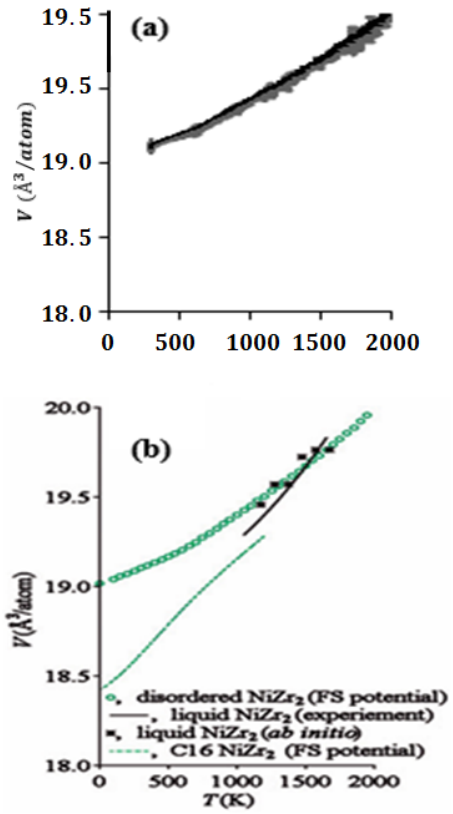


Figure 4.2: (Color Online). Panel (a): Specific volume as a function of temperature for our simulated system. Panel (b): Specific volume as a function of temperature. Reproduced from (50).

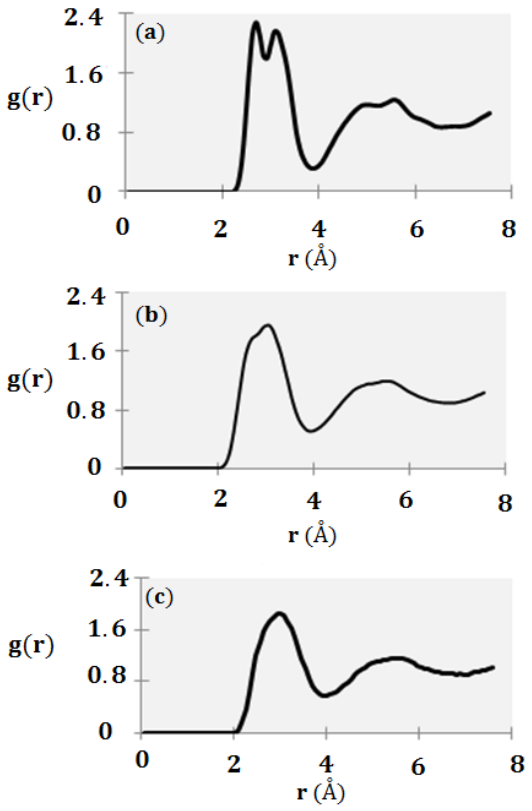


Figure 4.3: (Color Online). Radial Distribution Function at a temperature of (a): T=300 K $< T_g$, (b): moderate supercooling with T=1100 K, and (c): above the melting temperature at T=1500 K.

glass transition is the volume. The temperature dependence of the volume shows a "kink" at the glass transition temperature, $T_g$ (the thermal expansion coefficient, $\alpha \equiv \frac{1}{V}\frac{\partial V}{\partial T}$, has a discontinuity), providing an efficient way to determine $T_g$. The temperature dependence of the volume of our system during a quench to 300 K is depicted in panel (a) of Figure (4.2). There appears to be a subtle kink in the vicinity of $T \approx 700K$. This is in good agreement with the results in panel (b) of the same figure, which was produced by the author of the potential in (50), as well as previous numerical work performed under similar protocols (51).

In order to assess that our system is behaving as expected before applying shear stresses, we examine the behavior of the radial distribution functions at various temperatures. These results are shown in Figure (4.3). It is clear that system behaves as expected as the glass

transition is approached, and in comparison with (50), we see that the radial distribution functions (RDFs) measured in this work retain the overall shape and placement of the peaks. The height of the first peak (and behavior of the splitting of the first peak), however, is slightly different from those in (50) and we attribute this to the discrepancy in quench rates.

We modeled the external shear stress by defining a 4 angstrom-thick layer at the top of our simulation box, and applying an external force in the x direction on the atoms in this layer. In order to avoid fracturing in such a small system size at low temperatures, a force value of only 0.2 eV/A was used. A stronger force would be expected to make the effects more dramatic, but system size limitations did not allow for higher values. The force was left active for 100 timesteps to attempt to approximate an impulsive kick at the top of the box. No external forces were applied to the bottom of the box. After an observation time of $\tau_o$=16,000 timesteps, displacement data was extracted.

## 4.5 Measurement Results

To quantify the depth of penetration of the shear stress, we plot the displacement of each atom in the shear direction (x-direction) versus its position in the transverse height dimension (z-direction). The displacement represents the net movement in the shear direction from the timestep before the external shear stress was applied, up to the observation time $\tau_o$ (as described in methods section). The height of each particle corresponds to the vertical layer it is in at the observation time. Due to the periodic boundaries, only atoms in the layers from $z = \frac{L}{2}$ to $z = L$ at the observation time were considered. Figure (4.4) shows displacement data for four representative temperatures, i.) deep in the glassy phase (300K), ii.) at $T_g$ (700K), iii.) in the moderately supercooled regime (1300K), and iv.) above $T_{melt}$ (1500K). Thermal effects tended to produce large motions in the height dimension at

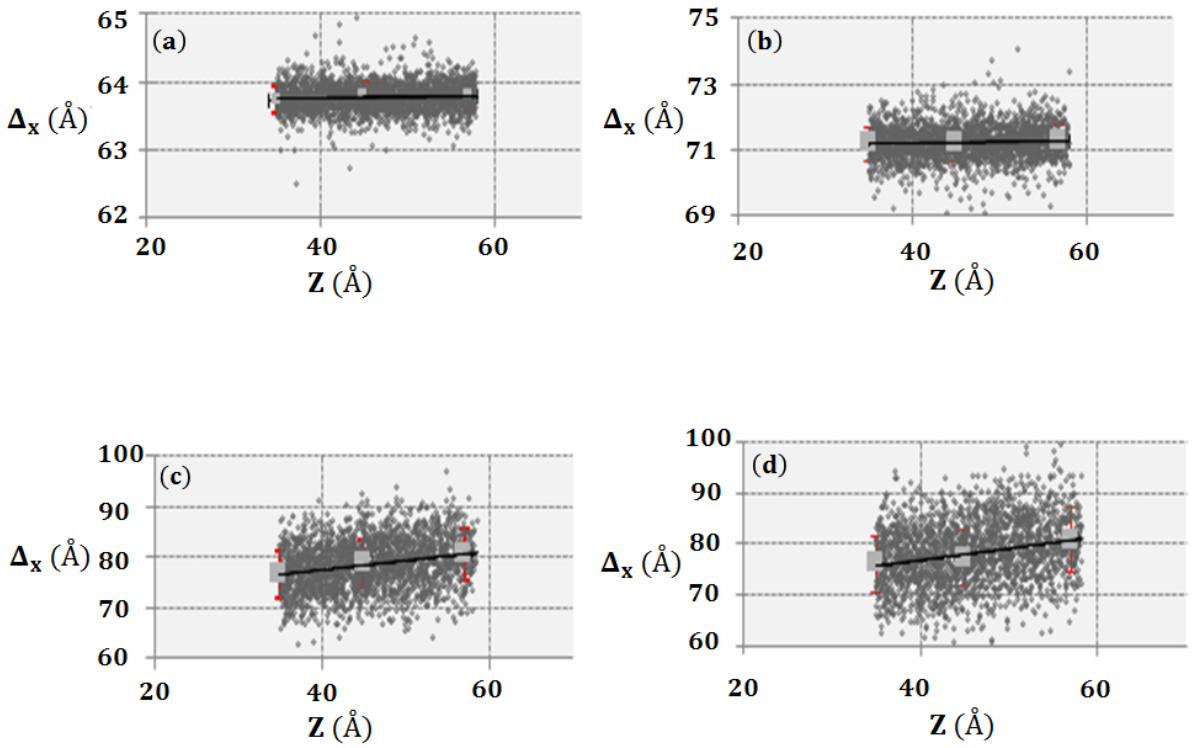


Figure 4.4: (Color Online). Typical Data at four [(a): 300 K, (b): 700 K, (c): 1300 K, (d): 1500 K] representative temperatures both above and below $T_g$ ($\approx$ 700 K). The red lines correspond to the standard deviation at the two boundaries and center of the material. It is noteworthy that they are significantly tighter than the data seems to suggest at this level of zoom. The black lines are the lines of fit from which the slope is extracted to define the length scale. Note the dramatically changing behavior as T is lowered.

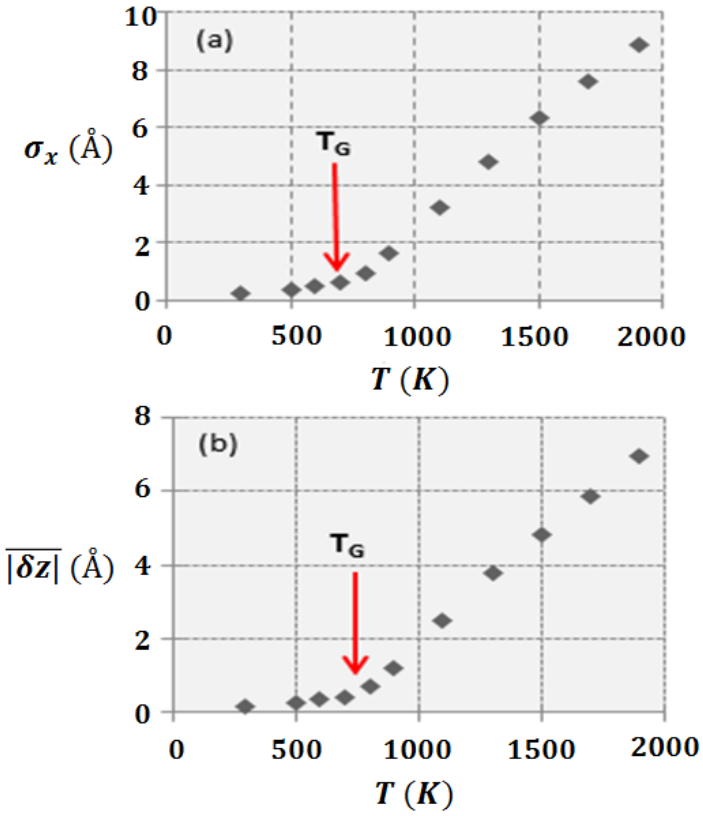


Figure 4.5: (Color Online). Panel (a): Plot of standard deviation of displacement in direction (x-axis) of applied shear as a function of temperature. Panel (b): Average displacement in height dimension (z-dimension) as a function of the temperature.

temperatures above $T_{melt}$, but the effects were not large enough to wash out the effect of shear penetration except at very high temperatures (1700-1900 K) . Figure (4.5) serves to quantify the impact of thermal noise. In panel (a), the standard deviation of displacement (at the observation time) in the direction of applied shear is plotted as a function of the temperature. As expected, the thermal noise decreases with decreasing temperatures becoming very small as $T_g$ is approached. In panel (b), the average magnitude of the particle displacements in the height (z) direction is plotted as a function of temperature. It is clear from panel (b) that

large scale thermal motion may play a role in "washing out" the shear penetration depth at the highest temperatures measured.

The general response function, $\mathcal{R}$, of our system to the externally imposed shear is a function of distance in the z direction to the imposed shear, temperature T, and observation time $\tau_o$;

$$\mathcal{R} = \mathcal{R}(z, T, \tau_o). \tag{4.1}$$

In this work, we chose a constant observation time, $\tau_o$, and varied the temperature to ascertain the penetration depth along the z axis. The penetration depth of the applied shear ultimately has some value depending on the temperature. However, our ability to extract the exact value depends on the observation time chosen. For sufficiently short observation times, the effects of the externally applied shear cannot penetrate the system at the lowest temperatures (near and below $T_g$). Therefore, the observation time has to be sufficiently long to capture the effect at low temperatures. As shown in Figure (4.6), for very long observation times at high temperatues, the effects of the external shear will be nill. Therefore, using an observation time which is very long would lead one to conclude a much deeper penetration depth at high temperatures (see Figure 4.6). Hence, choosing an appropriate observation time is important. For a couple representative temperatures we investigated the impact of observation time. In each case the duration for which the shear force was applied was constant; for this work we wanted to maintain an approximation of an impulsive kick to the system. Oscillatory shears have been discussed elsewhere. It was observed that at the lowest temperatures (T¡$T_A$), the results showed little change when observation times were changed by factors of two. For high temperatures, the observation time plays a more noticeable effect. Afte investigation, we found that the observation time employed in this work was

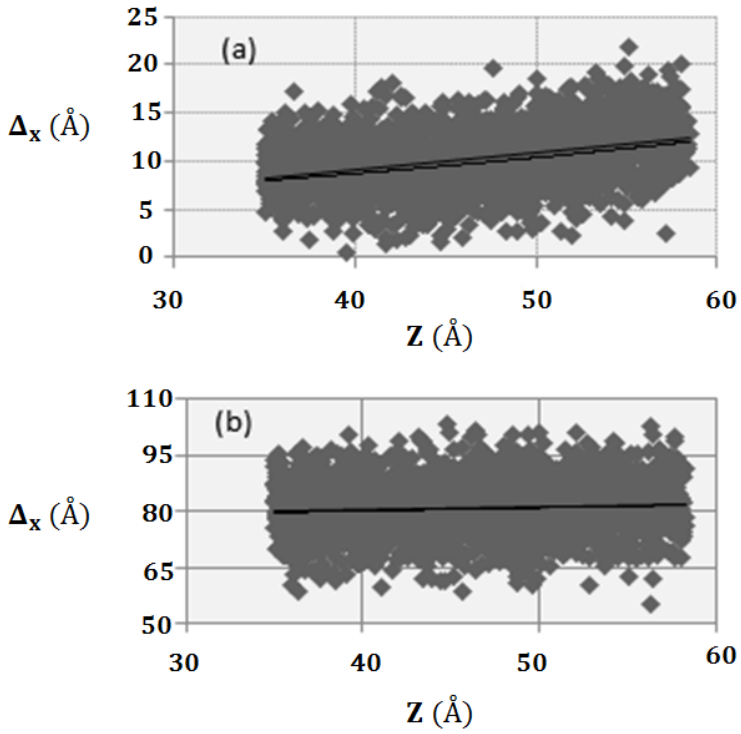


Figure 4.6: (Color Online) Displacement data for a random configuration at 1700 K. Panel (b) is the displacement for the observation time (16,000 timesteps), panel (a) is the data at an earlier time (3000 timesteps after the shear is turned off). As panel (b) shows, at high temperature the shear induced displacements appear to be far smaller at the standard observation time used in this work. Nevertheless, at earlier times, as seen in panel (a), the displacements are much more noticeable.

sufficient to capture the low temperature effect of the penetration, while not losing the high temperature impact except at the hightest temperatures studied.

Typically, one would expect the displacement response to decay exponentially with depth. As pictured in Figure (4.4), at these system sizes, the shear-induced displacement, while not very large, is still quite noticeable. As the displacement was not extremely large, we applied a linear regression to the data rather than an exponential one. These fits are

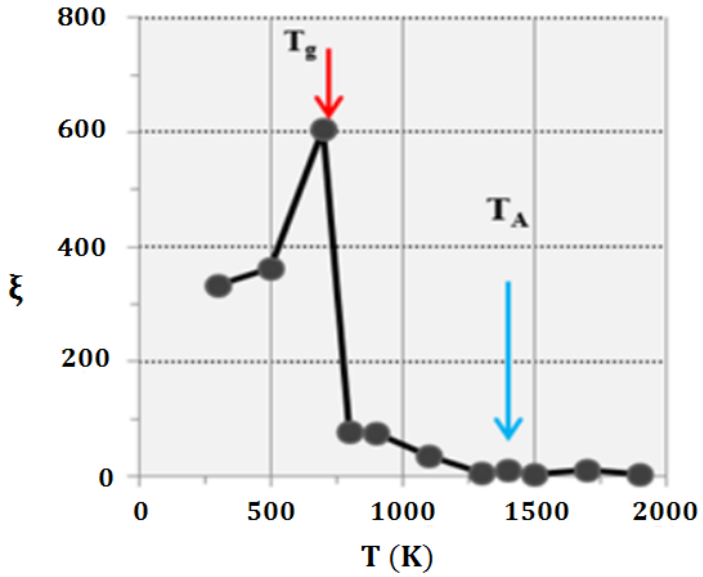


Figure 4.7: (Color Online). Plot of the length scale, $\xi$ versus temperature. All temperatures below $T_g$ were averaged over multiple independent runs, as were select, representative temperatures above $T_g$.

sufficient to quantify the penetration depth. Fits to the data were of the form,

$$\delta_x(z, \tau_o) = m * z + \delta_0 \tag{4.2}$$

where we denote by $\delta$, the displacement in the shear direction (x-direction) and z the height of the layer (both measured in angstroms). We define the rigidity length scale (the penetration depth) as

$$\xi \equiv \frac{1}{m} \tag{4.3}$$

where m is the slope in Eq. (4.2). For the temperatures noted above, the value of m was averaged over multiple runs, and this average was used in Eq. (4.3) for these temperatures.

The temperature dependence of the length scale ($\xi$) is shown in Figure (4.7). A dramatic growth of $\xi$ with decreasing temperature is evident. The first notable penetration

of the shear, beyond the layer to which the force was applied, occurs at a temperature marked $T_A(\approx 2T_g)$ (52). Below this temperature super-Arrhenius growth of the viscosity may be anticipated based upon collective effects (52; 53; 54; 55). The sudden, monotonic increase of $\xi$ at temperatures below $T_A$, provides direct support to earlier numerical studies, which found that metallic liquids begin to develop solid-like features once they are cooled below $T_A$ (52; 53). These solid-like features include the breakdown of the Stokes-Einstein relationship, exponential stretching of the relaxation functions, and the onset of cooperative structural rearrangements during the liquids relaxation process (1). Indeed, $T_A$ does appear to serve as a crossover temperature below which the liquid begins to exhibit a substantial rigid response to external forces, though it is a local and transient response. Putting all this together, our simulation results allow us to predict that marked growth of the shear penetration depth may commence at the same temperature as the breakdown of the Stokes-Einstein relation in real supercooled liquids. The penetration depth increases rapidly as the liquid is supercooled toward the glass transition temperature, $T_g$. Below the latter temperature, the material is glassy and exhibits structural rigidity on all practical timescales, such that shear perturbations propagate the length of the material and appear to diverge. As discussed previously, we performed multiple (typically six) independent measurements at all temperatures $T \leq T_g \approx 700K$, as well as most of the representative temperatures above $T_g$ (300-800, 1300, 1400, 1700K). At each of these temperatures, averaging was done to determine the slope, m, in the fit of Eq. (4.2). The apparently periodic nature of $\xi$ below $T_g$ can be attributed to noise due to the lengthscale being essentially divergent to the system size at these temperatures. This point is vividly made in Figure (4.8), which depicts the average slopes, m, as a function of temperature. The error bars on the points with multiple runs corresponds to the standard deviation in slopes. We see that, at temperatures near and below $T_g$, the combination of the average value and associated error bars lead to m being virtually indistinguishable from zero, consistent with the divergence of the penetration depth beyond the system size at the glass transition. It should also be immediately noticeable that

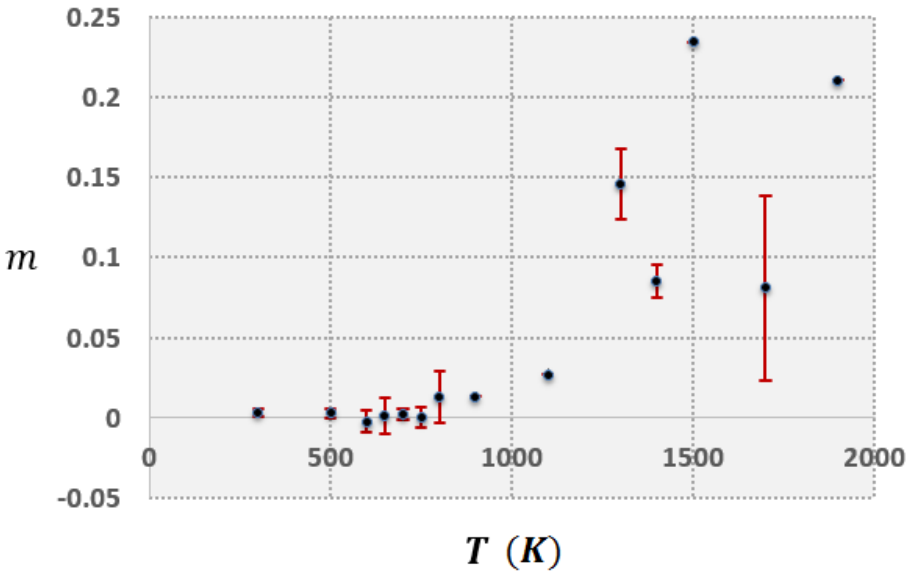


Figure 4.8: (Color Online). Plot of the average value of the slopes, m, at each of the measured temperatures along with their associated standard deviations $\sigma$ (when multiple runs were performed).

the data points associated with the value of the penetration depth at temperatures T=600, 650, and 750 K, are not plotted in Figure (4.7). This is because, as seen in Figure (4.8), the signal to noise ratio ($\frac{\sigma}{m}$) for these points was a factor of three for the data point at 600K and a factor of ten for the data points at 650 and 750 K. This large relative error is due to the fact that the length scale, $\xi$, is exceedingly large as the corresponding average slope m is very small, and in fact virtually indistinguishable from zero (see Eq. (4.3)). This corresponds to total penetration of the shear to beyond the system size, and the fluctuations about m=0, are to be expected due to ordinary thermal effects. Because of the large relative error in the aformentioned data points, we removed these data points from Figure (4.7) so as to not mask the overall monotonic increase of $\xi$ with incredible values. It may at first seem concerning that the data point at T=750 K is suggestive of near divergene considering it is above $T_g$. This is, in fact, not an issue, as the value of $T_g$ is not precise, and very likely falls within the T=700 to 750 K range for this system size and quench rate. Also, the close proximitiy to $T_g$ and limitations of resolution at this system size, would lead to the impact of the arrest

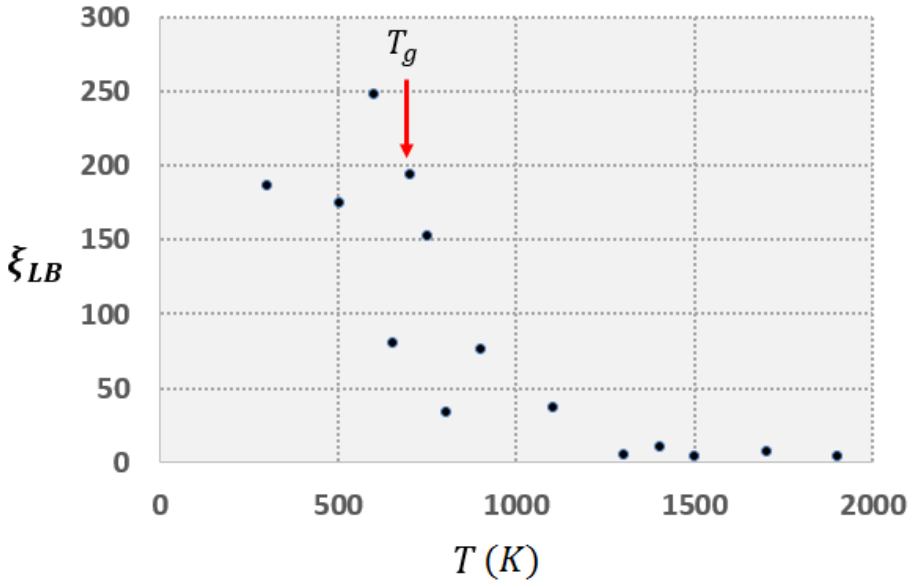


Figure 4.9: (Color Online). Lower bound, $\xi_{LB}$, on the shear penetration depth. See text.

at the glass transition strongly influencing temperatures asymptotically close to $T_g$. Clearly, Figure (4.8) serves not only to explain the fluctuations but also reinforces the idea that the penetration depth appears to diverge to the system size in the vicinity of $T_g$, and is perhaps the most consequential and rigorous result in this work.

As a lower bound on the shear penetration depth, in Figure (4.9) we plot

$$\xi_{LB} \equiv \frac{1}{m+\sigma}. \tag{4.4}$$

Because this is a lower bound, we can strongly assert, based on our data, that the penetration does indeed show dramatic increase upon supercooling. For temperatures below $T_g$, the length scale is so large and slopes so small, that the observed fluctuations of $\xi$ may be statistical (see Figure 4.8). We also conclude that the length scale becomes, at least, considerably larger than the system size at $T_g$, and may in fact diverge. For the impulsive kick we applied this will remain the case at all longer timescales of observation. However, if one were to apply a **static shear** at the top of the box and left this shear on for a time

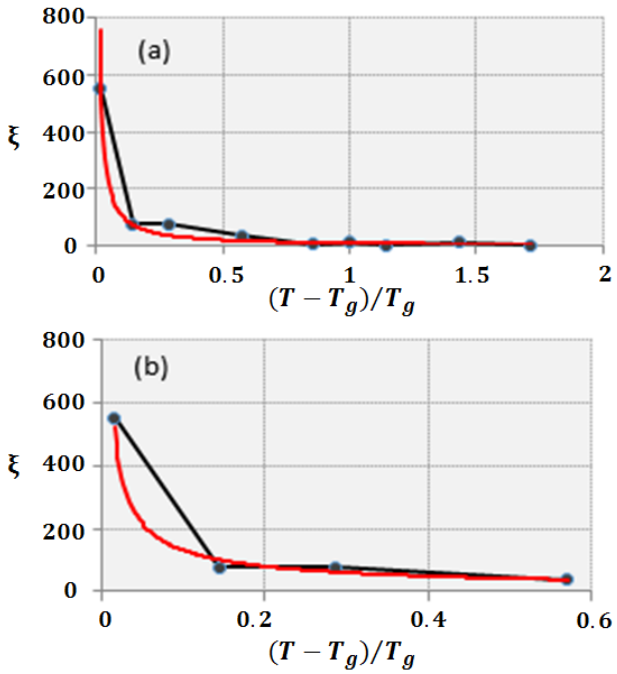


Figure 4.10: (Color Online). Power law fits to the shear penetration depth as a function of reduced temperature (measured relative to glass transition temperature $T_g$). Panel (a): $\xi \propto \left(\frac{T-T_g}{T_g}\right)^{-1}$. Panel (b): $\xi \propto \left(\frac{T-T_g}{T_g}\right)^{-0.71}$.

longer than the relaxation time, then even below $T_g$, the length may not diverge. On all practical timescales, though, it would, not diminishing this length as a natural candidate for the glass transition problem. The precise behavior of the penetration depth as the duration of the static shear stress is varied is an interesting problem, but requires a different type of analysis, and will be addressed in a future work.

## 4.6 Scaling Arguments

Previous studies have examined the behavior of various proposed length scales in the vicinity of $T_g$ (or the Vogel-Fulcher-Tammann temperature $T_0$ (7; 56; 57; 58). In (29), a diverging length scale associated with liquid-like defects at $T_g$ produced an exponent $\nu$=1;

This value constitutes an upper bound on the exponents reported in other works. Researchers in (59) found a critical exponent of $\nu$=0.875 for the largest icosahedral cluster size in a model metallic glass former (55). In both (60), focusing on inherent structures in a binary Lennard-Jones glass former, and in (61), by largely studying medium-range bond orientational order in colloidal liquids, scaling analyses gave exponents of $\nu \approx 2/3$, in rough agreement with a three-dimensional Ising exponent ($\nu$=0.625(1) (62)). We performed a similar scaling analysis of our data, fitting a function of the form

$$\xi \propto \left( \frac{T - T_g}{T_g} \right)^{-\nu}. \tag{4.5}$$

To represent the value of the length scale at $T_g$ itself, we interpolated the value at T=710K using the line connecting T=800K and T=700K. In addition, the data point at T=750 K, was excluded from this scaling analysis for reasons discussed above. When using the full range of temperatures in applying the power law fit, we extracted an exponent of $\nu$=1. This is depicted in Figure (4.10), panel (a). Decreasing the temperature range considered in the scaling to only include temperatures very close to $T_g$, caused the value of the exponent $\nu$ to decrease. This is depicted in panel (b) of Figure (4.10), where a value of $\nu$=0.713 was found. Clearly, as the scaling is applied to a more and more asymptotic region around $T_g$, the value of $\nu$ appears to approach a value consistent with Ising-like scaling. Our value for , is, thus, in rough agreement with previously suggested exponents extracted by different means. A similar study conducted in (33) studied the high temperature ($T \geq T_m$) correlations of the anisotropic part of the atomic level stress. In this work the authors found an exponent of $\nu \approx$0.7 for the low temperature extrapolation of the correlations in their two-dimensional system (the high crystallization rate at temperatures below $T_m$ thwarted a direct study at low temperatures). Our possible scaling may provide further evidence of a universal nature of the length scale at deep supercooling. As $T_g$ is not a true thermodynamic temperature, it

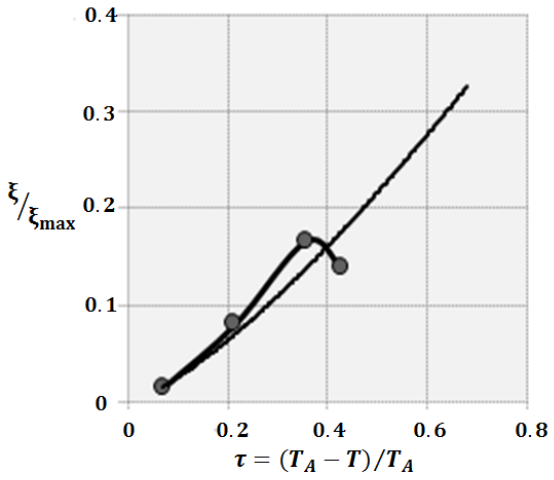


Figure 4.11: (Color Online). Power law scaling, $\xi \propto \left(\frac{T_A - T}{T_A}\right)^{\nu_A}$, in the asymptotic region below the crossover temperature, $T_A$.

is unclear what this scaling may mean, but it may be suggestive of universality in the glass transition.

In [69, 70] theoretical arguments for the scaling of the length scale about the crossover temperature, $T_A$, were provided. It was suggested when asymptotically approaching $T_A$ from below, that a characteristic structural domain size, l, scaled as

$$l = {\tau_A}^{\nu_A}, \tag{4.6}$$

where $\tau_A \equiv \frac{T_A - T}{T_A}$. We examined the shear penetration depth as a function of the reduced temperature, $\tau_A$, as depicted in Figure (4.11). We observed that a power law is a good fit in this region with an exponent, $\nu_A$ ≈1.335. If the lowest temperature (highest reduced

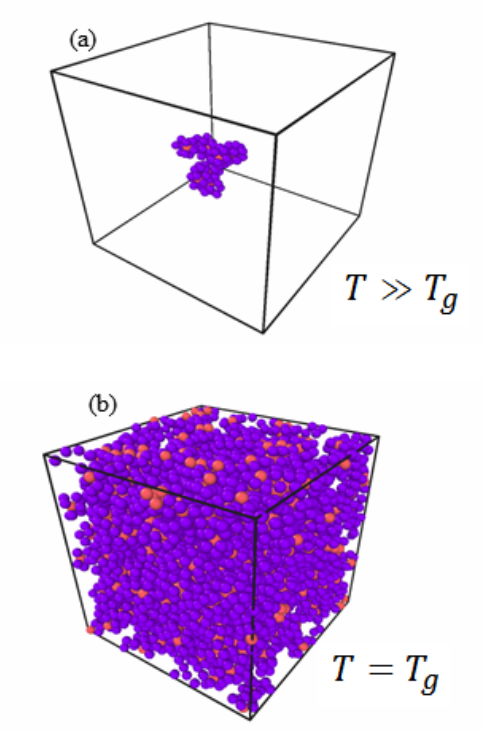


Figure 4.12: (Color Online). Depiction of growing interconnectivity of icosahedral clusters with supercooling in $Cu_{36}Zr_{64}$, a very similar metallic glass former. The Cu atoms are marked red and the Zr by purple. In Panel (a) we show the longest interconnected cluster at 1200 K. Panel (b) shows the longest connected cluster at $T_g$ (800 K for this system). Note that interconnecting icosahedra percolate at $T_g$. (These results are similar to those in (55).)

temperature) point in Figure (4.11) is removed, then a value of $\nu_A \approx 1.5$ will be obtained instead.

## 4.7 The Question of Structure

We have defined the shear penetration depth as the distance over which supercooled liquids can support shear appreciably. This definition is based on a simple physical picture of liquids as a continuum unable to globally support shear stress. With decreasing temperature the viscous inter-layer forces, rigidity, and the lifetime of connectivity increase. At $T_g$, the glass transition temperature, these quantities mirror those of crystals and the material is

solid. This scale has the added benefit that it may be readily experimentally accessible. Results from simulations on $NiZr_2$, a typical fragile glass, support this definition. In the current work, we applied, in simulatum, a shear force to the top layer of a $NiZr_2$ system. By measuring the penetration depth, $\xi$, we have demonstrated a dramatically increasing structural scale upon supercooling toward $T_g$. This leads to the conclusion that the shear penetration depth marks a very natural candidate for the structural length scale characterizing glassy dynamics. Furthermore, and of equal importance, the shear penetration depth can be measured experimentally. While it might be practically difficult, in theory, the penetration depth can accessed experimentally in a way that does not rely solely on scattering, and may, therefore, be easier to investigate. This is a major advanatage for this lengthscale, and sets it apart from previously proposed lengths.

We ultimately believe that the shear penetration depth is intimately connected to the structure of the supercooled liquid. However, as mentioned earlier, structure factors and radial distribution functions show little change upon supercooling to $T_g$, and long-range order of the type seen in crystalline solids does not appear to cause the kinetic arrest in glasses. Despite this, an activation barrier which grows with decreasing temperature is suggestive of cooperative particle motion in the supercooled liquid, and it is natural to suspect that this cooperativity likely arises due to structural changes accompanying supercooling and the propagation of some form of "amorphous" order. Further, that the activation energy increases beyond the standard enthalpy of fusion in most fragile liquids, suggests that local single particle "bond-breaking" ceases to be the primary mode of structural relaxation. It has been shown (53; 55; 63; 64; 65; 66; 67; 68) in extensive numerical studies that clusters of locally preferred structural order tend to grow and interconnect as temperature is lowered in supercooled liquids. These clusters locally minimize the relevant free energy and hence are stronger and more stable to fluctuations. Due to their locally stable nature and tight binding, the clusters resist thermal breakup and lock into a rigid structure forming a force

network that can propagate shear. The interlocking and cohesiveness of this network also serves to slow down the dynamics (65), as sufficiently large thermal fluctuations are needed to break the network and this becomes less likely with lower temperature. Interconnections of the clusters increase in length and lifetimes (53; 54; 65) upon lowering temperature, and eventually span the system size at the glass transition. This percolation of a structural network, which is depicted in Figure (4.12) for a cousin configuration, is very likely the source of the penetration depth as well as a leading cause of the arrest at the glass transition temperature $T_g$.

The fact that our length scale begins to grow substantially, only when supercooled beneath $T_A$, further suggests a structural origin for the glass transition. Indeed, it has been suggested, and extensively investigated, that $T_A$ marks the point at which locally preferred structures begin to form and persist in the liquid and solid-like properties begin to appear (52; 53; 54; 55). Taken together, there is significant evidence which suggests that percolation of locally preferred structures plays a role in the phenomenology of supercooled liquids.

In fragile glasses, this network has to form quickly over the temperature range encountered in typical experiments. This is likely due to the largely non-directional binding in fragile glasses which lacks the natural network found in strong covalent liquids. In metallic liquids, the network is likely icosahedral (53; 55; 63; 64; 66). In silicates (typical of the strong classification) a natural tetrahedral network with strong bonds and directionality is present. It has been suggested that (66) networks of locally preferred structures tend to form in fragile glasses being either icosahedral or crystal-like at short range.

As discussed above, the percolating structures begin to grown and persist starting at the temperature $T_A$. Additionally, it is known that the super-Arrhenius character of the viscosity sets in at the same $T_A$, as demonstrated in Figure Whatever. In Figure Whatever.2 we demonstrate that the penetration depth begins to grow dramatically starting around

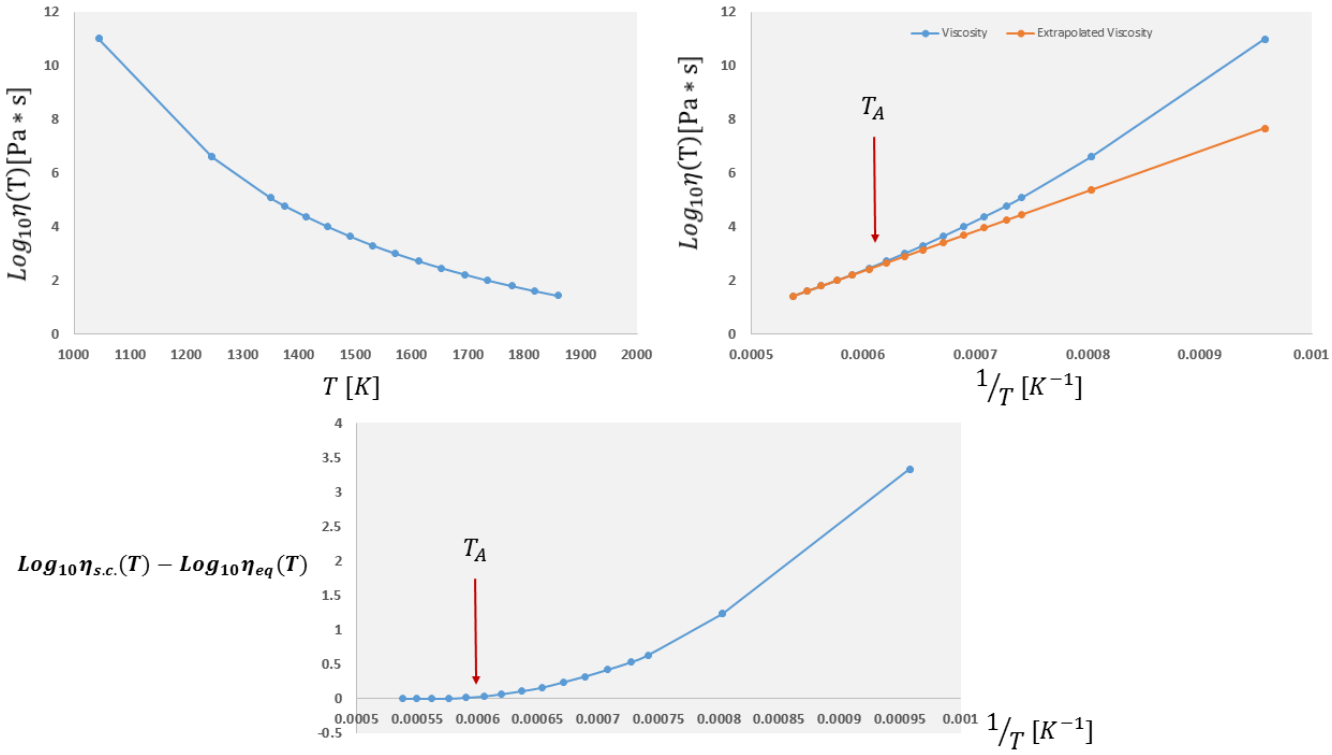


Figure 4.13: (Color Online). Top Left: Plot of Viscosity of prototypical glass former (composition proprietary). Top Right: Viscosity and Extrapolated Equilibirium Viscosity plotted versus reciprocal temperature. Bottom: Difference between viscosity and extrapolated high temperature viscosity. The first appreciable difference occurs at $T_A$.

the same temperature. These correlations are strongly suggestive that the penetration depth is intimately connected to both the super-Arrhenius character of the viscosity and the outgrowth of a 'backbone' of interconnected local structure. Additionally, that all three begin to grow at essentially the same temperature is immediately suggestive of a link between percolation of local structure and the temperature dependence of the viscosity in supercooled liquids.

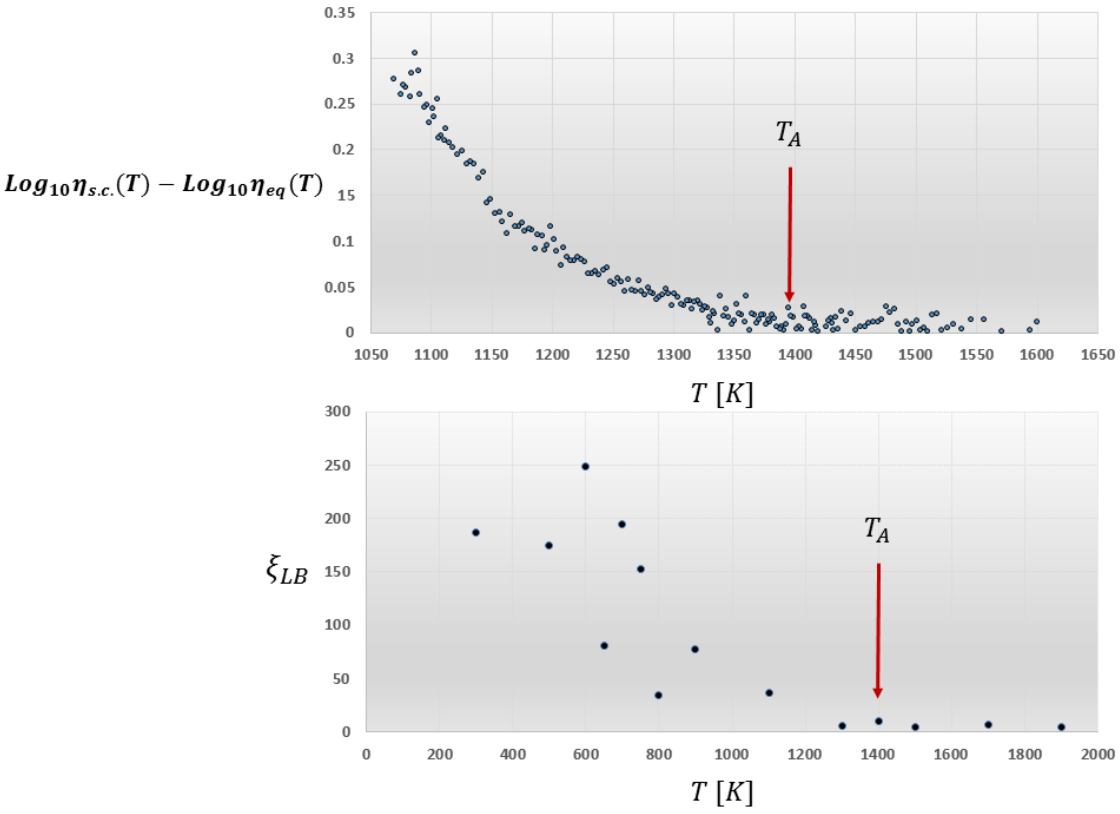


Figure 4.14: (Color Online). Top: Difference between viscosity and extrapolated high temperature viscosity plotted versus temperature for $Ni_{34}Zr_{36}$. Bottom: Temperature dependence of the lower bound of the shear penetration depth. Note that appreciable growth of the penetration depth sets in at the same temperature as the super-Arrhenius growth in the $Ni_{34}Zr_{36}$ system.

## 4.8 Conclusion

The notion that the shear penetration in amorphous solids is due to a system spanning network is a universal one. As discussed, a network forms over a narrow range in fragile glasses leading to the super-Arrhenius increase of viscosity and causing the rigidity. In strong glasses, a tetrahedral network forms at high temperature and becomes increasingly cohesive as the temperature is lowered to $T_g$. Other forms of a system spanning network can also exist. In colloids a frictional or contact network can be created by jamming, and in fact a rigidity length scale has been proposed for these systems (25). The formation of a contact network has also been shown to occur, albeit short-lived, in some discontinuous shear thickening fluids (67). This contact network may also play a role strong to fragile crossovers in high pressure thermal glasses.

Based on the above discussion, it is clear that a shear penetration length scale can be quite naturally extended to many, if not most, glassy systems. This leads naturally to the connection between slowing down and network formation. As such, being able to experimentally detect these structures and the length over which they exist in supercooled liquids is of critical importance to uncover how much, if any, role they truly play in glass formation.

# References


[1] A. Cavagna, Physics Reports, **476**, 551-124 (2009) [review]

[2] I. M. Kalogeras and HE. Hagg Lobland, Journal of Materials Education, **34**(3-4): 69-94 (2012) [review]

[3] L. Berthier and F. Biroli, Reviews of Modern Physics, **83**, April-June (2011) [review]

[4] G. L. Hunter and E. R. Weeks, Rep. Prog. Phys. **75**, 066501, (2011) [review]

[5] I. Procaccia, Eur. Phys. J. Special Topics, **178**, 81-122 (2009) [review]

[6] J. S. Langer, Rep. Prog. Phys., **77**,042501 (2014) [review]

[7] C. A. Angell, Science, **267**, 1924-1935 (1995)

[8] H. G. E. Hentschel, S. Karmakar, I. Procaccia, J. Zylberg, Phys. Rev. E **85**, 061501 (2012)

[9] A. Montanari, and G. Semerjian, J. Stat. Phys., **125**, 23 (2006)

[10] T. R. Kirkpatrick, D. Thirumalai, and P.G. Wolynes, Phys. Rev. A, **40**, 1045 (1989)

[11] T. R. Kirkpatrick and D. Thirumalai, Phys. Rev. Lett., **58**, 2091 (1987)

[12] T. R. Kirkpatrick and D. Thirumalai, Phys. Rev. B, **36**, 5388 (1987)

[13] T. R. Kirkpatrick and P. G. Wolynes, Phys. Rev. B., **36**, 8552 (1987)

[14] T. R. Kirkpatrick and D. Thirumalai, Phys. Rev. B., **37**, 5342 (1988)

[15] T. R. Kirkpatrick and D. Thirumalai, J. Phys. A, **22**, L149 (1989)

[16] G. Adam, and J. H. Gibbs, J. Chem. Phys., **43**, 139-146, (1965)

[17] D. R. Reichman, and P. Charbonneau, J. Stat. Mech: Theory and Experiment, Issue **05**, 05013 (2005)

[18] F. Ritort and P. Sollich, Adv. Phys., **52**, 219-342 (2003)

[19] R. Busch, Z. Evenson, I. Gallino, and S. Wei, arXiv:1405.2251v1 (2014)

[20] G. M. Hocky, T. E. Markland, and D. R. Reichman Phys. Rev. Lett., **108**, 225506 (2012)

[21] L. Berthier and W. Kob, Phys. Rev. E, **85**, 011102 (2012)

[22] S. Karmakar and I. Procaccia, Phys. Rev. E, **86**, Issue 6, id. 061502 (2012)

[23] J. Russo and H. Tanaka, PNAS, **112** 6920 (2015)

[24] T. Iwashita and T. Egami, Phys. Rev. E, **90**, Issue 5, 052307 (2014)

[25] C. P. Goodrich, W. G. Ellenbroek, and A. J. Liu, Soft Matter, **9**, 10993 (2013)

[26] A. Malins, J. Eggers, H. Tanaka, and C.P. Royall, Faraday Discuss., **167**, 405 (2013)

[27] R. Gutierrez, S. Karmakar, Y. G. Pollack, and I. Procaccia, Europhysics Lett., **111**, 56009 (2015)

[28] G. Biroli, S. Karmakar, and I. Procaccia, Phys. Rev. Lett., **111**, 165701 (2013)

[29] E. Aharanov, E. Bouchbinder, H. G. E. Hentschel, V. Ilyin, N. Makedonska, I. Procaccia, and N. Schupper, Euro. Phys. Lett. **77**, 56002 (2007)

[30] K. Trachenko, and V. V. Brazhkin, J. Phys.: Condens. Matter **20**, 075103 (2008)

[31] G. Biroli, J.-P. Bouchard, A. Cavagna, T. S. Grigera, and P. Verrocchio, Nature Physics, **4**, 771-775 (2008)

[32] V. A. Levashov, J. R. Morris, and T. Egami, J. Chem. Phys., **138**, 044507 (2013)

[33] B. Wu, T. Iwashita, and T. Egami, Phys. Rev. E., **91**, 032301 (2015)

[34] N. Lacevic, T. B. Schroder, F. W. Starr, S. C. Glotzer, J. Chem. Phys., **119**, Number 14, (2003)

[35] R. Richert, J. Phys.: Condens. Matter, **14**, R703-R738 (2002)

[36] H. Sillescu, J. Non-Cryst. Solids **243**, 81 (1999)

[37] M. D. Ediger, Ann. Rev. Phys. Chem. **51**, 99 (2000)

[38] W. Kob, C. Donati, S. J. Plimpton, P. H. Poole, and S. C. Glotzer, Phys. Rev. Lett. **79**, 2827 (1997)

[39] C. Donati, J. F. Douglas, W. Kob, S. J. Plimpton, P. H. Poole, and S. C. Glotzer, Phys. Rev. Lett. **80**, 2338 (1998)

[40] S. C. Glotzer, J. Non-Cryst. Solids **274**, 342 (2000)

[41] Y. Gebremichael, T. B. Schroder, F. W. Starr, and S. C. Glotzer, Phys. Rev. E **64**, 051503 (2001)

[42] J.-X. Lin, C. Reichhardt, Z. Nussinov, L. P. Pryadko, and C. J. Olson Reichhardt, Phys. Rev. E, **73**, 061401 (2006)

[43] P. Ronhovde, S. Chakrabarty, D. Hu, M. Sahu, K. K. Sahu, K. F. Kelton, N. A. Mauro, and Z. Nussinov, European Journal of Physics E, **34**, 105 (2011) [In particular see appendix S, therein for theoretical discussion of the shear penetration depth in glasses; P. Ronhovde, S. Chakrabarty, D. Hu, M. Sahu, K. K. Sahu, K. F. Kelton,

N. A. Mauro, and Z. Nussinov, Scientific Reports **2**, 329 (2012) ; Z. Nussinov, P. Ronhovde, Dandan Hu, S. Chakrabarty, M. Sahu, Bo Sun, N. A. Mauro, K. K. Sahu, arXiv: 1503.06126 (2015)]

[44] C. Donati, S. C. Glotzer, and P. H. Poole, PRL, **82**, 5064(4) (1999)

[45] S. Wei, I. Gallino, R. Busch, and C. A. Angell, Nature Physics, **7**, 178-182 (2011)

[46] J. Zaanen, Z. Nussinov, and S. I. Mukhin, Annals of Physics, **310**,181-260 (2004)

[47] M. Blodgett, T. Egami, Z. Nussinov, and K. F. Kelton, Nature Scientific Reports, **5**, 13837 (2015)

[48] H. Yoshino and M. Mezard, Phys. Rev. Lett. **105**, 015504 (2010)

[49] S. Plimpton, J. Comp. Phys., **117**, 1-19 (1995)

[50] M. I. Mendelev, M. J. Kramer, S. G. Hao, K. M. Ho, and C. Z. Wang, Philosophical Magazine, **92:35**, 4454-4469, DOI: 10.1080/14786435.2012.712220 (2012)

[51] F. J. Cherne, M. I. Baskes, and R. B. Schwarz, J. Non-Crystalline Solids, **317**, 45-51 (2003)

[52] D. Kivelson, S. A. Kivelson, X. Zhao, Z. Nussinov, and G. Tarjus, A Thermodynamic Theory of Supercooled Liquids, Physica A **219**, 27 (1995)

[53] R. Soklaski, V. Tran, Z. Nussinov, K. F. Kelton, and L. Yang, Philosophical Magazine, **96** (2016)

[54] T. Iwashita, D. M. Nicholson, and T. Egami, Phys. Rev. Lett., **110**, 205504 (2013)

[55] R. Soklaski, Z. Nussinov, Z. Markow, K. F. Kelton, and L. Yang, Phys. Rev. B, **87**, 184203 (2013)

[56] H. Vogel, Z. Phys. **22**, 645 (1921)

[57] G. S. Fulcher, J. Am. Ceram. Soc. **8**, 339 (1925)

[58] G. Tamann and W. Z. Hesse, Anorg. Allgem, Chem. **156**, 245 (1926)

[59] Z. W. Wu, F. X. Li, C. W. Huo, M. Z. Li, W. H. Wang, K. X. Liu, arXiv:1505.04601 (2015)

[60] M. Mosayebi, E. Del Gado, P. Ilg, and H. C. Ottinger, Phys. Rev. Lett., **104**, 205704 (2010)

[61] H. Tanaka, T. Kawasaki, H. Shintani, and K. Watanabe, Nature Materials, **9**, 324-331 (2010)

[62] R. Gupta and P. Tamayo, Int. J. Mod. Phys. C **07**, 305 (1996)

[63] Z. W. Wu, M. Z. Li, W. H. Wang, and K. X. Liu, Phys. Rev. B. **88**, 054202 (2013)

[64] J. Ding, Y. Cheng, and E. Ma, Acta Mater. **69**, 343-354 (2014)

[65] Y. Q. Cheng, H. W. Sheng, and E. Ma, Phys Rev B., **78**, 014207 (2008)

[66] M. Leocmach, and H. Tanaka, Nature Communications, **3**, 974 (2012)

[67] F. F. Abraham, arXiv:1504.05751 (2015)

[68] P. Crowther, F. Turci, and C. P. Royall, Journ. Chem. Phys., **143**, 044503 (2015)

[69] E. Brown, Physics **6**, 125 (2013)

[70] Zohar Nussinov, Physical Review B **69**, 014208 (2004)

[71] G. Tarjus, S. A. Kivelson, Z. Nussinov, and P. Viot, Journal of Physics: Condensed Matter **17**, R1143 (2005)

**An Energy Distribution Approach to Supercooled Liquids, Weingartner, Ph.D. 2017**